The Processes of Path Integration and Landmark-based Navigation in Human Adults

By

Yafei Qi

A thesis submitted in partial fulfillment of the requirements for the degree of

Doctor of Philosophy

Department of Psychology

University of Alberta

Abstract

An effective navigation process requires the ability to determine the navigators' current position and heading in the environment (referred to as self-localization) and localize the points of interest, such as home. Humans and non-human animals typically use self-motion cues (i.e., path integration) and landmarks (i.e., piloting) to keep track of their position and orientations and find their homes. Chapter 1 reviews the previous research regarding the usage of these two processes in human navigation and their contribution to determining orientation and briefly discusses the systematic homing errors observed in path integration. Chapter 2 presents a study that examined the usage of different landmarks in human orientation and Chapter 3 presents a study that examined the sources of systematic biases in human path integration. Chapter 4 summarizes the findings of the two studies and discusses the implications and limitations of these studies.

Chapter 2 involves a study investigating the roles of distal and proximal landmarks in determining human orientations. It has been a long-standing theoretical argument and foundational assumption in research paradigms that distal landmarks dominate as orientation cues over proximal landmarks. Participants learned object locations with proximal and distal landmarks in an immersive virtual environment. After walking a path without seeing objects or landmarks, participants were disoriented and pointed to the objects with the reappearance of a proximal landmark being rotated -50°, a distal landmark being rotated 50°, or both (Conflict). Heading errors were examined. Experiment 1 manipulated the relative cue precision. Results indicate that besides the relative cue precision, prior knowledge of distal cue dominance also influences orientation cue usage. In Experiments 2 and 3, participants walked a path stopping at one object location. Participants were informed of it explicitly in Experiment 2 but not in Experiment 3. Results showed that distal cue dominance still occurred in Experiment 3.

However, in Experiment 2, proximal cue dominance appeared, and it was not predicted by the relative cue precision. These results suggest that prior knowledge of proximal cue dominance might have been invoked by the instruction of locations. Consistent with the Bayesian inference model, human cue usage in orientation is determined by relative cue precision and prior knowledge. The choice of prior knowledge can be influenced by instructions.

Chapter 3 involves a study employing computational modeling to investigate potential sources of systematic biases observed in human path integration. Systematic biases (compression patterns in the inbound responses) have been well documented in human triangle completion tasks. Cross-validation modeling was used to compare three plausible theoretical models that assume that systematic errors occur in the encoding outbound path solely (encoding-error model), executing the inbound responses solely (execution-error model), and both (bi-component model), respectively. Unlike traditional triangle completion tasks with a single inbound response (i.e., the homing vector) for each outbound path, the triangle-completion task used in this study required participants to indicate three learned locations (including the home location) during the response phase. The results demonstrated that the bi-component model outperformed the other models in accounting for the systematic errors using multiple inbound responses. This finding suggests that both encoding the outbound path and executing the inbound responses contribute to the systematic biases in human path integration. Additionally, the results showed that the algorithm using only the home response could not distinguish among these three models, suggesting that the typical triangle-completion task with only the home response for each outbound path cannot determine the sources of the systematic biases.

Preface

Chapter 2 of this dissertation has been published as: Qi, Y., & Mou, W. (2023). Sources of systematic errors in human path integration. Journal of Experimental Psychology: Human Perception and Performance, 49(2), 197. Also, versions of this chapter have been presented at international conferences, i.e., the 2022 Psychonomic Society's Annual Meeting and iNAV Symposium.

Chapter 3 of this dissertation has not yet been published. A version of this chapter has been presented at the 2023 Psychonomic Society's Annual Meeting as Qi, Y., & Mou, W. (2023). Relative cue precision and prior knowledge contribute to the preference of proximal and distal landmarks in human orientation.

This thesis is an original work by Yafei Qi. The research project, of which this thesis is a part, received research ethics approval from the University of Alberta Research Ethics Board, Project Name "Human navigation", Pro00082900, July 23, 2018.

Acknowledgments

My journey through the five-and-a-half-year graduate program has drawn to a close, and it feels like time has passed by in the blink of an eye. I am deeply grateful for the help and support I have received from many individuals, and I would like to express my heartfelt appreciation to each one of them.

First and foremost, I want to extend my sincere gratitude to my supervisor, Dr. Weimin Mou. Your role as my mentor has been truly remarkable. You have provided me with insightful guidance and unwavering encouragement throughout my research journey. Your patience and dedication to your students have significantly influenced my personal and professional development, shaping me into the person I aspire to be in life. Your wisdom and passion for research have been a constant source of motivation, driving me to pursue my goals in the field. I feel incredibly fortunate to have had you as my supervisor. I also wish to express my gratitude to my supervisory committee members, Dr. Anthony Singhal and Dr. Peggy St. Jacques, for their invaluable feedback, guidance, and unwavering support.

To my supportive colleagues in the Virtual Reality and Spatial Cognition Lab—Xuehui Lei, Yue Chen, and Zijian Zhang—I extend my heartfelt thanks for engaging in enriching discussions related to my research and for being a constant source of companionship throughout these years. I would also like to acknowledge the contributions of all the research assistants who have collaborated with me: Jerry Wu, Mia Hawkins, Zhichun Qi, Andrea Ybanez, Gurleen Gill, and Subekshya Adhikari. Your dedication to data collection and the enjoyable moments you've shared with me have been deeply appreciated. Our lab has not just been a research space but a warm and supportive family.

I want to extend my thanks to my friends—Jiabi Wen, Peiran Yao, and Xinlei Cao—for the countless joyful moments and unwavering friendship you've provided. To my boyfriend, Yang Liu, I am grateful for your constant companionship, care, and support during this journey. You celebrated my achievements and provided strength during challenging times. Last, but certainly not least, I want to express my profound appreciation to my beloved parents, Liping Zhang and Xianbo Qi, who have consistently stood by me in every situation. Your unconditional love, trust, and support have been my unwavering pillars of strength.

Table of Contents

List of Tables

List of Figures

Chapter 1 General Introduction

Desert ants forage up to hundreds of meters and find their nest within 1 square centimeter of error (Gallistel, 1990; Wehner & Srinivasan, 1981). Puluwat sailors navigate canoes between islands separated by distances of up to 800 kilometers, arriving at their destination with ease (Gladwin, 1970). As for us, modern humans heavily rely on navigation for daily necessities including commuting to work and school, exploring restaurants and attractions across town, and hiking unfamiliar trails. Successful navigation requires the ability of determining navigators' current position and heading in the environment (referred to as self-localization) and localizing the points of interest (referred to as goal-localization). Humans and a wide range of mobile animals are able to navigate by means of two basic navigation processes: path integration relying on self-motion cues (Etienne & Jeffery, 2004; Loomis et al., 1993) and landmark-based navigation (also referred to as piloting) relying on landmark cues (Doeller & Burgess, 2008; Foo et al., 2005).

The current dissertation investigates two questions related to the navigation processes of path integration and piloting in human navigation. In Chapter 1, I first review the previous research regarding the usage of these two processes in human navigation and their contribution to determining orientation and discuss the systematic homing errors observed in path integration. Chapter 2 presents Study 1 which examined the roles of visual distal and proximal landmarks in providing spatial orientation. Chapter 3 presents Study 2 examining the potential sources of the systematic biases in human path integration using computational modeling. Chapter 4 summarizes the findings and implications of these studies and suggests possible future studies.

1.1 Path integration and piloting

Landmark-based navigation or piloting utilizes previously encoded visual landmarks in the environment to determine the positions and headings of navigators (e.g., Cheng & Spetch,

1998; Etienne et al., 1996, 2004; Foo et al., 2005; Wehner et al., 1996), as well as the locations of other objects (Doeller & Burgess, 2008; Hermer & Spelke, 1994; Zhou & Mou, 2016). Piloting relies on visual perception to encode the spatial relationships between visual items as well as the spatial relationships between those items and the navigators themselves (Cheng & Spetch; 1998; Doeller & Burgess, 2008; Mou & Zhang, 2014; Taube, 2007; Yoder et al., 2011). Some salient items (i.e., landmarks) can serve as reference points to specify other locations. As a result, people can localize themselves and their goals by recognizing familiar landmarks. For instance, a shopper might try to find their parked car by recalling that it was near the shopping cart corral outside of a grocery store. The shopping cart corral acts as a landmark, providing relative spatial information (e.g., distance and bearing) about the car's location. Regarding the landmark-based navigation, its accuracy does not require the continuous presence of landmarks; instead, navigators can intermittently refer to landmarks when necessary (Etienne et al., 2004; Yoder et al., 2011).

Path integration, also referred to as dead reckoning, is a navigation process through which organisms utilize cues generated by self-motion to keep track of their moving direction and velocity. This enables them to constantly update their position and orientation in relation to some known reference point (e.g., the starting point, home) as they move through their environment (Etienne et al., 1996; Mittelstaedt & Mittelstaedt, 1982). The self-motion cues include proprioceptive cues, vestibular cues, motor efference copies, and optic flow (Collett & Collett, 2000; Etienne & Jeffery, 2004; Kearns et al., 2002; Loomis et al., 1999; Tcheang et al., 2011). Path integration is a prevalent navigation method among many species, including desert ants (Muller & Wehner, 1988; Wehner & Wehner, 1986), rodents (Etienne & Jeffery, 2004), crabs

(Layne et al., 2003), fish (Hughes & Blight, 1999), honeybees (Dyer et al., 1993), geese (Saint Paul, 1982), gerbils (Mittelstaedt & Glasauer, 1991), and humans.

Path integration operates as a continuous process, where navigators perceive and estimate their moving distance and orientation (akin to specific vectors) from one moment to the next. Due to potential estimation noise in each vector, path integration is prone to accumulating errors from the summation of these vectors. As a result, path integration performs reasonably well in smaller-scale navigation, the cumulative uncertainty and errors can become substantial significantly over greater distances and durations of travel (Harootonian et al., 2020; Souman et al., 2009). In contrast, piloting operates intermittently and is unaffected by cumulative errors along the navigation path, as it relies on the stored long-term memory of environmental cues (Cheng & Spetch, 1998; Etienne et al., 2004).

Path integration and landmark-based navigation rely on distinct sensory inputs (self-motion cues vs. landmarks) and can operate independently. Humans and certain non-human species can exclusively employ either of these processes for navigation (Collett et al., 1999; Hermer & Spelke, 1994). For instance, blindfolded participants, (i.e., devoid of visual landmarks), can accurately turn to face the initial origin after physically walking a two-leg path with a turn between legs (Klatzky et al., 1998). Additionally, mice can learn to navigate to specific locations solely using visual landmark cues presented within a virtual environment displayed on a single computer monitor, without any physical movement (i.e., with the absence of self-motion cues) (Youngstrom & Strowbridge, 2012).

Human navigation in everyday life commonly incorporates a variety of accessible cues and is the outcome of the interaction between the processes of path integration and piloting. Even a simple activity like walking to a class in a distant building on campus may encompass

perceiving environmental objects and landmarks along the route, as well as sensing bodily motion during movement. Existing literature implies that the interaction between path integration and piloting is neither fixed nor enduring; rather, it is dynamic, adaptable, and guided by specific goals (Chen et al., 2017; Etienne et al., 1990; Zhao & Warren, 2015b). The interaction between path integration and piloting can be broadly categorized into two formats: cue combination and cue competition. In cue combination, individuals integrate spatial estimates based on self-motion cues and landmarks to generate an averaged estimation (Nardini et al., 2008; Zhao & Warren, 2015b). In contrast, in cue competition, individuals exclusively rely on the estimates of one cue while disregarding the other.

Regarding when the path integration and piloting systems interact, recent research (Mou & Zhang, 2014; Zhang et al., 2020; Zhang & Mou; 2017) has attempted to address it during human homing behaviors. Returning to the origin of a path, known as homing, is a fundamental navigation behavior (Loomis et al., 1993). Zhang et al. (2020) proposed the self-localization hypothesis, which speculates that navigators combine the self-motion and landmark cues in localizing themselves (e.g., estimating their heading) prior to determining the home location. Participants in their study learned the locations of five objects (one at the home location) before walking an outbound path starting from the origin (home). They were asked to replace these objects to the remembered locations when participants reached the end of the outbound path under four cue conditions: path-integration only (by removing the landmarks), landmark only (by rotating participants in place to disrupt their self-motion sense), both consistent cues and conflicting cues (by rotating the landmarks around participants covertly). The results of Zhang et al. (2020) showed that in homing behaviours the combination of path integration and piloting

occurs in determining navigators' self-localization (e.g., estimating their heading), instead of determining the home location.

1.2 Contributions of visual landmarks in orientation

Orientation in navigation generally refers to knowledge about one's direction or heading with respect to the external world and being oriented within an environment is essential for effective navigation. When lost in an unfamiliar place (e.g., in a theme park or a shopping center), knowing one's orientation can help determine the appropriate direction to head to find a way out. Also, a sense of direction during navigation is essential for establishing an understanding of the spatial relationships between different locations in space and improving the stability of internal representations of object location (Wang & Spelke, 2000).

1.2.1 Dominance of visual landmarks over self-motion cues in orientation

In humans, the utilization of visual landmarks seems to be predominant for orientation when they are accessible and perceived as stable (Foo et al., 2005; Mou & Zhang, 2014; Warren et al., 2001; Yoder et al., 2011). Mou and Zhang (2014) showed the dominance of landmarks over self-motion cues in determining navigators' headings. In their study, participants learned object arrays at the path origin, with distal landmarks indicating directions. They walked an outbound path with the absence of distal landmarks after learning. They replaced objects to the remembered locations after navigation with the reappearance of the distal landmarks being rotated covertly. The results showed that participants' heading estimates followed the rotated distal landmarks whereas participants' position estimates followed the self-motion cues, suggesting that the rotated distal landmarks overrode the self-motion cues to dominate participants' heading estimates. Piloting reset the heading representations produced by path integration might be attributed to the fact that path integration is prone to accumulating errors

during continuous locomotion. In contrast, piloting is not subject to accumulated errors during continuous locomotion and can be considered a method to intermittently correct the accumulated errors in path integration (Etienne et al., 2004; Foo et al., 2005; Kelly et al., 2008; Zhang & Mou, 2019).

The dominance of visual landmarks over self-motion cues in orientation was supported by neuroscience studies (Goodridge & Taube, 1995; Taube & Burton, 1995; Zugaro et al., 2000). Specifically, head direction cells displayed more consistent firing patterns in response to landmarks when directional information from self-motion cues conflicted with the directional information derived from environmental landmarks.

1.2.2 Distal and proximal visual landmarks in orientation

Landmarks are often considered to fall into two broad categories based on their proximity to the destination: close or proximal landmarks, and distant or distal landmarks (O'Keefe & Nadel, 1978). In general, distal landmarks are the cues located beyond the immediate surroundings of humans and animals. They can be observed from various angles and distances, often attached on or outside the behavioral enclosure, and cannot be directly contacted (Chan et al., 2012; Cressant et al., 1997; O'Keefe & Speakman, 1987; Parron et al., 2004). Distal landmarks are too distant to pinpoint a specific position in space (Jacobs & Schenk, 2003; Knierim & Hamilton, 2011). In contrast, proximal landmarks are objects that are located within immediate surroundings. They are visible only from a limited area and specific directions, usually part of the apparatus itself, and can be directly approached during exploration (Chan et al., 2012; Parron et al., 2004). Proximal landmarks allow precise encoding of a location in space (Cheng & Spetch 1998; Wilson & Alexander, 2008). During a picnic in the park, for example, a

water tower and a church in the distance can serve as distal landmarks and a specific gazebo and trees near the picnic area can function as proximal landmarks.

Although both distant and proximal landmarks are commonly used to support navigation behaviors, previous research has emphasized the predominant role of distal landmarks in providing orientational information, while proximal landmarks primarily offer locational information during navigation (Buckley et al., 2015; Bullens et al., 2010; Doeller & Burgess, 2008; Jacobs & Schenk, 2003; see Knierim & Hamilton, 2011, for a review).

These conclusions are primarily derived from neuroscientific evidence obtained through animal studies. In scenarios where familiar distal and proximal landmarks were subjected to opposing rotations, indicating conflicting orientations (i.e., double-rotation method), it was observed that distal cues exerted greater control than proximal cues over the preferred firing directions of the head direction cells and the firing fields of place cells (Knierim, 2002; Shapiro et al., 1997; Tanila et al., 1997; Yoganarasimha et al., 2006). Furthermore, other research demonstrates that the rotation of a set of objects situated near the periphery of the behavioral arena correspondingly resulted in the rotation of place fields (Cressant et al., 1999; Muller & Kubie, 1987); in contrast, the rotation of the same objects, when located near the center of the arena, failed to exert such a control (Cressant et al., 1997). Although distal cues are demonstrated to be the primary source of orientation information in animal studies, there has been research indicating the opposite (Brown & Skaggs, 2002; Renaudineau et al., 2007), implying that the privileged status of distal cues over proximal ones in determining orientation may not be absolute but rather flexible and contingent on other factors.

The rationale behind this proposition is rooted in the idea that distal landmarks offer a relatively consistent and precise reference for orientation as individuals navigate within a local

environment. By contrast, proximal landmarks tend to provide less precise orientational information during individuals' navigation because they are more subject to self-induced motion parallax (Benhamou & Poucet, 1998; Hebb, 1949; Nadel & Hupbach, 2006; O'Keefe & Nadel, 1978). For example, when people move around their picnic area, their locomotion only leads to minor directional changes with respect to a distal tower but more significant directional changes in relation to the nearby tree.

1.2.3 The purposes of Study 1

In the realm of human navigation, however, to our knowledge, there is a lack of direct empirical studies focused on examining the roles of distal and proximal landmarks in determining human orientations and the underlying mechanisms. Study 1 in Chapter 2 aims to close this gap. Experiment 1 of Study 1 was designed to investigate whether distal landmarks take precedence over proximal ones as orientation cues for humans and the crucial factors that influence the role of distal and proximal landmarks in providing spatial orientation. Experiments 2 and 3 of Study 1 were designed to identify the circumstances in which proximal landmarks can prevail over distal ones for orientations.

1.3 Systematic errors in human path integration

Certain animals, like desert ants and nocturnal hamsters, may have developed remarkable path integration abilities, allowing them to navigate back to their nest or home location with impressive accuracy (Müller & Wehner, 1988; Séguinot et al., 1993; Wehner & Wehner, 1986; Wittlinger et al., 2006), humans may possess coarse path integration abilities (Foo et al., 2005; Zhao & Warren, 2015a). Humans often exhibit systematic distortions in homing performance when relying on path integration, especially as the complexity of the path increases (Kearns et al., 2002; Kelly et al., 2008; Klatzky et al., 1999; Loomis et al., 1993).

The widely used task for investigating human path integration is known as the triangle-completion task. In this task, participants walk along an outbound path composed of two linear segments with a turn angle between them. Subsequently, they return to or point toward the starting point of the outbound path (Klatzky et al., 1998; Loomis et al., 1993). Participants' responses of the inbound path (i.e., homing vector) include the turn angle and leg length (see Figure 1.1). Participants usually overshot small values (illustrated in Figure 1.1A), and conversely, undershot large values (illustrated in Figure 1.1B), showing a compression pattern relative to the correct values of both turn angle (β) and path length (PO). This systematic distortion was distinguished from random errors (Chrastil & Warren, 2017; Harootonian et al., 2020).

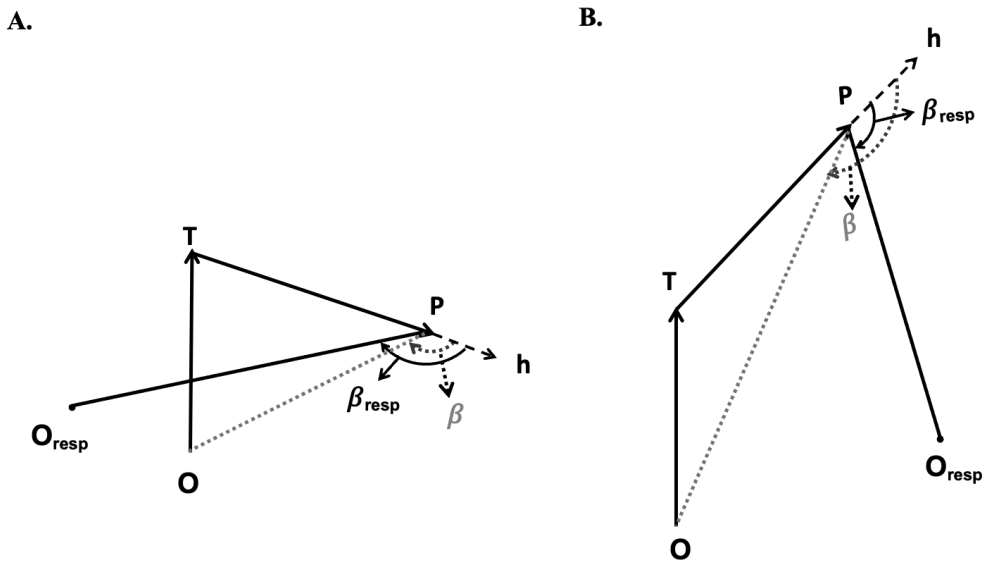

Figure 1.1. Illustration of the systematic distortion in performing triangle completion. A hypothetical participant walks a path starting at home location O, turns at T, stops at P, with the heading of h, and then pinpoints the home location at Oresp. β and PO denote the correct values of the inbound turn angle and path length to complete the triangle. βresp and POresp denote the participant's actual response of inbound turn angle and path length. (A) An illustration of

participants overshooting the relatively small inbound angle and length that they were supposed to produce. (B) An illustration of participants undershooting the relatively large inbound angle and length that they were supposed to produce.

The triangle-completion task has been deconstructed into three primary cognitive stages to help identify the source of the systematic errors (Fujita et al., 1993; Loomis et al., 1993). These stages involve: 1) Encoding the length and angles along the outbound path, requiring sensing the traversed path and forming the internal representations of the outbound path; 2) Integrating these internal representations to calculate desired inbound responses; and 3) Executing the desired inbound response. It is possible for systematic errors to accumulate during any of these processes.

1.3.1 Models of path integration

Previous work has proposed different models to account for the nature of the systematic bias observed in human path integration, and the evidence appears inconclusive (Chrastil & Warren, 2021; Fujita et al. 1993; Harootonian et al., 2020). The encoding-error model, a well-known model of path integration proposed by Fujita et al. (1993), suggests that systematic errors in the inbound response are due to errors in encoding of the outbound paths and there is no systematic error in either the integration of path segments via cognitive trigonometry or execution of the desired inbound responses. Moreover, the encoding-error model assumes that leg lengths are encoded by a constant linear encoding function and turn angles are encoded by another constant linear encoding function, both of which determine the corresponding encoded values based on the actual values of the outbound path. On one hand, several studies have fit their empirical data to the encoding-error model and found that the model accounts for a large

portion of the variance (Klatzky et al., 1999; May & Klatzky, 2000; Péruch et al., 1997; Wartenberg et al., 1998). On the other hand, there is evidence suggesting that several of its foundational assumptions do not hold up to scrutiny. Both the assumption of no execution error and the assumption of a constant encoding function have been subjected to questioning (Bakker et al., 1999, 2001; Chrastil & Warren, 2017; Harootonian et al., 2020; Klatzky et al., 1990, 1999).

Recent work, however, suggests that executing the inbound responses makes the largest contribution to systematic errors in path integration (Chrastil & Warren, 2021). Chrastil and Warren (2021) tested models of encoding errors solely (i.e., encoding-error model), execution errors solely (i.e., execution-error model), and both types of errors. They used distance and angle reproduction tasks to estimate participants' encoding functions and execution functions for triangle-completion tasks. Then the three models, using the corresponding functions (e.g., an encoding-error model used the encoding functions), generated the predictions for the inbound response errors in the triangle-completion task. The results showed that the execution-error model outperformed the encoding-error model in predicting path integration errors. Furthermore, the model incorporating both types of errors did not outperform the execution-error model. These results suggest that the observed systematic errors in inbound responses were sufficiently explained by the systematic errors in executing the inbound path, challenging the long-standing assumption that errors reflect encoding alone.

1.3.2 The purposes of Study 2

The purpose of Study 2 is to identify the potential sources of the systematic biases in human path integration using computational modeling. Study 2 compared three plausible theoretical models that assume that systematic errors in human path integration occur in the

encoding outbound path solely (encoding-error model), executing the inbound responses solely (execution-error model), and both (bi-component model), respectively. Different from the typical triangle-completion task with only one inbound response (i.e., the homing vector) for each outbound path, the triangle-completion task used in this study required participants to indicate three learned locations (including the home location) during the response phase. Previous studies (Mou & Zhang, 2014; Zhang et al., 2020) have indicated that multiple inbound responses enable to recover participants' encoded positions and headings at the endpoint of the outbound path. I conjectured that the contribution of encoding and execution processes to the systematic errors in the human triangle-completion task can be separated by using multiple inbound responses for each outbound path.

1.4 References

Able, K. P. (1991). Common themes and variations in animal orientation systems. *American Zoologist, 31*(1), 157-167.

Bakker, N. H., Werkhoven, P. J., & Passenier, P. O. (1999). The effects of proprioceptive and visual feedback on geographical orientation in virtual environments. *Presence, 8*(1), 36–53.

Bakker, N. H., Werkhoven, P. J., & Passenier, P. O. (2001). Calibrating visual path integration in VEs. *Presence, 10*(2), 216–224.

Benhamou, S., & Poucet, B. (1998). Landmark use by navigating rats (Rattus norvegicus) contrasting geometric and featural information. *Journal of Comparative Psychology, 112*(3), 317-322.

Boles, L. C., & Lohmann, K. J. (2003). True navigation and magnetic maps in spiny lobsters. *Nature, 421*(6918), 60-63.

Brown, J. E., & Skaggs, W. E. (2002). Concordant and discordant coding of spatial location in populations of hippocampal CA1 pyramidal cells. *Journal of Neurophysiology, 88*(4), 1605-1613.

Buckley, M. G., Haselgrove, M., & Smith, A. D. (2015). The developmental trajectory of intramaze and extramaze landmark biases in spatial navigation: An unexpected journey. *Developmental Psychology, 51*(6), 771-791.

Bullens, J., Nardini, M., Doeller, C. F., Braddick, O., Postma, A., & Burgess, N. (2010). The role of landmarks and boundaries in the development of spatial memory. *Developmental Science, 13*(1), 170-180.

Chan, E., Baumann, O., Bellgrove, M. A., & Mattingley, J. B. (2012). From objects to landmarks: the function of visual location information in spatial navigation. *Frontiers in Psychology, 3*, 304.

Chen, X., McNamara, T. P., Kelly, J. W., & Wolbers, T. (2017). Cue combination in human spatial navigation. *Cognitive Psychology, 95*, 105-144.

Cheng, K., & Spetch, M. L. (1998). Mechanisms of landmark use in mammals and birds. In S. Healy (Ed.), *Spatial representation in animals* (pp. 1–17). New York, NY: Oxford University Press.

Chrastil, E. R., & Warren, W. H. (2017). Rotational error in path integration: Encoding and execution errors in angle reproduction. *Experimental Brain Research, 235*(6), 1885-1897.

Chrastil, E. R., & Warren, W. H. (2021). Executing the homebound path is a major source of error in homing by path integration. *Journal of Experimental Psychology: Human Perception and Performance, 47*(1), 13-35.

Collett, M., & Collett, T. S. (2000). How do insects use path integration for their navigation?. *Biological Cybernetics, 83*(3), 245-259.

Collett, M., Collett, T. S., & Wehner, R. (1999). Calibration of vector navigation in desert ants. *Current Biology, 9*(18), 1031-1034.

Cressant, A., Muller, R. U., & Poucet, B. (1997). Failure of centrally placed objects to control the firing fields of hippocampal place cells. *Journal of Neuroscience, 17*(7), 2531-2542.

Cressant, A., Muller, R. U., & Poucet, B. (1999). Further study of the control of place cell firing by intra-apparatus objects. *Hippocampus, 9*(4), 423-431.

Doeller, C. F., & Burgess, N. (2008). Distinct error-correcting and incidental learning of location relative to landmarks and boundaries. *Proceedings of the National Academy of Sciences, 105*(15), 5909-5914.

Dyer, F. C., Berry, N. A., & Richard, A. S. (1993). Honey bee spatial memory: Use of route-based memories after displacement. *Animal Behaviour, 45*(5),1028-1030.

Etienne, A. S., & Jeffery, K. J. (2004). *Path integration in mammals*. Hippocampus, 14(2), 180-192.

Etienne, A. S., Maurer, R., Boulens, V., Levy, A., & Rowe, T. (2004). Resetting the path integrator: A basic condition for route-based navigation. *Journal of Experimental Biology, 207*(9), 1491-1508.

Etienne, A. S., Maurer, R., & Séguinot, V. (1996). Path integration in mammals and its interaction with visual landmarks. *Journal of Experimental Biology, 199*(1), 201-209.

Etienne, A. S., Teroni, E., Hurni, C., & Portenier, V. (1990). The effect of a single light cue on homing behaviour of the golden hamster. *Animal Behaviour, 39*(1), 17-41.

Fujita, N., Klatzky, R. L., Loomis, J. M., & Golledge, R. G. (1993). The encoding-error model of pathway completion without vision. *Geographical Analysis, 25*(4), 295-314.

Foo, P., Warren, W. H., Duchon, A., & Tarr, M. J. (2005). Do humans integrate routes into a cognitive map? Map-versus landmark-based navigation of novel shortcuts. *Journal of Experimental Psychology: Learning, Memory, and Cognition, 31(2)*, 195-215.

Gallistel, C. R. (1990). *The organization of learning.* The MIT Press.

Gladwin, T. (1970) *East is a big bird*. Cambridge, MA., Harvard University Press.

Goodridge, J. P., & Taube, J. S. (1995). Preferential use of the landmark navigational system by head direction cells in rats. *Behavioral Neuroscience, 109*(1), 49-61.

Harootonian, S. K., Wilson, R. C., Hejtmánek, L., Ziskin, E. M., & Ekstrom, A. D. (2020). Path integration in large-scale space and with novel geometries: Comparing vector addition and encoding-error models. *PLoS Computational Biology, 16*(5), e1007489.

Hebb, D. O. (1949). *The organization of behaviour*. Wiley-Interscience, New York.

Hermer, L., & Spelke, E. S. (1994). A geometric process for spatial reorientation in young children. *Nature, 370*(6484), 57–59.

Hughes, R. N., & Blight, C. M. (1999). Algorithmic behaviour and spatial memory are used by two intertidal fish species to solve the radial maze. *Animal Behaviour, 58*(3), 601-613.

Jacobs, L. F., & Schenk, F. (2003). Unpacking the cognitive map: the parallel map theory of hippocampal function. *Psychological Review, 110*(2), 285-315.

Kearns, M. J., Warren, W. H., Duchon, A. P., & Tarr, M. J. (2002). Path integration from optic flow and body senses in a homing task. *Perception, 31*(3), 349-374.

Kelly, J. W., McNamara, T. P., Bodenheimer, B., Carr, T. H., & Rieser, J. J. (2008). The shape of human navigation: How environmental geometry is used in maintenance of spatial orientation. *Cognition, 109*(2), 281-286.

Klatzky, R. L., Beall, A. C., Loomis, J. M., Golledge, R. G., & Philbeck, J. W. (1999). Human navigation ability: Tests of the encoding-error model of path integration. *Spatial Cognition and Computation, 1*(1), 31-65.

Klatzky, R. L., Loomis, J. M., Beall, A. C., Chance, S. S., & Golledge, R. G. (1998). Spatial updating of self-position and orientation during real, imagined, and virtual locomotion. *Psychological Science, 9*(4), 293-298.

Klatzky, R. L., Loomis, J. M., Golledge, R. G., Cicinelli, J. G., Doherty, S., & Pellegrino, J. W. (1990). Acquisition of route and survey knowledge in the absence of vision. *Journal of Motor Behavior, 22*(1), 19-43.

Knierim, J. J. (2002). Dynamic interactions between local surface cues, distal landmarks, and intrinsic circuitry in hippocampal place cells. *Journal of Neuroscience, 22*(14), 6254-6264.

Knierim, J. J., & Hamilton, D. A. (2011). Framing spatial cognition: Neural representations of proximal and distal frames of reference and their roles in navigation. *Physiological Reviews, 91*(4), 1245-1279.

Layne, J. E., Barnes, W. J. P., & Duncan, L. M. (2003). Mechanisms of homing in the fiddler crab Uca rapax 2. Information sources and frame of reference for a path integration system. *Journal of Experimental Biology, 206*(24), 4425-4442.

Lew, A. R. (2011). Looking beyond the boundaries: Time to put landmarks back on the cognitive map?. *Psychological Bulletin, 137*(3), 484-507.

Loomis, J. M., Klatzky, R. L., Golledge, R. G., Cicinelli, J. G., Pellegrino, J. W., & Fry, P. A. (1993). Nonvisual navigation by blind and sighted: Assessment of path integration ability. *Journal of Experimental Psychology: General*, 122(1), 73-91.

Loomis, J. M., Klatzky, R. L., Golledge, R. G., & Philbeck, J. W. (1999). Human navigation by path integration. In R. G. Golledge (Ed.), *Wayfinding: Cognitive mapping and other spatial processes* (pp. 125–151). Baltimore, MD: Johns Hopkins University Press.

May, M., & Klatzky, R. L. (2000). Path integration while ignoring irrelevant movement. *Journal of Experimental Psychology: Learning, Memory, and Cognition, 26*(1), 169–186.

Mittelstaedt, H., & Mittelstaedt, M. L. (1982). Homing by path integration. In F. Papi & H. G. Wallraff (Eds.), *Avian navigation* (pp. 290–297). Springer-Verlag.

Mittelstaedt, M. L., & Glasauer, S. T. E. F. A. N. (1991). Idiothetic navigation in gerbils and humans. *Zool. Jb. Physiol*, *95*, 427-435.

Mou, W., & Zhang, L. (2014). Dissociating position and heading estimations: Rotated visual orientation cues perceived after walking reset headings but not positions. *Cognition, 133*(3), 553-571.

Muller, R. U., & Kubie, J. L. (1987). The effects of changes in the environment on the spatial firing of hippocampal complex-spike cells. *Journal of Neuroscience, 7*(7), 1951-1968.

Müller, M., & Wehner, R. (1988). Path integration in desert ants, Cataglyphis fortis. *Proceedings of the National Academy of Sciences, 85*(14), 5287-5290.

Nadel, L., & Haupbach, A. (2006). Species comparisons in development: The case of the geometric 'module'. *Processes of Change in Brain and Cognitive Development: Attention and Performance XXI*, 499-511.

Nardini, M., Jones, P., Bedford, R., & Braddick, O. (2008). Development of cue integration in human navigation. *Current Biology, 18*, 689–693.

O'Keefe, J., & Nadel, L. (1978). *The hippocampus as a cognitive map* (Vol. 3, pp. 483-484). Oxford: Clarendon Press.

O'Keefe, J., & Speakman, A. 1. (1987). Single unit activity in the rat hippocampus during a spatial memory task. *Experimental Brain Research, 68*, 1-27.

Parron, C., Poucet, B., & Save, E. (2004). Entorhinal cortex lesions impair the use of distal but not proximal landmarks during place navigation in the rat. *Behavioural Brain Research, 154*(2), 345-352.

Péruch, P., May, M., & Wartenberg, F. (1997). Homing in virtual environments: Effects of field of view and path layout. *Perception, 26*(3), 301–311.

Renaudineau, S., Poucet, B., & Save, E. (2007). Flexible use of proximal objects and distal cues by hippocampal place cells. *Hippocampus, 17*(5), 381-395.

Saint Paul, U. V. (1982). Do geese use path integration for walking home? In F. Papi & H. G. Wallraff (Eds.), *Avian navigation* (pp. 298–307). Springer.

Séguinot, V., Maurer, R., & Etienne, A. S. (1993). Dead reckoning in a small mammal: the evaluation of distance. *Journal of Comparative Physiology A, 173*, 103-113.

Shapiro, M. L., Tanila, H., & Eichenbaum, H. (1997). Cues that hippocampal place cells encode: Dynamic and hierarchical representation of local and distal stimuli. *Hippocampus, 7*(6), 624-642.

Souman, J. L., Frissen, I., Sreenivasa, M. N., & Ernst, M. O. (2009). Walking straight into circles. *Current Biology, 19*(18), 1538-1542.

Tanila, H., Shapiro, M. L., & Eichenbaum, H. (1997). Discordance of spatial representation in ensembles of hippocampal place cells. *Hippocampus, 7*(6), 613-623.

Taube, J. S. (2007). The head direction signal: origins and sensory-motor integration. *Annual Review of Neuroscience, 30*, 181-207.

Taube, J. S., & Burton, H. L. (1995). Head direction cell activity monitored in a novel environment and during a cue conflict situation. *Journal of Neurophysiology, 74*(5), 1953-1971.

Tcheang, L., Bülthoff, H. H., & Burgess, N. (2011). Visual influence on path integration in darkness indicates a multimodal representation of large-scale space. *Proceedings of the National Academy of Sciences, 108*(3), 1152-1157.

Valerio, S., & Taube, J. S. (2012). Path integration: how the head direction signal maintains and corrects spatial orientation. *Nature Neuroscience, 15*(10), 1445-1453.

Wang, R. F., & Spelke, E. S. (2000). Updating egocentric representations in human navigation. *Cognition, 77*(3), 215-250.

Warren, W. H., Kay, B. A., Zosh, W. D., Duchon, A. P., & Sahuc, S. (2001). Optic flow is used to control human walking. *Nature Neuroscience, 4*(2), 213-216.

Wartenberg, F., May, M., & Péruch, P. (1998). Spatial orientation in virtual environments: Background considerations and experiments. In C. Freska, C. Habel, & K. F. Wender (Eds.), *Spatial Cognition* (pp. 469–489). Springer.

Wehner, R., Michel, B., & Antonsen, P. (1996). Visual navigation in insects: Coupling of egocentric and geocentric information. *Journal of Experimental Biology, 199*(1), 129-140.

Wehner, R., & Srinivasan, M. V. (1981). Searching behaviour of desert ants, genus Cataglyphis (Formicidae, Hymenoptera). *Journal of Comparative Physiology, 142*, 315-338.

Wehner, R., & Wehner, S. (1986). Path integration in desert ants. Approaching a long-standing puzzle in insect navigation. *Monitore Zoologico Italiano-Italian Journal of Zoology, 20*(3), 309-331.

Wilson, P. N., & Alexander, T. (2008). Blocking of spatial learning between enclosure geometry and a local landmark. *Journal of Experimental Psychology: Learning, Memory, and Cognition, 34*(6), 1369-1376.

Wittlinger, M., Wehner, R., & Wolf, H. (2006). The ant odometer: Stepping on stilts and stumps. *Science, 312*(5782), 1965-1967.

Yoder, R. M., Clark, B. J., & Taube, J. S. (2011). Origins of landmark encoding in the brain. *Trends in Neurosciences, 34*(11), 561-571.

Yoganarasimha, D., Yu, X., & Knierim, J. J. (2006). Head direction cell representations maintain internal coherence during conflicting proximal and distal cue rotations: Comparison with hippocampal place cells. *Journal of Neuroscience, 26*(2), 622-631.

Youngstrom, I. A., & Strowbridge, B. W. (2012). Visual landmarks facilitate rodent spatial navigation in virtual reality environments. *Learning & Memory, 19*(3), 84-90.

Zhang, L., & Mou, W. (2017). Piloting systems reset path integration systems during position estimation. *Journal of Experimental Psychology: Learning, Memory, and Cognition, 43*(3), 472-491.

Zhang, L., & Mou, W. (2019). Selective resetting position and heading estimations while driving in a large-scale immersive virtual environment. *Experimental Brain Research, 237*(2), 335-350.

Zhang, L., Mou, W., Lei, X., & Du, Y. (2020). Cue combination used to update the navigator's self-localization, not the home location. *Journal of Experimental Psychology: Learning, Memory, and Cognition. 46*(12), 2314-2339.

Zhao, M., & Warren, W. H. (2015a). Environmental stability modulates the role of path integration in human navigation. *Cognition, 142*, 96-109.

Zhao, M., & Warren, W. H. (2015b). How you get there from here: Interaction of visual landmarks and path integration in human navigation. *Psychological Science, 26*(6), 915-924.

Zhou, R., & Mou, W. (2016). Superior cognitive mapping through single landmark-related learning than through boundary related learning. *Journal of Experimental Psychology: Learning, Memory, and Cognition, 42*(8), 1316.

Zugaro, M. B., Tabuchi, E., & Wiener, S. I. (2000). Influence of conflicting visual, inertial and substratal cues on head direction cell activity. *Experimental Brain Research, 133*, 198-208.

Chapter 2 Relative cue precision and prior knowledge contribute to the preference of proximal and distal landmarks in human orientation

2.1 Abstract

A prevailing argument posits that distal landmarks dominate over proximal landmarks as orientation cues. However, no studies have tested this argument or examined the underlying mechanisms. This project aimed to close this gap by examining the roles of relative cue precision and prior knowledge in cue preference. Participants learned object locations with proximal and distal landmarks in an immersive virtual environment. After walking a path without seeing objects or landmarks, participants disoriented themselves by spinning in place and pointed to the objects with the presence of a proximal landmark being rotated -50°, a distal landmark being rotated 50°, or both (Conflict). Heading errors were examined. Experiment 1 manipulated the relative cue precision. Results showed that in Conflict condition, the observed weight on the distal cue (exceeding 0.5) changed with but remained higher than the weight predicted by the relative cue precision. This indicates that besides the relative cue precision, prior knowledge of distal cue dominance also influences orientation cue usage. In Experiments 2 and 3, participants walked a path stopping at one object location. Participants were informed of it explicitly in Experiment 2 but not in Experiment 3. Results showed that distal cue dominance still occurred in Experiment 3. However, in Experiment 2, proximal cue dominance appeared, and it was not predicted by the relative cue precision. These results suggest that prior knowledge of proximal cue dominance might have been invoked by the instruction of locations. Consistent with the Bayesian inference model, human cue usage in orientation is determined by relative cue precision and prior knowledge. The choice of prior knowledge can be influenced by instructions.

Keywords: Spatial orientation, distal landmark, proximal landmark, path integration, navigation

2.2 Introduction

To navigate successfully through an environment, people need to know their position (where they are located) and heading (which direction they are facing). To achieve these goals, people may utilize various spatial cues. On one hand, navigators can utilize cues derived from self-motion to track their travel direction and speed, allowing them to update their position and heading relative to a specific point within the environment. This process is referred to as path integration (Etienne & Jeffery, 2004; Mittelstaedt & Mittelstaedt, 1982). On the other hand, humans, being highly visual beings, have the remarkable ability to rely on previously encoded visual landmarks in the environment to determine their position and heading. This process is known as landmark-based navigation (Foo et al., 2005; Wehner et al., 1996) or piloting (Gallistel, 1990).

Visual landmarks have been classified into two main categories based on their proximity to the navigator: proximal landmarks and distal landmarks (O'Keefe & Nadel, 1978). Distal landmarks, generally located beyond the immediate "working space" of navigators, are cues that typically lie outside the enclosure and cannot be directly contacted with (Cressant et al., 1997; O'Keefe & Speakman, 1987; Parron et al., 2004). Distal landmarks are too far away to pinpoint a specific position in space (Jacobs & Schenk, 2003). In contrast, proximal landmarks refer to cues that can be directly approached during exploration within the immediate space of navigators (Parron et al., 2004), enabling precise encoding of spatial locations in space (Cheng & Spetch, 1998; Wilson & Alexander, 2008). During camping, for instance, while a mountain in the distance can be regarded as a distal landmark, a camping tent at the campsite can function as a proximal landmark.

While distal and proximal landmarks are commonly employed to facilitate navigational behavior, previous research has highlighted the different roles of these landmarks. In particular, distal landmarks primarily offer orientation information, whereas proximal landmarks primarily offer positional information during navigation (Buckley et al., 2015; Bullens et al., 2010; Doeller & Burgess, 2008; Jacobs & Schenk, 2003; see Knierim & Hamilton, 2011, for a review).

These conclusions are primarily based on neuroscientific evidence from animal studies, involving neurons that fire at precise spatial locations as an animal navigates (termed place cells) and neurons that fire when the animal's head points in a certain direction (termed head-direction cells). Some studies used a double-rotation method, where proximal and distal cues were rotated in opposite directions and showed that the distal cues exert greater control than proximal cues over the preferred firing directions of head direction cells and the firing fields of place cells (Knierim, 2002; Shapiro et al., 1997; Tanila et al., 1997; Yoganarasimha et al., 2006). Other studies only rotated three objects within a high-walled circular platform. They showed that the rotation of the objects controlled the head direction cell of rodents only when the objects were placed at the periphery of the platform but not when they were placed at the center of the platform (Cressant et al., 1997). Furthermore, Zugaro et al. (2001) also showed that the control of the rotating objects placed at the periphery of the platform disappeared when the walls were removed, allowing the rat to see the curtains in the surrounding square room. The preferred directions of the head direction cells did not align with the objects but instead remained fixed relative to the room. These findings suggest that the head-direction system may automatically utilize the most distal cues to establish orientations.

Can we generalize this conclusion that distal landmarks control orientations to human navigation? Unfortunately, there is no direct empirical evidence available to address this

question, to the best of our knowledge. The differences between rodent and human visual systems may impact how each navigates using visual landmarks (Ekstrom, 2015). Rodents possess a broader field of view but lower visual acuity than many other mammals (Douglas et al., 2005; Wallace et al., 2013), and they likely lack a specialized brain system for object processing akin to the high-resolution ventral stream in humans, which processes detailed object information through multiple stages (Kravitz et al., 2013). However, some researchers have put forward a theoretical argument suggesting that distal landmarks may still play a more significant role than proximal landmarks in determining human orientations (Nadel & Hupbach, 2006). The reasoning behind this theory is that distal landmarks, being situated farther away, provide a relatively constant orientation reference as individuals navigate within a local environment. For example, when people move around within their campsite, their locomotion only results in minor directional changes relative to a distant mountain. On the other hand, proximal landmarks offer less precise directional information due to the potential effects of self-induced motion parallax. When people move within their campsite, their locomotion can cause significant directional changes in relation to the camping tent, including the opposite directions before and after moving, leading to varying orientation estimates (Benhamou & Poucet, 1998; Hebb, 1949; Nadel & Hupbach, 2006; O'Keefe & Nadel, 1978). Thus, the greater precision of distal cues used for orientation leads to the dominance of distal cues in determining orientation.

This theoretical argument has been widely utilized in the field of human spatial cognition. It has been employed post-hoc to explain the notable finding that human toddlers relied on color walls in a large rectangular room but not in a small room to distinguish between two diagonal corners that are identical based on the room geometry (e.g., Cheng & Newcombe, 2005; Learmonth et al., 2002). Moreover, it has served as a foundational assumption in designing

paradigms to study human spatial behaviors (e.g., Doeller & Burgess, 2008; Padilla et al., 2017; Zhang & Mou, 2017). For instance, Doeller and Burgess (2008) employed distal mountains as orientation cues while examining how a boundary (a circular wall) and a within-boundary landmark (a traffic cone) competed with each other in encoding the locations of objects within the boundary.

Given the importance of this theoretical argument, it is surprising that there is no human study that systematically and directly investigates the extent to which distal landmarks dominate over proximal landmarks in determining orientations during human navigation. The current study was conducted to close this gap.

2.2.1 Explaining distal cue dominance by three hypotheses

We began by investigating whether the cue precision, which determines the dominance of distal landmarks, is dependent on or independent of a specific navigation environment. We proposed three hypotheses to guide this investigation. The first hypothesis, referred to as the *relative-precision hypothesis,* stipulates: the usage of distal and proximal cues for orientation is based on the relative precision of specific cues in a specific environment. The precision of a cue can be assessed by its inverse relationship with the variability observed when people estimate orientation using that cue alone (Chen et al., 2017; Cheng et al., 2007; Nardini et al., 2008). The usage of distal and proximal cues for orientation can be measured by relative distances between the observed heading estimates and the headings indicated by two conflicting cues. According to this hypothesis, when two cues are available to the navigator, they sense and evaluate the precision associated with each orientation cue and compare them to obtain their respective relative precision. The navigators' reliance on each cue in determining orientations is directly determined by its relative cue precision. Specifically, if we manipulate the relative precision of

two orientation cues through experimental settings, this hypothesis predicts that the observed reliance on these cues will also change accordingly.

In our everyday navigation scenarios, we may have engaged in the process of evaluating and comparing the relative precision of specific orientation cues, described in the first hypothesis, across numerous occasions. Consequently, we might have developed or acquired a predisposition (prior belief) to favor distal landmarks when estimating orientation. Building on this idea, we propose the second hypothesis, referred to as the *prior-beliefs hypothesis*. According to this hypothesis, the reliance on distal cues in determining orientations can be attributed to the prior beliefs held by navigators, which prioritize distal landmarks over proximal landmarks because distal landmarks are generally more precise in specifying directions. These prior beliefs are top-down in nature and exist prior to the availability of any specific landmark cues in a given navigation scenario, likely to enhance efficiency and reduce computational costs (McNamara & Chen, 2022). Specifically, distal cues are always preferred, and the degree of cue preference is not sensitive to manipulation of the relative precision of two orientation cues through experimental settings. Therefore, this hypothesis predicts that the observed reliance on these cues will remain fixed across different levels of relative cue precision. The influence of prior beliefs and knowledge has been the subject of investigation in human spatial memory for a long time (Huttenlocker et al., 1991; Sampaio et al., 2020) and has been extended to human navigation in recent years (Harootonian et al., 2020; Negen et al., 2020; Petzschner et al., 2012; Petzschner & Glasauer, 2011; Roy et. al, 2023; Wang et al., 2018; Wang & Mou, 2020; also see Newman et al., 2023 for a review).

The third hypothesis takes into account both relative precision and prior beliefs, and it is referred to as the *dual-factor hypothesis*. This hypothesis speculates that both the relative cue

precision and prior beliefs regarding the superiority of distal cues influence the usage of both distal and proximal landmarks for orientation. Before being presented with a specific navigational environment, navigators may hold beliefs, knowledge, and expectations about certain types of landmarks being more likely to be used for orientation compared to others. Subsequently, when navigators perform navigation tasks in a specific environment and need to determine orientation within it, they evaluate the precision of specific landmarks as orienting cues while also considering their preexisting prior beliefs. Navigators combine their prior knowledge with the information they sense from the navigation scenario to estimate orientations using these landmarks.

2.2.2 Explaining distal cue dominance under a Bayesian lens

According to the Bayesian inference (Wagenmakers, 2007),

$$\frac{\mathrm{P(Hd|E)}}{\mathrm{P(Hp|E)}} = \frac{\mathrm{P(E|Hd)}}{\mathrm{P(E|Hp)}} \times \frac{\mathrm{P(Hd)}}{\mathrm{P(Hp)}}. \qquad (1)$$

In general, Hd and Hp refer to two competing hypotheses[1]. E refers to evidence to compare hypotheses.

In the current context, Hd could be explained as "the hypothesis of using distal landmarks" and Hp could be explained as "the hypothesis of using proximal landmarks". E could be explained as evidence people perceive in the experimental environment to evaluate their hypotheses of using distant and proximal cues. As we only consider participants' using distal or proximal cues, $\mathrm{P(Hp|E)} = 1 - \mathrm{P(Hd|E)}, \mathrm{P(Hp)} = 1 - \mathrm{P(Hd)}$.

[1] The two competing hypotheses are two generic hypotheses in Bayesian inference, not related to the three hypotheses we proposed above.

The ratio $\frac{\mathrm{P(Hd|E)}}{\mathrm{P(Hp|E)}}$ is termed as the posterior odds. The ratio $\frac{\mathrm{P(Hd)}}{\mathrm{P(Hp)}}$ is termed as the prior odds. The ratio $\frac{\mathrm{P(E|Hd)}}{\mathrm{P(E|Hp)}}$ is termed as the likelihood ratio or the Bayes factor. Equation 1 can be rewritten as

$$\text{posterior odds} = \text{likelihood ratio} \times \text{prior odds} \qquad (2)$$

We assume that participants' cue usage in a given experiment reflects the posterior odds. As discussed earlier, participants' cue usage is measured by the weights assigned to each cue in the conflict condition (i.e., Wd and Wp, weights for distal cues and proximal cues respectively, $\mathrm{Wd} + \mathrm{Wp} = 1$). Thus, we get

$$\text{posterior odds} = \frac{\mathrm{Wd}}{\mathrm{Wp}}. \qquad (3)$$

Previous studies have indicated that when a flat prior is assumed (noted as prior=1), the weights assigned to each cue are determined by the relative cue precision and defined to be the reciprocal of the variances of each cue (Chen et al., 2017; Nardini et al., 2008). Thus, $\frac{\mathrm{Wd}}{\mathrm{Wp}}^{prior=1} = \frac{\sigma_p^2}{\sigma_d^2}$, here $\frac{\mathrm{Wd}}{\mathrm{Wp}}^{prior=1}$ refers to $\frac{\mathrm{Wd}}{\mathrm{Wp}}$ when a flat prior is assumed. According to Equation 3, the posterior odds should also be the reciprocal of the variances of each cue., i.e., $\text{posterior odds}^{\,prior=1} = \frac{\sigma_p^2}{\sigma_d^2}$. In addition, when a flat prior is assumed, the likelihood ratio is the same as the posterior odds, i.e., $\text{posterior odds}^{\,prior=1} = \text{likelihood ratio}^{prior=1}$. Therefore, when a flat prior is assumed, $\text{likelihood ratio}^{\,prior=1} = \frac{\sigma_p^2}{\sigma_d^2}$. Note that the likelihood ratio should be independent of the prior odds (i.e., $\text{likelihood ratio} = \text{likelihood ratio}^{\,prior=1}$), we get

$$\text{likelihood ratio} = \frac{\sigma_p^2}{\sigma_d^2} \qquad (4)$$

From Equations 2, 3, and 4, we get

$$\frac{\mathrm{Wd}}{\mathrm{Wp}} = \frac{\sigma_p^2}{\sigma_d^2} \times \text{prior odds} \quad (5)$$

Furthermore, we conceive of prior odds as the remembered prior knowledge of a collective of $\frac{\sigma_p^2}{\sigma_d^2}$. In particular, the prior knowledge can be specified as the geometric average of all $\frac{\sigma_p^2}{\sigma_d^2}$ that participants remember based on the experimental context.

$$\text{prior odds} = \left(\prod_{k=1}^{n} \left(\frac{\sigma_p^2}{\sigma_d^2}\right)_k\right)^{\frac{1}{n}} \quad (6)$$

Here, $\left(\frac{\sigma_p^2}{\sigma_d^2}\right)_k$ is a collective of cue variance ratios that people remembered, different from the $\frac{\sigma_p^2}{\sigma_d^2}$ that participants perceive in the current experiment.

In conclusion, Equation 5 presents a comprehensive Bayesian inference model that suggests cue preference is determined by both the relative cue precision and prior odds. If we assume $\frac{\mathrm{Wd}}{\mathrm{Wp}} = \frac{\sigma_p^2}{\sigma_d^2} \times \text{prior odds} > 1$, this model aligns with the two-factor hypothesis discussed earlier. Similarly, if we assume $\frac{\mathrm{Wd}}{\mathrm{Wp}} = \frac{\sigma_p^2}{\sigma_d^2} > 1$, it represents the relative-precision hypothesis. If we assume $\frac{\mathrm{Wd}}{\mathrm{Wp}} = \text{prior odds} > 1$, it characterizes the prior-knowledge hypothesis.

2.2.3 Is proximal dominance possible?

Although distal cues are demonstrated to be the primary source of orientation information in animal studies, there has been research indicating the opposite (Brown & Skaggs, 2002; Renaudineau et al., 2007). Renaudineau et al. (2007) conducted a study where they recorded the activity of place cells in rats while they engaged in a task of chasing food pellets on a circular platform containing three distinct proximal objects surrounded by a curtain with three distal visual patterns attached. The manipulation of both distal and proximal cue sets created a 180°

mismatch. Surprisingly, the results showed that although most place cells were not influenced significantly by either proximal or distal cues (i.e., remapping), the remaining cells were predominantly influenced by the proximal objects. This finding challenges the notion of distal cues' absolute dominance and suggests that other factors, such as the salience of landmarks, could modulate the effect. Renaudineau et al. (2007) used 3D objects as proximal cues on the platform, in contrast to other studies that utilized tactile surfaces as proximal cues (Knierim, 2002; Shapiro et al., 1997; Yoganarasimha et al., 2006). These 3D objects, acting as potential obstacles, might have hindered the rats' movement on the platform, thus carrying a higher level of salience. Consequently, the privileged status of distal cues over proximal ones in determining orientation may not be absolute but rather flexible and contingent on other factors.

Drawing inspiration from these intriguing findings, the second purpose of the current study is to investigate the specific circumstances under which proximal landmarks could prevail over distal ones in indicating orientations during human navigation.

The current study specifically focused on utilizing one single rotational symmetrical proximal landmark compared with distal landmarks. This focus was to eliminate any orientation information derived from the arrangement of multiple objects or the intrinsic orientation of a polarized object. While a single rotational symmetrical proximal landmark alone may not provide direct orientation information, the vector (comprising distance and direction) between the proximal landmark and the participant's own location can offer relevant orientation cues (Knierim & Hamilton, 2011). Real navigation scenarios often involve situations where individuals are aware of their position but uncertain about their orientation. For example, when exiting a subway station, individuals should know they are at the station, even if they are unsure

of their exact orientation at that moment. The vector between their current location and a familiar landmark can play a crucial role in helping them regain their orientation after feeling disoriented.

Therefore, considering the vectors between the positions of the navigators and a single proximal landmark is important for investigating whether distal landmarks dominate over proximal landmarks in orientation. This approach allows researchers to examine the influence of the relative position and direction of the proximal landmark in relation to the navigators, which can provide valuable insights into how individuals use different cues for orientation in real-world navigation scenarios.

In the literature, when researchers examine the roles of different visual cues in determining orientations, they often ensure that participants are deliberately disoriented, effectively preventing self-motion information from indicating orientations (e.g., Learmonth et al., 2002). However, it is important to note that disorientation could potentially impair human orientation representation while not necessarily affecting human position representations (Zhang et al., 2020). For instance, individuals may stand three meters north of a camping tent and then spin in place with their eyes closed. After sufficient spinning, they may find it difficult to accurately indicate their orientation with eyes remaining closed, but they would still be aware of their position - knowing that they are standing three meters north of the camping tent. Thus, people who lose their orientation but have position representations after spinning in place could still utilize the vectors between their positions and a single proximal landmark to regain their orientation when seeing the landmark. Their preference for distal landmarks or a proximal landmark in orientation could shed lights on whether distal landmarks dominate over proximal landmarks in orientation.

Is there a circumstance where people who lose their orientation but have position representations (e.g., when exiting a subway or after spinning in place) prefer one proximal landmark over distal landmarks to regain their orientation? We hypothesize that a proximal landmark may be preferred for orientation when navigators possess a clear and precise representation of their positions in relation to the proximal landmark. Our rationales are as follows.

As mentioned earlier, self-motion cues play a significant role in helping navigators estimate their position relative to fixed reference points during locomotion. This process, known as path integration, allows navigators to continuously track their positions relative to a familiar proximal landmark in the environment, represented by a vector pointing from their estimated position to the proximal landmark. By using this vector, navigators can determine their orientations in the environment. It is argued that path integration primarily operates in the local environment rather than the global environment (Lei & Mou, 2023; Wang & Brockmole, 2003). As a result, the process of path integration motivates navigators to encode the spatial representation of the local environment more extensively, enhancing the salience of the proximal landmark within that particular area. Based on this understanding, we conjecture that when the vector originating from their own position and pointing towards a nearby familiar landmark becomes highly salient and unambiguous, navigators are more likely to rely directly on this vector rather than seeking out distal landmarks to determine their orientations within the environment.

2.3 Current study and General Methods

Experiment 1 of the current study was designed to investigate whether navigators' reliance on distal and proximal landmarks for orientation is determined by relative cue precision,

prior beliefs, or a combination of both factors. Experiments 2 and 3 of the current study were designed to identify the circumstances in which proximal landmarks can prevail over distal ones for orientation.

All experiments were conducted within immersive virtual reality environments. The experimental paradigm was similar to those used in previous studies (Mou & Zhang, 2014; Zhang et al., 2020). Participants were positioned at the path origin and learned the locations of five target objects in the presence of both proximal and distal landmarks. After learning, all the landmarks and objects disappeared, and the participants walked an outbound path until reaching the testing position (the endpoint of the path). Participants were disoriented at the endpoint by spinning in place and then asked to place the targets back to their original locations.

Spinning in place at the end of the path was to disrupt the heading estimates based on self-motion cues. It did not impair the position estimates from self-motion so that the vector between participants' position and the proximal landmark could indicate orientations. Following the methods developed by previous studies (Mou & Zhang, 2014; Zhang et al., 2020), we calculated participants' representations of their headings and positions from participants' responses of replacing objects. We then compared the calculated heading estimates in different cue conditions to examine the relative importance of distal and proximal landmarks.

Participants replaced objects in three cue conditions: distal-landmark-only (DLM) condition, proximal-landmark-only (PLM) condition, and conflict-landmark (Conflict) condition. Specifically, in the DLM condition, one of the three distal landmarks reappeared at random, but its location was rotated 50° clockwise (clockwise is positive in the current project) around the center of the circular wall. In the PLM condition, the proximal landmark reappeared, but its location was rotated 50° counter-clockwise (i.e., -50°) around the endpoint of the path. In the

Conflict condition, both a distal landmark rotated 50° and a proximal landmark rotated -50° reappeared.

In the DLM and PLM conditions, participants were hypothesized to rely on the rotated distal landmark (subjected to 50° rotation) or proximal landmark (subjected to -50° rotation) to estimate their heading during testing. The angular difference between the direction of the actual heading (h) and the estimated heading (h') is referred to as the heading error, η, (i.e., η = h' - h). Consequently, the predicted heading error based on the rotated distal landmarks in the DLM condition would be -50° (i.e., $\eta_{Predict\_Dlm}$ = -50°) (see the illustration in Figure 2.1) and the predicted heading error based on the rotated proximal landmarks in the PLM condition would be 50° (i.e., $\eta_{Predict\_Plm}$ = 50°).

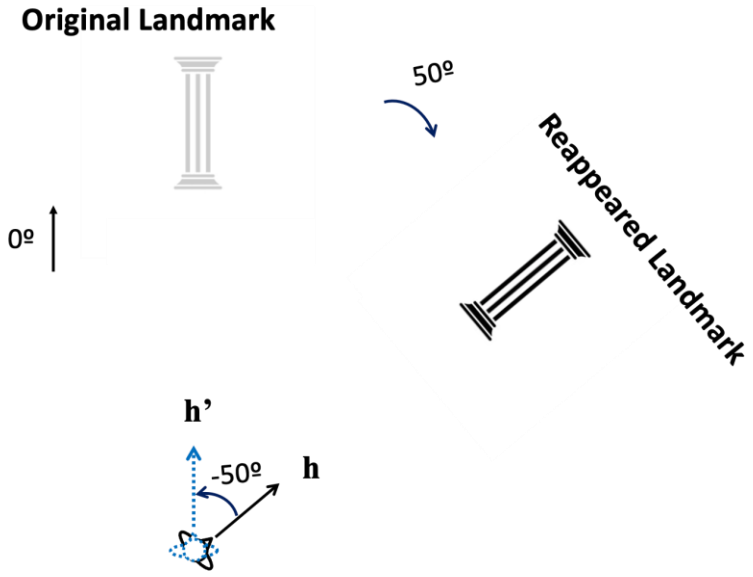

Figure 2.1. A hypothetical participant after disorientation sees a landmark that has been rotated with a degree of X (e.g., 50º). If their real heading is h and they think the reappeared landmark is in its original direction, then their estimated of their heading (h') should be –X (e.g., -50°) relative to h. In other words, the heading error η (h' – h) is –X (e.g., -50º) (i.e., η = h' – h = 0º - 50º).

We calculated the relative variance of the heading errors in the DLM and PLM conditions to reflect the relative cue precision. We then calculated the predicted weight on the distal cue ($W_{Predicted\_Dlm}$) based on the relative cue precision.

$$W_{Predicted\_Dlm} = \frac{\sigma_{Plm}^2}{\sigma_{Plm}^2 + \sigma_{Dlm}^2} \quad (7)$$

Where σ_{Plm}^2 and σ_{Dlm}^2 are the variances of heading estimates measured in the PLM and DLM conditions, respectively.

We measure the observed weight assigned to the distal landmark cue ($W_{\text{Observed\_Dlm}}$) for heading estimates in the Conflict condition for each participant using the following equation (Equation 12 in Chen et al., 2017; Equation 1 in Nardini et al., 2008):

$$W_{Observed\_Dlm} = \frac{\eta_{Observed\_Conf} - \eta_{Predict\_Plm}}{\eta_{Predict\_Dlm} - \eta_{Predict\_Plm}} \quad (8)$$

Where $\eta_{Predict\_Dlm}$ = -50° and $\eta_{Predict\_Plm}$= 50°. $\eta_{Observed\_Conf}$ denotes the observed heading error in the Conflict condition. E.g., a $\eta_{Observed\_Conf}$ of -50° indicates that participants rely solely on the rotated distal cue for heading estimates in the Conflict condition, assigning a weight of 1 to the distal cue.

We compared the weights assigned to the distal cue based on their relative precision ($W_{Predicted\_Dlm}$) with the observed weights of the distal cue ($W_{Observed\_Dlm}$) in the Conflict condition. Any difference between these two weights would indicate that prior knowledge contributes to cue usage. For example, prior knowledge that distal landmarks are more precise than proximal landmarks in determining orientation (i.e., prior odds>1) would lead to a larger observed weight ($W_{Observed\_Dlm}$) than the predicted weight ($W_{Predicted\_Dlm}$). Wang et al. (2018) used a similar approach to demonstrate that the knowledge of a street configuration being more

stable than a single building led to a larger observed weight to the street layout than the predicted weight to the street based on the relative cue precision in a conflicting condition.

2.4 Experiment 1

The purpose of Experiment 1 was to investigate whether the usage of distal and proximal landmarks for orientation is due to the relative cue precision (i.e., relative-precision hypothesis), prior beliefs in the superiority of the distal cue (i.e., prior-belief hypothesis), or involves a combination of both factors (i.e., dual-factor hypothesis). We assumed that a proximal landmark further away from the participants, given similarly precise representations of participants' positions, could provide more precise orientation information based on the vector between the proximal landmark and participants' positions. When the precision of the distal cue is fixed, a further proximal landmark could lead to a higher relative precision of the proximal landmark or a lower relative precision of the distal cues. Accordingly, we manipulated the relative cue precision by using a longer distance (3.2m in Experiment 1a)[2] or a shorter distance (1.6m in Experiment 1b) between the testing position and the proximal landmark, respectively.

Figure 2.2 illustrates the predictions on the results of Experiments 1a and 1b based on the three hypotheses. All hypotheses had the same prediction on the predicted weight. In particular, $W_{Predicted\_Dlm}$ should be smaller for a longer distance (3.2m) as a further proximal landmark could lead to a lower relative precision of the distal cues. However, these three hypotheses differed in their prediction about the observed weight. According to the relative-precision hypothesis, which claims that the utilization of distal landmarks as orienting cues is solely based

[2] We did not randomly assign participants to the conditions of longer or shorter distance. Therefore, we use Experiments 1a and 1b.

on considerations of relative cue precision, $W_{Observed\_Dlm}$ would align with $W_{Predicted\_Dlm}$. According to the prior-knowledge hypothesis, which claims that the dominance of distal cues is driven only by the prior knowledge that distal landmarks are superior for orientation, $W_{Observed\_Dlm}$ would not be influenced by variations in $W_{Predicted\_Dlm}$. According to the dual-factors hypothesis, which claims that both of the above contribute to the utilization of orienting cues, $W_{Observed\_Dlm}$ would change in accordance with variations in $W_{Predicted\_Dlm}$ but would exceed $W_{Predicted\_Dlm}$ due to extra preference for distal cues imposed by prior knowledge.

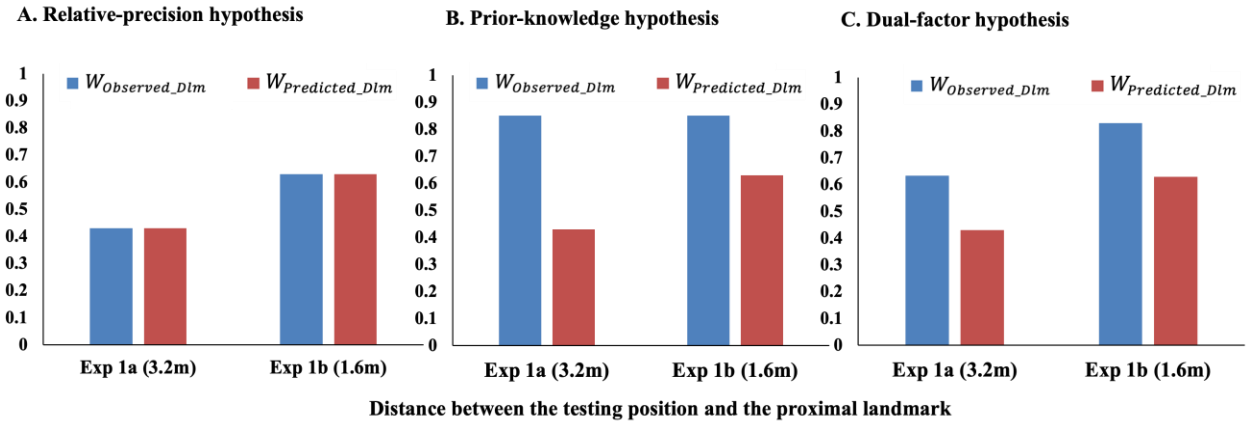

Figure 2.2. As the distance between the testing position and the proximal landmark varies in Experiments 1a and 1b, the predicted relationship between the weights assigned to the distal cue based on its relative precision ($W_{Predicted\_Dlm}$) with the observed weights of the distal cue ($W_{Observed\_Dlm}$) based on the three different hypotheses. ***(A)*** *relative-precision hypothesis.* ***(B)*** *prior-belief hypothesis.* ***(C)*** *dual-factor hypothesis. The relative precision of the distal cue (i.e., $W_{Predicted\_Dlm}$ shown in red bars) was manipulated by the experimental setup and thus consistent across all three hypotheses.*

2.4.1 Method

2.4.1.1 Participants. In Experiment 1a and Experiment 1b, each had 28 undergraduate students[3] from the University of Alberta participating (14 males). They received course credits as compensation for their participation. This study was approved by the University of Alberta Research Ethics Board and all participants provided written informed consent. The sample size of this study was chosen by assuming a medium effect size (Cohen's dz = 0.5) to compare the predicted and observed weights using a paired t test. We used a sample size of 28 participants to reach a power of 72%[4] at the 0.05 level for a two-tailed and paired *t*-test (find the MATLAB code for the power analysis at https://doi.org/10.7939/r3-na1j-g302).

2.4.1.2 Materials and design. The physical experimental space was a 4 × 4 m room. A virtual environment was rendered using WorldViz Vizard software (Santa Barbara, California). The environment was displayed using a head-mounted display (HMD, Oculus Rift S) with a 115º diagonal field of view, a resolution of 1280 × 1440 pixels per eye, and an 80 Hz refresh rate. Participants' head positions and orientations were tracked with an InterSense IS-900 (InterSense, Inc., MA) motion tracking system. To mask possible acoustic cues for orientation, white noise was played via HMD, and four fans were dispersed and positioned along the periphery of the experimental room, operated in rotation mode to generate noise during the whole experiment in all conditions.

---

[3] About 20% of participants dropped out due to motion sickness and were replaced.

[4] We adopted a power value above 70% but below 80% because we chose to use multiple experiments to reduce the chances of false positives and false negatives.

The virtual environment (see a screenshot in Figure 2.3A) had a grassy ground plane and a circular wall with a radius of 50 meters and a height of 10 meters. The center of the circular wall was also the center of the physical room.

Three distinctive items (i.e., a grey tower, a yellow pillar, and a black lamp, each approximately 40 m high) served as distal landmarks. The distal landmarks were positioned at a distance of 50 m from the center of the circular wall (so overlapping with the wall), with each adjacent pair separated by an angular distance of 30º relative to the center of the circular wall.

The path origin (O) was located 1.6 meters away from the center of the wall and aligned in the direction opposite to the distal landmarks. Specifically, in Experiment 1a, the midpoint of the path OP is at the center of the circular wall (see Figure 2.3B). In Experiment 1b, the endpoint of the path (P) is at the center of the circular wall (see Figure 2.3C).

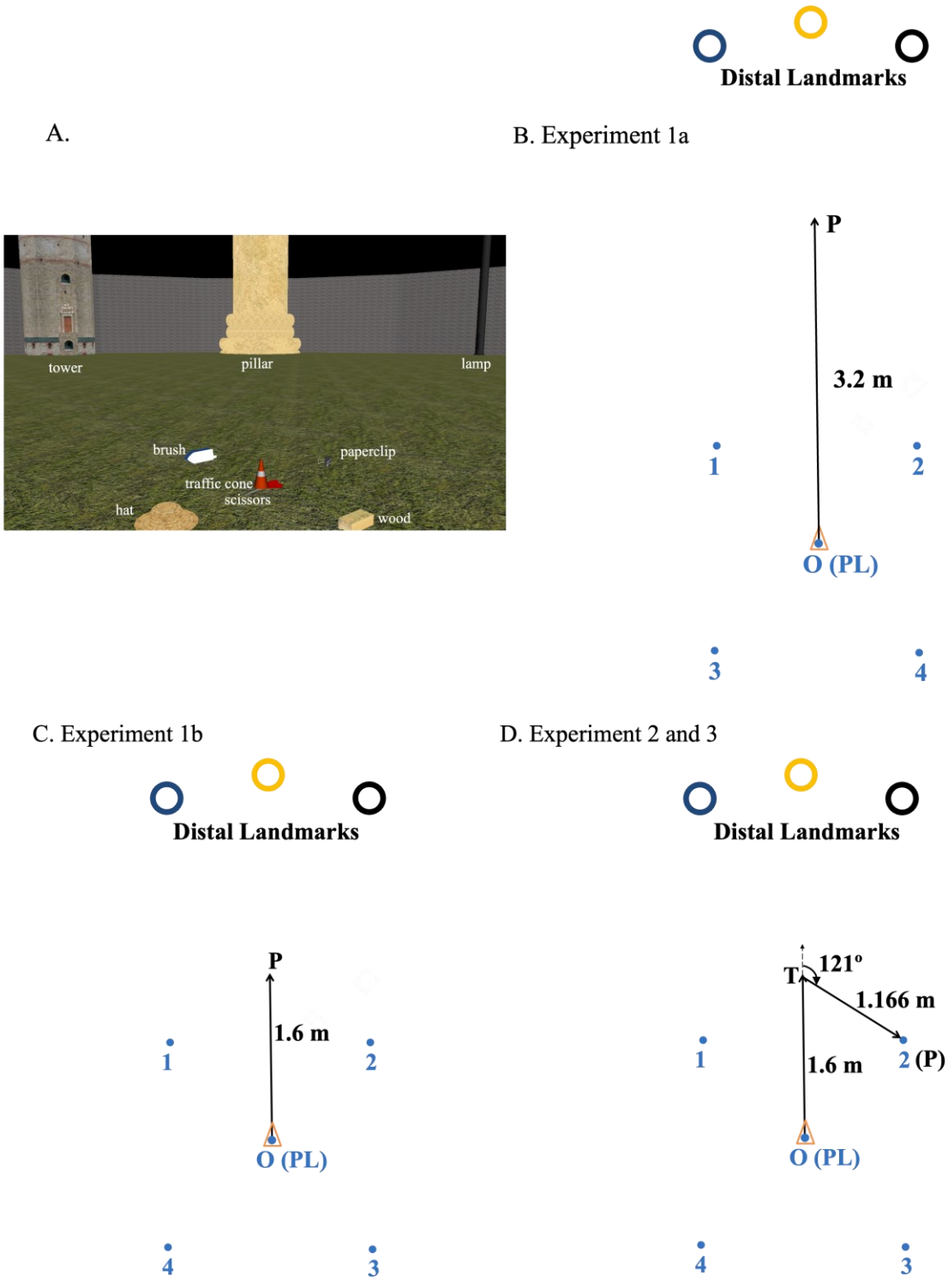

Figure 2.3. A screenshot of the virtual environment and schematic diagrams of path configurations in all experiments. ***(A)****. A screenshot of the experimental environment includes five target objects (e.g., scissors, brush, paperclip, wood, and hat), a proximal landmark (i.e.,*

traffic cone), and three distal landmarks (i.e., tower, pillar, and lamp). The labels of the objects and landmarks are added for readers only. ***(B, C & D)*** *Solid arrow lines represent the walking paths from the origin (O) to the end of the path (P) and the 2-leg paths used in Experiments 2 and 3 include the turning point (T) as well. Five dots in blue denote five target objects, the center object placed at the origin (O) of the path, and the other four (numbered 1–4) shape a square shape. The triangle in orange is denoted as the proximal landmark (PL). Three colored circles denote the three distal landmarks. In the interest of clarity, we use the initial walking direction (i.e., the direction of* $\overrightarrow{OP}$ *in Experiment 1 and the direction of* $\overrightarrow{OT}$ *in Experiments 2 and 3) as the reference direction (referred to as 0°) in the current study.*

A rotational symmetric traffic cone with a height of 0.3 m (see Figure 2.3A), located at the path origin, served as the proximal landmark (PL). Participants learned the locations of five targets (e.g., the scissors, brush, paperclip, wood, and hat in Figure 2.3A, respectively) and the traffic cone before walking an outbound path. One of the targets (scissors in Figure 2.3A or O in Figure 2.3B) overlapped with the traffic cone at the origin (O). The other four targets (brush, paperclip, wood, and hat in Figure 2.3A or 1, 2, 3, 4 in Figure 2.3B) were located 1.41 m from the origin at relative directions 315º, 45, 135º, and 225º clockwise to the initial walking direction (i.e., the direction of $\overrightarrow{OP}$ in Experiment 1) respectively, forming a square shape (Mou & Zhang, 2014). The association between these five target objects and their positions was randomized among participants but consistent for each participant across paths.

The lengths of the walking path (i.e., OP in Figures 2.3B and 2.3C) were 3.2 meters and 1.6 meters in Experiments 1a and 1b, respectively. The outbound path was marked by poles (with a radius of 0.05 meters and a height of 1.5 meters). The origin was indicated by a red pole, and

the testing position was indicated by a green pole. These poles appeared sequentially to guide participants' walking and disappeared once the participant reached the locations.

There are three cue conditions, differing only in the testing phase. Participants were required to indicate the locations of targets with the presence of different landmark cues: 1) a shifted proximal landmark being rotated -50° around the endpoint of the path (PLM condition), 2) a shifted distal landmark being rotated 50° (DLM condition), and 3) both two above (Conflict condition). No feedback was given during the testing phase.

All participants completed the four paths in each of the three cue conditions (12 path trials in total). Across the four paths, the relationship among the path, objects, and landmarks was constant in the virtual environment but the four paths started from different locations in the physical room (1.6 m north, south, east, or west of the room center).

Path trials were blocked by condition, with four paths randomly presented within each block. For half of the participants, the order of the blocks was PLM-DLM-Conflict conditions and for the other half, the order of the blocks was DLM-PLM-Conflict conditions. For each path trial, participants were required to indicate the locations of all five targets which were probed in a random order with no time limit. Participants' responses of the objects' locations were recorded.

The primary dependent variable was derived from the heading error on each path trial, which is the angular difference between participants' correct heading and their estimates of their heading during testing (see data analysis below for the details of the calculation).

2.4.1.3 Procedure. Each experimental trial consisted of a learning phase and a testing phase. In an immersive virtual environment, participants saw a red pole with a traffic cone (i.e., the proximal landmark) overlapping its base, along with three distinctive structures in the distance (i.e., distal landmarks) and a circular wall surrounding all of them. Participants were

instructed to walk to the location of the red pole (i.e., the origin of the path). Once participants reached the location, the red pole with the traffic cone disappeared. Participants were then instructed to maintain their orientation by aligning themselves with the direction indicated by the red arrows appearing at their feet, ensuring they faced directly toward the central distal landmark (i.e., the pillar). This facing direction aligns with the initial walking direction as well. Afterward, the red arrow disappeared and five target objects and the proximal landmark (i.e., the traffic cone) were presented.

In the learning phase, participants learned the locations of all five objects, the location of the proximal landmark, and the directions of three distal landmarks. The learning time is one minute in the first trial and fifteen seconds in the remaining 11 trials given that the object-location pairs remained consistent for each participant across trials. Then all objects and landmarks were removed, and participants were probed by a floating model of one of the targets of landmarks and asked to replace it back to the original location (for the proximal landmark and target objects) or direction (for the distal landmarks) by using a virtual stick. After each pointing response, the probed item was displayed in its correct location as feedback for two seconds. Once all objects and landmarks had been replaced once with feedback, they all appeared in their correct positions, providing participants with the opportunity to review them again if needed. Then they were removed.

Participants walked from the origin toward a green pole located at P, which indicated the end of the path. Upon participants reaching the green pole, the green pole disappeared, and they were disoriented in place to disrupt their heading estimates from path integration (although their position estimates from path integration remain intact). Regarding the disorientation, participants were asked to sit on a spinning chair and were spun by an experimenter while performing a task

of counting backward for 12 seconds (approximately 80º per second). The initial direction of rotation was randomly determined, and the direction may change during the rotation.

In the testing phase, all five targets were probed in random order and participants were required to indicate the locations of targets with the presence of different landmark cues. No feedback was given during the testing phase.

Participants completed two practice trials to familiarize themselves with the experimental procedure before starting the formal experimental trials. In the practice trials, different target objects and the paths were used. Furthermore, the proximal and one of the distal landmarks reappeared in their original locations after participants were disorientated at the end of the path.

2.4.1.4 Data Analysis. Figure S2.1 in the Supplementary materials of Chapter 2 defines the relationship between homing, position, and heading errors. We calculated the estimated position (P') and heading (h') in the testing phase on each experimental path for each participant employing a bidimensional regression (Friedman & Kolner, 2003; Zhang et al., 2020). Figure S2 provides examples of using this approach for all three conditions. This approach involved establishing a mapping function (f) representing the transforming relationship (scale, rotation, and translation) between the configurations of correct locations (i.e., locations 1, 2, 3, 4, and O, the dependent variable) and the replaced object locations (i.e., locations 1', 2', 3', 4', and O', the independent variable) (e.g. O=f(O'), see Figure 3 in Zhang et al., 2020 and Figure S2.2 in the Supplementary materials of Chapter 2). The mean r^2 values for the regression models across paths and participants exceeded .82 in all experiments of the current project, indicating a high level of coherence in participants' responses across objects within individual paths. Participants' position and heading estimates (P' and h') were calculated by applying the mapping function (f),

with the participants' testing position (P) and heading (h) as the independent values, respectively, i.e., P' = f (P), h' = f (h).

Using the estimated position (P') and heading (h'), we calculated the angular errors of heading (η = h' - h), position, and home estimates for each path trial and for each participant. In the interest of brevity, we only present the results of errors in heading estimates. The results of errors in position and goal estimates are presented in the Supplementary materials of Chapter 2 (see Table S2.1, Figure S2.4, and Figure S2.8 for main results).

We referred to the heading error for each path trial and each participant as an individual heading error. For each participant, we calculated the circular mean and circular standard deviation (SD_DLM, SD_PLM, SD_Conflict) across individual heading errors in the same cue condition (referred to as participant-level circular mean and standard deviation). The circular mean in the Conflict condition was used to calculate the observed weight assigned to the distal landmark cue ($W_{Observed\_Dlm}$) based on Equation 2. The circular standard deviations in the DLM and PLM conditions were utilized to calculate the predicted weight ($W_{Predicted\_Dlm}$) based on Equation 1 (σ_{Dlm} = SD_DLM, σ_{Plm} = SD_PLM). The comparison between the observed and predicted weights enables us to compare the three potential theoretical hypotheses.

The group-level circular means of the participant-level circular mean and their corresponding confidence intervals were also calculated for each condition. The confidence interval (CI) of the mean was used to identify whether the observed group-level circular mean in the single cue conditions (i.e., DLM and PLM conditions) was determined by the rotated angle of the given cue. For instance, if the confidence interval of the group-level mean heading error in the PLM condition encompasses 50° (which is the heading error predicted by the rotated proximal landmark), it implies that the heading estimates were determined by the proximal

landmark (Batschelet, 1981). The variability of circular means of heading errors was examined by the parametric test for concentration across the conditions (Batschelet, 1981, p. 122). For each condition, we also conducted the Rayleigh *Z* test to assess whether the mean heading errors had uniform distributions across participants, which would indicate a random estimation.

2.4.2 Results

Before we discuss the results of heading errors in detail, we will summarize the results of homing and position errors briefly. The detailed results of homing and position errors are included in the supplementary materials.

For homing errors, in the PLM and Conflict conditions, where the proximal landmark was presented during the test, their circular means were the same as the rotation angle of the proximal landmark (see Table S2.1, Figure S2.3) and their standard deviations (SDs) were very small (see Figure S2.4). These results indicate that participants used the rotated proximal landmark as the home location. In the DLM condition, where the proximal landmark was not available, their circular means followed those of the heading errors, and their SDs were large. These results indicate that homing errors were attributed to both position errors based on self-motion and heading errors based on distal landmarks.

For position errors, in the PLM and DLM conditions, their circular means did not show any systematic error, and their SDs were comparable between these two conditions. These results indicate that participants relied on their self-motion information to estimate their position. In the Conflict condition, their circular means appeared to be the sum of heading errors and homing errors, and their SDs appeared to be the same as the SDs of the heading errors.

The summarized results for homing errors and position errors were consistent across all experiments, so they will not be repeated for the following experiments.

2.4.2.1 Participant-level circular means of heading errors. Participant-level circular means and their mean and confidence interval in all conditions are plotted in Figure 2.4. The group-level circular mean and circular standard deviation are summarized in Table 2.1. The Rayleigh Z test showed that the heading errors in all conditions were clustered around one direction (Zs ≧12.75, ps < .001).

Table 2.1. Predicted heading errors based on distal or proximal landmarks and the circular means (circular standard deviations) of the participant-level heading errors in each cue condition of all experiments.

Conditions	Prediction from distal landmarks	Prediction from proximal landmarks	Observed mean heading errors (standard deviation)			
			Exp 1a	Exp 1b	Exp 2	Exp 3
DLM	-50°		-39.1° (28.4°)	-46.5° (23.8°)	-43.9° (16.3°)	-43.5° (12.2°)
PLM		50°	43.9° (32.4°)	46.8° (50.8°)	57.1° (21.6°)	21.8° (64.9°)
Conflict	-50°	50°	-11.9° (28.4°)	-29.3° (23.7°)	36.4° (30.2°)	-38.7° (28.8°)

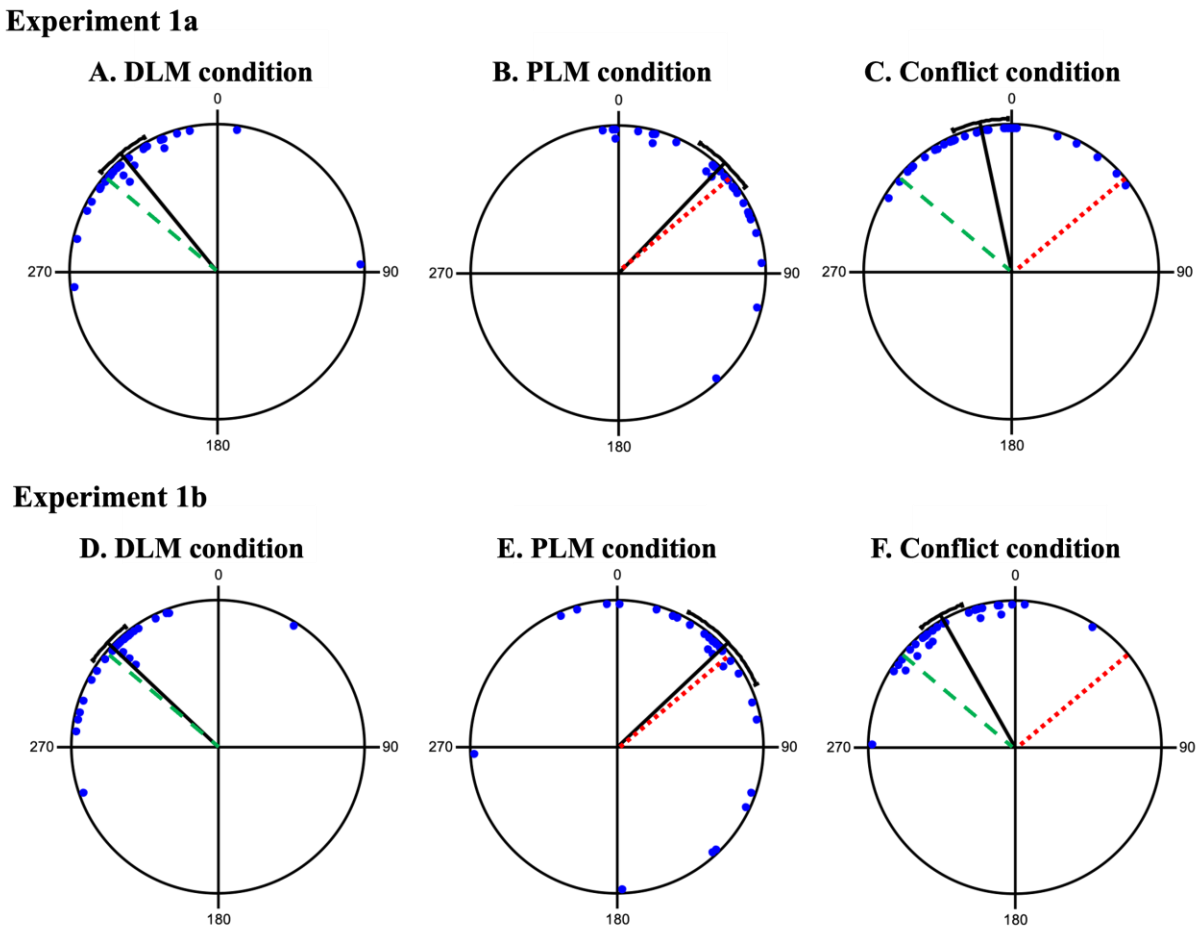

Figure 2.4. Observed and predicted heading errors in the DLM (panels A and D), PLM (panels B and E), and Conflict conditions (panels C and F) in Experiments 1a and 1b. Each blue dot indicates one participant-level circular mean of heading errors across paths. The solid black line indicates the group-level circular mean of the heading errors across participants. The black arc indicates the 95% confidence interval of the group-level circular mean. The dotted red line indicates the predicted heading error based on the rotated proximal landmark (50°). The dashed green line indicates the predicted heading error based on the rotated distal landmark (-50°).

In the DLM condition, the heading estimates clustered around the predicted heading errors (-50°) based on the rotated distal landmark (the dashed green line in Figures 2.4A and

2.4D) in both Experiments 1a and 1b (mean heading error = -39.1°, 95% CI [-49.6°, –28.6°] and mean heading error = -46.5°, 95% CI [-55.3°, –37.7°], respectively). These results indicate that participants used the rotated distal landmark for estimating their headings after disorientation.

In the PLM condition, the heading estimates clustered around the predicted heading errors (50°) based on the rotated proximal landmark (the dotted red line in Figures 2.4B and 2.4E) in both Experiments 1a and 1b (mean heading error = 43.9°, 95% CI [31.9°, 55.8°] and mean heading error = 46.8°, 95% CI [27.9°, 65.8°], respectively). These results indicate that participants used the rotated proximal landmarks for heading estimation after disorientation when path integration enabled them to estimate their position.

In the Conflict condition, the mean heading error was -11.9° with a 95% confidence interval [-22.4°, -1.4°] in Experiment 1a (Figure 2.4C) and the mean heading error was -29.3° with a 95% confidence interval [-38.1°, -20.6°] in Experiment 1b (Figure 4F). The 95% CI of the heading errors did not encompass the predictions based on either displaced distal (-50°) or proximal cues (50°), indicating that the participants do not rely entirely on either distal or proximal landmarks to determine their headings.

In Experiment 1a, there were no significant differences in the variability of heading errors across any conditions, all Fs(27,27) $\leq$1.29, ps > .05 (Batschelet, 1981, p. 122). However, in Experiment 1b, the heading errors were more variable in the PLM condition than in the DLM and Conflict conditions, Fs(27,27) $\geq$ 3.92, ps < .01. There were no significant differences in the variability of heading errors between DLM and Conflict conditions, F(27,27) = 1.01, p > .05.

2.4.2.2 Participant-level circular standard deviation of heading errors.

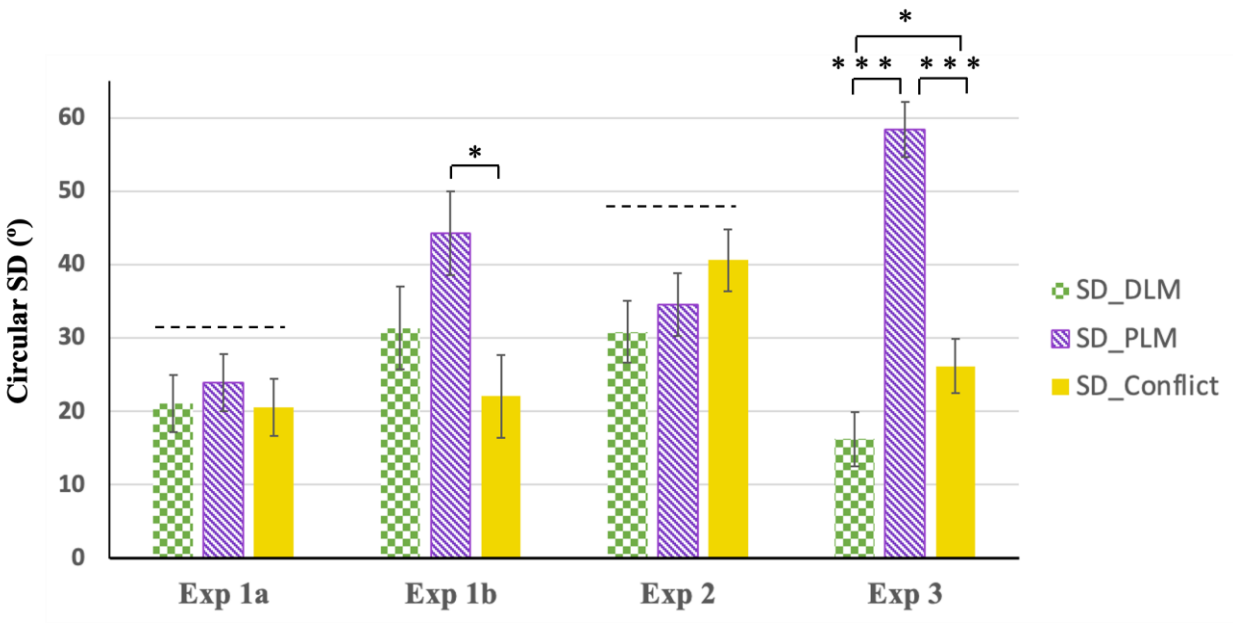

*Figure 2.5. The means of participant-level circular standard deviations of the heading errors in all conditions of all experiments. The solid lines represent significant comparisons (.01 < *p < .05, ***p < .001) and the dashed line represents an insignificant comparison (p > .05). Error bars represent ± 1 SE of the means (from the MSE of each repeated-measure ANOVA).*

The means of participant-level circular standard deviations in all conditions are plotted in Figure 2.5. We conducted repeated-measure ANOVA with one within-subject factor (cue condition: DLM, PLM, and Conflict) for Experiment 1a and 1b respectively. There were no significant differences among conditions in Experiment 1a, $F(2, 54) = .22$, $p = .80$, $MSE = 421.46$, $\eta_p^2 = .008$, $BF_{01}=7.8$, indicating that the means of the participant-level SDs of heading errors were comparable across all conditions in Experiment 1a.

There was a significant difference among conditions in Experiment 1b, $F(2, 54) = 3.88$, $p = .03$, $MSE = 897.31$, $\eta_p^2 = .126$. In particular, the SD in the PLM condition was significantly larger than that in the Conflict condition, $t(27) = 2.67$, $p = .01$, Cohen's $dz = .50$, but did not

differ from that in the DLM condition, $t(27) = 1.52$, $p = .14$, Cohen's $dz = 0.29$, $BF_{01} = 1.80$. The SD in the DLM condition did not differ from that in the Conflict condition, $t(27) = 1.31$, $p = .20$, Cohen's $dz = 0.25$, $BF_{01} = 2.30$.

2.4.2.3 Predicted and observed weights. In the Conflict condition, participants consistently favored the usage of the distal landmark over the proximal landmark. The observed weight on the distal landmark was significantly larger than the observed weight on the proximal landmark in Experiment 1a (mean $W_{Observed\_Dlm} = .612$, mean $W_{Observed\_Plm} = .388$) 5, t(27) = 2.06, p = .049, Cohen's dz = .39 and in Experiment1b (mean $W_{Observed\_Dlm} = .792$, mean $W_{Observed\_Plm} = .208$), t(27) = 6.38, p < .001, Cohen's dz = 1.21.

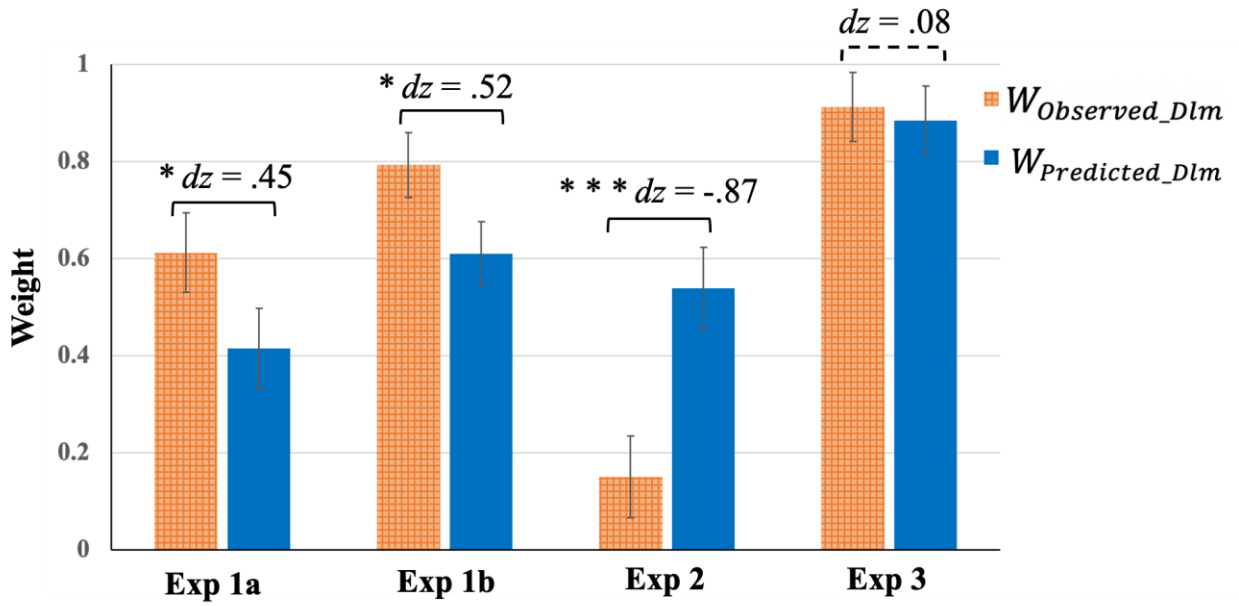

[5] This comparison is equivalent to comparing $W_{Observed\_Dlm}$ with .5. For example, $W_{Observed\_Dlm} > W_{Observed\_Plm}$ means $W_{Observed\_Dlm} > .5$.

*Figure 2.6. The observed weights of the distal cue ($W_{Observed\_Dlm}$) and the weights of the distal cue based on its relative precision ($W_{Predicted\_Dlm}$) in all experiments. The solid lines represent significant comparisons (.01 < *p < .05, ***p < .001) and the dashed line represents an insignificant comparison (p > .05). Cohen's dz values are listed. Error bars represent ± 1 SE of the means.*

The mean predicted weights of the distal cue based on its relative precision ($W_{Predicted\_Dlm}$) and the observed weights of the distal cue ($W_{Observed\_Dlm}$) across participants in the two experiments are plotted in Figure 2.6. The relative precision obtained from the distal landmark significantly increased from Experiment 1a (mean $W_{Predicted\_Dlm}$ = .42) to 1b (mean $W_{Predicted\_Dlm}$ = .61), $t(54) = -2.03$, $p = .047$, Cohen's $d = -.54$, providing evidence for the validity of our manipulation of relative precision of distal and proximal cues.

To differentiate the three hypotheses, we first tested the prediction of the relative-precision hypothesis: the predicted weights rely solely on the relative cue precision. We conducted paired-sample *t*-tests comparing the observed weights of the distal cue ($W_{Observed\_Dlm}$) with predicted weights of distal cues based on its relative precision ($W_{Predicted\_Dlm}$) for each experiment separately. The observed weights of the distal cue were significantly larger than the predicted weights based on the relative precision in Experiment la (mean $W_{Observed\_Dlm}$ = .612, mean $W_{Predicted\_Dlm}$ = .415), $t(27) = 2.40$, $p = .02$, Cohen's $dz = .45$ and Experiment lb (mean $W_{Observed\_Dlm}$ = .792, mean $W_{Predicted\_Dlm}$ = .610), $t(27) = 2.74$, $p = .01$, Cohen's $dz = .52$. These results demonstrate that compared to the predicted weights relying solely on the relative cue precision, participants actually assigned greater weights to the

distal cues under the Conflict conditions, undermining the relative-precision hypothesis (see Figure 2.2a).

We tested the prediction of the prior-knowledge hypothesis: the observed weight should not increase with the predicted weights from Experiment 1a to 1b (Figure 2.2b). We conducted an independent samples *t*-test comparing the observed weights ($W_{Observed\_Dlm}$) in Experiments 1a and 1b. It revealed that the observed weights were smaller in Experiment 1a than 1b, $t(54) = -2.531$, $p = .014$, Cohen's $d = -.68$. This result undermined the prior-knowledge hypothesis, which suggests that orientation cue usage should not be influenced by variations in relative cue precision between Experiments 1a and 1b.

However, the results that observed weights ($W_{Observed\_Dlm}$) were larger than the predicted weights and increased with the predicted weights from Experiment 1a to 1b were consistent with the dual-factor hypothesis (see Figure 2.2c).

In addition, we examined whether the prior odds in Experiments 1 and 2 are consistent. We calculated the group-level prior odds based on the mean observed weights and the mean predicted weights for both experiments using the following equation.

$$\text{prior odds} = \frac{mean\ W_{observed\_Dlm}}{1-mean\ W_{observed\_Dlm}} \div \frac{mean\ W_{predicted\_Dlm}}{1-mean\ W_{predicted\_Dlm}} \quad (9)$$

Here, $\frac{mean\ W_{observed\_Dlm}}{1-mean\ W_{observed\_Dlm}}$ represents the posterior and $\frac{mean\ W_{predicted\_Dlm}}{1-mean\ W_{predicted\_Dlm}}$ represents the likelihood ratio on the group level[6].

[6] To calculate the group level prior odds, we could also use mean observed weight ratios as the posterior odds and mean predicted weight ratios as the likelihood ratio. However, it is hard to assume that weight ratios follow a normal distribution. Thus, mean weight ratios might not be a valid estimate of group level posterior or likelihood ratio.

Prior odds were 2.22 (i.e., $\frac{0.61}{1-0.61} \div \frac{0.415}{1-0.415}$) for Experiments 1a and 2.43 for Experiment 1b, indicating that they were consistent. To further qualify it, we test whether the mean $W_{observed\_Dlm}$ in Experiment 1a can be recovered if we replace the prior odds in Experiment 1a with that in Experiment 1b, following Equation 10.

$$\frac{recovered\ mean\ W_{observed\_Dlm}}{1-recovered\ mean\ W_{observed\_Dlm}}^{expA} = \frac{mean\ W_{predicted\_Dlm}}{1-mean\ W_{predicted\_Dlm}}^{expA} \times \text{prior odds}^{expB} \quad (10)$$

Equation 10 calculated the $recovered\ mean\ W_{observed\_Dlm}$ in one experiment (e.g., expA) derived from the prior odds from another experiment (e.g., expB). If the prior odds in both experiments are consistent, then the $recovered\ mean\ W_{observed\_Dlm}$ should be consistent with the real $mean\ W_{observed\_Dlm}$ in the same experiment (e.g., expA).

Therefore, $recovered\ mean\ W_{observed\_Dlm}^{exp1a}$ is a weight estimate derived from the prior odds from Experiment 1b (specifically, $\frac{recovered\ mean\ W_{observed\_Dlm}}{1-recovered\ mean\ W_{observed\_Dlm}}^{exp1a} = \frac{mean\ W_{predicted\_Dlm}}{1-mean\ W_{predicted\_Dlm}}^{exp1a} \times \text{prior odds}^{exp1b} = \frac{0.415}{1-0.415} \times 0.243$. We obtained $recovered\ mean\ W_{observed\_Dlm}^{exp1a} = 0.633$). We then compared the real mean observed weights of Experiment 1a ($mean\ W_{observed\_Dlm}$= 0.61) to the $recovered\ mean\ W_{observed\_Dlm}^{exp1a}$ (the value = 0.633). A one-sample t-test showed that they did not significantly differ, $t(27) = -0.383$, $p = .71$, Cohen's $dz = -0.072$., BF01= 4.66. This result indicated that the prior odds from Experiments 1a and 1b were exchangeable and thus consistent.

2.4.3 Discussion

Consistent with previous research findings from animal studies (Knierim, 2002; Shapiro et al., 1997; Yoganarasimha et al., 2006) and theoretical arguments about human navigation (Bullens et al., 2010; Nadel & Hupbach, 2006), Experiment 1 confirmed that distal cues exert an

advantage in competition with proximal cues (i.e., observed weight of distal cues larger than .5). Furthermore, the dominance of distal cues was attributed to both the relative cue precision and the top-down cue preference of the distal cues based on the prior knowledge of cue precision.

The results of Experiment 1 favor the dual-factor hypothesis over the other two hypotheses. Participants favored the distal landmark over the proximal one, using both the relative precision of specific cues and prior knowledge. When the relative precision of cues was altered in Experiments 1a and 1b, participants did not apply a constant weight to the distal landmark for orientation, which contradicts the prior-knowledge hypothesis. Additionally, participants assigned greater weights to distal cues than the predicted weight based on the relative cue precision, displaying a constant and significantly higher utilization (with constant prior odds of 2.22 - 2.43), which is incompatible with the relative-precision hypothesis. These results, however, are consistent with the dual-factor hypothesis, which predicts that while considering the relative cue precision of landmarks for orientation, navigators exhibit an additional top-down preference for distal landmarks.

Experiments 2 and 3 further investigated whether there are circumstances in which proximal cues can override distal cues to dominate participants' heading estimates. We hypothesized that when participants have a clear understanding of the spatial relationship between their current position and the proximal landmark in the environment (represented by a vector pointing from their position to the proximal landmark), they are more inclined to utilize this vector than distal landmarks to determine orientations in the environment. If this top-down inclination is large enough, proximal landmarks can override distal cues to dominate participants' heading estimates.

2.5 Experiment 2

The purpose of Experiment 2 was to test situations in which a proximal landmark can override a distal one in determining participants' heading estimation. Participants walked a two-leg path that led to a previously learned object location (e.g., a brush in Figure 2.3A). In addition to utilizing path integration to estimate their own position, as in Experiment 1, participants also received verbal instructions upon reaching the end of the path, informing them of their current location (e.g., "You are now at the location of the brush"). Given the well learned spatial relationship between this object and the proximal landmark established during the learning phase, we hypothesized that when path integration and verbal instructions enable participants to have a clear understanding of their position relative to the proximal landmark, they might have a top-down preference for the vector involving the proximal landmark in determining their orientations. This extra top-down preference might cause the proximal landmark to be favored over the distal landmark for orientation in the conflicting condition.

2.5.1 Method

2.5.1.1 Participants. 28 undergraduate students from the University of Alberta participated in Experiment 2 and received course credits in return.

2.5.1.2 Materials, Design, and Procedure. Experiment 2 was similar to Experiment 1 except for the following changes. After the learning phase, participants walked a two-leg path (O-T-P, see Figure 2.3D). The turning point of the paths (T indicated by a red pole) was always at the center of the physical room (also the center of the virtual circular wall). Upon participants reaching the turning point T, the red pole disappeared, and they were asked to turn left or right to walk to a green pole indicating the end of the path (P). The end of the path (P) was one of the learned locations of the target objects (i.e., the target object labeled 1 or 2 in Figure 2.3). And

participants were informed of their current location when they were at the end of the path by verbal instructions from experimenters (e.g., “You are now at the location of the brush”).

Across the four paths starting from different locations in the physical room, two had a turning angle of -121°, led to a left turn, and ended at the location of the target 1 in the upper left of the object array (see Figure 2.3D). The other two paths had a turning angle of 121°, led to a right turn, and ended at the location of the target 2 in the upper right of the object array (see Figure 2.3D). The lengths of the first (OT) and second legs (TP) are 1.6 m and 1.166 m, respectively.

2.5.2 Results

2.5.2.1 Participant-level circular means of heading errors. The heading errors for each participant across paths in all conditions are plotted in Figure 2.7. The mean heading errors across participants are summarized in Table 2.1. The Rayleigh *Z* test showed that the heading errors in all conditions were clustered around one direction (Zs $\geqq$ 21.20, ps < .001).

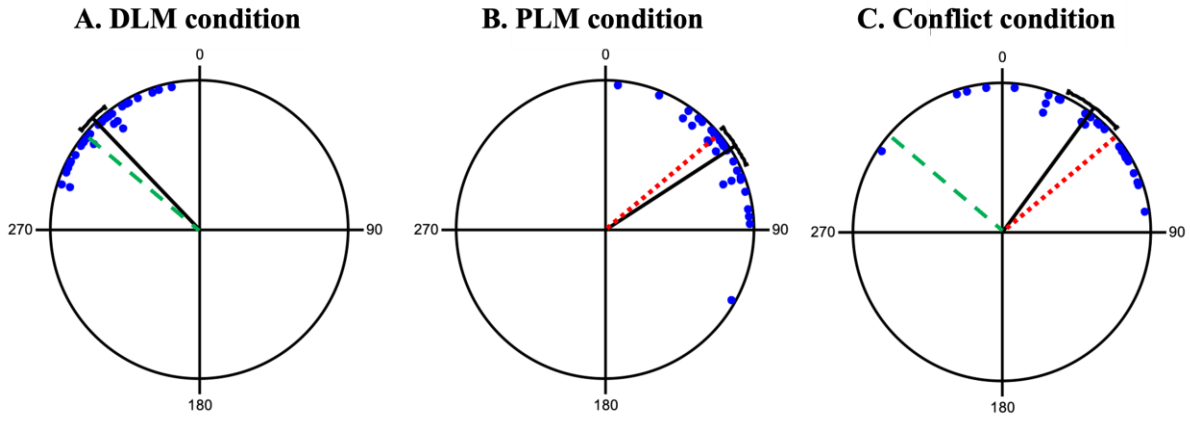

Figure 2.7. Observed and predicted heading errors in the DLM (panel A), PLM (panel B), and Conflict conditions (panel C) in Experiment 2. Each blue dot indicates one participant-level circular mean of heading errors across paths. The solid black line indicates the group-level

circular mean of the heading errors across participants. The black arc indicates the 95% confidence interval of the group-level circular mean. The dotted red line indicates the predicted heading error based on the rotated proximal landmark (50°). The dashed green line indicates the predicted heading error based on the rotated distal landmark (-50°).

In the DLM condition, the heading estimates clustered around the predicted heading errors (-50°) based on the rotated distal landmark (the dashed green line in Figure 2.7A), mean heading error = -43.9°, 95% CI [-49.9°, –37.8°]. These results indicate that participants used the distal landmark for estimating their headings after disorientation.

In the PLM condition, the heading estimates clustered around the predicted heading errors (50°) based on the rotated proximal landmark (the dotted red line in Figure 2.7B), mean heading error = 57.07°, 95% CI [49.05°, 65.08°]. These results indicate that participants used proximal landmarks for heading estimation after disorientation when they were aware of their position.

In the Conflict condition, the mean heading error was 36.4° with a 95% confidence interval [25.2°, 47.5°]. The confidence interval of the heading errors did not encompass the predictions based on either displaced distal (-50°) or proximal cues (50°).

The variability of heading errors in the PLM condition did not differ significantly from that in the DLM or Conflict conditions, Fs(27,27) ≤ 1.88, ps > .05. However, the variability of heading errors in the Conflict condition was significantly greater than that in the DLM condition, $F(27,27) = 3.25$, $p < .01$.

2.5.2.2 Participant-level circular standard deviation of heading errors. Participant-level circular standard deviations of all conditions in Experiment 2 are plotted in Figure 2.5. A

repeated-measure ANOVA with one within-subject factor (cue condition: DLM, PLM, and Conflict) was conducted. The results show no significant differences among conditions, $F(2, 54) = 1.36$, $p = .27$, $MSE = 502.41$, $\eta_p^2 = .048$, $B_{01} = 2.92$, indicating that the SDs of heading errors across paths were comparable for all conditions in Experiment 2.

2.5.2.3 Predicted and observed weights. In the Conflict condition, the observed weight on the distal landmarks was significantly smaller than the observed weight on the proximal landmark (mean $W_{Observed\_Dlm} = .151$, mean $W_{Observed\_Plm} = .849$), $t(27) = -5.93$, $p < .001$, Cohen's $dz = -1.12$. This suggests the proximal landmark was favored over the distal landmark.

The mean predicted weights of the distal cue based on its relative precision ($W_{Predicted\_Dlm}$) and the observed weights of the distal cue ($W_{Observed\_Dlm}$) across participants in Experiment 2 are plotted in Figure 2.6. A paired-sample *t*-test shows that the observed weight was significantly smaller than the predicted weight (mean $W_{Observed\_Dlm} = .151$, mean $W_{Predicted\_Dlm} = .539$), $t(27) = -4.62$, $p < .001$, Cohen's $dz = .87$. This suggests a top-down inclination of using the proximal landmark.

In addition, we calculated the prior odds for Experiment 2 (see Equation 9), which was 0.152. We tested whether the prior odds in Experiment 2 were consistent with the odds of Experiment 1. Using Equation 10, we recovered the mean observed weight for Experiment 2 by using the prior odds from Experiment 1b (prior odds = 2.43). The recovered $mean\ W_{observed\_Dlm}$ for Experiment 2 was 0.74. We then compared it with the real mean observed weights of Experiment 2 ($mean\ W_{observed\_Dlm} = 0.151$) using a one-sample t-test. The results showed that the mean observed weight of Experiment 2 was significantly smaller than the recovered mean observed weight based on the prior odds from Experiment 1b, $t(27) = -10.01$, p

< .001, Cohen's *dz* = -1.89. This result indicated that the prior odds from Experiment 2 was much smaller than that from Experiment 1.

2.5.3 Discussion

Experiment 2 demonstrates that a proximal landmark can override a distal one to dominate participants' heading estimates when they were clearly aware of their positions relative to the proximal landmark ($W_{Observed\_Dlm}$ smaller than .5). Importantly, the predicted weight based on the relative cue precision did not show any dominance of the proximal landmark ($W_{Predicted\_Dlm}$ = .539, not smaller than .5) (we will interpret this result in the General Discussion). Therefore, this dominance of the proximal landmark in Experiment 2 should be primarily attributed to participants' choice of prior knowledge that favors the proximal landmark, in contrast to the choice of prior knowledge that favors the distal landmark in Experiment 1.

In Experiment 2, participants were tested at the location of a target previously learned before walking the path. They were explicitly informed about this location after completing the walk. This information should have helped participants clearly understand their position at the end of the path. Indeed, the participant-level circular means of position errors approached zero (Table S2.1 and Figure S2.9), and the standard deviations (SDs) of position errors were small (Figure S2.8), especially when compared with those from Experiments 1a and 1b (Table S2.1, Figure S2.7, and Figure S2.8). Consequently, the vector from the participant's own position pointing towards the familiar nearby landmark became highly salient. In this context, participants might have relied on their prior knowledge, favoring the proximal landmarks.

One concern may be the possibility that the proximal dominance appeared in heading estimates because participants overall preferred the proximal landmark over the distal landmark, attributed to smaller position errors in PLM condition than in DLM condition. However,

participants' position estimates in the PLM and DLM conditions were comparable (Table S2.1, Figure S2.8, and Figure S2.9). This result was expected as participants relied on the same self-motion information and instruction of self-location in both conditions. The results of Experiment 2 extended the dual-factor hypothesis by showing proximal cue dominance (i.e., $\frac{\mathrm{Wd}}{\mathrm{Wp}} = \frac{\sigma_p^2}{\sigma_d^2} \times \text{prior odds} < 1$) and suggested that the prior knowledge used in Bayesian inference is not fixed and the choice of prior knowledge is affected by top-down variables. While participants in Experiments 1a and 1b used the prior knowledge that favored the distal landmarks, the salience of the vector to the proximal landmark in Experiment 2 might have invoked a top-down inclination to choose the prior knowledge of favoring the proximal landmark, which was large enough to demonstrate the dominance of proximal landmarks.

However, it is not clear whether a clear understanding of their testing location (overlapping with one target) was attributed to the path integration process during walking or to the explicit instruction of the testing location. Experiment 3 addressed this issue.

2.6 Experiment 3

The purpose of Experiment 3 was to test whether a proximal cue would still override a distal cue in determining participants' heading estimation if there was no explicit instruction. Participants walked a path and arrived at the location of one object they had previously learned but were not explicitly informed of their location upon arrival. They had to depend entirely on path integration to estimate their position.

2.6.1 Method

2.6.1.1 Participants. 14 males and 14 females from the University of Alberta participated in the experiment and received course credits in return.

2.6.1.2 Materials, Design, and Procedure. Experiment 3 was similar to Experiment 2 except that after walking the two-leg path (O-T-P), participants were not informed of their endpoint location (P) by verbal instructions from experimenters.

2.6.2 Results

2.6.2.1 Participant-level circular means of heading errors. The heading errors for each participant across paths in all conditions are plotted in Figure 2.8. The mean heading errors across participants are summarized in Table 2.1. The Rayleigh *Z* test showed that the heading errors in all conditions were clustered around one direction (Zs $\geqq 7.75$, ps $< .001$).

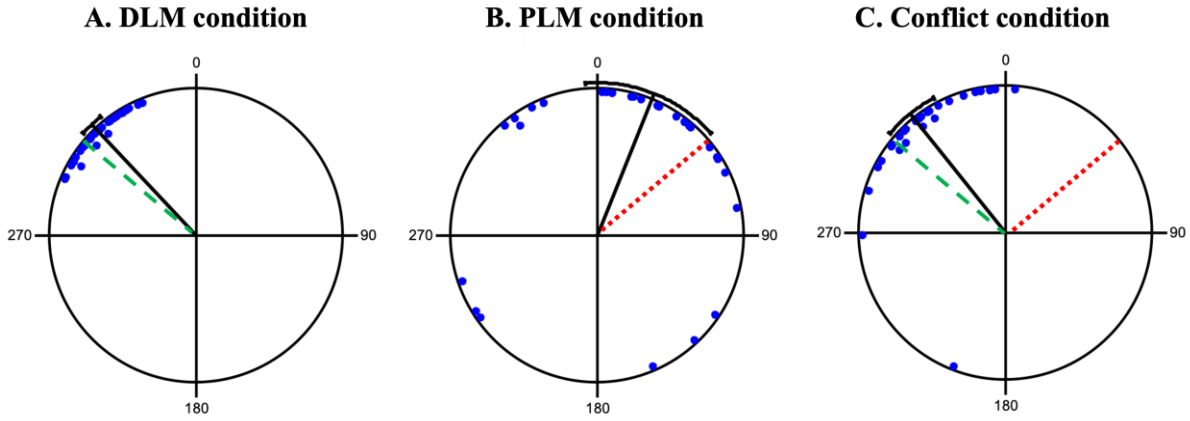

Figure 2.8. Observed and predicted heading errors in the DLM (panel A), PLM (panel B), and Conflict conditions (panel C) in Experiment 3. Each blue dot indicates one participant-level circular mean of heading errors across paths. The solid black line indicates the group-level circular mean of the heading errors across participants. The black arc indicates the 95% confidence interval of the group-level circular mean. The dotted red line indicates the predicted heading error based on the rotated proximal landmark (50°). The dashed green line indicates the predicted heading error based on the rotated distal landmark (-50°).

In the DLM condition, the heading estimates clustered around the predicted heading errors (-50°) based on the rotated distal landmark (the dashed green line in Figure 2.8A), mean heading error = -43.5°, 95% CI [-48.0°, –39.0°]. These results indicate that participants used the distal landmark for estimating their headings after disorientation.

In the PLM condition, the mean heading error was 21.85° with a 95% confidence interval [-4.53°, 48.22°] (see Figure 2.8B). The mean heading error did not differ from 0°. These results indicate that participants might have had difficulty in using the proximal landmark for estimating their headings after disorientation.

In the Conflict condition, the mean heading error was -38.7° with a 95% confidence interval [-49.38°, -28.12°] (see Figure 2.8C). These results indicate that participants primarily used the distal landmark for heading estimates.

The heading errors were more variable in the PLM condition than in the DLM and Conflict conditions, Fs(27,27) $\geq$ 4.02, ps < .01. The heading errors were more variable in the Conflict condition than in the DLM condition, $F(27,27) = 5.36$, $p < .01$.

2.6.2.2 Participant-level circular standard deviation of heading errors. Participant-level circular standard deviations of all conditions in Experiment 3 are plotted in Figure 2.5. A repeated-measure ANOVA with one within-subject factor (cue condition: DLM, PLM, and Conflict) was conducted. There were significant differences among conditions, $F(2, 54) = 34.71$, $p < .001$, $MSE = 391.57$, $\eta_p^2 = .56$. In particular, the SD in the PLM condition was significantly larger than that in the DLM and Conflict conditions, $t(27) = 9.02$, $p < .001$, Cohen's $dz = 1.70$, and $t(27) = 4.93$, $p < .001$, Cohen's $dz = .93$, respectively. The SD in the Conflict condition was significantly larger than that in the DLM condition, $t(27) = 2.26$, $p = .03$, Cohen's $dz = .43$.

2.6.2.3 Predicted and observed weights. In the Conflict condition, the observed weight on the distal landmark was significantly larger than the observed weight on the proximal cues, (mean $W_{Observed\_Dlm}$ = .912, mean $W_{Observed\_Plm}$ = .088), $t(27) = 6.96$, $p < .001$, Cohen's dz = 1.32. This suggests participants favored the utilization of the distal landmark over the proximal landmark.

The mean weights of the distal cue based on its relative precision ($W_{Predicted\_Dlm}$) and the observed weights of the distal cue ($W_{Observed\_Dlm}$) across participants in Experiment 3 are plotted in Figure 2.6. A paired-sample t-test shows that these two weights did not significantly differ (mean $W_{Observed\_Dlm}$ = .912, mean $W_{Predicted\_Dlm}$ = .884), $t(27) = .41$, $p = .69$, Cohen's dz = .08. To qualify this null effect, BF_{01}= 4.63.

We compared the prior odds of Experiment 3 with those of previous Experiments. We calculated the prior odds for Experiment 3 (see Equation 9), and it was 1.36. To test whether the prior odds of Experiment 3 was different from the prior odds of Experiment 2, we recovered the mean observed weight for Experiment 3 based on the prior odds from Experiment 2 (prior odds = 0.152) (see Equation 10). The recovered $mean\ W_{observed\_Dlm}$ of Experiment 3 was 0.537 and significantly smaller than the mean observed weight of Experiment 3 ($mean\ W_{Observed\_Dlm}$ = 0.912), $t(27) = 6.33$, $p < .001$, Cohen's dz = 1.197. This result indicated that the prior odds from Experiment 3 was larger than that from Experiment 2.

To test whether the prior odds of Experiment 3 was different from the prior odds of Experiment 1, we recovered the mean observed weight for Experiment 3 using the prior odds from Experiment 1b (prior odds = 2.43) (see Equation 10). The recovered $mean\ W_{observed\_Dlm}$ of Experiment 3 was 0.949, which was not different from the mean observed weight of Experiment 3 ($mean\ W_{Observed\_Dlm}$ = 0.912), $t(27) = -0.622$, $p = .539$, Cohen's dz = -0.117,

BF01= 4.22. This result indicated that the prior odds from Experiments 3 and Experiment 1b were exchangeable and thus consistent.

2.6.3 Discussion

In contrast to the dominance of the proximal landmark in Experiment 2, the results of Experiment 3 showed the dominance of the distal landmark. Furthermore, while there was a top-down preference for the proximal landmark in Experiment 2, the results of Experiment 3 did not show such a top-down preference for the proximal landmark. These results indicate that the instruction of the testing location in Experiment 2 was the key to invoking the top-down process of preferring the proximal landmark, which then caused the dominance of proximal landmarks in determining the orientation.

In Experiment 3, the navigators were required to rely on path integration to estimate their positions during walking. However, errors in position estimation via path integration can accumulate rapidly, particularly with increasing path complexity (e.g., more legs in a path) (Kearns et al., 2002; Kelly et al., 2008; Rieser & Rider, 1991). Indeed, the SDs of position errors in DLM and PLM conditions were very large in Experiment 3, compared with previous experiments (see Figure S2.8). In addition, the participant-level circular means of position errors in DLM and PLM conditions varied more in Experiment 3 (see Figure S2.10), compared with Experiment 2 (Figure S2.9). Because position errors in DLM and PLM conditions should be attributed to self-motion cues, it suggests that participants in Experiment 3 might not have estimated their positions accurately based on self-motion. Therefore, participants might not have known that they were standing at a location that had been well-learned. As depicted in Figure 2.8B, it is evident that the heading errors of some participants deviated significantly from the predicted values in the PLM condition. Additionally, the heading errors in the PLM condition

were much more variable than in the DLM condition in Experiment 3, whereas they were comparable in Experiment 2 (see Figures 2.7 and 2.8). The participant-level standard deviations of heading errors in the PLM condition were much larger than in the DLM condition in Experiment 3, whereas they were comparable in Experiment 2 (see Figure 2.5). Therefore, in the absence of verbal instructions regarding navigators' self-location, the vector connecting their estimated self-location to the reappeared proximal landmark might be noisy and less salient. This lack of clarity prevented the top-down preference for the proximal landmark based on vector salience from being invoked, which could have otherwise demonstrated the dominance of proximal landmarks.

Interestingly, the observed weights of the distal landmark were also not significantly higher than the predicted weights based on relative cue precision, failing to show the additional weight attributed to the prior knowledge demonstrated in Experiment 1. One possible explanation for this is a ceiling effect. The predicted weight of the distal landmark based on the relative cue precision alone was 0.884, while the predicted weight of the distal landmark based on the relative cue precision and prior odds from Experiment 1b (i.e., the recovered $mean\ W_{Observed\_Dlm}$ based on the prior odds of 2.43) was 0.949. Participants might still have used the prior odds from Experiment 1 as suggested by the fact that the observed weight of the distal landmark did not differ from that recovered based on the prior odds from Experiment 1b. The observed weight (0.913) was numerically larger than the prediction based on the relative-cue hypothesis (0.884). However, achieving a significant difference within such a limited room for improvement (from 0.884 to 0.949) can be quite difficult.

2.7 General Discussion

The purpose of this project was to test the long-standing theoretical argument that distal landmarks dominate over proximal landmarks as orientation cues (e.g., Hebb, 1938; 1949; Knierim & Hamilton, 2011; Nadel & Hupbach, 2006; O'Keefe & Nadel, 1978) and explore the underlying mechanisms in human navigation. The study yielded two main findings. Firstly, both the relative cue precision of specific landmarks and the pre-existing prior knowledge of the superiority of distal cues as orientation cues contribute to distal dominance. Secondly, it was observed that a proximal landmark dominated over a distal one as an orientation cue when navigators were explicitly informed of their self-location. This proximal dominance was primarily attributed to a top-down preference for proximal landmarks, as evidenced by a significantly smaller observed weight on distal landmarks compared to the predicted weights based on the relative cue precision.

Since there was no direct study testing the theoretical argument of distal dominance, the project proposed three hypotheses to conceptualize the underlying mechanisms. The first hypothesis, known as the relative-precision hypothesis, suggests that cue usage is determined by the relative cue precision, which is reciprocal to the relative variance of estimates based on individual cues. This hypothesis attributes the distal dominance to the smaller variance (i.e., larger cue precision) based on distal cues compared to proximal cues in a specific environment. Consequently, it predicts a comparable observed weight in the Conflict condition and the predicted weight based on the relative cue precision (Figure 2.2a). However, this hypothesis was undermined by the larger observed weight on the distal cues than the predicted weight in Experiments 1a and 1b (see Figure 2.6). Additionally, it was not consistent with the smaller observed weight on the distal cues than the predicted weight in Experiment 2. Although this hypothesis was consistent with the finding in Experiment 3, it seems to be an exceptional case.

The comparable observed and predicted weights in Experiment 3 might be attributed to a ceiling effect, wherein the predicted weight on the distal landmarks is too large to be increased further.

The second hypothesis, the prior-knowledge hypothesis, posits that people develop prior knowledge that distal landmarks are more precise than proximal landmarks across life experiences, primarily due to the general reduction in motion parallax relative to distal landmarks compared to proximal landmarks (Benhamou & Poucet, 1998; Nadel & Hupbach, 2006). According to this hypothesis, individuals might rely solely on this prior knowledge and disregard the relative cue precision in the specific environment when estimating their orientations. Therefore, the hypothesis predicts that the observed weights on the distal landmarks should be larger than .5 and consistent across varied relative cue precision (Figure 2.2b). However, this hypothesis was contradicted by the finding that the observed weight on the distal landmarks increased with the predicted weight from Experiment 1a to Experiment 1b (Figure 2.6). Additionally, it was inconsistent with the observed weight on the distal landmark, which was smaller than .5 in Experiment 2. Furthermore, it fails to explain the changes in the observed weights from Experiment 2 to Experiment 3.

The third hypothesis, the dual-factor hypothesis, posits that both the relative cue precision in a specific experiment and a prior belief of distal dominance contribute to distal dominance. This hypothesis provides a reasonable explanation for the effects of relative cue precision and the larger observed weight on the distal landmarks than the predicted weight in Experiment 1a and Experiment 1b (see Figure 2.2c and Figure 2.6). However, the dual-factor hypothesis appears inconsistent with the observed proximal dominance and the smaller observed weight than the predicted weight in Experiment 2. Originally, the dual-factor hypothesis was proposed to explain the underlying mechanism of distal dominance, assumed but not yet tested in the literature. It

solely considered the prior knowledge of distal dominance. To fit the findings in Experiments 2 and 3, the dual-factor hypothesis should be modified. In the modified dual-factor hypothesis, people can choose the prior knowledge of proximal dominance based on instructions. By incorporating both the relative cue precision and the chosen prior knowledge, the modified dual-factor hypothesis can better account for the observed variations in orientation cue preferences across different experimental conditions.

The modified dual-factor hypothesis, which incorporates both the relative precision of individual cues and the influence of top-down cognitive variables, appears to be consistent with findings from previous studies that have examined other pairs of competing cues (e.g., Chen et al., 2017; Wang et al., 2018; Zhao & Warren, 2015b). Chen et al. (2017) demonstrated that participants' cue preference for path integration and landmarks was biased towards the middle points of the estimates between these two cues, deviating from the predicted weights based on relative precision. This suggested that participants adopted a strategy of considering the average of the two estimates, rather than solely relying on one cue. Wang et al. (2018) found that when a building and a street configuration indicated conflicting orientations, participants exhibited a stronger preference for the street configuration compared to what could be predicted based solely on the accuracy of individual cues. This extra cue preference for the street configuration was attributed to participants' prior knowledge that a street configuration is more stable than a building. Specifically, when participants detected changes in the spatial relationship between a building and a street configuration, they assigned additional weight to the street configuration. In Zhao and Warren's study (2015b), when the landmarks unexpectedly shifted by 115º, participants' homing responses were completely influenced by the shifted landmarks, even though the shift exceeded the estimated discrimination threshold of path integration in this task.

The dominance of landmarks in the homing direction was attributed to participants' belief and knowledge that the path integration process is noisy and that landmarks were more precise and stable cues.

These findings collectively support the idea proposed in the modified dual-factor hypothesis, suggesting that this integrated approach of considering both relative cue precision and prior knowledge (aka Bayesian inference model of human cognition) may indeed reflect a universal principle for how humans weigh different cues in various navigation scenarios.

It is important to note that the choice of prior knowledge based on top-down variables appears to be too flexible and post-hoc. This concern was addressed as we carefully examined the consistency of the prior odds across experiments. Indeed, our results showed that participants might use consistent prior knowledge in similar situations. In all experiments without the instruction of self-location, the results showed consistent prior odds (2.2, 2.43, and 1.36 for Experiments 1a, 1b, and 3 respectively). When we used the prior odds of Experiment 1b to recover the observed weights of Experiment 1a and Experiment 3, the recovered observed weights were comparable to real mean observed weights (0.633 vs. 0.612 for Experiment 1a and 0.949 vs. 0.912 for Experiment 3), suggesting that these prior odds were exchangeable and thus consistent. Participants only appeared to use a different prior odd (0.152) when they were informed of their location in Experiment 2. As this is the first and only report of a consistent effect of prior knowledge when participants were not given instruction and a different effect of prior knowledge when participants were given instruction, further research in this area will help solidify and validate the significance of these findings.

The theoretical argument of distal dominance in orientations is widely used as a foundational assumption in research paradigms studying human navigation (e.g., Bullens et al.,

2010; Doeller & Burgess, 2008; Zhao & Warren, 2015a; Zhou & Mou, 2019). This argument considers the transient nature often associated with proximal landmarks (Cheng & Spetch, 1998) and also takes into account the less precise direction information provided by proximal landmarks due to motion parallax (Nadel & Hupbach, 2006). However, this theoretical argument has limitations as it does not fully consider the role of the vector between a proximal landmark and the navigator's self-location.

When people move in the environment, they can update the vector between a proximal landmark and their self-location (Etienne et al., 1996; Rieser, 1989; Wang & Spelke, 2002). This vector can provide orientation information especially when people walk a simple path. For example, individuals who walk three meters south from their camping tent and then spin themselves in place until losing orientation should regain their orientation by seeing the camping tent again, as they have updated the vector between the tent and their self-location during walking. The importance of the vector is more obvious in a familiar environment, in which the locations of objects are well learned. People should easily know their orientation when standing at the location of one object and seeing the location of the other object. At the campsite, for example, people who have learned their car is west of the camping tent should know they are facing east when standing beside the car and directly facing the tent. Consequently, the vector between a proximal landmark and people's self-location at one object can be sufficient to indicate orientations, making it not necessary to learn or use distal landmarks, potentially leading to proximal landmark dominance. In particular, when individuals have not thoroughly learned the distal landmark, relative cue precision favors the proximal landmark over the distal one, leading to proximal landmark dominance. Furthermore, this preference for proximal landmarks based on relative cue precision, established over time in environments individuals are familiar

with, can become a stored form of prior knowledge. This prior knowledge is then activated when participants encounter a familiar environment, further contributing to the dominance of proximal landmarks.

The current project provides clear evidence indicating the important role of the vector between a proximal landmark and the self-location in orientation estimates. When participants walked a simple path, the variances of heading estimates in the single cue conditions were comparable in Experiment 1a, showing comparable cue precision. Therefore, it is not always true that less precise direction information is provided by proximal landmarks due to motion parallax (Nadel & Hupbach, 2006). More strikingly, when participants were informed of their location at one object, a proximal landmark even dominated the heading estimates in the Conflict condition of Experiment 2. These findings provide compelling evidence that people rely on the vector between a proximal landmark and their self-location in orientation estimates. When this vector is precise and salient, the privileged status of distal landmarks in establishing orientation can be eliminated or even reversed.

The proximal dominance observed in Experiment 2 could indeed be attributed to the knowledge of the vector between the proximal landmark and the self-location overlapping one object. The experimental setup, where participants and the proximal landmark were positioned together at the center of an object array forming a rectangle, allowed participants to learn vectors from their self-location pointing to each object. During the navigation, participants moved to a new location in the environment and were then informed of their self-location being at one of the learned object's positions. At this point, participants could directly see the reappeared proximal landmark, which had been covertly shifted to a new location. This perceived vector, from the navigators' current location to the reappeared proximal landmark, corresponded to the reverse of

one of the previously learned vectors. Given this direct and salient perceived vector, participants might have efficiently used it to determine their orientation, which resulted in the observed proximal dominance in orientation estimates in Experiment 2. This finding underscores the significance of considering the influence of perceived vectors in navigation tasks, as it can override the traditional dominance of distal landmarks in orientation judgments.

As mentioned earlier, the direct and highly salient vector perceived from self-location to the landmark could contribute to the observed proximal dominance in Experiment 2, potentially influenced by relative cue precision, prior knowledge, or a combination of both. However, it is important to note that the relative cue precision in Experiment 2 did not predict proximal dominance ($W_{Predicted\_Dlm}$ = .539, not smaller than .5). The reason that the relative cue precision in Experiment 2 did not favor proximal landmarks may be attributed to the fact that participants were required to learn both distal and proximal landmarks in the current study, which might have resulted in comparable cue precision between distal and proximal landmarks even when participants were explicitly instructed of their self-location. In familiar environments of daily life, however, people may not need to learn distal landmarks and favor proximal landmarks.

The knowledge of the vector between the proximal landmark and the self-location overlapping one object might have been influenced by explicit instruction provided to the participants in Experiment 2. In contrast, in Experiment 3, where explicit verbal information was not given, participants did not show any top-down preference for the proximal cue and, instead, exhibited distal dominance. The lack of top-down preference for the proximal cue in Experiment 3 suggests that without explicit instruction, participants may not have been able to pinpoint their testing location unambiguously (see Figures S2.8 and S2.10), possibly due to error-prone path integration (e.g., Kelly et al., 2008). As a result, they may have faced difficulties in using the

knowledge of the vector between the proximal landmark and the self-location overlapping one object to assign more weight to proximal landmarks compared to what could be predicted based on relative cue precision.

Why should prior knowledge be considered in spatial orientation? Research indicates that the dominance of distal landmarks in the directional system may stem from evolutionary adaptations, which likely offered advantages to our ancestors in hunting and avoiding predators (Nadel & Hupbach, 2006; Renaudineau et al., 2007). Rapidly establishing their orientation and finding their way back to a safe shelter would have significantly enhanced their chances of survival. In this context, using prior knowledge favoring distal landmarks in orientations could have expedited spatial orientation and provided a reliable means of navigation in unfamiliar or open environments. Similarly, in a familiar environment with well-established spatial relationships between objects, using prior knowledge favoring proximal landmarks in orientation can also expedite spatial orientation. This strategy may be particularly effective in familiar settings, where proximity to known landmarks can quickly and accurately indicate one's orientation. Moreover, we speculate that the reliance of proximal landmarks could be a flexible and adaptive strategy contingent on the environment. For instance, in a consistently foggy environment, our ancestors might have favored proximal over distal cues. Overall, by incorporating both prior knowledge and the relative precision of individual cues, individuals can make more accurate and expedient decisions in orientation tasks. The choice of which prior knowledge to rely on likely varies with the environmental context.

There is one important methodological contribution from the current study. To thoroughly examine the influence of prior knowledge, we should manipulate prior knowledge. One straightforward approach is to provide participants with enough training examples so that they

can develop prior knowledge before the test. However, it is not clear if training examples are effective in developing prior knowledge different from the prior knowledge that participants have developed throughout their lives. Even if they are, it would be time-consuming to train. The current study suggests that we can use instruction to prime some prior knowledge (as in Experiment 2), as a more efficient way to manipulate prior knowledge.

2.8 Conclusions

The competition between proximal and distal landmarks in providing spatial orientation is indeed influenced by two seemingly independent crucial factors: the precision of each landmark in indicating orientation and the prior knowledge. In general, participants may have prior knowledge favoring distal landmarks as a superior orienting cue, which often results in distal dominance. However, the dynamics of this competition can change when navigators possess a clear and precise understanding of their position relative to a proximal landmark (for instance, they are informed that they are standing at a location they have previously learned). In such cases, they can choose the prior knowledge favoring the proximal landmark, leading to proximal dominance in orientation.

2.9 References

Batschelet, E. (1981). *Circular statistics in biology*. London, UK: Academic Press.

Benhamou, S., & Poucet, B. (1998). Landmark use by navigating rats (Rattus norvegicus) contrasting geometric and featural information. *Journal of Comparative Psychology, 112*(3), 317-322.

Brown, J. E., & Skaggs, W. E. (2002). Concordant and discordant coding of spatial location in populations of hippocampal CA1 pyramidal cells. *Journal of Neurophysiology, 88*(4), 1605-1613.

Buckley, M. G., Haselgrove, M., & Smith, A. D. (2015). The developmental trajectory of intramaze and extramaze landmark biases in spatial navigation: An unexpected journey. *Developmental Psychology, 51*(6), 771-791.

Bullens, J., Nardini, M., Doeller, C. F., Braddick, O., Postma, A., & Burgess, N. (2010). The role of landmarks and boundaries in the development of spatial memory. *Developmental Science, 13*(1), 170-180.

Chen, X., McNamara, T. P., Kelly, J. W., & Wolbers, T. (2017). Cue combination in human spatial navigation. *Cognitive Psychology, 95*, 105-144.

Cheng, K., & Newcombe, N. S. (2005). Is there a geometric module for spatial orientation? Squaring theory and evidence. *Psychonomic Bulletin & Review, 12*, 1-23.

Cheng, K., Shettleworth, S. J., Huttenlocher, J., & Rieser, J. J. (2007). Bayesian integration of spatial information. *Psychological Bulletin, 133*(4), 625-637.

Cheng, K., & Spetch, M. L. (1998). *Mechanisms of landmark use in mammals and birds*. In S. Healy (Ed.), Spatial representation in animals (pp. 1–17). Oxford University Press.

Cressant, A., Muller, R. U., & Poucet, B. (1997). Failure of centrally placed objects to control the firing fields of hippocampal place cells. *Journal of Neuroscience, 17*(7), 2531-2542.

Doeller, C. F., & Burgess, N. (2008). Distinct error-correcting and incidental learning of location relative to landmarks and boundaries. *Proceedings of the National Academy of Sciences, 105*(15), 5909-5914.

Douglas, R. M., Alam, N. M., Silver, B. D., McGill, T. J., Tschetter, W. W., & Prusky, G. T. (2005). Independent visual threshold measurements in the two eyes of freely moving rats and mice using a virtual-reality optokinetic system. *Visual Neuroscience, 22*(5), 677-684.

Ekstrom, A. D. (2015). Why vision is important to how we navigate. *Hippocampus, 25*(6), 731-735.

Etienne, A. S., & Jeffery, K. J. (2004). Path integration in mammals. *Hippocampus, 14*(2), 180-192.

Etienne, A. S., Maurer, R., & Séguinot, V. (1996). Path integration in mammals and its interaction with visual landmarks. *Journal of Experimental Biology, 199*(1), 201-209.

Foo, P., Warren, W. H., Duchon, A., & Tarr, M. J. (2005). Do humans integrate routes into a cognitive map? Map-versus landmark-based navigation of novel shortcuts. *Journal of Experimental Psychology: Learning, Memory, and Cognition, 31(2)*, 195-215.

Friedman, A., & Kohler, B. (2003). Bidimensional regression: Assessing the configural similarity and accuracy of cognitive maps and other two-dimensional data sets. *Psychological Methods, 8*(4), 468-491.

Gallistel, C. R. (1990). *The organization of learning.* The MIT Press.

Harootonian, S. K., Wilson, R. C., Hejtmánek, L., Ziskin, E. M., & Ekstrom, A. D. (2020). Path integration in large-scale space and with novel geometries: Comparing vector addition and encoding-error models. *PLoS Computational Biology*, *16*(5), e1007489.

Hebb, D. O. (1938). Studies of the organization of behavior. I. Behavior of the rat in a field orientation. *Journal of Comparative Psychology*, *25*(2), 333-352.

Hebb, D. O. (1949). *The organization of behaviour*. Wiley-Interscience, New York.

Huttenlocher, J., Hedges, L. V., & Duncan, S. (1991). Categories and particulars: Prototype effects in estimating spatial location. *Psychological Review, 98*(3), 352-376.

Jacobs, L. F., & Schenk, F. (2003). Unpacking the cognitive map: the parallel map theory of hippocampal function. *Psychological Review, 110*(2), 285-315.

Kearns, M. J., Warren, W. H., Duchon, A. P., & Tarr, M. J. (2002). Path integration from optic flow and body senses in a homing task. *Perception, 31*, 349-374.

Kelly, J. W., McNamara, T. P., Bodenheimer, B., Carr, T. H., & Rieser, J. J. (2008). The shape of human navigation: How environmental geometry is used in maintenance of spatial orientation. *Cognition, 109*(2), 281-286.

Knierim, J. J. (2002). Dynamic interactions between local surface cues, distal landmarks, and intrinsic circuitry in hippocampal place cells. *Journal of Neuroscience, 22*(14), 6254-6264.

Knierim, J. J., & Hamilton, D. A. (2011). Framing spatial cognition: Neural representations of proximal and distal frames of reference and their roles in navigation. *Physiological Reviews, 91*(4), 1245-1279.

Kravitz, D. J., Saleem, K. S., Baker, C. I., Ungerleider, L. G., & Mishkin, M. (2013). The ventral visual pathway: An expanded neural framework for the processing of object quality. *Trends in Cognitive Sciences, 17*(1), 26-49.

Learmonth, A. E., Nadel, L., & Newcombe, N. S. (2002). Children's use of landmarks: Implications for modularity theory. *Psychological Science, 13*(4), 337-341.

Lee, S. A., & Spelke, E. S. (2010). A modular geometric mechanism for reorientation in children. *Cognitive Psychology, 61*(2), 152-176.

Lei, X., & Mou, W. (2023). Visual re-anchoring in misaligned local spaces impairs global path integration. *Journal of Experimental Psychology: Learning, Memory, and Cognition*. *49*(5), 728-742.

Lew, A. R. (2011). Looking beyond the boundaries: Time to put landmarks back on the cognitive map?. *Psychological Bulletin, 137*(3), 484-507.

McNamara, T. P., & Chen, X. (2022). Bayesian decision theory and navigation. *Psychonomic Bulletin & Review*, *29*, 721-752

Mittelstaedt, H., & Mittelstaedt, M. L. (1982). *Homing by path integration.* In Avian navigation (pp. 290-297). Springer, Berlin, Heidelberg.

Mou, W., & Zhang, L. (2014). Dissociating position and heading estimations: Rotated visual orientation cues perceived after walking reset headings but not positions. *Cognition, 133*(3), 553-571.

Nadel, L., & Haupbach, A. (2006). Species comparisons in development: The case of the geometric 'module'. *Processes of Change in Brain and Cognitive Development: Attention and Performance XXI*, 499-511.

Nardini, M., Jones, P., Bedford, R., & Braddick, O. (2008). Development of cue integration in human navigation. *Current Biology, 18*(9), 689-693.

Negen, J., Bird, L. A., King, E., & Nardini, M. (2020). The difficulty of effectively using allocentric prior information in a spatial recall task. *Scientific Reports*, *10*(1), 7000.

Newman, P. M., Qi, Y., Mou, W., & McNamara, T. P. (2023). Statistically optimal cue integration during human spatial navigation. *Psychonomic Bulletin & Review*, 1-22.

O'Keefe, J., & Nadel, L. (1978). *The hippocampus as a cognitive map* (Vol. 3, pp. 483-484). Oxford: Clarendon Press.

O'Keefe, J., & Speakman, A. 1. (1987). Single unit activity in the rat hippocampus during a spatial memory task. *Experimental Brain Research, 68*, 1-27.

Padilla, L. M., Creem-Regehr, S. H., Stefanucci, J. K., & Cashdan, E. A. (2017). Sex differences in virtual navigation influenced by scale and navigation experience. *Psychonomic Bulletin & Review, 24*, 582-590.

Parron, C., Poucet, B., & Save, E. (2004). Entorhinal cortex lesions impair the use of distal but not proximal landmarks during place navigation in the rat. *Behavioural Brain Research, 154*(2), 345-352.

Pecchia, T., & Vallortigara, G. (2010). View-based strategy for reorientation by geometry. *Journal of Experimental Biology, 213*(17), 2987-2996.

Petzschner, F. H., & Glasauer, S. (2011). Iterative Bayesian estimation as an explanation for range and regression effects: A study on human path integration. *Journal of Neuroscience, 31*(47), 17220-17229.

Petzschner, F. H., Maier, P., & Glasauer, S. (2012). Combining symbolic cues with sensory input and prior experience in an iterative Bayesian framework. *Frontiers in Integrative Neuroscience*, *6*, 58.

Renaudineau, S., Poucet, B., & Save, E. (2007). Flexible use of proximal objects and distal cues by hippocampal place cells. *Hippocampus, 17*(5), 381-395.

Rieser, J. J. (1989). Access to knowledge of spatial structure at novel points of observation. *Journal of Experimental Psychology: Learning, Memory, and Cognition*, *15*(6), 1157-1165.

Rieser, J. J., & Rider, E. A. (1991). Young children's spatial orientation with respect to multiple targets when walking without vision. *Developmental Psychology, 27*(1), 97-107.

Roy, C., Wiebusch, D., Botsch, M., & Ernst, M. O. (2023). Did it move? Humans use spatio-temporal landmark permanency efficiently for navigation. *Journal of Experimental Psychology: General, 152*(2), 448-463.

Sampaio, C., Jones, M., Engelbertson, A., & Williams, M. (2020). Bayesian priors in estimates of object location in virtual reality. *Psychonomic Bulletin & Review, 27*, 1309-1316.

Shapiro, M. L., Tanila, H., & Eichenbaum, H. (1997). Cues that hippocampal place cells encode: Dynamic and hierarchical representation of local and distal stimuli. *Hippocampus, 7*(6), 624-642.

Tanila, H., Shapiro, M. L., & Eichenbaum, H. (1997). Discordance of spatial representation in ensembles of hippocampal place cells. *Hippocampus, 7*(6), 613-623.

Wallace, D. J., Greenberg, D. S., Sawinski, J., Rulla, S., Notaro, G., & Kerr, J. N. (2013). Rats maintain an overhead binocular field at the expense of constant fusion. *Nature, 498*(7452), 65-69.

Wang, L., & Mou, W. (2020). Effect of room size on geometry and features cue preference during reorientation: Modulating encoding strength or cue weighting. *Quarterly Journal of Experimental Psychology, 73*(2), 225-238.

Wang, L., Mou, W., & Dixon, P. (2018). Cue interaction between buildings and street configurations during reorientation in familiar and unfamiliar outdoor environments. *Journal of Experimental Psychology: Learning, Memory, and Cognition, 44*(4), 631-644.

Wang, R. F., & Brockmole, J. R. (2003). Human navigation in nested environments. *Journal of Experimental Psychology: Learning, Memory, and Cognition*, *29*(3), 398-404.

Wang, R. F., & Spelke, E. S. (2002). Human spatial representation: Insights from animals. *Trends in Cognitive Sciences*, *6*(9), 376-382.

Wehner, R., Michel, B., & Antonsen, P. (1996). Visual navigation in insects: Coupling of egocentric and geocentric information. *Journal of Experimental Biology, 199(1)*, 129-140.

Wilson, P. N., & Alexander, T. (2008). Blocking of spatial learning between enclosure geometry and a local landmark. *Journal of Experimental Psychology: Learning, Memory, and Cognition, 34*(6), 1369-1376.

Yoganarasimha, D., Yu, X., & Knierim, J. J. (2006). Head direction cell representations maintain internal coherence during conflicting proximal and distal cue rotations: Comparison with hippocampal place cells. *Journal of Neuroscience, 26*(2), 622-631.

Zhang, L., & Mou, W. (2017). Piloting systems reset path integration systems during position estimation. *Journal of Experimental Psychology: Learning, Memory, and Cognition, 43*(3), 472-491.

Zhang, L., Mou, W., Lei, X., & Du, Y. (2020). Cue combination used to update the navigator's self-localization, not the home location. *Journal of Experimental Psychology: Learning, Memory, and Cognition. 46*(12), 2314-2339.

Zhao, M., & Warren, W. H. (2015a). How you get there from here: Interaction of visual landmarks and path integration in human navigation. *Psychological Science, 26*(6), 915-924.

Zhao, M., & Warren, W. H. (2015b). Environmental stability modulates the role of path integration in human navigation. *Cognition, 142*, 96-109.

Zhou, R., & Mou, W. (2019). The effects of cue placement on the relative dominance of boundaries and landmark arrays in goal localization. *Quarterly Journal of Experimental Psychology*, *72*(11), 2614-2631.

Zugaro, M. B., Berthoz, A., & Wiener, S. I. (2001). Background, but not foreground, spatial cues are taken as references for head direction responses by rat anterodorsal thalamus neurons. *The Journal of neuroscience, 21*(14), RC154.

Chapter 3 Sources of systematic errors in human path integration

3.1 Abstract

Triangle completion is a task widely used to study human path integration, an important navigation method relying on idiothetic cues. Systematic biases (compression patterns in the inbound responses) have been well documented in human triangle completion. However, the sources of systematic biases remain controversial. We used cross-validation modeling to compare three plausible theoretical models that assume that systematic errors occur in the encoding outbound path solely (encoding-error model), executing the inbound responses solely (execution-error model), and both (bi-component model), respectively. The data for cross-validation modeling are from a previous study (Qi et al., 2021), in which participants learned three objects' locations (one at the path origin, that is, home) very well before walking each outbound path and then pointed to the objects' original locations after walking the outbound path. The modeling algorithm used one inbound response (i.e., response to the home) or multiple inbound responses (i.e., responses to two non-home locations and the home) for each outbound path. The algorithm of using multiple inbound responses demonstrated that the bi-component model outperformed the other models in accounting for the systematic errors. This finding suggests that both encoding the outbound path and executing the inbound responses contribute to the systematic biases in human path integration. In addition, the results showed that the algorithm using only the home response could not distinguish among these three models, suggesting that the typical triangle-completion task with only the home response for each outbound path cannot determine the sources of the systematic biases.

Keywords: path integration; encoding-error model; execution-error model, cross-validation; triangle completion

3.2 Introduction

Path integration is the navigation process that employs idiothetic cues (i.e., proprioception, vestibular, and optic flow) and integrates the distances traveled and angles turned during motion so that navigators can continuously update their position and heading with respect to fixed reference locations in space (Etienne et al., 1996; Mittelstaedt & Mittelstaedt, 1982). The fixed locations can be the origin of the path traveled (e.g., the nest for an animal who is out for foraging) or remembered important locations in the environment (e.g., the grocery store for a human individual who will visit later after traveling from home to office). Thus, path integration plays an important role in navigation, especially when allothetic cues (e.g., visual landmarks) are scarce or navigation occurs in darkness (Klatzky et al., 1998).

Path integration is ubiquitous among mobile animals, including ants (Müller & Wehner, 1988), bees (Collett & Collett, 2000), rodents (Etienne & Jeffery, 2004), birds (Saint Paul, 1982), mammals (Mittelstaedt & Mittelstaedt, 1980), and humans (Loomis et al., 1999). Critically, path integration has been suggested as one important means of constructing spatial knowledge of the environment (Gallistel, 1990). By tracking the path lengths and turn angles, and linking routes between known places, path integration enables one to acquire a labeled graph that incorporates local metric information (Chrastil & Warren, 2014; Warren et al., 2017) or a cognitive map that includes globally consistent metric information (Jacobs & Schenk, 2003; Wang, 2016).

Path integration is not an error-free process. Errors in path integration can be accumulated quickly with the increase of the complexity of the path, for example with the increase of the number of legs in a path (Kelly et al., 2008; Rieser & Rider, 1991). Previous studies using triangle-completion tasks have found that the human participants' homebound behavior exhibits systematic distortion (Kearns et al., 2002; Klatzky et al., 1999; Loomis et al.,

1993). In the triangle-completion task, participants walked an outbound path, which consists of two linear segments and a turn angle between them, and then returned to or pointed to the origin of the outbound path (Klatzky et al., 1998; Loomis et al., 1993). Participants' responses of the inbound path (i.e., homing vector) include the turn angle and path length. Participants usually overshot small values, and conversely, undershot large values, showing a compression pattern relative to the correct values of both turn angle and path length. This systematic distortion was distinguished from random errors (Chrastil & Warren, 2017; Harootonian et al., 2020).

A compression pattern relative to the correct values has been widely and long reported in magnitude judgments of various types of stimuli including size, weight, brightness, loudness, and duration (Stevens & Greenbaum, 1966). Stevens and Greenbaum (1966) referred to the compression pattern as the regression effect and attributed the effect primarily to participants' tendency to shrink the judgment range under their control. Other researchers attributed the compression pattern to the stimulus range controlled by experimenters (e.g., Teghtsoonian & Teghtsoonian, 1978). Petzschner and Glasauer (2011) proposed a Bayesian model to explain the compression pattern in reproducing a previewed distance or angle. Participants in their study walked a distance to approach a visible target or turned an angle to face a visible target. They then reproduced the distance or angle without the presence of the target. The results showed that participants biased their reproduced magnitudes towards the mean of the previewed magnitudes. Hence, participants not only used the perceived magnitudes in the specific trial but also used the prior distribution of the magnitudes (Harootonian et al., 2022; McNamara & Chen, 2021). The prior knowledge could be learned from past trials (see also Harootonian et al., 2020). Note that other studies suggested that prior knowledge could be primarily determined by experiences outside the experiment (e.g., categorical information, Huttenlocher et al., 1991).

A strict Bayesian approach assumes that separate estimates of the true value (prior or perceived magnitude) are combined in judgment but do not change the representation of the perceived magnitude (Zhang & Mou, 2017). Hence, the representation of the perceived magnitude should be free of compression. However, to explain the compression pattern reported in the triangle-completion task, researchers proposed that compression could occur both in executing the inbound path (Chrastil & Warren, 2021) and in encoding the outbound path (Fujita et al., 1993; Harootonian et al., 2020). The latter proposal implies that participants might use the Bayesian inference in encoding rather than in response. Thus, examining the sources of the compression pattern reported in triangle completion is not only theoretically important in human navigation but also in broad fields of experimental psychology.

Performing the triangle-completion task requires three cognitive stages (Fujita et al., 1993). The initial stage involves sensing the traversed path and forming internal representations of leg lengths and turn angles, referred to as the encoding process. In the second stage, the internalized representations are employed to compute the desired inbound responses (i.e., inbound path length and turn angle), referred to as the integration process. Ultimately, the desired inbound response is executed, referred to as the execution process. The important yet inconclusive theoretical question is which stage or stages the systematic errors originate from (Chrastil & Warren, 2021; Fujita et al., 1993; Harootonian et al., 2020). Answering this question is important to advance our understanding of the nature of human path integration.

One intuitive answer is that systematic errors in the inbound path length and turn angle originated from the execution process. However, Klatzky, Loomis, and their colleagues (Fujita et al., 1993; Klatzky et al., 1999; Loomis et al., 1999) provided innovative insights that systematic errors in encoding the outbound path can also well explain the systematic errors appearing in the

inbound path length and turn angle. Their influential model, the encoding-error model, assumes that while the systematic errors originate from encoding the outbound path, the subsequent processes, i.e., computing the desired inbound responses via cognitive trigonometry and executing it, are free of systematic errors (Fujita et al., 1993).

There are three important theoretical contributions of the encoding-error model. First, it indicates that *counter-intuitively* the systematic errors appearing in response measures may not originate from execution and instead from encoding. Second, it suggests that human path integration may significantly differ from animal path integration. Animals may only represent and update the homing vector but do not encode the outbound path in memory (e.g., Benhamou & Séguinot, 1995; Etienne & Jeffery, 2004; Wehner et al., 1996). This type of spatial updating is referred to as continuous updating. In contrast, spatial updating with encoding of the outbound path in memory is referred to as configural updating (He & McNamara, 2018; Loomis et al., 1999; Wiener et al., 2011). Hence, while researchers hypothesize that animal path integration is continuous updating (Wiener et al., 2011, p. 62), the encoding-error model suggests that human path integration is configural updating. Last, the encoding-error model suggests that humans can develop configural knowledge of the outbound path. This configural knowledge is different from route knowledge because the configural knowledge can support a novel short-cut between two points on the outbound path and thus is more like a survey (map-like) knowledge. Therefore, path integration can be a means to develop map-like knowledge (Gallistel, 1990).

More specifically, the encoding-error model stipulates that there are two linear functions, the encoding function of leg lengths and the encoding function of turn angles, which determine the encoded values from the actual values of the outbound path. Each encoding function has two parameters, the slope, and the intercept. Therefore, for each given outbound path, the

corresponding internal representation of the path can be described by the encoding functions. As a result, the desired inbound response can be calculated from the encoding functions assuming no systematic bias in the integration process. Given that the desired inbound response is executed without systematic bias, the encoding-error model can predict the participants' inbound response, at least on average. Fujita et al. (1993) fit the encoding-error model with empirical data of triangle completion. They estimated the parameters of the encoding functions by minimizing the discrepancy between the model's predictions and participants' actual responses to the path origins. For both functions, the slope tended to be smaller than 1 and the intercept tended to be larger than 0, showing a compression pattern of the encoded values relative to the correct values. Moreover, the modeling results showed that the encoding-error model fit the data very well. The performance of the encoding-error model was still impressive when data from other studies were applied, suggesting that encoding distortion captured the path integration errors under a variety of situations (Klatzky et al., 1999; May & Klatzky, 2000; Péruch et al., 1997; Wartenberg et al., 1998).

However, the demonstration that systematic distortion can be attributed to the encoding component (Fujita et al., 1993) does not exclude the possibility that systematic distortion can also be attributed to the execution component alone (referred to as the execution-error model). Intuitively, an execution-error model stipulating that execution errors follow a compression pattern (a linear function to predict the response values from the correct values with a slope less than 1 and an intercept larger than 0) can readily explain the observed compression pattern of the response values relative to the correct values. Thus, it is challenging to dissociate the encoding-error model from the execution-error model empirically. We speculate that due to this challenge, Fujita et al. (1993) did not contrast the encoding-error model with the execution-error model to

prove the relative superiority of the encoding-error model. Although testing the encoding-error model is theoretically critical, no other modeling work had been conducted to further test the encoding-error model until two recent studies reported by Harootonian et al. (2020) and Chrastil and Warren (2021).

Harootonian et al. (2020) still assumed that systematic errors occur in the encoding process rather than in the integration or execution process, similar to the original encoding-error model. However, they proposed that the systematic errors primarily occur in encoding the leg lengths but not in encoding the turn angles whereas the original encoding-error model claimed systematic errors in both leg lengths and turn angles of the outbound path. Furthermore, different encoding functions were used for the lengths of the first and the second legs whereas the original encoding-error model used one common function for both legs. They fit their model and the original encoding-error model to data in a triangle-completion task in which participants returned home after walking an outbound path on an omnidirectional treadmill. The model comparison results showed superior performance of their model over the original encoding-error model. However, as designed to examine variants of the encoding-error model, this study still cannot distinguish between the encoding-error model and the execution-error model.

More relevantly, Chrastil and Warren (2021) tested models of encoding errors solely, execution errors solely, and both types of errors. In their study, participants did both simple tasks (e.g., distance or angle reproduction tasks) and triangle-completion tasks. They used data of *reproduction tasks* to estimate the parameters of the encoding and execution functions for triangle-completion tasks. Then the three models, using the corresponding functions (e.g., an encoding-error model used the encoding functions), generated the predictions for the inbound response errors in the triangle-completion task. The results of the model comparison showed that

the execution-error model performed better than the encoding-error model. Furthermore, the model including both types of errors did not perform better than the execution-error model. These results suggest that the observed systematic errors in inbound responses were sufficiently explained by the systematic errors in executing the inbound path, but not by the systematic errors in encoding the outbound path. The finding of Chrastil and Warren (2021) is theoretically important as it is the first modeling work clearly indicating that systematic errors in the human triangle-completion task are not solely contributed to the encoding errors, undermining the key argument of the encoding-error model (Fujita et al., 1993).

However, the finding of Chrastil and Warren (2021) could not decisively lead to the conclusion that systematic errors in inbound responses are primarily attributed to systematic execution errors either. One critical concern is whether the reproduction tasks that Chrastil and Warren (2021) employed could truly measure parameters for the *pure* encoding and execution functions. In particular, in their reproduction tasks, participants walked a distance or turned an angle (encoding path). After being stopped by a sound, they reproduced the distance or the angle (response path). By assuming that there were only systematic encoding errors in the encoding path or only systematic execution errors in the response path, Chrastil and Warren separately estimated the parameters of the encoding and execution functions from the reproduction tasks. However, their assumption may be inaccurate because there could be both systematic errors in encoding and execution (Chrastil & Warren, 2014).

Chrastil and Warren (2021) also measured the distance error in a blind-walking task. They then subtracted the errors in the blind-walking task from the errors in the reproduction task to get the pure encoding function. Specifically, in blind-walking, participants perceived an egocentric distance visually and then walked an equivalent distance while being blindfolded

(Chrastil & Warren, 2014). Assuming that there were no systematic encoding errors in perceiving an egocentric distance visually and considering that the response path was the same in the blind walking and the reproduction task, Chrastil and Warren attributed the difference of the errors in these two tasks to the pure encoding errors. Nevertheless, visual perceiving distance may introduce systematic encoding errors. Previous research suggested that there is a calibration/recoupling between locomotor displacement and the visually perceived distance (Rieser et al., 1990; 1995), hence systematic encoding errors in locomotion may also occur in visual perceiving distance. Consequently, these methods were not perfect to estimate either encoding or execution functions if there were indeed both systematic encoding and execution errors. In addition, one may also wonder whether the functions derived from the reproduction tasks are the same as those used in a much more complicated triangle-completion task.

Therefore, the sources of systematic biases in the inbound responses of the triangle-completion task are still not clear. The primary purpose of the current study was to further test the sources of systematic biases. Adopting a model cross-validation approach (Arlot & Celisse, 2010; Refaeilzadeh et al., 2009), we tested three models: the encoding-error model, the execution-error model, and a bi-component model with both encoding and execution biases. We used the data of the triangle-completion task from Qi et al. (2021) for both model fitting and model validation. In the step of model fitting, we used half data to estimate the parameters of different models (i.e., encoding functions for the encoding-error model, execution functions for the execution-error model, and both functions for the bi-component model). In the step of model validation, we compared the performance of the three models in explaining the other half data. Because we estimated the parameters of encoding/execution functions directly using the data of

the triangle-completion task, we avoided the issues of estimating encoding/execution functions from other independent tasks (e.g., reproduction tasks) discussed above.

Note that in a typical triangle-completion task, participants had one inbound response (i.e., homing vector) for each outbound path. Mou and Zhang (2014) indicated that from only one inbound response, researchers cannot correctly recover (or calculate) participants' representations of their positions and orientations that guide their inbound responses at the end of the outbound path. They argued that many possible pairs of position and orientation representations at the end of the outbound path could lead to the same homing vector. Because position and orientation representations at the end of the outbound path are not only the outcome of the represented outbound path but also determine the desired inbound responses, we conjectured that from one inbound response, we could not determine the represented outbound path and desired inbound responses. Mou and Zhang (2014) further demonstrated that from multiple inbound responses, they could calculate participants' representations of their position and orientation at the end of the outbound path (see also Qi et al., 2021; Zhang & Mou, 2017; Zhang et al., 2020). Following this result, we conjectured that from multiple inbound responses for one single outbound path, we could determine the represented outbound path and the desired inbound responses and then could estimate the encoding and execution functions. Unlike the typical triangle-completion task in which participants only need to make a single response (i.e., the homing vector), participants in Qi et al. (2021) were required to indicate multiple locations (including home location) that they had learned before walking a two-segment path. Thus, using the data from Qi et al. (2021), the current study validated models using multiple inbound responses for each outbound path.

3.3 Current study

3.3.1 Description of the data

The data used for model fitting and model validation in the current study came from the path integration conditions of the four experiments in Qi et al. (2021)[7]. Figure 3.1 illustrates the path configurations and object arrays used in the four experiments of Qi et al. (2021). The experimental task was conducted in an immersive virtual environment. Participants in Qi et al. (2021) learned the locations of three objects (i.e., A, B, and C in Figure 3.1) while standing at the origin O (i.e., the home location). O overlapped with either B or C across experiments. After learning, the objects disappeared. Participants traveled along the two outbound legs, i.e., OT and TP. At the endpoint of the outbound path (i.e., P), participants reported the three objects' locations (including home location) by pinpointing the locations individually on the floor using a virtual stick in different cue conditions. Relevant to the current study, participants in the path integration condition only had iditothetic cues. There were 28 participants in each of the four experiments (112 participants in total). Each participant completed 8 outbound paths (three responses for each path) in the path integration condition.

As depicted in Figure 3.1, the length of the outbound path can be 0.9 m or 1.8 m. And the turn angle on the outbound path can be -20º, ±50º, -70º, ±80º, ±100º, 110º, ±130º, or 160º relative to the direction along the first outbound leg OT (reference direction). Clockwise is positive.

---

[7] The primary purpose of Qi et al. (2021) was to investigate how people combine self-motion and landmark cues to find home and non-home goal locations. Qi et al. (2021) did not examine the sources of systematic errors of path integration.

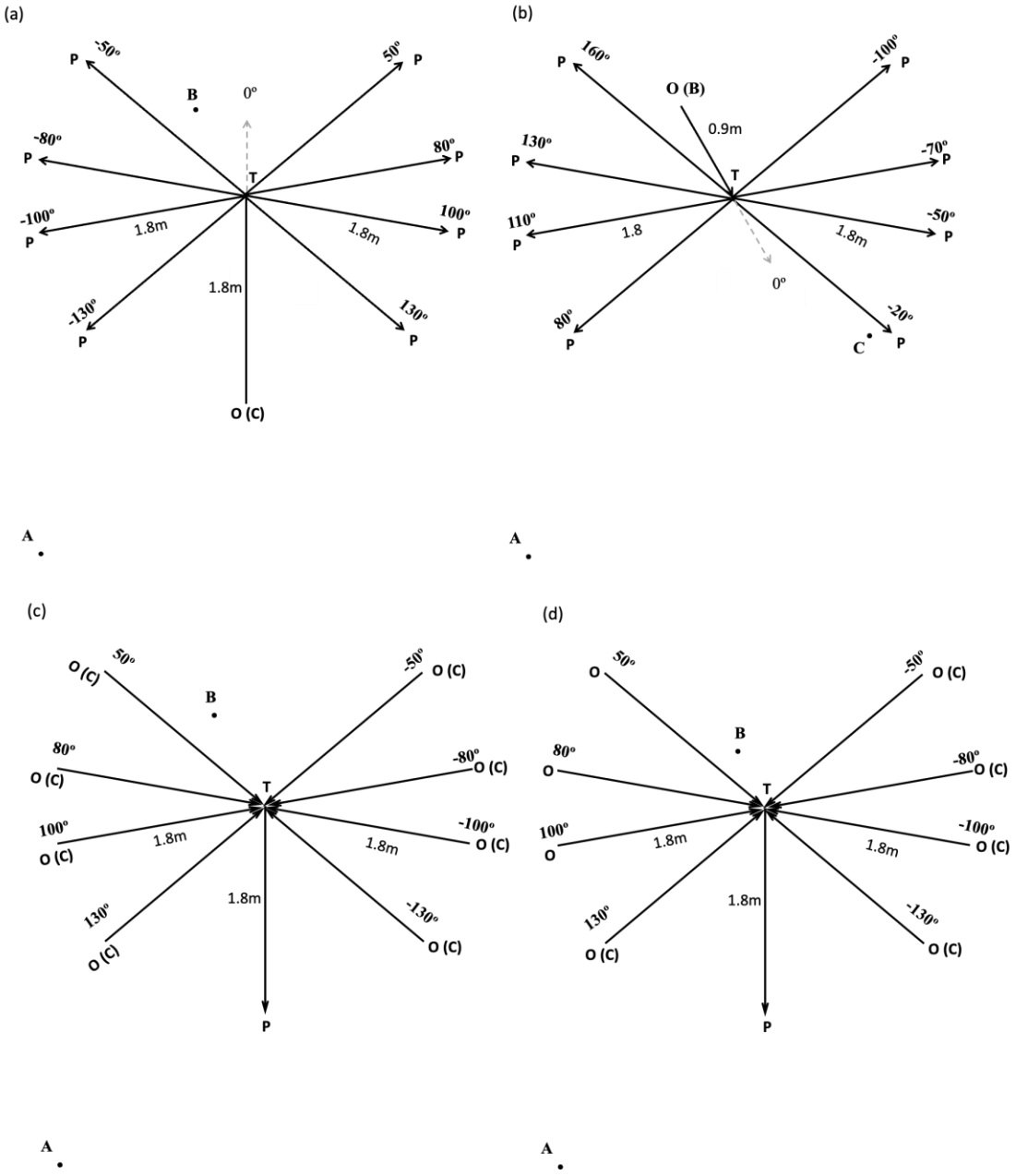

Figure 3.1. The schematic of outbound path configurations and locations of target objects in four experiments (a, b, c, and d corresponding to experiments 1, 2, 3, and 4 respectively) of Qi et al. (2021). O is the learning location and A, B, and C are the three target locations. An outbound path is comprised of origin O, turning point T, and end point P. The values of turn angles (positive if participants turned right from the direction of OT) and leg lengths are superimposed on each outbound path.

3.3.2 The compression pattern of the response inbound path length and turn angle

The response measures include the inbound path length and the inbound turn angle for each target location (A, B, and C in Figure 3.1). Figure 3.2 depicts examples of the response measures for a target location overlapping with the origin (home target, O) and for a non-home target (A).

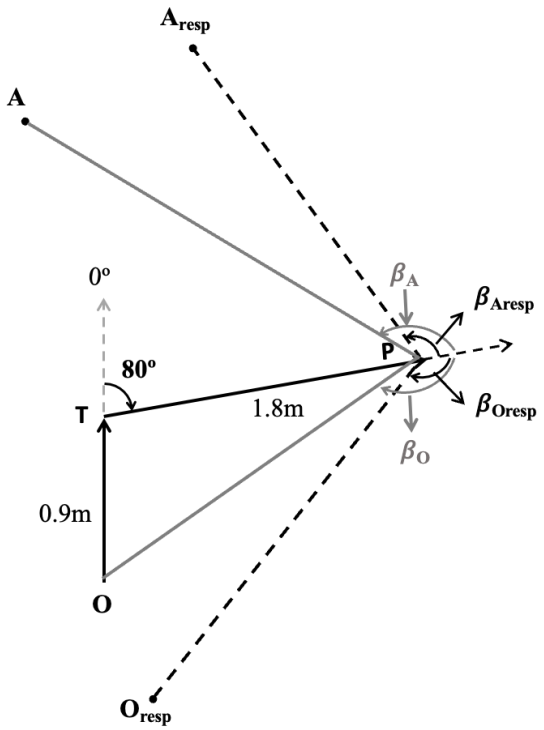

Figure 3.2. Illustrating the response measures of the current study. O and A are the correct locations of two targets whereas O_{resp} and A_{resp} are the response locations of two targets (O is the home, A is a non-home target). β_O and β_A are the correct inbound turn angles for the targets O and A. β_{Oresp} and β_{Aresp} are the response inbound turn angles for the targets O and A.

The response inbound path length (e.g., PO_{resp}) is the length between the end of the outbound path (i.e., P) and the response target location that the participant pinpointed using a virtual stick (e.g., O_{resp}). The response inbound turn angle (e.g., β_{Oresp}) is the angular difference between the participant's heading at P (i.e., the direction of TP) and the direction from P to the response target location (e.g., O_{resp}). The correct inbound path length (e.g., PO) is the length between the end of the outbound path (i.e., P) and the correct target location (e.g., O). The correct inbound turn angle (e.g., β_O) is the angular difference between the participant's heading at P (i.e., the direction of TP) and the direction from P to the correct target location (e.g., O). In the rest of this paper, we will only use O to represent all target locations regardless of whether it is the home location or non-home location.

Figure 3.3A plots the response inbound path length (including all three target objects for each outbound path) as a function of correct inbound path length, yielding a linear regression line (the yellow line with markers in Figure 3.3A) with a slope less than 1 and a positive intercept ($y = 0.633x + 2.201$, $r = .243$). That is, participants tended to overshoot the small distances that they were supposed to produce and reversely, tended to undershoot the large distances. Figure 3.3B plots the response inbound turn angle as a function of the correct inbound turn angle, yielding a linear regression line with a slope less than 1 and a positive intercept ($y = 0.864x + 28.257$, $r = .632$). That is, participants overturned small angles and underturned large angles. Overall, consistent with previous research (Klatzky et al., 1990; Loomis et al., 1993), the current study confirmed a compression pattern relative to correct values of the inbound responses in triangle completion. Note that the regression line did not cross with the diagonal line (y = x) at the mean of x, referred to as *bias to the mean*, for either length (mean = 2.5m) or angle (mean = 129º). Instead, participants overestimated all correct lengths and angles (referred to as *bias to the upper*

extreme). Findings of *bias to the extremes* rather than *bias to the mean* were reported in previous studies (e.g., Chrastil & Warren, 2020, Figure 3.7A for length; Harootonian et al., 2020, for angle and length; Klatzky et al., 1999, Figure 3.3 for angle; also see Stevens & Greenbaum, 1966 for a variety of different stimuli). The results of *biases to the extreme* could occur because participants might use the prior distribution of the encoding values and response values from their experiences prior to the experiment (Klatzky et al., 1999) as well as from their experiences in the prior trials (Harootonian et al., 2020; Petzschner & Glasauer, 2011). Specifically, participants in the current study might have the overall bias to point to their back (categorical information about the prior, Huttenlocher et al., 1991) because 80% of the correct angles (2156/2688) were larger than 90º (see Figure S3.1). In addition, Mou and Zhang (2014) suggested that participants might overall overestimate the inbound lengths using a virtual stick for pointing responses because the length of the virtual stick might be underestimated in virtual environments, which might partially explain the *bias to the upper extreme* for length.

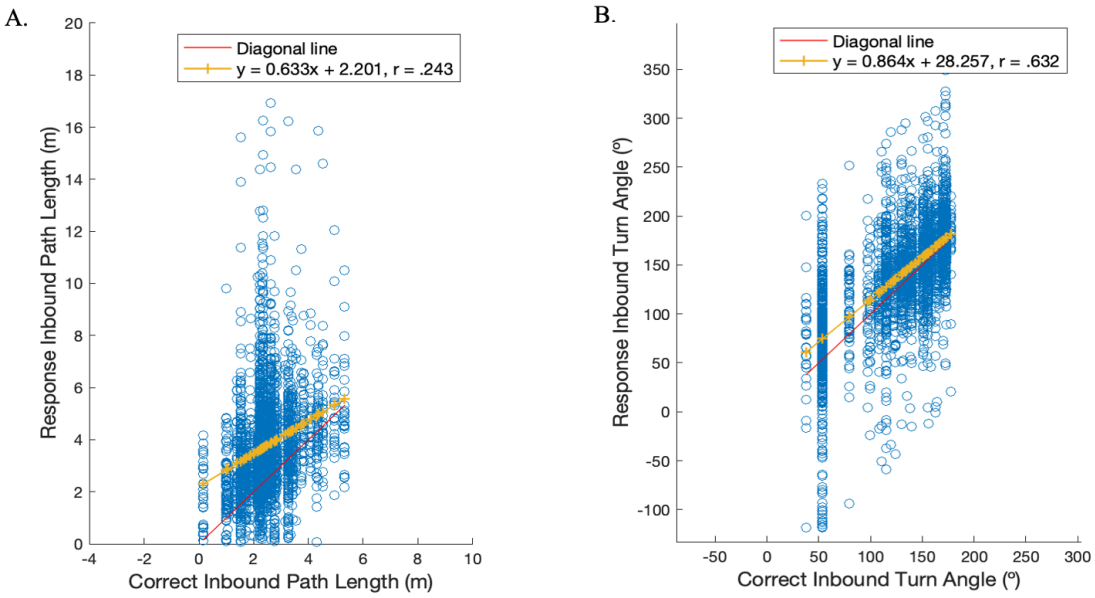

Figure 3.3. (A) The response inbound length as a function of the correct inbound length. (B) The response inbound turn angle as a function of the correct inbound turn angle. The diagonal lines in red (y = x) indicate the perfect inbound response. The yellow lines indicate the regression lines. Each dot indicates one individual pair of predicted and response values from all three targets and all 896 outbound paths (2688 dots in total).

3.4 Specifications of individual models

To examine the sources of the compression patterns of inbound responses relative to the correct values, we formulated three theoretically plausible models (i.e., the encoding-error model, the execution-error model, and the bi-component model). In addition, we also included a baseline model that assumes no systematic bias and used the correct values as the predicted values for the inbound responses.

3.4.1 The encoding-error model

The encoding functions of the outbound path length and the outbound turn angle comprise a set of 4 parameters, 2 for each function. $\theta_{L\_s}^{enc}$, $\theta_{L\_i}^{enc}$ are the slope and the intercept of the linear function for encoding the outbound path length whereas $\theta_{A\_s}^{enc}$, $\theta_{A\_i}^{enc}$ are the slope and the intercept of the linear function for encoding the outbound turn angle. Same as the original encoding-error model, $\theta_{L\_s}^{enc}$, $\theta_{L\_i}^{enc}$ are used for both the first and second legs of the outbound path. Thus, the encoded values of leg length L_e and turn angle α_e can be represented with these parameters,

$$L_e = \theta_{L\_s}^{enc} \times L + \theta_{L\_i}^{enc}, \quad (1)$$

$$\alpha_e = \theta_{A\_s}^{enc} \times \alpha + \theta_{A\_i}^{enc}, \quad (2)$$

where L and α are the correct length and turn angle of the outbound path, respectively (see values in Figure 3.1).

As depicted in Figure 3.4A, hypothetical participants encode outbound segment L1, L2, and turn angle α as L_{1e}, L_{2e}, and α_e. According to Formulas 1 and 2, $L_{1e} = \theta_{L\_s}^{enc} \times L1 + \theta_{L\_i}^{enc}$, $L_{2e} = \theta_{L\_s}^{enc} \times L2 + \theta_{L\_i}^{enc}$, $\alpha_e = \theta_{A\_s}^{enc} \times \alpha + \theta_{A\_i}^{enc}$.

In a Cartesian coordinate system, by means of theorems of trigonometry, the encoded outbound path can be represented in terms of vectors, $\overrightarrow{OT_e} = \frac{L_{1e}}{L1} \times \overrightarrow{OT}$, and $\overrightarrow{T_eP_e} = L_{2e} \times \frac{\overrightarrow{T_eP_e}}{||\overrightarrow{T_eP_e}||}$.

Where the $\left\|\overrightarrow{T_eP_e}\right\|$ is the length of the vector of $\overrightarrow{T_eP_e}$. $\frac{\overrightarrow{T_eP_e}}{||\overrightarrow{T_eP_e}||}$ equals to the unit vector (a vector with the length of 1) with the direction of the vector $\overrightarrow{OT}$ being rotated by the angle of α_e.

Accordingly, the participants consider themselves standing at P_e and facing the direction of h_e, same as the direction of $\overrightarrow{T_eP_e}$. To pinpoint the target location, they intend to produce the desired inbound vector $\overrightarrow{P_eO}$, which consists of the desired inbound turn angle β_e and the desired inbound path length L_{3e}:

$$\overrightarrow{P_eO} = -(\overrightarrow{OT_e} + \overrightarrow{T_eP_e}), \quad (3)$$

$$\beta_e = \text{dir}(\overrightarrow{P_eO}) - (\text{dir}\left(\overrightarrow{OT}\right) + \alpha_e), \quad (4)$$

$$L_{3e} = \left\|\overrightarrow{P_eO}\right\|. \quad (5)$$

Where the dir $(\overrightarrow{P_eO})$ is the direction of $\overrightarrow{P_eO}$ and dir $\left(\overrightarrow{OT}\right)$ is the direction of $\overrightarrow{OT}$. The direction of a vector is specified by the angular distance from a fixed reference direction in the virtual environment (e.g., the UP direction in Figure 3.1) to the vector. Where the $\left\|\overrightarrow{P_eO}\right\|$ is the length of the vector of $\overrightarrow{P_eO}$.

As there is no systematic bias in executing the inbound path based on the assumptions of the encoding-error model, the participants are able to implement the desired inbound path length and turn angle without bias (e.g., $L_r = L_{3e}$, $\beta_r = \beta_e$ in Figure 3.4A) while standing at P and facing the direction of h actually. Thus, the predicted response vector $\overrightarrow{PO_{pred}}$ can be given by

$$\overrightarrow{PO_{pred}} = L_{3e} \times \frac{\overrightarrow{PO_{pred}}}{||\overrightarrow{PO_{pred}}||}, \quad (6)$$

where $\frac{\overrightarrow{PO_{pred}}}{||\overrightarrow{PO_{pred}}||}$ equals to the unit vector with the direction of the vector $\overrightarrow{OT}$ being rotated by the angle of $(\alpha + \beta_e)$.

We then get the predicted response location O_{pred}.

$$O_{pred} = P + \overrightarrow{PO_{pred}}. \quad (7)$$

Where O_{pred} and P represent the coordinates in the Cartesian coordinate system used in Qi et al. (2021), where the direction of UP in Figure 3.1 is y positive and the direction of RIGHT in Figure 3.1 is x positive.

Thus, following Formula 1-7, the coordinates of the predicted response location O_{pred} can be expressed in terms of parameters $\theta_{L\_s}^{enc}$, $\theta_{L\_i}^{enc}$, $\theta_{A\_s}^{enc}$, and $\theta_{A\_i}^{enc}$, and several constants (e.g., L1, L2, and α) for each path.

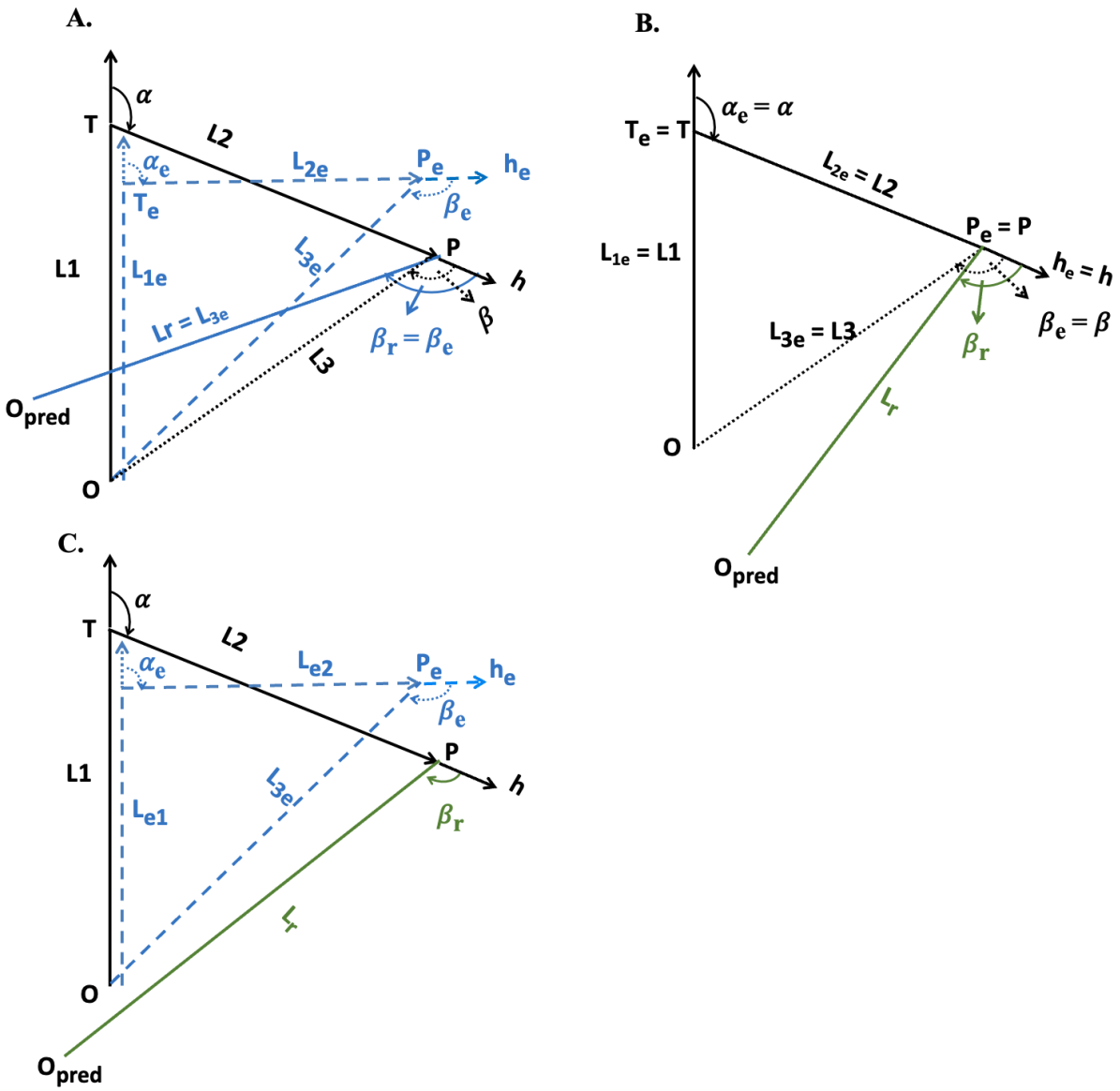

Figure 3.4. Illustration of predictions of different models. In each panel, the outbound path of a participant, O-T-P (solid black), consists of lengths L1 and L2 and turn angle α. H is the participant's heading at the end of the outbound path. The prediction of the participants' inbound path, PO_{pred} (solid blue indicating inbound responses without systematic errors or solid green indicating inbound responses with systematic execution errors), consists of length L_r and inbound turn angle β_r. O_{pred} is the predicted location of O. (A) the encoding-error model. The encoded outbound path, O-Te-Pe (blue dotted), consists of lengths L1e and L2e and turn angle

æ, which are determined by the encoding functions. h_e *is the encoded heading at the end of the outbound path. The desired inbound responses are free of execution errors (i.e.,* $L_r = L_{3e}$ *and* $\beta_r = \beta_e$*). (B) the execution-error model. The outbound path is free of encoding errors (*$\alpha_e = \alpha$ *and* $P_e = P$*). The inbound responses (*L_r *and* β_r*) are solely determined by the execution functions. (C) the bi-component model. The inbound responses (*L_r *and* β_r*) are determined by the systematic errors in encoding (blue dots) according to the encoding functions and in execution (green solid) according to execution functions.*

3.4.2 The execution-error model

The execution-error model assumes that the process of encoding is independent of the systematic bias and the navigators estimate their self-localization (i.e., T_e = T and P_e = P in Figure 3.4B) accurately.

The execution functions for inbound path length and angle have 2 parameters, respectively. While $\theta_{L\_s}^{exe}$ and $\theta_{L\_i}^{exe}$ are the slope and intercept for the inbound path length, $\theta_{A\_s}^{exe}$ and $\theta_{A\_i}^{exe}$ are the slope and intercept for inbound turn angle.

The executed values of inbound length L_r and turn angle β_r (see Figure 3.4B) can be represented as:

$$L_r = \theta_{L\_s}^{exe} \times L_{3e} + \theta_{L\_i}^{exe}, \quad (8)$$

$$\beta_r = \theta_{A\_s}^{exe} \times \beta_e + \theta_{A\_i}^{exe}, \quad (9)$$

where L_{3e} and β_e equal to the correct length L3 and turn angle β for the inbound path, respectively, because there is no systematic error in encoding the outbound path.

Therefore, the predicted response vector $\overrightarrow{PO_{pred}}$ can be calculated according to Formula 10:

$$\overrightarrow{PO_{pred}} = L_r \times \frac{\overrightarrow{PO_{pred}}}{||\overrightarrow{PO_{pred}}||}. \quad (10)$$

Where $\frac{\overrightarrow{PO_{pred}}}{||\overrightarrow{PO_{pred}}||}$ equals to the unit vector with the direction of the vector $\overrightarrow{OT}$ being rotated by the angle of $(\alpha + \beta_r)$.

As a result, the predicted location O_{pred} can be calculated by Formula 7.

3.4.3 The bi-component model

Since the bi-component model presumes that both the encoding and execution processes contribute to systematic errors, it incorporates the previously described encoding functions for the outbound path and execution functions for the inbound path (see Figure 3.4C).

Specifically, Formula 1 through 5 still holds in encoding the outbound path and estimating the desired inbound response, i.e., L_{3e} and β_e, for the current model. Formula 8-10 still holds when executing the desired inbound response through the execution functions. As a result, Formula 7 can be used to calculate the model's predicted response location O_{pred}.

3.4.4 The baseline model

The baseline model presumes no systematic bias in both encoding and execution stages, i.e., the slopes are one and the intercepts are zero for all the encoding functions and the execution functions. Thus, the baseline model directly used the correct values of the target locations to predict participants' response locations ($O_{pred} = O$).

Note that Harootonian et al. (2020) showed the influence of the immediately preceding trial. Participants tended to bias the encoded distance of the current trial towards the encoded distance of the previous trial (e.g., a larger distance in the previous trial would lead to overestimation of a short distance in the current trial), which indicates that the Bayesian prior of the true value assimilates the information of the immediately preceding trial. According to the

three models interested in the current study (encoding-error model, execution-error model, and bi-component model), a Bayesian prior could be considered in encoding the outbound path, executing the inbound path, or in both, predicting history effects in different processes. To simply the model comparison, we did not add parameters of the history effect to the models in the current study.

3.5 Cross-validation for models without considering participant variable

We conducted cross-validation for models without considering participants' differences in their compression patterns in either encoding or response functions. Therefore, one value of each parameter (e.g., eight free parameters, $\theta_{L\_s}^{enc}$, $\theta_{L\_i}^{enc}$, $\theta_{A\_s}^{enc}$, $\theta_{A\_i}^{enc}$, $\theta_{L\_s}^{exe}$, $\theta_{L\_i}^{exe}$, $\theta_{A\_s}^{exe}$, and $\theta_{A\_i}^{exe}$ for the bi-component model) was estimated for all participants.

For each model, the technique of 5 times of 2-fold (5 × 2) cross-validation (Alpaydm, 1999; Dietterich, 1998) was employed for the computational modeling of the response locations. To be specific, the original dataset (all 896 outbound paths, 8 paths × 4 experiments × 28 participants for each experiment) was partitioned randomly into two equal subsamples, S1 and S2, with 448 outbound paths each. One subsample (e.g., S1) was assigned to the model training to estimate the model parameters, and the other (e.g., S2) was used for the model validation. Then, the two subsamples were swapped, that is, S2 was used for model training and S1 was the subsample to test the model performance. The above random subsampling and cross-validation operations were repeated 5 rounds. Each half of the dataset was applied to both model fitting and validation in each round. Afterward, model performance in model validation can be averaged across the ten folds (5 × 2 folds) to obtain a more robust estimation of the model performance by reducing the impact of sampling (partitioning) errors.

The process of modeling was carried out using two different algorithms. One only used the data of the home response location for every outbound path, as in the previous typical triangle-completion studies, whereas the other used all three response locations for every outbound path. As we speculated above, only using the response to the home for every outbound path, cross-validation modeling may not distinguish the three models (single-component models and the bi-component model). In contrast, using the responses to three locations for every outbound path, cross-validation modeling may distinguish the three interested models.

3.5.1 Model fitting

The functions of each model were determined (i.e., the parameters of θs were estimated) by making the models' predictions (O_{pred}) as closely as possible to the participants' responses (O_{resp}). The discrepancy was measured by the mean squared error (MSE) between the predicted and response locations across all outbound paths and all targets (3 for the algorithms using multiple response locations and 1 for the algorithms using home response locations only) in training subsamples (the data used for model fitting):

$$\text{MSE} = \frac{1}{n}\sum_{i=1}^{n}\left[\left(O_{xi}^{pred} - O_{xi}^{resp}\right)^2 + \left(O_{yi}^{pred} - O_{yi}^{resp}\right)^2\right], \quad (11)$$

where the $(O_{xi}^{pred}, O_{yi}^{pred})$ is the predicted location based on the model, $(O_{xi}^{resp}, O_{yi}^{resp})$ is the response location, and n is the number of data points.

Then using Matlab's fminsearch function, we found the value of parameters that minimize the MSE for each model. The fminsearch function can detect the minimal value of an objective function (e.g., MSE) by means of various optimization algorithms. To boost the possibility of locating a global minimum rather than a local one for the objective function, the search ran 500 iterations and each time started with random initial values of parameters. After

500 iterations, the fitting procedure located the minimum of MSE at an optimal solver, and this solver was the set of best-fitting parameters.

Table 3.1 summarizes the averaged ten-fold results of fitting different models to response data, including parameters and fitting performance, using two distinct algorithms (see Supplementary Materials of Chapter 3 and Table S3.1 for results of individual folds). These parameters would be held for the subsequent model validation.

For brevity, the encoding-error model is referred to as Model 1, the execution-error model as Model 2, the bi-component model as Model 3, and the baseline model as Model 0 (abbreviated as M1, M2, M3, and M0, respectively in the following sections).

The fitting performance of a specific model *M* is evaluated by the squared root of the MSE (RMSE), the percentage of the variance of the baseline model explained by the individual model (Partial R^2 = 1- $\frac{MSE\ of\ M}{MSE\ of\ M0}$), and the maximum log-likelihood (MaxLogL).

To calculate the maximum log-likelihood, we assumed that the deviations of the predicted locations from the response locations ($O_{xi}^{pred} - O_{xi}^{resp}, O_{yi}^{pred} - O_{yi}^{resp}$), referred to as the locational residuals, were from a bivariate normal distribution with zero means ($\mu = (0,0)$) and undetermined covariance matrix (Σ). The maximum log-likelihood of the locational residuals were calculated by Formula 12 (Jordan, 2003; Taboga, 2021):

$$\text{MaxLogL} = \log\left[\left(\frac{1}{\sqrt{2\pi}}\right)^{cn} \times e^{-\frac{cn}{2}} \times \left|\hat{\Sigma}\right|^{-\frac{n}{2}}\right]. \quad (12)$$

Where c is the dimension of the data (c = 2 for the locational residuals), and n refers to the number of the data points (n = 498 × 3 for the algorithms of using multiple locations and n = 498 for the algorithms of using the home response locations only). $\hat{\Sigma}$ is

$$\begin{bmatrix} \frac{1}{n}\sum_{i=1}^{n}\left(O_{xi}^{pred}-O_{xi}^{resp}\right)^2 & \frac{1}{n}\sum_{i=1}^{n}\left(O_{xi}^{pred}-O_{xi}^{resp}\right)\left(O_{yi}^{pred}-O_{yi}^{resp}\right) \\ \frac{1}{n}\sum_{i=1}^{n}\left(O_{xi}^{pred}-O_{xi}^{resp}\right)\left(O_{yi}^{pred}-O_{yi}^{resp}\right) & \frac{1}{n}\sum_{i=1}^{n}\left(O_{yi}^{pred}-O_{yi}^{resp}\right)^2 \end{bmatrix}$$ from

each individual models. $\left|\hat{\Sigma}\right|$ is the determinant of the matrix.

Table 3.1. Model fitting performance using multiple locations (upper) or only home response locations (lower). Parameters are estimated slopes and intercepts of encoding functions ($\theta_{L\_s}^{enc}$ and $\theta_{L\_i}^{enc}$ for length, $\theta_{A\_s}^{enc}$ and $\theta_{A\_i}^{enc}$ for angle) and execution functions ($\theta_{L\_s}^{exe}$ and $\theta_{L\_i}^{exe}$ for length, $\theta_{A\_s}^{exe}$ and $\theta_{A\_i}^{exe}$ for angle) for all four models in the model fitting. The RMSE, maximum log-likelihood, and partial r-squared are goodness-of-fit measures. M0 = the baseline model, M1=the encoding-error model, M2 = the execution-error model, M3 = the bi-component model.

	Multiple response locations										
	Parameters								5×2 Fitting		
	$\theta_{L\_s}^{enc}$	$\theta_{L\_i}^{enc}$	$\theta_{A\_s}^{enc}$	$\theta_{A\_i}^{enc}$	$\theta_{L\_s}^{exe}$	$\theta_{L\_i}^{exe}$	$\theta_{A\_s}^{exe}$	$\theta_{A\_i}^{exe}$	RMSE	MaxLogL	Partial R^2
M0	1	0	1	0	1	0	1	0	3.178	-5961.9	0
M1	1.04	0.48	0.79	18.38	1	0	1	0	3.076	-5882.2	0.063
M2	1	0	1	0	0.70	1.29	0.78	41.11	3.054	-5865.2	0.077
M3	0.82	0.78	0.84	20.42	0.69	1.10	0.82	34.21	3.017	-5831.5	0.099
	Home response locations only										
	Parameters								5×2 Fitting		
	$\theta_{L\_s}^{enc}$	$\theta_{L\_i}^{enc}$	$\theta_{A\_s}^{enc}$	$\theta_{A\_i}^{enc}$	$\theta_{L\_s}^{exe}$	$\theta_{L\_i}^{exe}$	$\theta_{A\_s}^{exe}$	$\theta_{A\_i}^{exe}$	RMSE	MaxLogL	Partial R^2
M0	1	0	1	0	1	0	1	0	2.805	-1867.1	0
M1	0.68	0.67	0.45	23.43	1	0	1	0	2.620	-1815.5	0.128
M2	1	0	1	0	0.42	2.10	0.47	84.21	2.625	-1816.8	0.124
M3	2.53	3.94	0.48	26.20	0.73	0.11	1.18	12.55	2.618	-1815.0	0.129

Table 3.1 shows that the bi-component model (M3) is the best model according to the three goodness-of-fit measures numerically when all three response locations were included in the model fitting. In contrast, although the three models of interest (M1-M3) are better than the base model (M0), they could not distinguish from each other when only the home response locations were included in the model fitting. However, the superiority of the bi-component model (M3) using all three response locations might be attributed to the fact that the bi-component model (M3) has more free parameters than the encoding-error model and the execution-error model (M1 and M2). This issue could be addressed by some model selection criteria (e.g., AIC, Akaike, 1973 or BIC, Schwarz, 1978) that penalize free parameters to be estimated. This issue could also be addressed by cross-validation which applied the estimated parameters to independent data (i.e., test subsamples) so that there is no free parameter in any models. The current study used the second approach. We still conducted AIC and BIC analyses for the training subsamples as some readers might be interested (see Supplementary materials of Chapter 3 and Table S3.3).

3.5.2 Model validation

In each round of cross-validation (five rounds in total), after fitting models to each training subsample (S1 or S2), we evaluated the generalizability of models using the corresponding test subsample (S2 or S1). Table 3.2 shows the averaged validation performance over ten test subsamples after performing the cross-validation five times for all four models (see Supplementary materials of Chapter 3 and Table S3.2 for results of individual folds).

More specifically, for each model, the estimated parameters derived from each training subsample were applied to predict the response locations for the corresponding test subsample that were not involved in estimating the parameters. The residuals between the predicted and

response locations were used to calculate the RMSE, maximum log-likelihood, and partial r-squared.

Table 3.2. Model validation performance using multiple locations (upper) or only home response locations (lower). Parameters are the same as in Table 3.1 from model fitting. The RMSE, maximum log-likelihood, and partial r-squared are generalizability measures, which were calculated by applying the parameters to the test subsamples.

	Multiple response locations										
	Parameters								5×2 Validation		
	$\theta_{L\_s}^{enc}$	$\theta_{L\_i}^{enc}$	$\theta_{A\_s}^{enc}$	$\theta_{A\_i}^{enc}$	$\theta_{L\_s}^{exe}$	$\theta_{L\_i}^{exe}$	$\theta_{A\_s}^{exe}$	$\theta_{A\_i}^{exe}$	RMSE	MaxLogL	Partial R^2
M0	1	0	1	0	1	0	1	0	3.178	-5961.9	0
M1	1.04	0.48	0.79	18.38	1	0	1	0	3.085	-5889.9	0.058
M2	1	0	1	0	0.70	1.29	0.78	41.11	3.060	-5868.9	0.073
M3	0.82	0.78	0.84	20.42	0.69	1.10	0.82	34.21	3.031	-5843.6	0.090
	Home response locations only										
	Parameters								5×2 Validation		
Model	$\theta_{L\_s}^{enc}$	$\theta_{L\_i}^{enc}$	$\theta_{A\_s}^{enc}$	$\theta_{A\_i}^{enc}$	$\theta_{L\_s}^{exe}$	$\theta_{L\_i}^{exe}$	$\theta_{A\_s}^{exe}$	$\theta_{A\_i}^{exe}$	RMSE	MaxLogL	Partial R^2
M0	1	0	1	0	1	0	1	0	2.805	-1867.1	0
M1	0.68	0.67	0.45	23.43	1	0	1	0	2.632	-1819.2	0.120
M2	1	0	1	0	0.42	2.10	0.47	84.21	2.633	-1819.1	0.119
M3	2.53	3.94	0.48	26.20	0.73	0.11	1.18	12.55	2.634	-1819.8	0.118

Table 3.2 indicates that the bi-component model (M3) is the best model according to the three generalizability measures when all three response locations were included in the model

evaluation. In contrast, although the encoding-error model, execution-error model, and the bi-component model (M1, M2, and M3) are better than the baseline model (M0), they could not distinguish from each other when only the home response locations were included in the model evaluation.

These conclusions were quantified by the maximum likelihood ratios (LRs) analysis. Because all models have the same number of free parameters for the test subsamples, LRs can be directly calculated from the MaxLogLs without adjustment due to difference in parameter numbers. Table 3.3 summarizes the results.

Table 3.3. Maximum likelihood ratio (LR) between models (row model over column model) in model validation using multiple locations (left) or only home response locations (right).

	Multiple response locations				Home response locations only			
LR	M0	M1	M2	M3	M0	M1	M2	M3
M1	$1.86 \times 10^{31**}$				$6.70 \times 10^{20**}$			
M2	$2.31 \times 10^{40**}$	$1.25 \times 10^{9**}$			$7.55 \times 10^{20**}$	$1.13^{—}$		
M3	$2.37 \times 10^{51**}$	$1.28 \times 10^{20**}$	$1.02 \times 10^{11**}$		$3.66 \times 10^{20**}$	$0.55^{—}$	$0.49^{—}$	

Note: * indicates clear evidence, i.e., LR > 3 or LR <1/3, and ** indicates strong evidence, i.e., LR > 10 or LR <1/10. ⁻ indicates no evidence (Glover & Dixon, 2004).

The results of the maximum likelihood ratio shown in Table 3.3 demonstrate that there is strong evidence in favor of the bi-component model (M3) over the encoding-error model (M1) and the execution-error model (M2) when the cross-validation included multiple response locations, whereas there was no clear evidence favoring any models when the cross-validation included only home response locations.

Furthermore, we adopted Alpaydin's 5×2cv combined F test to examine the differences in models' performance (Alpaydm, 1999, see also Raschka, 2018). To compare the results of two competing models, the difference in the value of RMSE (dRMSE) between them was calculated, generating 5 × 2 difference matrices (RMSEs of ten-folds in validation of each model are listed in Table S3.2). d_i^j was used to denote the dRMSE value on the *j*th (*j* = 1, 2) fold of the *i*th (*i* = 1, …, 5) round in a difference matrix and d_i^{avg} denotes the averaged RMSE difference in the *i*th round, $d_i^{avg} = (d_i^1 + d_i^2) / 2$.

Then the estimated variance of the difference for the *i*th round is given by

$$s_i^2 = \left(d_i^1 - d_i^{avg}\right)^2 + \left(d_i^2 - d_i^{avg}\right)^2. \quad (13)$$

The F statistic is calculated as:

$$f = \frac{\sum_{i=1}^{5}\sum_{j=1}^{2}\left(d_i^j\right)^2}{2\sum_{i=1}^{5} s_i^2}, \quad (14)$$

which approximately follows an F distribution with (10, 5) degrees of freedom.

Table 3.4 summarizes the mean dRMSE of all pairs of the models and the corresponding significance of Alpaydin's F-test. Consistent with the results indicated by Table 3.3, when three locations' data were included (left panel), the results show that the bi-component model ($RMSE_{M3}$ = 3.031) significantly outperforms the encoding-error model ($RMSE_{M1}$ = 3.085, p < .001) and the execution-error model ($RMSE_{M2}$ = 3.060, p = .02) in predicting the actual responses. The execution-error model presents significantly better performance than the encoding-error model (p < .01). All the three models of interest have substantially better predictive performance than the baseline model ($RMSE_{M0}$ = 3.178, all p values < .001).

By contrast, when only the data of home response locations were used in the cross-validation (right panel), there was no significant difference in RMSE among M1, M2, and M3

although RMSEs in these three models, approximately 2.63, were significantly smaller than that of the baseline model (M0) ($RMSE_{M0}$ = 2.805, all *p* values < .01).

Table 3.4. Alpaydin's F-test examining the differences in RMSE (dRMSE) between models (the row model minus the column model) when using multiple locations (left) or only home response locations (right).

	Multiple response locations					Home response locations only				
dRMSE	M0	M1	M2	M3		dRMSE	M0	M1	M2	M3
M1	-.093**					M1	-.174***			
M2	-.118***	-.025**				M2	-.172***	.001—		
M3	-.147**	-.056***	-.029*			M3	-.171***	.002—	.001—	

Note: Asterisks denote significant dRMSE (***p < .001; **p < .01; *p < .05) and a dash (—) indicates non-significant dRMSE.

Figure 3.5 visually presents locational residuals of model validation. We calculated the *mean predicted locations* of each target (three for multiple response locations or one for home only) in each outbound path (32 in total) across the ten folds of the test subsamples based on different models. We also calculated the *mean response location* of the target across participants who replaced this target. The *locational residual* of one target for one model is the difference between the *mean predicted location* based on this model and the *mean response location* of the target across participants (mean predicted location – mean response location).

Figure 3.5A, employing multiple response locations, reveals clear differences in predictive performance among all these models. In particular, the bi-component model achieves

more centric dots and a smaller area of 95% density contours of the residual distributions compared with other competing models, indicating that it is capable to predict the actual responses of the participants more accurately. By contrast, Figure 3.5B, employing only the home response locations, shows that apart from the baseline model, the performance of the other three models is not distinguishable (the dots of various colors are mixed up and the ellipses overlap).

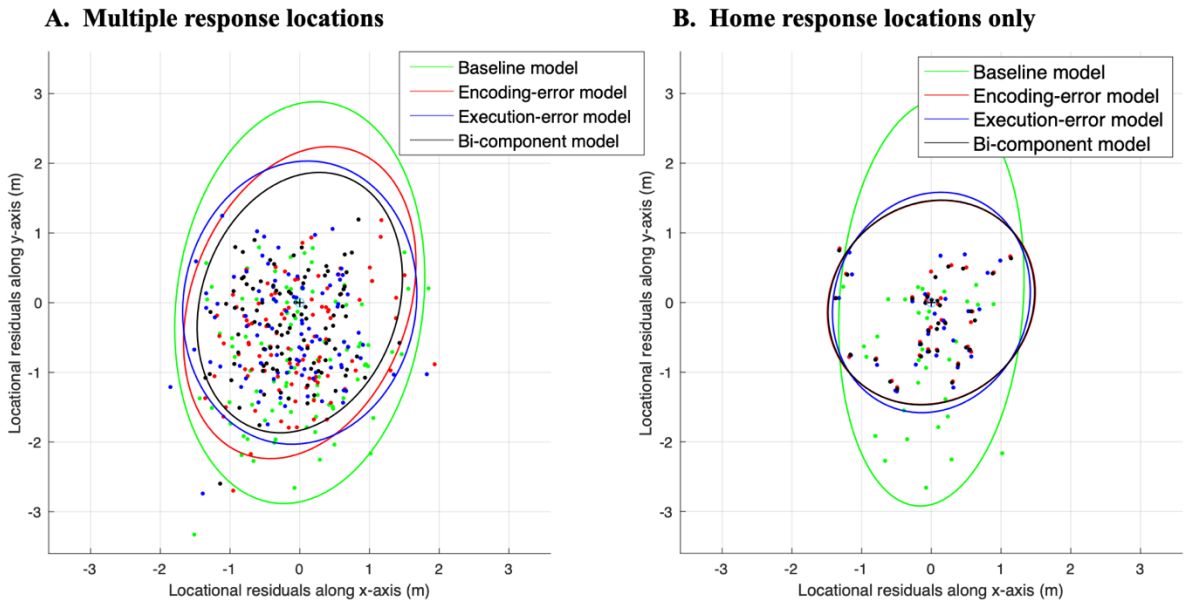

Figure 3.5. Visualizing the differences (locational residuals) between mean response locations and mean predicted locations from different models using (A) multiple response locations or (B) only home response locations. The open circle with a cross at (0, 0) indicates the response location, the coordinate of which varied in real experiments but is set to (0, 0) as a reference. Individual dots represent coordinates of the locational residuals for all targets (96 targets in A and 32 in B). Ellipses indicate the 95% density contours of the bivariate normal distributions with zero means ($\mu = (0,0)$) and covariance matrix (Σ) of the locational residuals according to

the baseline model (green), encoding-error model (red), execution-error model (blue), and bi-component model (black), respectively.

3.5.3 Model recovery

The results of 5 × 2 cross-validation indicated that the bi-component model was the best model to predict the response locations. Furthermore, although the algorithm of using all three objects can dissociate the bi-component model from the encoding-error and execution-error models, the algorithm of using only home response locations cannot. Because both these conclusions are dependent on the cross-validation methods used in the current project, these conclusions will be significantly strengthened if the cross-validation methods used in the current project can be shown to distinguish the true model from other models using the *simulated* response locations produced by each of the three models (the encoding-error, execution-error, and bi-component models).

For each model (i.e., the true model), we generated simulated response locations for all ten subsamples (5 × 2 folds). Using the corresponding parameters derived from model fitting using multiple objects (e.g., the values for M1, M2, and M3 in the upper table of Table 3.1), we calculated the predicted locations for all three targets for each of the 448 outbound paths in each subsample. Using the corresponding RMSE in the upper table of Table 3.1, we generated random noises for both dimensions (x and y) of all predicted locations from a normal distribution ($\mu = 0$, $\sigma = \frac{\mathrm{RMSE}}{\sqrt{2}}$). Each simulated response location is then the sum of the predicted location and the noise. We applied both algorithms of 5 × 2 cross-validation (using multiple response locations or using only home response locations) to the simulated response locations and examined whether the generalizability measure (i.e., LR) in the model validation could distinguish the true model

from other models. We created 100 sets of simulated response locations and conducted 5 × 2 cross-validation for all of them[8].

The frequency of successfully distinguishing the true model from other models could also indicate the discriminability of the cross-validation methods. For each true model, we calculated the likelihood ratio between any two models for each of the 100 simulations and classified the likelihood ratios into different categories (see details in Supplementary materials of Chapter 3 and Figure S3.2). Figure 3.6 presents the confusion matrix in model recovery. The best model was determined only when it had likelihood three times higher than both other two models. The results showed that the algorithm of using multiple response locations can successfully distinguish the true model from other models. Occasionally the algorithm could not find the best model (i.e., no model had likelihood three times than both other two models) (e.g., for true model M2, 18% chance of failure to find the best model). However, in most instances, the algorithm recovered the true model (98% for true model M1, 82% for true model M2, and 100% for true model M3) and never recovered any competing models. By contrast, the algorithm of using home response locations cannot clearly distinguish the true model from other models. In most cases, the algorithm could not find the best model (with a rate larger than 49%). Consequently, the algorithm could recover the true model at a low rate (23% for true model M1, 50% for true model M2, and 7% for true model M3). The algorithm also at times recovered competing models.

---

[8] Note that it takes about 3.5 hours to finish 5 × 2 cross-validation for each simulation subsample using all three response locations of each outbound path.

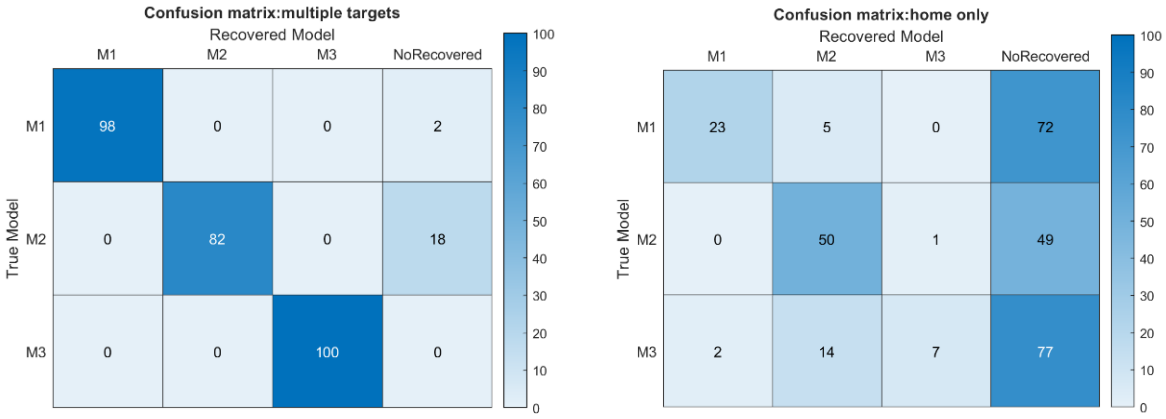

Figure 3.6. Confusion matrices in model recovery using multiple response locations (left) or home response locations only (right). The number in each cell indicates the frequency of the recovered model being the best model. NoRecoved means that no best model was recovered by the algorithm.

3.5.4 Similarity of parameters' values estimated from real and simulated response locations

The algorithm using multiple response locations estimated 16 parameters (four parameters for M1, four for M2, and eight for M3, see Table 3.1) based on participants' response locations. Similarly, this algorithm could also estimate 16 parameters based on simulated locations produced by each true model. The similarity between the estimated parameters based on real and simulated response locations should reflect the similarity between real and simulated response locations, thus indicating the closeness between the true model that produced the real response locations and each model. The model closest to the true model should be the best model. The similarity between parameters based on real response locations and simulated response locations from different models were illustrated by Figure 3.7 (see exact parameters in Table S3.4. The parameter distance was shortest when the simulated locations were produced by M3 (RMSE = 9.44, 6.8, and 1.5 for M1, M2, and M3 respectively). The parameters based on

simulated locations from M3 explained the largest proportion of the total variance of the 16 parameters based on real response locations ($r^2 = 1 - \frac{MSE}{Var}$, r^2 = .46, .72, and .99 for M1, M2, and M3 respectively). The rates of likelihood of M3 over other models were larger than 3.33×10^{10} (logL = -58.64, -53.38, and -29.15 for M1, M2, and M3 respectively). Therefore, the similarity between real and simulated response locations from M3 was largest, indicating M3 was the best model.

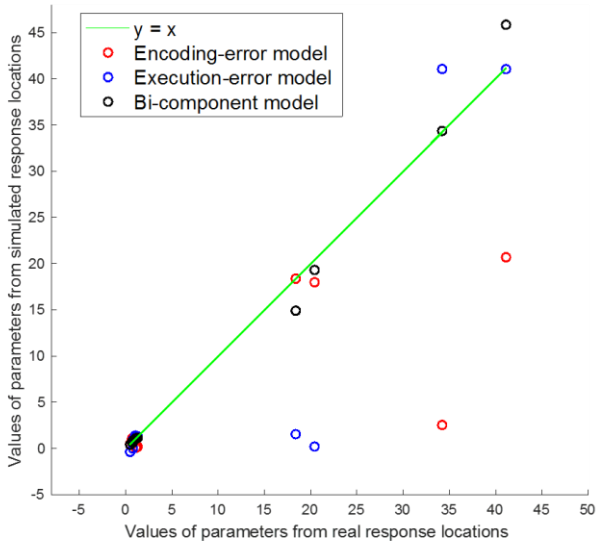

Figure 3.7. Illustrating the similarity of estimated parameters based on real data and simulated data from different models. The diagonal lines in green (y = x) indicate the ideal outcome that the parameters derived from real data are perfectly recovered from simulated data. Open dots depict the individual pairs of values of parameters based on real and simulated response locations for each model.

3.5.5 Predictive performance on the response error of participants

In addition, we compared the predictive performance of different models in terms of participants' response error (inbound path length or turn angle), consistent with previous studies

(Chrastil & Warren, 2021; Fujita et al., 1993). We conducted the following analyses of the mean predicted locations of targets across the ten-fold test subsamples, which were used in model validation. The predicted inbound path ($\overrightarrow{PO_{Pred}}$) was calculated from the testing position (P) to the predicted location (O_{pred}) based on each model. The predicted error (inbound path length or turn angle) was defined as the difference between the predicted and correct values for each target and each unique outbound path (32 different types of paths, 8 in each of the four experiments). The individual response error (inbound path length or turn angle) was defined as the difference between the response and correct values. The mean response error for each target and each unique outbound path was the average of the individual response errors across participants for the specific target and the specific outbound path.

Figure 3.8 illustrates the mean predictive performance of different models in terms of inbound length error and angle error. It shows that the bi-component model (M3) had the highest correlation coefficients for both inbound length (see *r*s in Figure 3.8A) and angle errors (Figure 3.8C) when the cross-validation included multiple response locations of each outbound path. Nevertheless, the correlation coefficients of the three models were comparable when the cross-validation only included the home response location of each outbound path (see *r*s in Figure 3.8B and Figure 3.8D).

A. Multiple response locations

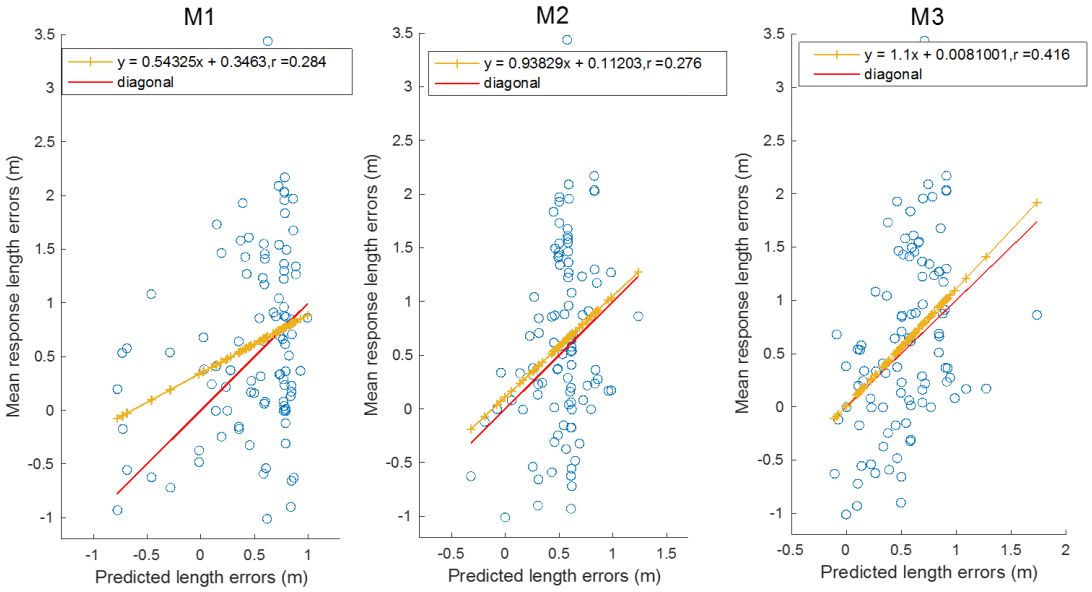

B. Home response locations only

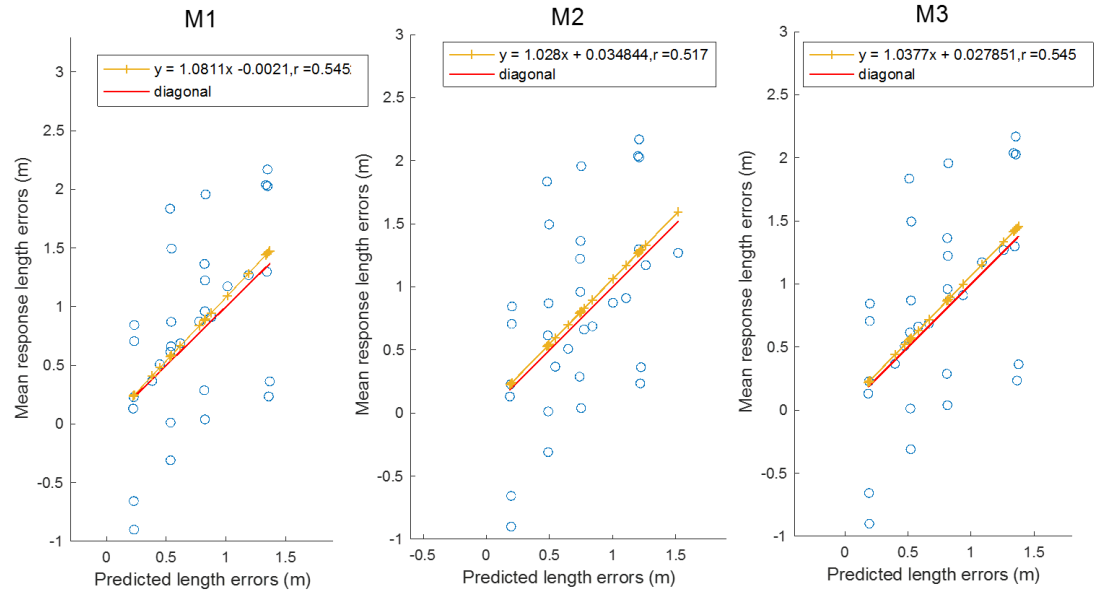

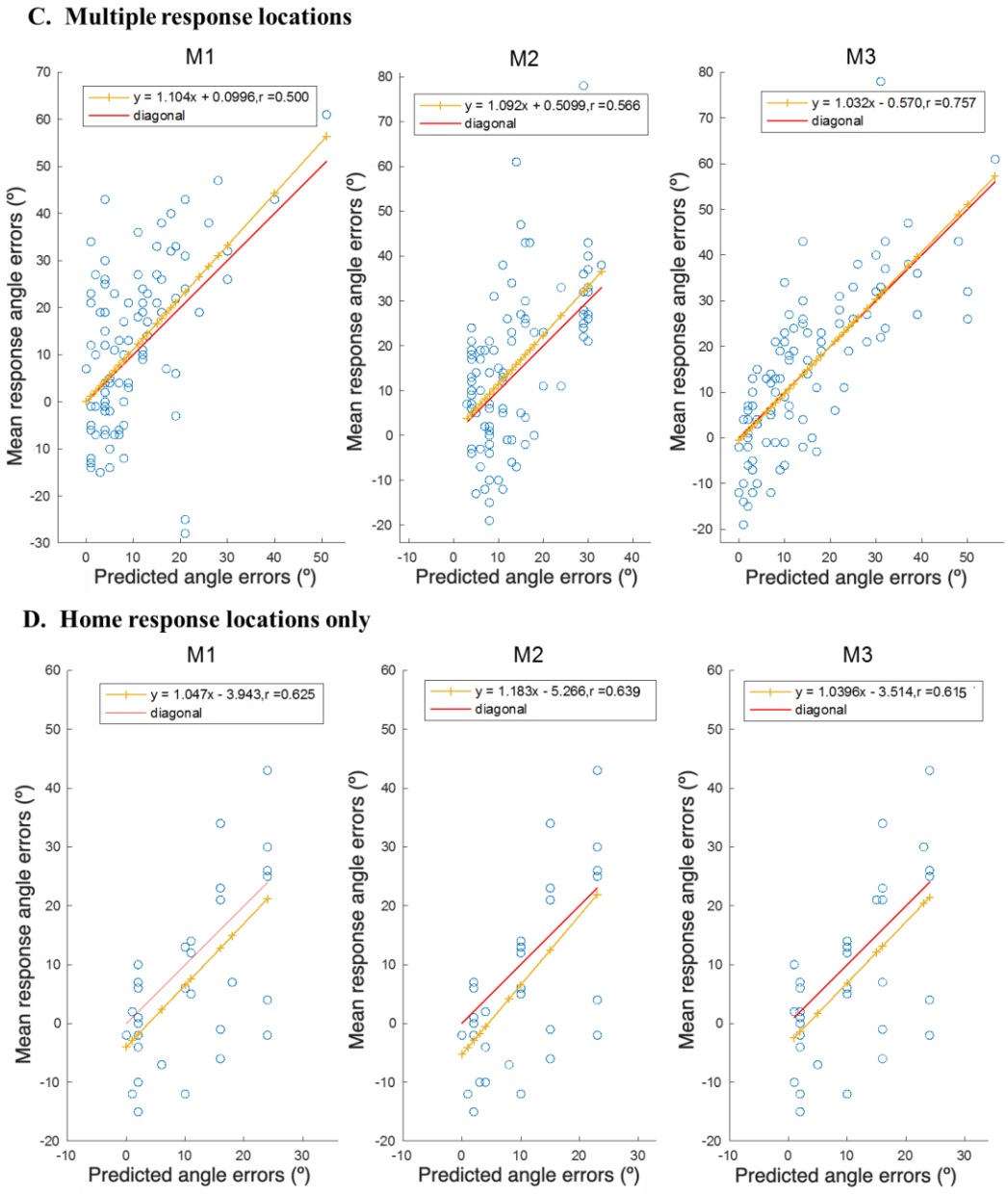

Figure 3.8. Illustrating the predicted errors in inbound path length (panels A and B) and turn angle (panels C and D) as a function of the mean response errors using multiple response locations or only home response locations. The diagonal lines in red (y = x) indicate the ideal outcome that the response errors are perfectly predicted. The yellow lines indicate the regression lines. Open dots depict the individual pairs of predicted errors and mean response errors across

participants, for each object, and for each path (32 paths in total), according to the encoding-error model (M1), execution-error model (M2), and bi-component model (M3), respectively.

The likelihood ratios were computed to compare the models' performance in predicting inbound length errors and angle errors. Following Glover and Dixon (2004), the likelihood ratio of favoring Model$_i$ over Model$_j$ (i.e., λ_{ij}) can be computed as

$$\lambda_{ij} = \left(\frac{1-r_j^2}{1-r_i^2}\right)^{\frac{n}{2}}, \quad (15)$$

where the r_i^2 and r_j^2 are squared mean correlation coefficients from Model$_i$ and Model$_j$ in Figure 3.8, indicating the variance that is explained by Model$_i$ and Model$_j$, respectively, and *n* is the number of data points. In the current example, *n* equals 96 (i.e., 32 paths × 3 response locations) for taking multiple response locations or equals 32 (i.e., 32 paths × 1 response location) for taking only home response locations into the cross-validation.

The results of likelihood ratios for the three competing models are reported in Table 3.5. For both length and angle errors, the method of employing multiple response locations demonstrates compelling evidence (i.e., five out of six likelihood ratios of over 100) that the bi-component model is superior to the encoding-error and execution-error models in describing mean response errors. However, no clear evidence (i.e., no likelihood ratios of over 2) is presented by employing only home response locations, showing that it cannot distinguish between models in terms of predictive power.

Table 3.5. Maximum likelihood ratios (λ) for competing models (row model over column model) in predicting inbound path length errors (left) and turn angle errors (right) using multiple locations or only home response locations.

	Length errors						Angle errors					
	Multiple response locations			Home response locations only			Multiple response locations			Home response locations only		
λ	M1	M2	M3	M1	M2	M3	M1	M2	M3	M1	M2	M3
M1												
M2	0.8			0.5—			113.1^{**}			1.6—		
M3	161.5^{**}	203.9^{**}		1.0—	1.9—		$5.6 \times 10^{11**}$	$4.9 \times 10^{9**}$		0.7—	0.5—	

Note: * indicates clear evidence, i.e., LR > 3 or LR <1/3, and ** indicates strong evidence, i.e., LR > 10 or LR <1/10. — indicates no evidence (Glover & Dixon, 2004).

3.6 Groups of participants differing in compression pattern of the response

In the cross-validation described above, we did not consider the participant variable. For each model, we estimated the best model parameters being applied to all participants. However, participants might differ in the compression pattern (i.e., some had a strong compression pattern whereas others had a weak compression pattern), so the best model parameters for each group might be significantly different from each other. Therefore, the conclusions on a model comparison based on the best model parameters for all participants and based on the best model parameters for each group of participants might not be consistent. We considered the variability of participants' responses in their triangle completion and classified participants into two groups based on the compression pattern of the inbound responses.

As illustrated in Figure 3.9, the participants showed variations in their compression pattern (e.g., the slopes of the regression lines) of the inbound responses. The dots inside the blue box in Figure 3.9C-D represent the participants who showed a compression pattern (i.e., with a slope between 0 and 1, and intercept larger than 0) or had strong compression whereas the dots outside the blue box represent the participants who did not show compression pattern or had

weak compression. Considering compression patterns in both length and angle, we could also divide participants into four groups based on both (47 in strong for both, 13 in weak for both, 22 in strong for angle and weak for length, 30 in weak for angle and strong for length). However, we might not be able to conduct meaningful 5 × 2 cross-validations for all four groups, especially the group with only 13 participants. Hence, we divided participants into two groups instead of four so that we had enough participants in each group for 5 × 2 cross-validations.

Across the regression lines of individual participants, the correlation coefficient (r) was significantly higher in the inbound turn angle (Figure 3.9D) than in the inbound path length (Figure 3.9C) (mean $r = 0.65$ for angle and mean $r = 0.39$ for length), $t\,(111) = 6.36$, $p < .001$, Cohen's $dz = .60$. Moreover, the number of participants showing significant correlations ($p \leq .05$) was significantly larger in the regression for inbound turn angle (Figure 3.9D) than for the inbound path length (Figure 3.9C) (61 participants for angle and 22 participants for length, sharing 5 participants with significant correlations in both), McNemar's $\chi^2\,(1) = 16.01$, $p < .001$. Hence, the compression patterns of individual participants in terms of inbound turn angle were much more reliable than in terms of inbound path length. Consequently, we classified the participants into two groups according to their compression on the inbound turn angle: the strong compression group (69 participants showing compression) and the weak compression group (43 participants showing no compression). Moreover, the distribution of participants in compression groups in terms of length was independent of in terms of angle ($\chi^2\,(1) = .03$, $p = .86$), indicating that the strong and weak compression groups only based on angle had similar proportions of participants with strong and weak compression in length. Therefore, the strong compression group had strong compression in angle and average compression in length whereas the weak compression group had weak compression in angle and average compression in length.

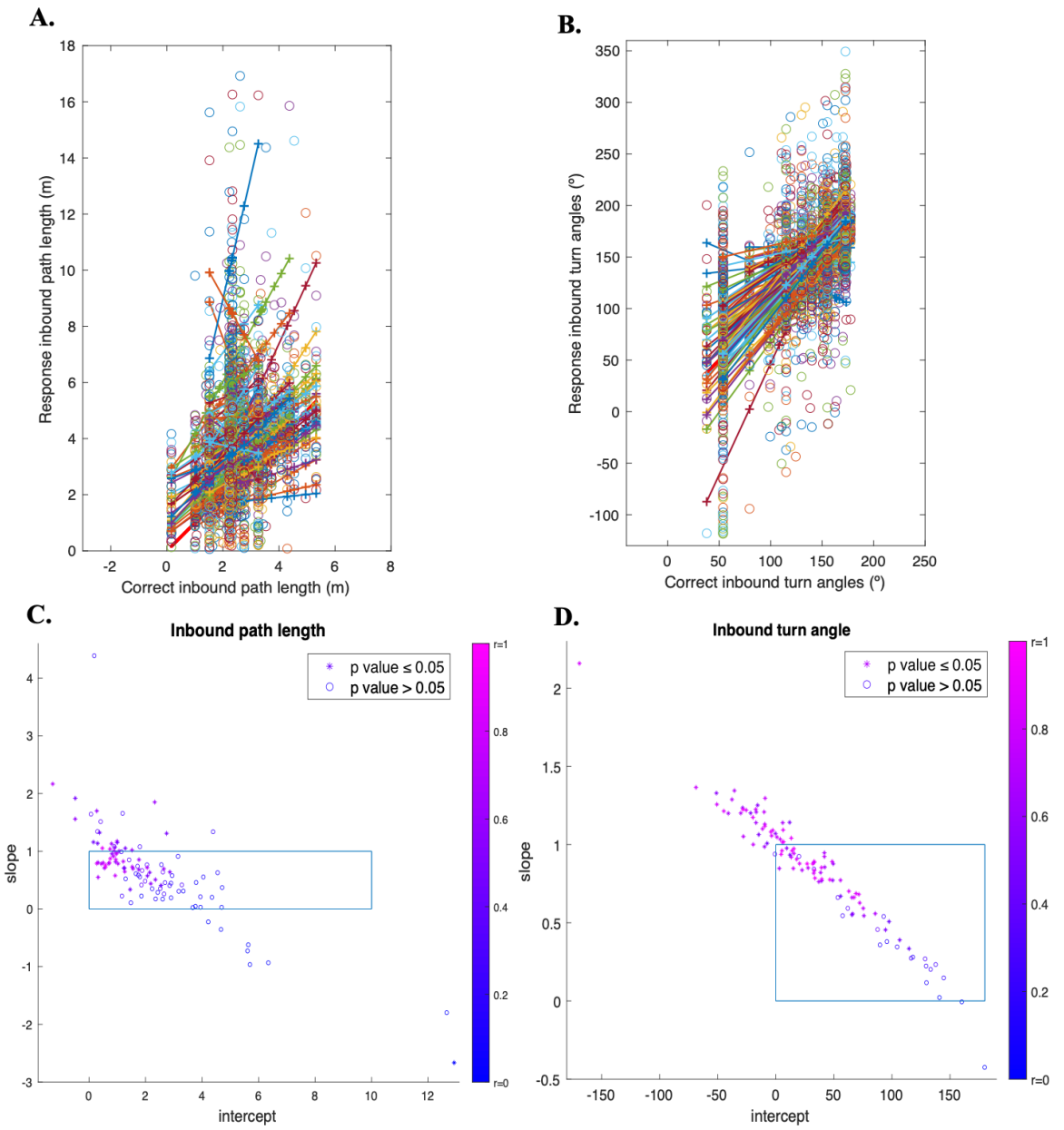

Figure 3.9. Each line indicates the linear regression of response values on the correct values for one participant in terms of inbound path length (A) and turn angle (B), respectively. (C-D) illustrate the slope-intercept, correlation coefficient (i.e., r-value), and its significance (i.e., p-value) of the linear regression relationship in terms of inbound path length (C) and turn angle (D), respectively.

We conducted model validation for each group using the model parameters estimated in the model fitting described in section 3.5.1 (see details in Supplementary materials of Chapter 3 and Tables S3.5-S3.8). Model validation based on the parameters from the algorithm using multiple locations showed that all the three models (M1-M3) even performed worse than the baseline model (M0) for the weak compression group (negative Partial R^2 in Table S3.5) although the bi-component model (M3) was still the best model for the strong compression group. These findings suggest that the best model parameters for all participants might not be appropriate for the weak compression group. Therefore, it is important to conduct cross-validation for each group and then calculate the overall model performance.

3.7 Cross-validation for different groups

We conducted 5 × 2 cross-validations for each group of compression. As we primarily used model validation performance in model comparison, we did not report the fitting results of two compression groups for the interest of brevity (see Supplementary materials of Chapter 3 Table S3.9 for the averaged fitting performance across ten folds).

3.7.1 Model validation

As illustrated in Tables 3.6, 3.7, and 3.8, the algorithm using home response locations only could not differentiate the three models (M1-M3) regardless of the compression group.

The algorithm using multiple response locations showed different model comparison results for the strong and weak compression groups. For the strong compression group, generalizability measures in Table 3.6, likelihood ratios in Table 3.7, and the results of *Alpaydin's F-test on* dRMSE in Table 3.8 (also see Table S3.10 for RMSEs of individual folds) all suggest that the bi-component model (M3) was the best. By contrast, for the weak compression group,

none of the generalizability measures, likelihood ratios, or *Alpaydin's F-test* on dRMSE could differentiate the four models including the baseline model.

Table 3.6. Model validation performance for the strong (upper) and weak (lower) compression groups. Parameters are estimated from model fitting for each corresponding group. The RMSE, maximum log-likelihood, and partial r-squared are generalizability measures, which were calculated by applying the parameters to the test subsamples.

	Strong compression group										
	Multiple response locations										
	Parameters								5×2 Validation		
Model	$\theta_{L\_s}^{enc}$	$\theta_{L\_i}^{enc}$	$\theta_{A\_s}^{enc}$	$\theta_{A\_i}^{enc}$	$\theta_{L\_s}^{exe}$	$\theta_{L\_i}^{exe}$	$\theta_{A\_s}^{exe}$	$\theta_{A\_i}^{exe}$	RMSE	MaxLogL	Partial R^2
M0	1	0	1	0	1	0	1	0	3.382	-3770.4	0
M1	1.14	0.49	0.79	15.45	1	0	1	0	3.214	-3692.0	0.096
M2	1	0	1	0	0.60	1.86	0.68	58.50	3.125	-3645.5	0.146
M3	0.64	1.19	0.88	18.69	0.57	1.76	0.72	52.07	3.084	-3623.2	0.168
	Home response locations only										
	Parameters								5×2 Validation		
Model	$\theta_{L\_s}^{enc}$	$\theta_{L\_i}^{enc}$	$\theta_{A\_s}^{enc}$	$\theta_{A\_i}^{enc}$	$\theta_{L\_s}^{exe}$	$\theta_{L\_i}^{exe}$	$\theta_{A\_s}^{exe}$	$\theta_{A\_i}^{exe}$	RMSE	MaxLogL	Partial R^2
M0	1	0	1	0	1	0	1	0	3.037	-1190.9	0
M1	0.84	0.58	0.46	18.64	1	0	1	0	2.738	-1139.7	0.186
M2	1	0	1	0	0.44	2.42	0.50	81.24	2.745	-1140.7	0.182
M3	2.88	0.84	0.43	12.46	0.72	0.86	1.51	12.50	2.743	-1140.5	0.183
	Weak compression group										
	Multiple response locations										
	Parameters								5×2 Validation		
Model	$\theta_{L\_s}^{enc}$	$\theta_{L\_i}^{enc}$	$\theta_{A\_s}^{enc}$	$\theta_{A\_i}^{enc}$	$\theta_{L\_s}^{exe}$	$\theta_{L\_i}^{exe}$	$\theta_{A\_s}^{exe}$	$\theta_{A\_i}^{exe}$	RMSE	MaxLogL	Partial R^2

M0	1	0	1	0	1	0	1	0	2.817	-2169.2	0
M1	0.86	0.46	0.80	21.2	1	0	1	0	2.814	-2169.3	0.002
M2	1	0	1	0	0.85	0.46	1.00	2.96	2.816	-2170.0	5.48E-04
M3	0.81	0.56	0.80	21.9	0.92	0.17	1.04	-1.73	2.810	-2168.3	0.005

	Home response locations only										
	Parameters								5×2 Validation		
Model	$\theta_{L\_s}^{enc}$	$\theta_{L\_i}^{enc}$	$\theta_{A\_s}^{enc}$	$\theta_{A\_i}^{enc}$	$\theta_{L\_s}^{exe}$	$\theta_{L\_i}^{exe}$	$\theta_{A\_s}^{exe}$	$\theta_{A\_i}^{exe}$	RMSE	MaxLogL	Partial R^2
M0	1	0	1	0	1	0	1	0	2.379	-662.8	0
M1	0.51	0.69	0.44	33.0	1	0	1	0	2.329	-657.0	0.041
M2	1	0	1	0	0.44	1.43	0.44	84.44	2.328	-656.9	0.042
M3	1.54	11.7	2.25	17.8	0.58	0.06	2.24	17.13	2.342	-659.1	0.029

Table 3.7. Maximum likelihood ratio (LR) between models (row model over column model) in model validation for the strong (upper) and weak (lower) compression groups using multiple locations (left) or only home response locations (right).

Strong compression group

	Multiple response locations				Home response locations only			
LR	M0	M1	M2	M3	M0	M1	M2	M3
M1	$1.06 \times 10^{34**}$				$1.64 \times 10^{22**}$			
M2	$1.72 \times 10^{54**}$	$1.62 \times 10^{20**}$			$6.03 \times 10^{21**}$	$0.37^{—}$		
M3	$8.03 \times 10^{63**}$	$7.58 \times 10^{29**}$	$4.66 \times 10^{9**}$		$7.84 \times 10^{21**}$	$0.48^{—}$	$1.30^{—}$	

Weak compression group

	Multiple response locations				Home response locations only			
LR	M0	M1	M2	M3	M0	M1	M2	M3
M1	$0.88^{—}$				322.58^{**}			
M2	$0.43^{—}$	$0.49^{—}$			370.37^{**}	$1.15^{—}$		

M3	2.50⁻	2.84⁻	5.81*	40.32**	0.13*	0.11*

Note: * indicates clear evidence, i.e., LR > 3 or LR <1/3, and ** indicates strong evidence, i.e., LR > 10 or LR <1/10. ⁻ indicates no evidence (Glover & Dixon, 2004).

Table 3.8. Alpaydin's F-test examining the differences in RMSE (dRMSE) between models (the row model minus the column model) for the group with strong (upper) and weak (lower) compression patterns when using multiple locations (left) or only home response locations (right).

Strong compression group									
Multiple response locations					Home response locations only				
dRMSE	M0	M1	M2	M3	dRMSE	M0	M1	M2	M3
M1	-.168**				M1	-.299**			
M2	-.257***	-.125**			M2	-.292**	.007⁻		
M3	-.298***	-.13***	-.041*		M3	-.294***	.005⁻	.002⁻	
Weak compression group									
Multiple response locations					Home response locations only				
dRMSE	M0	M1	M2	M3	dRMSE	M0	M1	M2	M3
M1	.003⁻				M1	.050⁻			
M2	.001⁻	-.002⁻			M2	.051⁻	-.001⁻		
M3	.007⁻	-.004⁻	-.006⁻		M3	.037⁻	.014⁻	.014⁻	

We also compared the overall performance of all models by combining the locational residuals of the two compression groups (see Tables 3.9-3.11 for generalizability measures, likelihood ratios, and the results of *Alpaydin's F-test*). Figure 3.10 visually illustrates the

locational residuals of individual targets achieved by different models using the two algorithms. All results suggest that the bi-component model was the best based on the cross-validation using multiple response locations whereas there was no best model based on the cross-validation using home response.

Table 3.9. The overall performance of model validation of the two compression groups using multiple locations (upper) or only home response locations (lower). Parameters are the weighted average of the best parameters for each group (weighted by the numbers of participants in different groups). The RMSE, maximum log-likelihood, and partial r-squared are generalizability measures, which were based on the combined locational residuals of the two compression groups.

	Multiple response locations										
	Parameters								5×2 Validation		
Model	$\theta_{L\_s}^{enc}$	$\theta_{L\_i}^{enc}$	$\theta_{A\_s}^{enc}$	$\theta_{A\_i}^{enc}$	$\theta_{L\_s}^{exe}$	$\theta_{L\_i}^{exe}$	$\theta_{A\_s}^{exe}$	$\theta_{A\_i}^{exe}$	RMSE	MaxLogL	Partial R^2
M0	1	0	1	0	1	0	1	0	3.179	-5964.5	0
M1	1.03	0.48	0.79	17.64	1	0	1	0	3.069	-5878.0	0.067
M2	1	0	1	0	0.70	1.32	0.81	37.18	3.012	-5828.4	0.102
M3	0.71	0.95	0.85	19.91	0.70	1.15	0.84	31.41	2.984	-5803.2	0.118
	Home response locations only										
	Parameters								5×2 Validation		
	$\theta_{L\_s}^{enc}$	$\theta_{L\_i}^{enc}$	$\theta_{A\_s}^{enc}$	$\theta_{A\_i}^{enc}$	$\theta_{L\_s}^{exe}$	$\theta_{L\_i}^{exe}$	$\theta_{A\_s}^{exe}$	$\theta_{A\_i}^{exe}$	RMSE	MaxLogL	Partial R^2
M0	1	0	1	0	1	0	1	0	2.805	-1868.3	0
M1	0.72	0.63	0.45	24.14	1	0	1	0	2.591	-1807.2	0.146
M2	1	0	1	0	0.44	2.04	0.48	82.47	2.595	-1807.9	0.143

M3	2.37	5.03	1.13	14.50	0.66	0.55	1.79	14.28	2.600	-1809.7	0.141

Table 3.10. The overall results of the maximum likelihood ratio (LR) between models (row model over column model) in model validation using multiple locations (left) or only home response locations (right).

	Multiple response locations				Home response locations only			
LR	M0	M1	M2	M3	M0	M1	M2	M3
M1	$3.86 \times 10^{37**}$				$3.47 \times 10^{26**}$			
M2	$1.29 \times 10^{59**}$	$3.35 \times 10^{21**}$			$1.69 \times 10^{26**}$	$0.49^{—}$		
M3	$1.08 \times 10^{70**}$	$2.80 \times 10^{32**}$	$8.36 \times 10^{10**}$		$2.74 \times 10^{25**}$	0.08^{**}	0.16^{*}	

Note: * indicates clear evidence, i.e., LR > 3 or LR <1/3, and ** indicates strong evidence, i.e., LR > 10 or LR <1/10. ¯ indicates no evidence (Glover & Dixon, 2004).

Table 3.11. The overall results of Alpaydin's F-test examining the differences in RMSE (dRMSE) between models (the row model minus the column model) when using multiple locations (left) or only home response locations (right).

	Multiple response locations				Home response locations only				
dRMSE	M0	M1	M2	M3	dRMSE	M0	M1	M2	M3
M1	$-.110^{*}$				M1	$-.214^{**}$			
M2	$-.167^{***}$	$-.057^{**}$			M2	$-.210^{**}$	$.004^{—}$		
M3	$-.195^{***}$	$-.085^{***}$	$-.028^{*}$		M3	$-.207^{**}$	$.008^{—}$	$.003^{—}$	

Note: Asterisks denote significant dRMSE (***p < .001; **p < .01; *p < .05) and a dash (¯) indicates non-significant dRMSE.

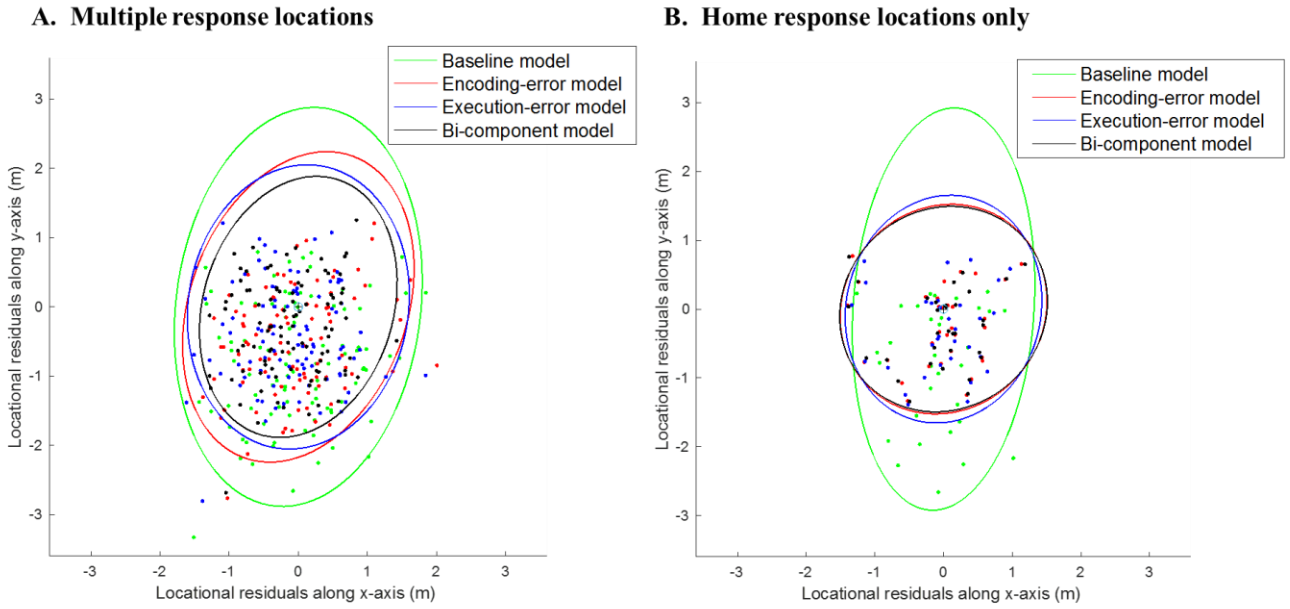

Figure 3.10. Visualizing the differences (locational residuals) between mean response locations and mean predicted locations from different models using (A) multiple response locations or (B) only home response locations. The open circle with a cross at (0, 0) indicates the response location, the coordinate of which varied in real experiments but is set to (0, 0) as a reference. Individual dots represent coordinates of the locational residuals for all targets (96 targets in A and 32 in B). Ellipses indicate the 95% density contours of the bivariate normal distributions with zero means ($\mu = (0,0)$) and covariance matrix (Σ) of the locational residuals according to the baseline model (green), encoding-error model (red), execution-error model (blue), and bi-component model (black), respectively.

3.7.2 Model recovery using varied values of parameters across participants

In the model recovery described above (see section 3.5.3), we used the fixed values of model parameters for all participants (Table 3.1) to produce simulated locations based on each true model. The simulation results indicated that the algorithm using multiple responses could recover the true models very well whereas the algorithm using home locations could not recover the true models (see Figure 3.6 for the confusion matrix). As participants showed different compression patterns (Figure 3.9), it is important to examine whether the algorithms can still recover the true model when varied values of model parameters are used to create simulated locations (below we refer to it as *model recovery with varied parameter values* and refer to the previous one as *model recovery with fixed parameter values*). Note that we conducted 5 × 2 cross-validations for strong and weak compression groups to address the issue of participants' differences in the compression pattern. Unfortunately, 5 × 2 cross-validation is not feasible for each participant. Conducting model recovery with varied parameter values is especially important as it can further address the issue of participants' differences in compression patterns. If we demonstrate that 5 × 2 cross-validations using the multiple response locations can recover the true model in model recovery with varied parameter values, our conclusion based on 5 × 2 cross-validations using the multiple response locations should also be able to recover the true model using participants' response locations.

Same as the *model recovery with fixed parameter values*, we still created 100 sets of simulated response locations from each model and conducted 5 × 2 cross-validations for all of them in conducting *model recovery with varied parameter values*. Difference from the *model recovery with fixed parameter values,* we used varied values for each of the intercept and slope parameters. Specifically, we sampled each parameter from a uniform distribution with a mean same as the fixed value of the model parameters in *model recovery with fixed parameter values*

(i.e., the parameters illustrated in Table 3.1). The range of the uniform distribution for slope parameters was twice the distance between the mean slope and 1 (i.e., the upper limit). The range of the uniform distribution for intercept parameters was twice the distance between the mean intercept and 0. For example, $\theta_{L\_s}^{enc}$ in M3 (a slope parameter in Table 3.1) was sampled from a uniform distribution U (0.82 - |1 – 0.82|, 0.82 + |1 – 0.82|). $\theta_{A\_i}^{exe}$ in M3 (an intercept parameter in Table 3.1) was sampled from a uniform distribution U (34.21 - |0 – 34.21|, 34.21 + |0 – 34.21|). As a result, we created 112 samples for each parameter of each model and then assigned them randomly to 112 participants. Using the outbound paths and target locations of each participant, we created the simulated response locations based on each model by applying the assigned values of model parameters.

Figure 3.11 presents the confusion matrix in model recovery (frequency in each category of likelihood ratio in model validation was reported in Supplementary materials of Chapter 3 Figure S3.3.). The results showed that the algorithm of using multiple response locations upon most occasions can successfully distinguish the true model from other models (64% for true model M1, 84% for true model M2, and 100% for true model M3). By contrast, the algorithm of using home response locations cannot clearly distinguish the true model from other models. In most cases, the algorithm could not find the best model (with a rate larger than 55%). Consequently, the algorithm could recover the true model at a very low rate (12% for true model M1, 28% for true model M2, and 9% for true model M3). Moreover, the algorithm also at times recovered distracting models.

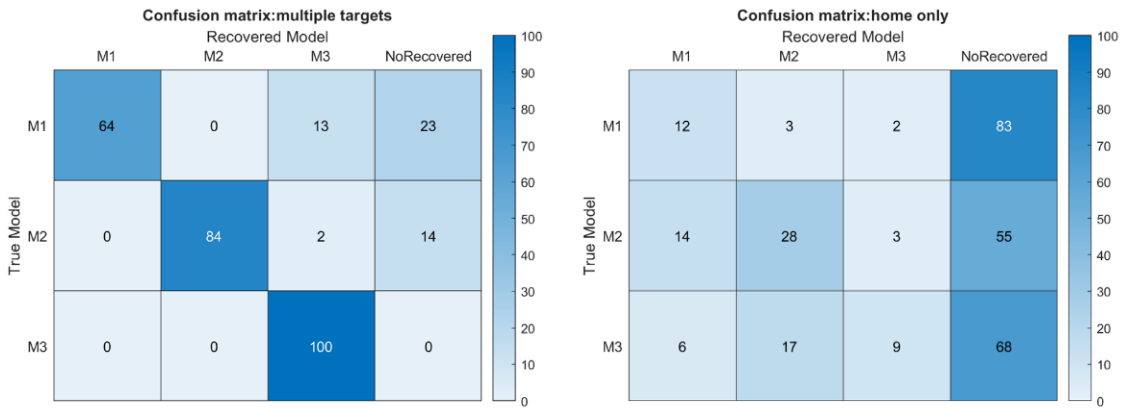

Figure 3.11. Confusion matrices in model recovery using multiple response locations (left) or home response locations only (right). The number in each cell indicates the frequency of the recovered model being the best model. NoRecoved means that no best model was recovered by the algorithm.

3.7.3 Similarity of parameters values estimated from real and simulated response locations

The similarity between parameters based on participants' response locations and based on simulated locations from different models was illustrated in Figure 3.12 (see exact parameters in Supplementary materials of Chapter 3 and Table S3.11). The parameter distance was shortest when the simulated locations were produced by M3 (RMSE= 8.59, 6.82, and 1.13 for M1, M2, and M3 respectively). The parameters based on simulated locations from M3 explained the largest proportion of the total variance of the 16 parameters based on participants' response locations ($r^2 = 1 - \frac{MSE}{Var}$, r^2 = .56, .72, and .99 for M1, M2, and M3 respectively). The ratios of likelihood of M3 over other models were larger than 2.97×10^{12} (logL = -57.11, -53.41, and -24.69 for M1, M2, and M3 respectively). Therefore, the similarity between participants' response locations and simulated locations from the bi-component model was the largest, suggesting the bi-component model was the best.

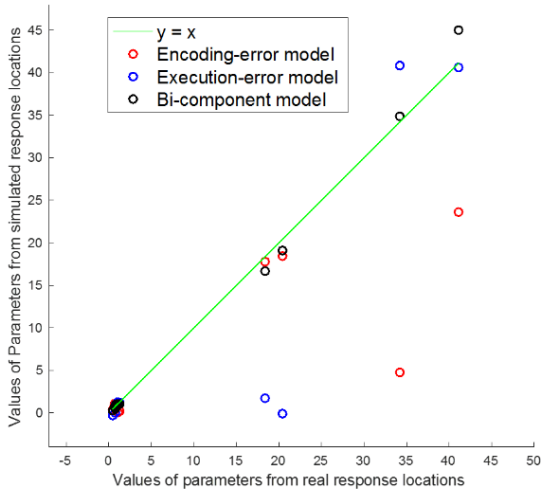

Figure 3.12. Illustrating the similarity of estimated parameters based on real data and simulated data from different models. The diagonal lines in green (y = x) indicate the ideal outcome that the parameters derived from real data are perfectly recovered from simulated data. Open dots depict the individual pairs of values of parameters based on real and simulated response locations for each model.

3.7.4 Predictive performance on the response error of participants based on best parameters for each group

We compared the predictive performance of different models in terms of inbound length error and angle error, using the best parameters for each group. The predicted error and the mean response error (in terms of inbound path length or turn angle) for each target and each unique outbound path were defined and calculated in the same way mentioned above (2.4.5).

Figure 3.13 illustrates the mean predictive performance of different models in terms of inbound length error and angle error. Table 3.12 shows that the bi-component model (M3) had the highest correlation coefficients for both inbound length (Figure 3.13A) and angle errors (Figure 3.13C) when the cross-validation included multiple response locations of each outbound path.

Nevertheless, the correlation coefficients of the three models (Figure 3.13B and Figure 3.13D) were comparable when the cross-validation only included the home response location of each outbound path.

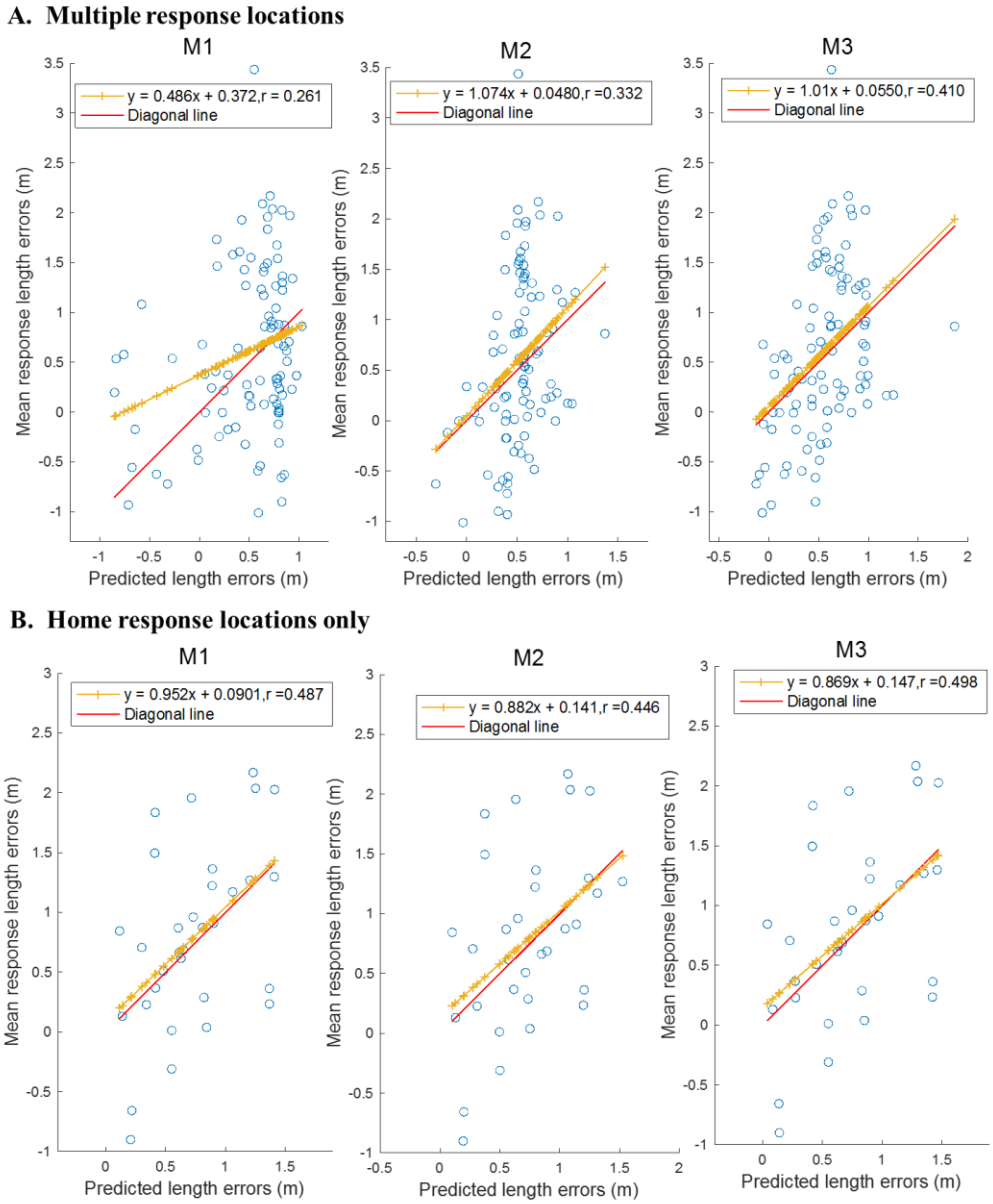

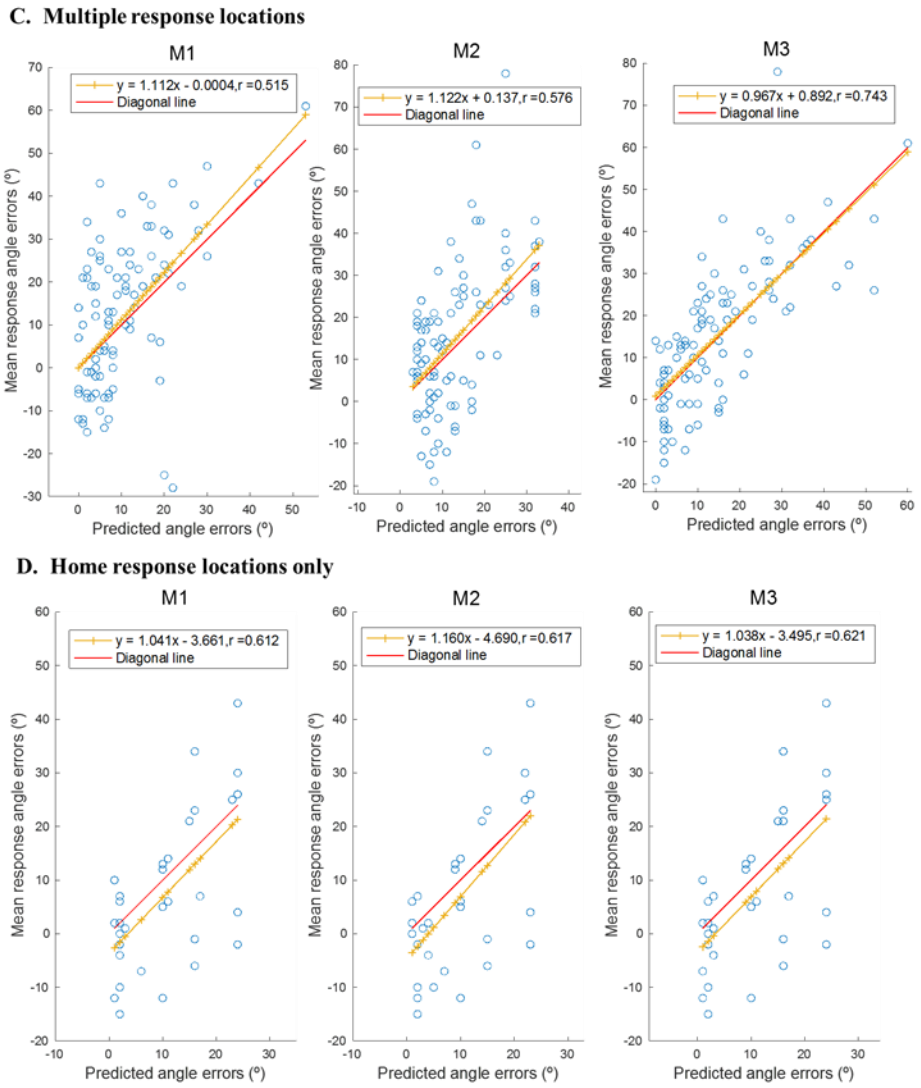

Figure 3.13. The overall performance of the predicted errors in inbound path length (panels A and B) and turn angle (panels C and D) as a function of the mean response errors using multiple response locations or only home response locations. The diagonal lines in red (y=x) indicate the ideal outcome that the response errors are perfectly predicted. The yellow lines indicate the regression lines. Open dots depict the individual pairs of predicted errors and mean response errors across participants, for each object and each path (32 paths in total), according to the

encoding-error model (M1), execution-error model (M2), and bi-component model (M3), respectively.

Table 3.12. Maximum likelihood ratios (λ) for competing models (row model over column model) in predicting inbound path length errors (left) and turn angle errors (right) using multiple locations or only home response locations.

	Length errors						Angle errors					
	Multiple response locations			Home response locations only			Multiple response locations			Home response locations only		
λ	M1	M2	M3	M1	M2	M3	M1	M2	M3	M1	M2	M3
M1												
M2	9.2^{*}			$0.5^{—}$			95.3^{**}			$1.2^{—}$		
M3	232.2^{**}	25.2^{**}		$1.3^{—}$	$2.8^{—}$		$2.1 \times 10^{10**}$	$2.2 \times 10^{8**}$		$1.3^{—}$	$1.1^{—}$	

Note: * indicates clear evidence, i.e., LR > 3 or LR <1/3, and ** indicates strong evidence, i.e., LR > 10 or LR <1/10. $^{—}$ indicates no evidence (Glover & Dixon, 2004).

3.8 Discussion

The primary purpose of the current study was to identify the possible sources of the systematic biases in human path integration. We used model cross-validation to compare three plausible theoretical models (the encoding-error model, the execution-error model, and the bi-component model) in explaining the systematic errors of the inbound responses when participants only had idiothetic cues in the path integration conditions of Qi et al. (2021). There are two important findings. First, cross-validation modeling using all three inbound responses for each outbound path indicated that the bi-component model outperformed the encoding-error model (Fujita et al., 1993) and the execution-error model (Chrastil & Warren, 2021). This finding

suggests that systematic biases in human path integration occurred in both encoding the outbound path and executing the desired inbound responses. Second, modeling using only the home response for each outbound path failed to distinguish among these three models.

To the best of our knowledge, the current study provided the first modeling evidence indicating that there are systematic biases in both encoding the outbound path (path lengths and turn angles) and in executing the desired inbound responses (path lengths and turn angles) in the triangle-completion task. The finding of both encoding and execution biases unified the encoding-error model (Fujita et al., 1993) and the execution-error model (Chrastil & Warren, 2021) into the bi-component model.

Although the finding of the current study appears to challenge the encoding-error model by undermining its assumption that there is no systematic bias in execution, it supports the key theoretical claims of the encoding-error model (Fujita et al., 1993; Klatzky et al., 1999; Loomis et al., 1993; Loomis et al., 1999). According to the encoding-error model (one version of the configural updating models), people encode the configuration of the outbound path by encoding the leg lengths and turn angles between legs. People calculate the inbound response based on the remembered outbound path. Therefore, the systematic biases (compression patterns) in encoding the outbound path should lead to the appearance of systematic biases in the inbound responses. The evidence of systematic encoding errors (i.e., the encoding functions of the bi-component model) provided by the current study is consistent with these claims. Note that although Fujita et al. (1993) showed that the encoding-error model well explained the compression patterns in the inbound responses, it could not remove the possibility that the compression patterns in the inbound responses were caused solely by the systematic biases in executing the inbound

responses. Thus, we believe that the current study indeed provides clearer evidence for the encoding biases by separating the encoding biases from the execution biases.

The current evidence of systematic execution errors is in line with the past studies (Bakker et al., 1999, 2001), which demonstrated systematic inaccuracies in simply producing specific angles. Specifically, the participants in Bakker et al. (1999) were required to produce cardinal angles (e.g., 90º, 180º, 270º) around a point under different combinations of sensory feedback. Note that in this task participants did not need to encode the angles by locomotion or visually but were only informed of the angles verbally. The significant undershoot pattern in all conditions would reflect the systematic errors in execution.

Chrastil and Warren (2021) provided the first modeling evidence to indicate that there are systematic execution errors in the triangle-completion task. They separately estimated the encoding functions and the execution functions from reproduction tasks (the simple translation and rotation tasks) by assuming that there were only encoding biases or execution biases. They argued that if people only have systematic biases in encoding but not in execution, the encoding functions estimated from the reproduction task should well explain the systematic errors in the triangle-completion task. Their modeling results showed that the discrepancy between the predicted and observed inbound responses was greater when the predicted values were only based on the encoding functions than when the predicted values were only based on the execution functions. Thus, these results suggested that there were systematic execution errors. However, it is not clear whether the encoding functions or execution functions from the simple translation and rotation tasks are the same as those functions in the triangle-completion task. The current study, using cross-validation modeling, estimated encoding functions and execution functions in the triangle-completion task using half of the data measured in the triangle-

completion task per se, instead of using other independent and simpler tasks (e.g., reproduction tasks in Chrastil & Warren, 2021). Therefore, the current study avoided the issues of assuming that the encoding functions or execution functions from the reproduction tasks are the same as those functions in the triangle-completion task. As the current study still showed that there are systematic biases in execution, separately from encoding biases, it provided clearer evidence for execution biases, one of the key claims of the execution-error model.

Chrastil and Warren (2021) also showed that the model with both encoding functions and execution functions did not outperform the model with only execution functions. In contrast, the current study indicated that both encoding biases and execution biases contributed to the biases in inbound responses. This discrepancy might occur because these two studies used different methods of estimating the encoding functions and execution functions. Chrastil and Warren (2021) estimated the encoding functions and the execution functions from reproduction tasks by assuming that there were only encoding biases or execution biases. They then used these encoding and execution functions in the model with both encoding and execution biases. However, the best parameters of encoding functions in the model with both biases may differ from the best parameters of encoding functions in the model with only encoding biases. Similarly, the best parameters of execution functions in the model with both biases may differ from the best parameters of execution functions in the model with only execution biases. By contrast, the current study estimated the encoding functions and the execution functions for the bi-component model independently rather than simply borrowing the encoding functions estimated for the encoding-error model and the execution functions estimated for the execution-error model. As shown in Tables 3.1 and 3.2, the parameters of encoding functions in the encoding-error model (M1) differ from the parameters of encoding functions in the bi-

component model (M3). The parameters of execution functions in the execution-error model (M2) also differ from the parameters of execution functions in the bi-component model (M3).

The finding that the bi-component model was the best is not attributed to more free parameters of the bi-component model than the other two models. In model validation, as the models were validated using the other halves of the data (test subsamples), the numbers of free parameters were the same for all three models. The likelihood ratio still showed the superiority of the bi-component model (see Table 3.3, left sub-table for multiple response locations). Furthermore, the findings of cross-validation modeling using the simulated response locations (multiple response locations) clearly indicated that if the true model was the encoding-error model (M1) or the execution-error model (M2), the bi-component model (M3) never outperformed the true model when the simulated locations were created using fixed values of parameters (Figure 3.6, upper panel) and seldom outperformed the true model when the simulated locations were created using varied values of parameters (Figure 3.11, upper panel).

In addition to using cross-validation, using multiple inbound responses for each outbound path is also critical to differentiate the bi-component model from the other two models. Different from the typical triangle-completion task with only one inbound response (i.e., the homing vector) for each outbound path, the triangle-completion task used in Qi et al. (2021) required participants to indicate three learned locations (including the home location) during the response phase. Previous studies indicated that one inbound response may not be able to recover participants' encoded positions and headings at the endpoint of the outbound path (e.g., Mou & Zhang, 2014). As one inbound response can be caused by many possible encoded positions and headings at the endpoint of the outbound path, this implies that the errors in the inbound response can be attributed to the encoding biases alone, the execution biases alone, or the

combination of both. In contrast, multiple inbound responses (multiple target locations) for each outbound path can recover the participants' encoded positions and headings at the endpoint of the outbound path (e.g., Mou & Zhang, 2014; Qi et al., 2021; Zhang et al., 2020). Thus, we conjectured that the encoding functions and the execution functions can be separated by a cross-validation algorithm using multiple inbound responses (multiple target locations) for each outbound path. These insights were confirmed by the modeling results based on the empirical data of Qi et al. (2021) (see Tables 3.3 and 3.4) and based on the simulated data (see Figures 3.6 and 3.11 and also Tables S3.4 and S3.11).

One may argue that the different discrimination abilities of the algorithms using multiple response locations and using home response locations alone might be attributed to the number of data points. The number in the former was three times that in the latter. According to Formulas 12 and 15, the likelihood ratio is the proportion of x^n (x is the ratio of RMSE, n is the data number). To address this issue, we calculated $\sqrt[3]{LR}$ for the LRs of M3 over M1 (LR_{31}) and M2 (LR_{32}) in model validation using multiple response locations (see Table 3.3 left, $LR_{31} = 1.28 \times 10^{20}$ and $LR_{32} = 1.02 \times 10^{11}$). The results were 5.04×10^6 and 4672.33, which still showed strong evidence favoring M3. Therefore, the evidence of favoring M3 using multiple response locations and the lack of evidence of favoring M3 only using home response locations should not be attributed to the different number of data points.

The current study supported the bi-component model, which considers linear functions to represent the working mechanisms of both encoding and execution processes, on the basis of previous research (Chrastil & Warren, 2014; 2021; Fujita et al., 1993; Loomis et al., 1993). However, we do not claim that there would be an immutable set of parameters for the current model across all pathways and contexts. Klatzky et al. (1999) reflected that the parameters of the

encoding functions based on the encoding-error model varied with the values of the outbound path (e.g., the path lengths of 1-3m or 4-6m). In addition, we admit that the encoding functions could also vary as Harootonian et al. (2020) showed that encoding functions of turn angles could be removed from their version of the encoding-error model when participants walked much longer paths.

We acknowledge that the current study examined the sources of systematic biases in homing when participants pointed to the targets including the home object. In other studies, which tackled similar research questions (Chrastil & Warren, 2021; Fujita et al., 1993; Harootonian et al., 2020), participants physically walked back home. We do not believe that this method discrepancy should undermine the conclusion of the current study because of the following evidence. First of all, although not as often as walking to the origin, pointing to the origin was still often used in the history of studying human path integration. In a review chapter on human path integration, Loomis and his colleagues wrote "Other variants of path completion have had the subject indicate only the direction of the origin from the dropoff point, typically by pointing to it using a protractor (e.g., Able & Gergits, 1985; Adler & Pelkie, 1985; Baker, 1985; Gould, 1985; Klatzky et al., 1998; Rieser & Frymire, 1995; Sadalla & Montello, 1989; Sholl, 1989)." (Loomis et al., 1999, p. 134). Hence, pointing, in addition to walking, can be used to study path integration.

Second, to our best knowledge, there is no study showing that walking and pointing to the origin led to different conclusions about human navigation. Rather, studies using either pointing or walking showed the same results. Tcheang et al. (2011) showed that participants after adapting to a smaller vision-locomotion gain (i.e., visual cues indicated a smaller turn angle than did locomotion), overestimated the inbound turn angle in the following triangle completion task

without vision. This result indicated that participants underestimated the turn angle in the outbound path because of the smaller gain. Du et al. (2020) replicated this result although participants in Tcheang et al. (2011) walked to the origin while participants in Du et al. (2020) pointed to the origin. Hence, underestimating the turn angle in the outbound path led to overestimating the inbound turn angle regardless of whether the response methods were walking or pointing. Thus, pointing, in addition to walking, can examine the biases of encoding the outbound path.

Can pointing, in addition to walking, be used to examine the biases of executing the desired inbound path? Walking (including walking forward and turning the body) and pointing appear to be two different kinds of actions. While walking is gradual (e.g., step by step), pointing seems more immediate. One may assume that execution biases occur in gradual actions but not in immediate actions. Following this assumption, one may speculate that pointing has very minimal execution errors. This speculation sounds reasonable but is inconsistent with the findings of the current study. The current study demonstrated the compression patterns (slope is smaller than 1 and intercept is larger than 0) in both inbound path length and inbound turn angle on the group level and individual levels (Figures 3.3 and 3.9). Furthermore, the best model (i.e. the bi-component model) clearly showed the compression pattern in the execution functions for both length ($\theta_{L\_s}^{exe}$ = 0.69 and $\theta_{L\_i}^{exe}$ = 1.10) and angle ($\theta_{A\_s}^{exe}$ = 0.82 and $\theta_{A\_i}^{exe}$ = 34.21) (see Table 3.1 for M3 using multiple locations). Therefore, pointing can reflect the execution biases. Hence, there is no reason to believe that the compression patterns in inbound pointing responses in the current study were caused by a mechanism different from that caused the compression patterns in inbound walking responses.

We speculated that one of the reasons why pointing to the origin was less used than walking to the origin in the research of human path integration is that in real environments, pointing may generally only indicate the direction of the origin whereas walking can indicate both direction and distance of the origin. However, nowadays in immersive virtual environments, participants could point to the exact location of the home with a virtual stick in a relatively small environment (e.g., up to 6m in Qi et al. (2021), see Figure S3.1 in the current chapter). We argue that pointing is a more effective way to study human path integration. First, it is fast to collect participants' pointing responses than walking responses. Second, there are fewer safety issues or space requirements to collect participants' pointing responses than walking responses. Last, it is possible to collect several inbound pointing responses for a single outbound path, which is important as the current study showed that the algorithm using multiple responses could differentiate models but the algorithm using homing only could not differentiate models.

Participants in the current study pointed to three objects after each outbound path, which provided a unique opportunity to differentiate models. However, one may be wondering whether the task of pointing to multiple objects invokes spatial updating mechanisms different from that used in pointing to the home location only. When people keep track of three objects during locomotion, they might only be able to update self-to-object vectors and have no extra resources to update the path configuration at the same time. In contrast, when people only keep track of the home location, they might have enough resources to update both the self-to-object vector and path configuration. Hence, participants pointing to three objects in the current study might have been less likely to have configual updating than those who only had a homing response in the typical homing studies (Kearns et al., 2002; Klatzky et al., 1999). We appreciated this concern

but argued that this concern had been addressed by the learning procedure in the paradigm of pointing to multiple objects used in the current study.

Mou and Zhang (2014), when originally introducing the paradigm of pointing to multiple objects in the inbound phase, acknowledged and addressed the issue of different memory loads in the paradigms of pointing to multiple objects and pointing to the origin only. They wrote "participants were allowed enough time to learn the directions of five objects accurately (see details in Experiment 1 for the evidence). When participants replaced the objects, they used a visible virtual stick to indicate the positions without any time pressure to ensure that they executed their responses as accurately as possible." (Mou & Zhang, 2014, p.557). Zhang et al. (2020) directly compared the paradigm of pointing to multiple objects with the paradigm of pointing to the home location when they investigated whether the Bayesian cue combination occurred prior to or during homing. Their results in experiments 1 and 2 showed the same results, that is no Bayesian cue combination in homing occurred when the second leg of the outbound path was much longer than the first leg of the outbound path. Furthermore, Lu et al. (2020) showed that online/offline spatial updating (analogue to continuous/configural updating) was not only determined by the number of objects to update during locomotion but also by the fidelity of spatial memory. When the same objects were placed at the same locations across all updating trials, participants appeared to use offline spatial updating regardless of the number of objects to update.

Therefore, as long as participants had well-learned target locations before walking the outbound path in the paradigm of pointing to multiple objects, they used the updating mechanisms similar to participants in the typical homing paradigm. Participants in the current study (i.e., Qi et al., 2021) had enough time to learn the three object locations. Furthermore, they

saw the non-home objects at the same locations across all outbound paths so they should have learned the locations of objects very well. As a result, in addition to execution biases, the current study showed encoding biases, suggesting that participants in the current study still used configural updating.

5. Conclusions

The results of modeling, using multiple inbound responses for each outbound path, support a bi-component model that incorporates both systematic biases in encoding the outbound path and executing the desired inbound responses to account for the systematic errors (regression to mean pattern) in the inbound responses. In addition, the results of modeling using only the home response for each outbound path could not dissociate the bi-component model from the encode-error model and the execution-error model. Our findings reconcile the execution-error model with the encoding-error model of human path integration. Furthermore, the current study demonstrates that cross-validation modeling using multiple inbound responses for each outbound path can be a powerful tool to understand human path integration.

3.9 References

Akaike, H. (1973). Information theory and an extension of the maximum likelihood principle. In B. N. Petrov & F. Caski (Eds.), *Second international symposium on information theory* (pp. 267-281). Budapest: Akademiai Kiado.

Alpaydm, E. (1999). Combined 5× 2 cv F test for comparing supervised classification learning algorithms. *Neural Computation*, *11*(8), *1885-1892*.

Arlot, S., & Celisse, A. (2010). A survey of cross-validation procedures for model selection. *Statistics Surveys, 4*, 40-79.

Bakker, N. H., Werkhoven, P. J., & Passenier, P. O. (1999). The effects of proprioceptive and visual feedback on geographical orientation in virtual environments. *Presence: Teleoperators & Virtual Environments, 8*(1), 36-53.

Bakker, N. H., Werkhoven, P. J., & Passenier, P. O. (2001). Calibrating visual path integration in VEs. *Presence, 10*(2), 216-224.

Benhamou, S., & Séguinot, V. (1995). How to find one's way in the labyrinth of path integration models. *Journal of Theoretical Biology, 174*(4), 463-466.

Chrastil, E. R., & Warren, W. H. (2014). Does the human odometer use an extrinsic or intrinsic metric?. *Attention, Perception, & Psychophysics, 76*(1), 230-246.

Chrastil, E. R., & Warren, W. H. (2017). Rotational error in path integration: Encoding and execution errors in angle reproduction. *Experimental Brain Research, 235*(6), 1885-1897.

Chrastil, E. R., & Warren, W. H. (2021). Executing the homebound path is a major source of error in homing by path integration. *Journal of Experimental Psychology: Human Perception and Performance, 47*(1), 13-35.

Collett, M., & Collett, T. S. (2000). How do insects use path integration for their navigation?. *Biological Cybernetics, 83*(3), 245-259.

Dietterich, T. G. (1998). Approximate statistical tests for comparing supervised classification learning algorithms. *Neural Computation, 10*(7), 1895-1923.

Du, Y., Mou, W., & Zhang, L. (2020). Unidirectional influence of vision on locomotion in multimodal spatial representations acquired from navigation. *Psychological Research, 84*(5), 1284-1303.

Etienne, A. S., & Jeffery, K. J. (2004). Path integration in mammals. *Hippocampus, 14*(2), 180-192.

Etienne, A. S., Maurer, R., & Séguinot, V. (1996). Path integration in mammals and its interaction with visual landmarks. *The Journal of Experimental Biology, 199*(1), 201-209.

Fujita, N., Klatzky, R. L., Loomis, J. M., & Golledge, R. G. (1993). The encoding-error model of pathway completion without vision. *Geographical Analysis, 25*(4), 295-314.

Gallistel, C. R. (1990). *The organization of learning*. Cambridge, MA: MIT Press.

Glover, S., & Dixon, P. (2004). Likelihood ratios: A simple and flexible statistic for empirical psychologists. *Psychonomic Bulletin & Review, 11*(5), 791-806.

Harootonian, S. K., Ekstrom, A. D., & Wilson, R. C. (2022). Combination and competition between path integration and landmark navigation in the estimation of heading direction. *PLoS Computational Biology, 18*(2), e1009222.

Harootonian, S. K., Wilson, R. C., Hejtmánek, L., Ziskin, E. M., & Ekstrom, A. D. (2020). Path integration in large-scale space and with novel geometries: Comparing vector addition and encoding-error models. *PLoS Computational Biology, 16*(5), e1007489.

He, Q., & McNamara, T. P. (2018). Spatial updating strategy affects the reference frame in path integration. *Psychonomic Bulletin & Review, 25*(3), 1073-1079.

Huttenlocher, J., Hedges, L. V., & Duncan, S. (1991). Categories and particulars: Prototype effects in estimating spatial location. *Psychological Review, 98*(3), 352-376.

Jacobs, L. F., & Schenk, F. (2003). Unpacking the cognitive map: The parallel map theory of hippocampal function. *Psychological Review, 110*(2), 285-315.

Jordan, M. I. (2003). *An Introduction to Probabilistic Graphical Models.* Chapter 13, Unpublished manuscript. Department of Statistics, University of California. https://people.eecs.berkeley.edu/~jordan/prelims/chapter13.pdf

Kearns, M. J., Warren, W. H., Duchon, A. P., & Tarr, M. J. (2002). Path integration from optic flow and body senses in a homing task. *Perception, 31*(3), 349-374.

Kelly, J. W., McNamara, T. P., Bodenheimer, B., Carr, T. H., & Rieser, J. J. (2008). The shape of human navigation: How environmental geometry is used in maintenance of spatial orientation. *Cognition, 109*(2), 281-286.

Klatzky, R. L., Beall, A. C., Loomis, J. M., Golledge, R. G., & Philbeck, J. W. (1999). Human navigation ability: Tests of the encoding-error model of path integration. *Spatial Cognition and Computation, 1*(1), 31-65.

Klatzky, R. L., Loomis, J. M., Beall, A. C., Chance, S. S., & Golledge, R. G. (1998). Spatial updating of self-position and orientation during real, imagined, and virtual locomotion. *Psychological Science, 9*(4), 293-298.

Klatzky, R. L., Loomis, J. M., Golledge, R. G., Cicinelli, J. G., Doherty, S., & Pellegrino, J. W. (1990). Acquisition of route and survey knowledge in the absence of vision. *Journal of Motor Behavior, 22*(1), 19-43.

Loomis, J. M., Klatzky, R. L., Golledge, R. G., Cicinelli, J. G., Pellegrino, J. W., & Fry, P. A. (1993). Nonvisual navigation by blind and sighted: Assessment of path integration ability. *Journal of Experimental Psychology: General, 122*(1), 73-91.

Loomis, J. M., Klatzky, R. L., Golledge, R. G., & Philbeck, J. W. (1999). Human navigation by path integration. *Wayfinding behavior: Cognitive Mapping and Other Spatial Processes*, 125-151.

Lu, R., Yu, C., Li, Z., Mou, W., & Li, Z. (2020). Set size effects in spatial updating are independent of the online/offline updating strategy. *Journal of Experimental Psychology: Human Perception and Performance, 46*(9), 901-911.

May, M., & Klatzky, R. L. (2000). Path integration while ignoring irrelevant movement. *Journal of Experimental Psychology: Learning, Memory, and Cognition, 26*, 169–186.

McNamara, T. P., & Chen, X. (2021). Bayesian decision theory and navigation. *Psychonomic Bulletin & Review*, 1-32.

Mittelstaedt, H., & Mittelstaedt, M. L. (1982). Homing by path integration In F. Papi & H. G. Wallraff (Eds.), *Avian navigation* (pp. 290–297). Berlin, Germany: Springer-Verlag.

Mittelstaedt, M. L., & Mittelstaedt, H. (1980). Homing by path integration in a mammal. *Die Naturwissenschaften, 67*(11), 566-567.

Mou, W., & Zhang, L. (2014). Dissociating position and heading estimations: Rotated visual orientation cues perceived after walking reset headings but not positions. *Cognition, 133*(3), 553-571.

Müller, M., & Wehner, R. (1988). Path integration in desert ants, Cataglyphis fortis. *Proceedings of the National Academy of Sciences, 85*(14), 5287-5290.

Péruch, P., May, M., & Wartenberg, F. (1997). Homing in virtual environments: Effects of field of view and path layout. *Perception, 26*(3), 301-311.

Petzschner, F. H., & Glasauer, S. (2011). Iterative Bayesian estimation as an explanation for range and regression effects: A study on human path integration. *Journal of Neuroscience, 31*(47), 17220-17229.

Qi, Y., Mou, W., & Lei, X. (2021). Cue combination in goal-oriented navigation. *Quarterly Journal of Experimental Psychology, 74*(11), 1981-2001.

Raschka, S. (2018). MLxtend: Providing machine learning and data science utilities and extensions to Python's scientific computing stack. *Journal of Open Source Software, 3*(24), 638.

Refaeilzadeh, P., Tang, L., & Liu, H. (2009). Cross-validation. *Encyclopedia of Database Systems, 5*, 532-538.

Rieser, J. J., Ashmead, D. H., Talor, C. R., & Youngquist, G. A. (1990). Visual perception and the guidance of locomotion without vision to previously seen targets. *Perception, 19*(5), 675-689.

Rieser, J. J., Pick, H. L., Ashmead, D. H., & Garing, A. E. (1995). Calibration of human locomotion and models of perceptual-motor organization. *Journal of Experimental Psychology: Human Perception and Performance, 21*(3), 480-497.

Rieser, J. J., & Rider, E. A. (1991). Young children's spatial orientation with respect to multiple targets when walking without vision. *Developmental Psychology*, *27*(1), 97-107.

Saint Paul, U. V. (1982). Do geese use path integration for walking home? In F. Papi, & H. G. Wallraff (Eds.), *Avian navigation* (pp. 298–307). New York: Springer.

Schwarz, G. (1978). Estimating the dimension of a model. *The Annals of Statistics*, 461-464.

Stevens, S. S., & Greenbaum, H. B. (1966). Regression effect in psychophysical judgment. *Perception & Psychophysics, 1*(5), 439-446.

Taboga, Marco (n.d.). *Multivariate normal distribution - Maximum Likelihood Estimation*. StatLect. https://www.statlect.com/fundamentals-of-statistics/multivariate-normal-distribution-maximum-likelihood.

Teghtsoonian, R., & Teghtsoonian, M. (1978). Range and regression effects in magnitude scaling. *Perception & Psychophysics, 24*(4), 305-314.

Tcheang, L., Bülthoff, H. H., & Burgess, N. (2011). Visual influence on path integration in darkness indicates a multimodal representation of large-scale space. *Proceedings of the National Academy of Sciences, 108*(3), 1152-1157.

Wang, R. F. (2016). Building a cognitive map by assembling multiple path integration systems. *Psychonomic Bulletin & Review, 23*(3), 692-702.

Warren, W. H. (2019). Non-euclidean navigation. *Journal of Experimental Biology, 222*(jeb187917), 1–10.

Warren, W. H., Rothman, D. B., Schnapp, B. H., & Ericson, J. D. (2017). Wormholes in virtual space: From cognitive maps to cognitive graphs. *Cognition, 166*, 152-163.

Wartenberg, F., May, M., & Péruch, P. (1998). Spatial orientation in virtual environments: Background considerations and experiments. In C. Freska, C. Habel & K. F. Wender (Eds.), *Spatial cognition* (pp. 469-489). Berlin: Springer.

Wehner, R., Michel, B., & Antonsen, P. (1996). Visual navigation in insects: Coupling of egocentric and geocentric information. *The Journal of Experimental Biology*, *199*(1), 129-140.

Wiener, J. M., Berthoz, A., & Wolbers, T. (2011). Dissociable cognitive mechanisms underlying human path integration. *Experimental Brain Research, 208*(1), 61-71.

Wiener, J. M., & Mallot, H. A. (2006). Path complexity does not impair visual path integration. *Spatial Cognition and Computation, 6*(4), 333-346.

Yamamoto, N., Meléndez, J. A., & Menzies, D. T. (2014). Homing by path integration when a locomotion trajectory crosses itself. *Perception, 43*(10), 1049-1060.

Zhang, L., & Mou, W. (2017). Piloting systems reset path integration systems during position estimation. *Journal of Experimental Psychology: Learning, Memory, and Cognition, 43*(3), 472-491.

Zhang, L., Mou, W., Lei, X., & Du, Y. (2020). Cue combination used to update the navigator's self-localization, not the home location. *Journal of Experimental Psychology: Learning, Memory, and Cognition, 46*(12), 2314-2339.

Chapter 4 General Discussion

Humans and non-human animals use self-motion cues (i.e., path integration) and landmarks (i.e., piloting) to keep track of their position and orientations and find their homes. The current dissertation work aims to provide new evidence to understand humans' two primary navigational processes. In Chapter 4, I first summarize the findings of the two studies presented in Chapters 2 and 3 and then discuss the implications of these findings.

4.1 Summary

Study 1 in Chapter 2 investigated the underlying mechanisms of utilizing distal and proximal landmarks to establish spatial orientation. In this study, participants familiarized themselves with the locations of objects with the presence of both proximal and distal landmarks and then walked a path. After participants spun at the end of the path to disrupt their orientations, they pointed to the objects when a clockwise-shifted proximal landmark (Proximal-Landmark condition), a counter-clockwise-shifted distal landmark (Distal-Landmark condition), or both reappeared (Conflict condition). Experiment 1 manipulated the relative cue precision by varying the distance between the testing position and the proximal landmark. The results revealed that in the Conflict condition, the observed weight on the distal cue (exceeding 0.5) changed with but remained higher than the weight predicted by the relative cue precision. This indicates that in addition to the relative cue precision, participants in general may hold a prior belief favoring distal landmarks as a superior orienting cue, which frequently results in distal dominance.

Experiments 2 and 3 investigated when participants could change cue dominance and prefer proximal landmarks for orientation. Participants walked a path stopping at one learned object location. Participants were informed of it explicitly in Experiment 2 but not in Experiment 3. Results showed proximal cue dominance in Experiment 2 but distal cue dominance in Experiment 3. The observed weight on the distal cue was lower than the predicted weight based

on relative cue precision in Experiment 2, and these two did not differ in Experiment 3, suggesting a top-down preference for the proximal landmark (invoked by the instruction of locations) attributing to the proximal landmark dominance. When navigators possess a clear and precise understanding of their position relative to a proximal landmark, a proximal landmark can override a distal one and become the dominant orientation cue. In such cases, people confidently use this knowledge to favor the proximal landmark, leading to proximal dominance in orientation. Therefore, orientation cue usage is determined by the relative precision of the cues available in the specific experiments and top-down factors (e.g., beliefs and instructions).

Study 2 in Chapter 3 examined the contributions of potential sources of systematic errors in human triangle completion. This study used cross-validation modeling to compare three plausible theoretical models: (1) encoding-error model, which assumes systematic biases in encoding the outbound path alone, (2) execution-error model, which assumes systematic biases in executing the inbound responses alone, (3) bi-component model, which assumes systematic biases in both encoding the outbound path and executing the inbound responses. The data of the triangle completion for cross-validation modeling were obtained from a prior study (Qi et al., 2021). In this earlier research, participants well-learned three objects' locations, one of which was located at the starting point (home). They then walked each outbound path and subsequently pointed to the objects' original locations after completing the outbound path. The modeling algorithm used one inbound response (i.e., response to the home location) or multiple inbound responses (i.e., responses to two non-home locations and the home) for each outbound path.

The results of the modeling demonstrated that the bi-component model outperformed the other models in accounting for the systematic errors when using multiple inbound responses for each outbound path. This finding suggests that both encoding the outbound path and executing

the inbound responses contribute to the systematic biases in human path integration, unifying two opposite models in the literature (i.e., encoding-error model and execution-error model). In addition, the results of Study 2 showed that using only the home response in the algorithm could not distinguish among these three models, suggesting that the typical triangle-completion task with only the home response for each outbound path cannot determine the sources of the systematic biases. In summary, this study helps to advance our understanding of the mechanisms underlying human path integration and also provides important contributions to the research methods to study human path integration.

Study 1 and Study 2 are closely connected. In Study 1, participants used path integration for position estimation in DLM and PLM conditions (particularly when explicit instructions were not provided in Experiments 1 and 3), and used the landmark provided for heading estimation. The transition from one-legged paths in Experiment 1 to two-legged paths in Experiment 3 led to increased errors in position estimation via path integration. This finding is echoed in Study 2, which identifies the encoding of the outbound path as a key factor in the systematic biases observed in human path integration.

4.2 Implications of the current studies

The two studies in this dissertation shed light on how human adults acquire spatial representation during navigation by relying on the processes of path integration and piloting. In this section, I will discuss two aspects of the implications of the current findings.

4.2.1 Utilizing proximal landmarks for positional information in experimental paradigms

There are numerous studies employing experimental paradigms in which distal landmarks orientation information, whereas proximal landmarks offer positional information during navigation (e.g., Buckley et al., 2015; Bullens et al., 2010; Doeller & Burgess, 2008; Padilla et

al., 2017; Zhang & Mou, 2017). For example, Bullens et al. (2010) employed distant extramaze (e.g., arrays of LED lights) as orientation cues while examining how children encode object locations relative to a boundary (a circular wall) and a proximal intramaze landmark (a traffic cone).

It is noteworthy that Study 1 in the current dissertation clearly demonstrates that a proximal landmark can provide orientation information and may even override a distal landmark to dominate participants' heading estimates when they were clearly aware of their positions relative to the proximal landmark. Therefore, when formulating experimental paradigms that incorporate one or multiple proximal landmarks intended solely for conveying positional information, it becomes crucial to exercise caution regarding the potential utilization of these proximal landmarks for orientation purposes.

To illustrate, suppose one is designing an experiment to investigate whether navigators combine cues from path integration (self-motion cues) and piloting (visual cues) to estimate their current position, rather than their home location. This could further examine Zhang et al.'s (2020) self-localization hypothesis, which posits that the combination of path integration and piloting occurs in navigators' self-localization but not in homing. In a typical paradigm, participants learn the locations of target objects in the presence of proximal and distal landmarks. Subsequently, participants traverse a path without seeing objects/landmarks and are required to indicate the objects' locations at the end of the path. Distal landmarks would be available for participants to orient themselves upon reaching the end of the path. However, the availability of different positional cues (i.e., self-motion cues and proximal landmarks) would be manipulated, generating different conditions to examine cue combination in position estimations, such as a *path-integration-only* condition with self-motion cues, a *landmark-only* condition with proximal

landmark, and a *both-cue* condition with proximal landmark and self-motion cues. In *both-cue* condition, navigators can update the vector between their self-location and the proximal landmark during walking relying on self-motion cues, and this vector can provide orientation information. It is plausible that participants employ self-motion cues for determining their position and the proximal landmark for orientation in the *both-cue* condition, which deviates from the intended objective of the design and cannot test the cue combination in position estimations appropriately.

In order to minimize the likelihood of the proximal landmark being utilized for orientation in this experimental setup, one effective approach is to locate the landmark and the navigators' response location in close proximity, to a certain extent. The closer they are, the less effectively it functions as an orientation cue. The findings from Experiment 1 of Study 1 have demonstrated that the precision of the orientation cue diminishes as the distance between the proximal landmark and participants' response position varies, ranging from 3.2 meters to 1.6 meters.

4.2.2 The format of spatial knowledge based on path integration

Humans and other animals navigate and develop spatial awareness through path integration, but the fundamental format of resulting spatial knowledge remains a subject of debate (Tobler, 1976; Trullier et al., 1997; Tversky, 1993). The metric cognitive map hypothesis, initially introduced by Tolman (1948), has been a prevailing theory (Gallistel & Cramer, 1996; O'Keefe & Nadel, 1978). According to this hypothesis, a cognitive map retains metric details of known locations within a common coordinate system (Gallistel, 1990; O'Keefe & Nadel, 1978; Tolman, 1948). It assumes accurate measurement of distances and angles and requires precise integration to create a globally accurate metric representation.

However, the current findings of substantial systematic encoding errors pose a problem for the concept of a metric cognitive map. Instead, these findings suggest that the format of spatial knowledge on the basis of path integration may be better suited for constructing a labeled graph (also known as a cognitive graph). A labeled graph is a place graph with local metric information. In this representation, edge weights approximate path lengths, while node labels provide estimates of the angles between adjacent paths at intersections (as depicted in Figure 1 in Warren et al., 2017 or Warren, 2019). Notably, a labeled graph does not demand highly precise encoding (Warren, 2019). The quantitative information it preserves remains local and tends to exhibit biases and imprecision, resulting in spatial knowledge that lacks geometric consistency (Warren, 2019).

Additionally, other empirical evidence suggests that path integration is more suited for constructing a labeled graph. Firstly, path integration may not operate continuously and automatically but rather intermittently. In an environment with stable visual landmarks for piloting, the operation of path integration may be suppressed or completely deactivated. In such scenarios, the unexpected disappearance of these landmarks can lead to complete disorientation among navigators (Zhao and Warren, 2015a). Moreover, familiar landmarks could reset the representation derived from path integration, such as navigators' orientation and position estimates. (Mou & Zhang, 2014; Zhang & Mou, 2017; Zhao & Warren, 2015b). Consequently, the path integration system is better suited for capturing local, incremental measurements of approximate travel distances and turn angles, which are then incorporated into a cognitive graph.

4.3 Limitations and future research

The study in Chapter 2 investigated whether distal landmarks dominate over proximal landmarks as orientation cues. This study focused on a single independent proximal landmark to

avoid the orientation indicated by the configuration of multiple landmarks. Previous studies suggest that the spatial arrangement of multiple proximal landmarks and their placement within the environment can have a significant impact on their role as orientation cues (Lee & Spelke, 2010; Pecchia & Vallortigara, 2010; for review, see Lew, 2011). The specific geometric configuration of landmarks and their relationship to the navigational space may influence how they interact with distal landmarks in determining orientations. In addition, the current studies used relatively simple and short paths. The generalizability of the findings to navigation scenarios with complex and long paths remains an open question that requires further research. Therefore, considering these factors in future research will be essential for gaining a comprehensive understanding of how humans integrate and utilize different cues for spatial orientation in various navigation scenarios.

The study in Chapter 3 investigated the sources of systematic errors in human triangle completion and supported the bi-component model. Additional studies are needed to examine the applicability of the bi-component model under various conditions, such as path integration on more complex paths, since navigators may adopt different navigational strategies depending on the complexity of the path (Klatzky et al., 1990; Wiener et al., 2011; Wiener & Mallot, 2006). On simple pathways, navigators are more likely to remember the path configuration, and calculate the vector to go home only when needed (that is, an offline process), which is a configural strategy. On complex pathways, however, storing the presentation of the path configuration is challenging for navigators, and they tend to switch to continuously updating the homing vector (that is, an online process), which is a continuous strategy. Wiener and Mallot (2006) demonstrated that participants pointed homeward even faster and more accurately as path complexity increased while maintaining the overall path length, turn angle, and turning direction

constant. In addition, an outbound path with path crossover might also be hard to encode the configuration (Fujita et al., 1993; Klatzky et al., 1990). However, Yamamoto et al. (2014) found that the presence of path crossover in traveled paths caused little impact on path integration performance. Future studies may test the bi-component model using outbound paths with more turns and path crossover.

Another potential limitation of the current bi-component model is presuming minimal systematic integration errors, as with previously proposed models of path integration (Benhamou & Séguinot, 1995; Chrastil & Warren, 2021; Fujita et al., 1993; Harootonian et al., 2020). The integration errors emerge from computing the desired inbound responses based on the internalized representation of the traversed path. In addition to cognitive maps, humans also build labeled graphs (Warren, 2019; Warren et al., 2017), and the difference between these two may reflect the involvement of integration errors. One conjecture is that as the complexity of the outgoing path increases, the integration errors will subsequently surge (if one keeps using the configural navigation strategy). Future modeling studies may consider some possible systematic biases in the integration errors instead of assuming that there were random integration errors.

4.4 References

Benhamou, S., & Séguinot, V. (1995). How to find one's way in the labyrinth of path integration models. *Journal of Theoretical Biology, 174*(4), 463-466.

Buckley, M. G., Haselgrove, M., & Smith, A. D. (2015). The developmental trajectory of intramaze and extramaze landmark biases in spatial navigation: An unexpected journey. *Developmental Psychology, 51*(6), 771-791.

Bullens, J., Nardini, M., Doeller, C. F., Braddick, O., Postma, A., & Burgess, N. (2010). The role of landmarks and boundaries in the development of spatial memory. *Developmental Science, 13*(1), 170-180.

Chrastil, E. R., & Warren, W. H. (2021). Executing the homebound path is a major source of error in homing by path integration. *Journal of Experimental Psychology: Human Perception and Performance, 47*(1), 13-35.

Doeller, C. F., & Burgess, N. (2008). Distinct error-correcting and incidental learning of location relative to landmarks and boundaries. *Proceedings of the National Academy of Sciences, 105*(15), 5909-5914.

Fujita, N., Klatzky, R. L., Loomis, J. M., & Golledge, R. G. (1993). The encoding-error model of pathway completion without vision. *Geographical Analysis, 25*(4), 295-314.

Gallistel, C. R. (1990). *The organization of learning*. Cambridge, MA: The MIT Press.

Harootonian, S. K., Wilson, R. C., Hejtmánek, L., Ziskin, E. M., & Ekstrom, A. D. (2020). Path integration in large-scale space and with novel geometries: Comparing vector addition and encoding-error models. *PLoS Computational Biology, 16*(5), e1007489.

Klatzky, R. L., Loomis, J. M., Golledge, R. G., Cicinelli, J. G., Doherty, S., & Pellegrino, J. W. (1990). Acquisition of route and survey knowledge in the absence of vision. *Journal of Motor Behavior, 22*(1), 19-43.

Lee, S. A., & Spelke, E. S. (2010). A modular geometric mechanism for reorientation in children. *Cognitive Psychology, 61*(2), 152-176.

Mou, W., & Zhang, L. (2014). Dissociating position and heading estimations: Rotated visual orientation cues perceived after walking reset headings but not positions. *Cognition, 133*(3), 553-571.

O'Keefe, J., & Nadel, L. E. (1978). *The hippocampus as a cognitive map*. Oxford: Clarendon Press.

Padilla, L. M., Creem-Regehr, S. H., Stefanucci, J. K., & Cashdan, E. A. (2017). Sex differences in virtual navigation influenced by scale and navigation experience. *Psychonomic Bulletin & Review, 24*, 582-590.

Pecchia, T., & Vallortigara, G. (2010). View-based strategy for reorientation by geometry. *Journal of Experimental Biology, 213*(17), 2987-2996.

Qi, Y., Mou, W., & Lei, X. (2021). Cue combination in goal-oriented navigation. *Quarterly Journal of Experimental Psychology, 74*(11), 1981-2001.

Tobler, W. R. (1976). *The geometry of mental maps.* In R. G. Golledge & G. Rushton (Eds.), Spatial choice and spatial behavior (pp. 69–82). Columbus, OH: Ohio State University Press.

Tolman, E. C. (1948). Cognitive maps in rats and men. *Psychological Review, 55*, 189–208.

Trullier, O., Wiener, S. I., Berthoz, A., & Meyer, J.-A. (1997). Biologically based artificial navigation systems: Review and prospects. *Progress in Neurobiology, 51*, 483–544.

Tversky, B. (1993). *Cognitive maps, cognitive collages, and spatial mental models*. Spatial information theory a theoretical basis for GIS. Springer.

Warren, W. H. (2019). Non-euclidean navigation. *Journal of Experimental Biology, 222*,1-10.

Warren, W. H., Rothman, D. B., Schnapp, B. H., & Ericson, J. D. (2017). Wormholes in virtual space: From cognitive maps to cognitive graphs. *Cognition, 166*, 152-163.

Wiener, J. M., Berthoz, A., & Wolbers, T. (2011). Dissociable cognitive mechanisms underlying human path integration. *Experimental Brain Research, 208*(1), 61-71.

Wiener, J. M., & Mallot, H. A. (2006). Path complexity does not impair visual path integration. *Spatial Cognition and Computation, 6*(4), 333-346.

Yamamoto, N., Meléndez, J. A., & Menzies, D. T. (2014). Homing by path integration when a locomotion trajectory crosses itself. *Perception, 43*(10), 1049-1060.

Zhang, L., & Mou, W. (2017). Piloting systems reset path integration systems during position estimation. *Journal of Experimental Psychology: Learning, Memory, and Cognition, 43*(3), 472-491.

Zhang, L., Mou, W., Lei, X., & Du, Y. (2020). Cue combination used to update the navigator's self-localization, not the home location. *Journal of Experimental Psychology: Learning, Memory, and Cognition. 46*(12), 2314-2339.

Zhao, M., & Warren, W. H. (2015a). How you get there from here: Interaction of visual landmarks and path integration in human navigation. *Psychological Science, 26*(6), 915-924.

Zhao, M., & Warren, W. H. (2015b). Environmental stability modulates the role of path integration in human navigation. *Cognition, 142*, 96-109.

Supplementary materials of Chapter 2

The relationship between heading errors, position errors, and homing errors

Figure S2.1 illustrates the angular error for participants' heading, position, and homing estimates, denoted as η, π, θ, respectively.

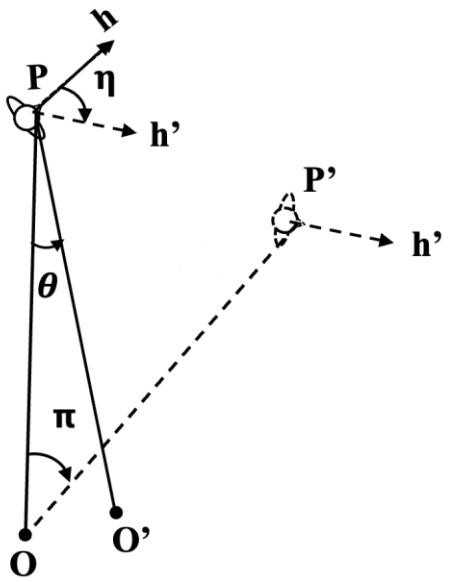

Figure S2.1. Illustrating the response measures of the current study. A hypothetical participant starts from his or her original position O (home) and ends at the position P and with the heading *h* after navigation. His or her estimates of P and *h* are P' and *h*'. He or she points to O' as the estimate of O. Heading error (η) is the angle from the direction *h* to the direction *h*'. Position error (π) is the angle from $\overrightarrow{OP}$ to $\overrightarrow{OP'}$. Homing error (θ) is the angle from $\overrightarrow{PO}$ to $\overrightarrow{PO'}$.

Previous research has demonstrated the relationship between heading errors, position errors, and homing errors: the homing error (θ) depends on both heading error (η) and the position error (π), as described by the following equation (Zhang et al., 2020, Equations 5).

$$\theta = \pi - \eta \qquad \text{(S1)}$$

Figure S2.2 provides examples of a presentative participant (specifically, Participant No. 14 from Experiment 1a) to illustrate the bidimensional regression approach used in calculating the estimated positions and headings for all three conditions.

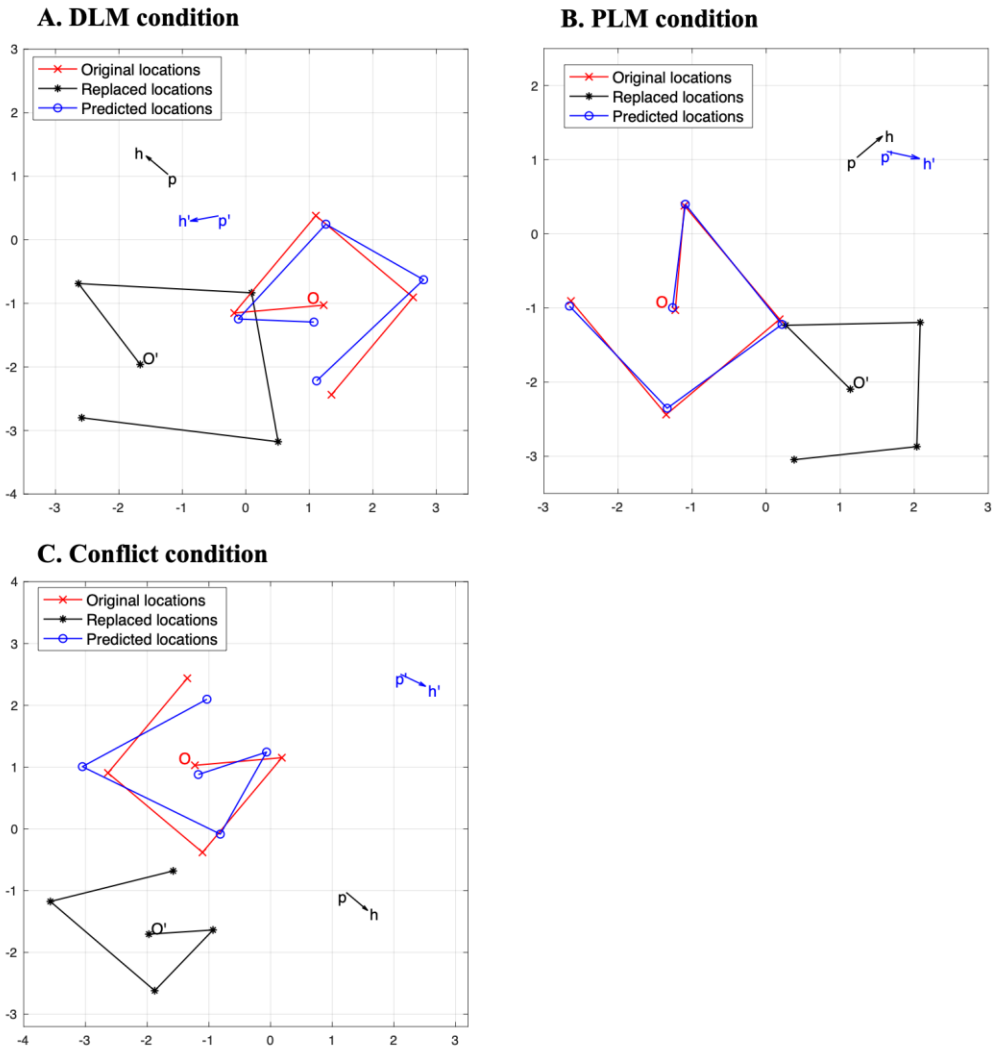

Figure S2.2. Demonstrating the bidimensional regression approach used for calculating estimated positions and headings. A participant memorizes the original locations of five targets (e.g., target O). After navigation, the participant replaces the targets at a testing position P with a heading direction h. Conceptually, the bidimensional regression generates a prediction function, encompassing a transformation matrix that includes uniform scaling, rotation, and translation.

This prediction function converts the replaced locations (e.g., O') to the predicted locations that minimize the overall distance from the original locations (e.g., O) (Friedman & Kohler, 2003). Subsequently, the prediction function calculates h' and P' using h and P as the predictor values, respectively. Lines connect the locations solely to illustrate their configuration, aiding readers in understanding the relationships among the three configurations.

Predictions of homing errors and position errors

The home location (i.e., the origin of the path) was overlapped with the traffic cone (i.e., the proximal landmark) before navigation. For the PLM and Conflict conditions, the traffic cone (being rotated -50°) reappeared when participants were asked to replace targets after navigation. For the PLM and Conflict conditions, the predicted homing error (θ) would be -50° (see Table S2.1) if participants used the reappeared proximal landmark to indicate the home location. For the DLM condition, participants would use the distal landmark for heading estimates (η = -50°) and path integration for position estimates (π = 0°). The predicted homing error for the DLM condition would be 50° based on the Equation 1 (θ = π – η = 50°).

Participants were disoriented at the endpoint of the path so that their heading estimates from path integration was disrupted but their position estimates from path integration remain intact. For the single-cue conditions (DLM and PLM conditions), participants were expected to use the reappeared landmark for estimating headings and rely on path integration for position estimates. The predicted position errors for DLM and PLM conditions are 0° (π = 0°). For the Conflict condition, as the predicted homing error (θ) is -50°, the predicted position error would be π = θ + η = -50 + η. For example, if participants use the rotated distal landmark for heading estimates (i.e., η = -50°, W_{Dlm} = 1), the predicted position error would be -100° (π = θ + η = -50°

+ (-50°) = -100°); if participants use the rotated proximal landmark for heading estimates (i.e., η = 50°, W_{Dlm} = 0), the predicted position error would be 0° (π = θ + η = -50°+50° = 0°).

Table S2.1. Predicted homing and position errors and the circular means (circular standard deviations) of the participant-level homing and position errors in each cue condition of all experiments. W_{Dlm} = 1 indicates that participants use distal landmarks for heading. W_{Dlm} = 0 indicates that participants use the proximal landmark for heading.

Conditions	DLM	PLM	Conflict	
Predicted homing errors	50°	-50°	-50°	
Observed homing errors (Exp 1a)	25.0° (45.7°)	-51.4° (3.9°)	-50.8° (2.7°)	
Observed homing errors (Exp 1b)	19.4° (63.8°)	-49.7° (2.1°)	-47.7° (10.1°)	
Observed homing errors (Exp 2)	37.7° (24.6°)	-49.9° (5.7°)	-46.5° (14.6°)	
Observed homing errors (Exp 3)	36.0° (57.1°)	-52.7° (8.7°)	-52.4° (5.8°)	
Predicted position errors	0°	0°	-100° (W_{Dlm} = 1)	0° (W_{Dlm} = 0)
Observed position errors (Exp 1a)	-14.4° (27.7°)	-8.2° (31.4°)	-62.2° (26.5)	
Observed position errors (Exp 1b)	-2.4° (53.9°)	-8.7° (48.2°)	-75.2° (26.7°)	
Observed position errors (Exp 2)	-3.1° (9.5°)	6.0° (15.7°)	-7.1° (21.2°)	
Observed position errors (Exp 3)	-6.5° (44.5°)	-26.6° (66.1°)	-86.1° (27.7°)	

Results of homing errors and position errors

For each participant, we calculated the circular mean and circular standard deviation (referred to as participant-level circular mean and standard deviation) across individual homing

errors and position errors in the same cue condition, respectively. The group-level circular means of the participant-level circular mean and their corresponding confidence intervals were also calculated for each condition.

Homing errors of Experiment 1

Participant-level circular means of the homing errors and their mean and confidence interval in all conditions are plotted in Figure S2.3. The group-level circular mean and circular standard deviation are summarized in Table S2.1. The Rayleigh *Z* test showed that the homing errors in all conditions were clustered around one direction (Zs $\geqq 8.11$, ps $< .001$).

Participant-level circular means: In the DLM condition, the mean homing error was 25.0° with a 95% confidence interval [8.2°, 41.8°] in Experiment 1a (Figure S2.3A) and the mean homing error was 19.4° with a 95% confidence interval [-6.1°, 45.0°] in Experiment 1b (Figure S2.3D).

In the PLM condition, the homing estimates clustered around the predicted homing errors (-50°) based on the rotated proximal landmark (the dotted orange line in Figure S2.3B and S2.3E) in both Experiments 1a and 1b (mean homing error = -51.4°, 95% CI [-52.8°, -49.96°] and mean homing error = -49.7°, 95% CI [-50.5°, -48.9°], respectively).

In the Conflict condition, the homing estimates clustered around the predicted homing errors (-50°) based on the rotated proximal landmark (the dotted orange line in Figure S2.3C and S2.3F) in both Experiments 1a and 1b (mean homing error = -50.8°, 95% CI [-51.9°, -49.8°] and mean homing error = -47.7°, 95% CI [-51.5°, -43.97°], respectively).

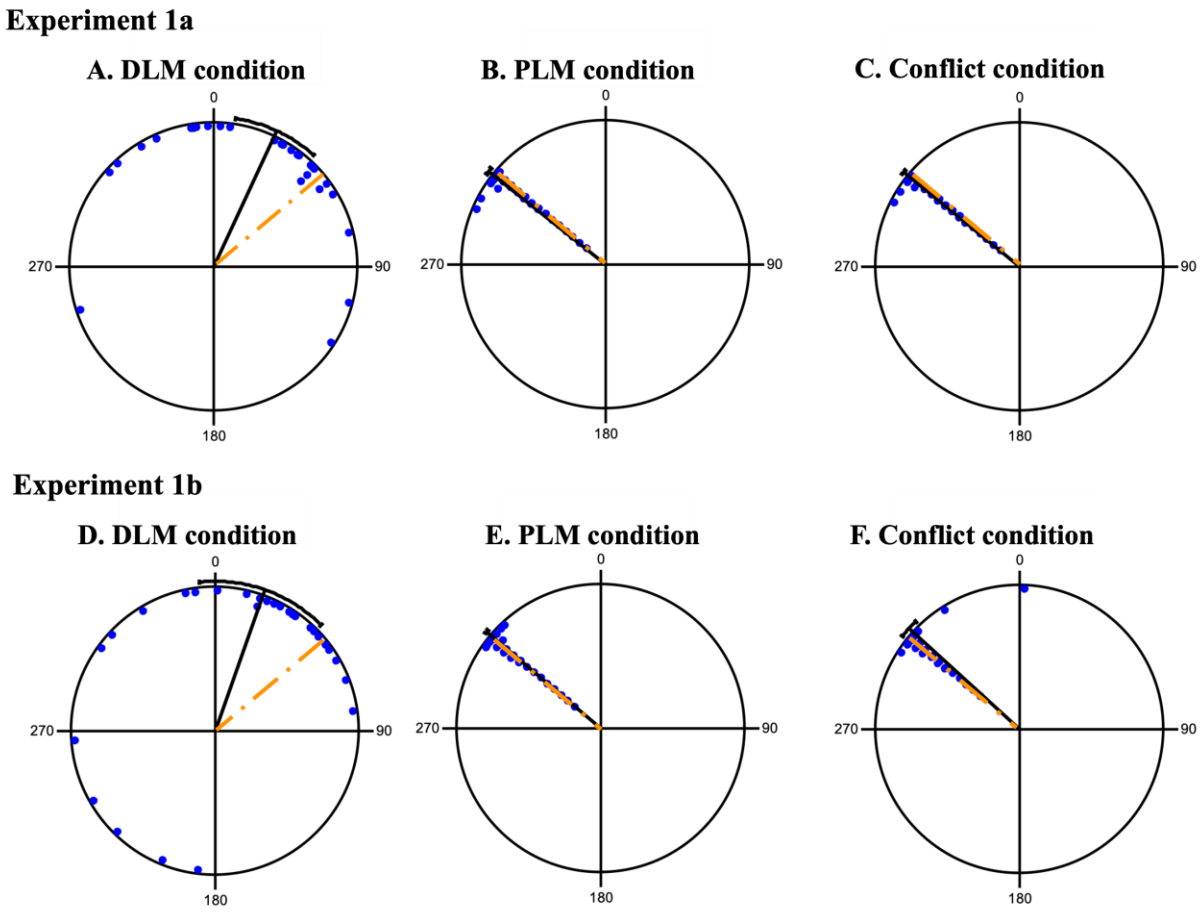

Figure S2.3. Observed and predicted homing errors in the DLM (panels A and D), PLM (panels B and E), and Conflict conditions (panels C and F) in Experiments 1a and 1b. Each blue dot indicates one participant-level circular mean of homing errors across paths. The solid black line indicates the group-level circular mean of the homing errors across participants. The black arc indicates the 95% confidence interval of the group-level circular mean. The dotted orange lines indicate the predicted homing errors in corresponding conditions.

Participant-level circular standard deviation: The means of participant-level circular standard deviations in all conditions are plotted in Figure S2.4. We conducted repeated-measure ANOVA with one within-subject factor (cue condition: DLM, PLM, and Conflict) for

Experiment 1a and 1b respectively. There was significant difference among conditions in Experiment 1a, $F(2, 54) = 60.25$, $p < .001$, $MSE = 151.23$, $\eta_p^2 = .69$. The SD in the DLM condition was significantly larger than that in the PLM condition, $t(27) = 7.70$, $p < .001$, Cohen's $dz = 1.45$ and that in the Conflict condition, $t(27) = 7.87$, $p < .001$, Cohen's $dz = 1.48$. The SDs in the PLM and Conflict conditions did not differ, $t(27) = 0.84$, $p = .41$, Cohen's $dz = 0.16$, $BF_{01} = 3.61$.

There was a significant difference among conditions in Experiment 1b, $F(2, 54) = 34.64$, $p < .001$, $MSE = 445.67$, $\eta_p^2 = .56$. The SD in the DLM condition was significantly larger than that in the PLM condition, $t(27) = 6.52$, $p < .001$, Cohen's $dz = 1.23$ and that in the Conflict condition, $t(27) = 5.92$, $p < .001$, Cohen's $dz = 1.12$. The SDs in the PLM and Conflict conditions did not differ, $t(27) = 0.17$, $p = .87$, Cohen's $dz = 0.03$, $BF_{01} = 4.93$.

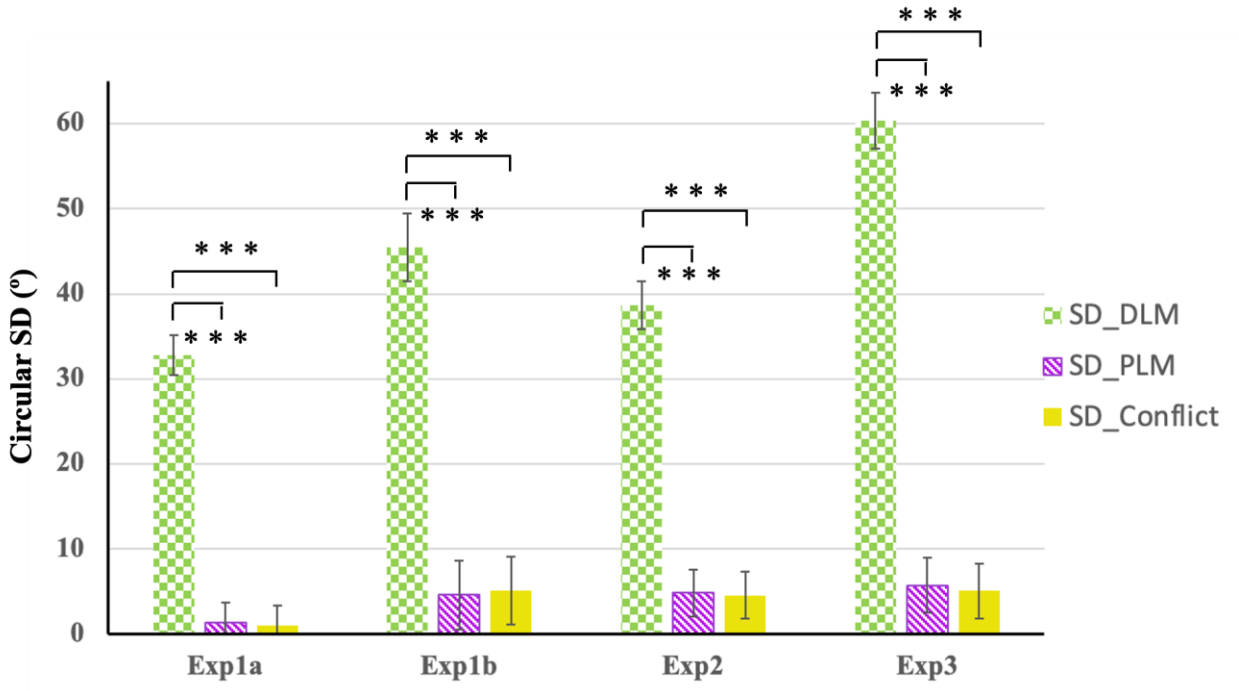

*Figure S2.4. The means of participant-level circular standard deviations of the homing errors in all conditions of all experiments. The solid lines represent significant comparisons (***p*

< .001). Error bars represent ± 1 SE of the means (from the MSE of each repeated-measure ANOVA).

Homing errors of Experiment 2

Participant-level circular means: In the DLM condition, the mean homing error was 37.7° with a 95% confidence interval [28.6°, 46.8°] in Experiment 2 (Figure S2.5A).

In the PLM condition, the homing estimates clustered around the predicted homing errors (-50°) based on the rotated proximal landmark (the dotted orange line in Figure S2.5B) in Experiment 2 (mean homing error = -49.9°, 95% CI [-51.9°, -47.8°]).

In the Conflict condition, the homing estimates clustered around the predicted homing errors (-50°) based on the rotated proximal landmark (the dotted orange line in Figure S2.5C) in Experiment 2 (mean homing error = -46.5°, 95% CI [-51.9°, -41.1°]).

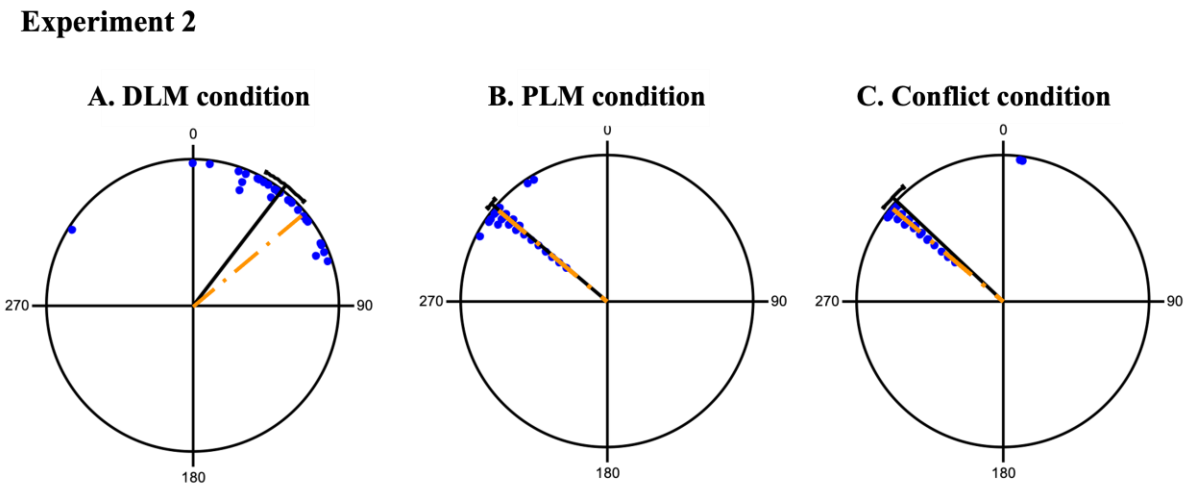

Figure S2.5. Observed and predicted homing errors in the DLM (panel A), PLM (panel B), and Conflict conditions (panel C) in Experiment 2. Each blue dot indicates one participant-level circular mean of heading errors across paths. The solid black line indicates the group-level circular mean of the heading errors across participants. The black arc indicates the 95%

confidence interval of the group-level circular mean. The dotted orange lines indicate the predicted homing errors in corresponding conditions.

Participant-level circular standard deviation: The means of participant-level circular standard deviations in all conditions are plotted in Figure S2.4. We conducted repeated-measure ANOVA with one within-subject factor (cue condition: DLM, PLM, and Conflict). There was a significant difference among conditions, $F(2, 54) = 50.42$, $p < .001$, $MSE = 213.50$, $\eta_p^2 = .65$. The SD in the DLM condition was significantly larger than that in the PLM condition, $t(27) = 8.60$, $p < .001$, Cohen's $dz = 1.63$ and that in the Conflict condition, $t(27) = 7.77$, $p < .001$, Cohen's $dz = 1.47$. The SDs in the PLM and Conflict conditions did not differ, $t(27) = 0.07$, $p = .94$, Cohen's $dz = 0.01$, $BF_{01} = 4.98$.

Homing errors of Experiment 3

Participant-level circular means: In the DLM condition, the mean homing error was 36.0° with a 95% confidence interval [14.1°, 57.8°] in Experiment 3 (Figure S2.6A). The predicted homing error for the DLM condition (50°) was encompassed in the 95% CI.

In the PLM condition, the homing estimates clustered around the predicted homing errors (-50°) based on the rotated proximal landmark (the dotted orange line in Figure S2.6B) in Experiment 3 (mean homing error = -52.7°, 95% CI [-55.9°, -49.5°]).

In the Conflict condition, the homing estimates clustered around the predicted homing errors (-50°) based on the rotated proximal landmark (the dotted orange line in Figure S2.6C) in Experiment 3 (mean homing error = -52.4°, 95% CI [-54.5°, -50.2°]).

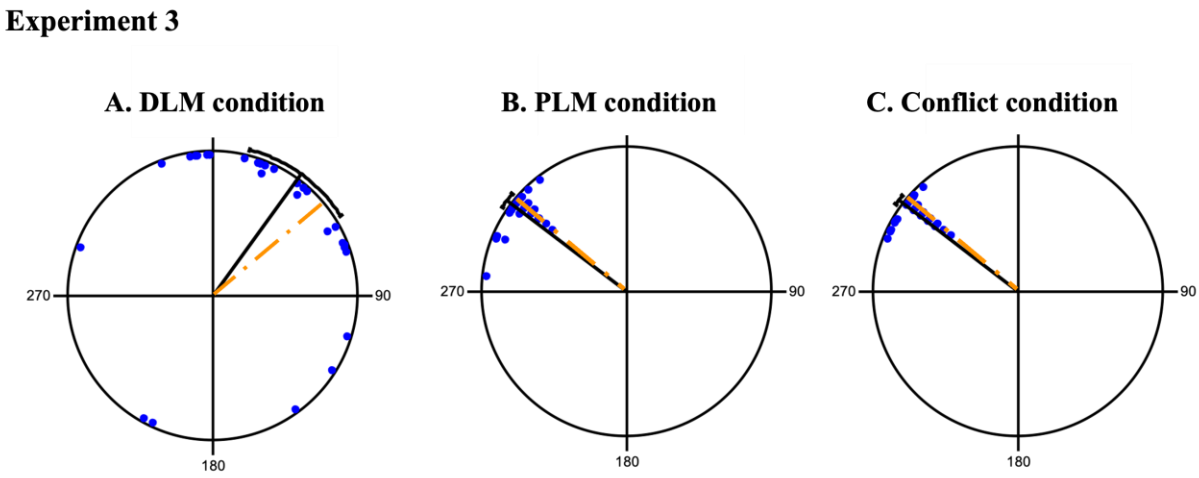

Figure S2.6. Observed and predicted homing errors in the DLM (panel A), PLM (panel B), and Conflict conditions (panel C) in Experiment 3. Each blue dot indicates one participant-level circular mean of heading errors across paths. The solid black line indicates the group-level circular mean of the heading errors across participants. The black arc indicates the 95% confidence interval of the group-level circular mean. The dotted orange lines indicate the predicted homing errors in corresponding conditions.

Participant-level circular standard deviation: The means of participant-level circular standard deviations in all conditions are plotted in Figure S2.4. We conducted repeated-measure ANOVA with one within-subject factor (cue condition: DLM, PLM, and Conflict). There was a significant difference among conditions, $F(2, 54) = 95.34$, $p < .001$, $MSE = 295.78$, $\eta_p^2 = .78$. The SD in the DLM condition was significantly larger than that in the PLM condition, $t(27) = 10.67$, $p < .001$, Cohen's $dz = 2.02$ and that in the Conflict condition, $t(27) = 9.87$, $p < .001$, Cohen's $dz = 1.87$. The SDs in the PLM and Conflict conditions did not differ, $t(27) = 0.29$, $p = .78$, Cohen's $dz = 0.05$, $BF_{01} = 4.80$.

Position errors

Position errors of Experiment 1

Participant-level circular means of the position errors and their mean and confidence interval in all conditions are plotted in Figure S2.7. The group-level circular mean and circular standard deviation are summarized in Table S2.1. The Rayleigh *Z* test showed that the position errors in all conditions were clustered around one direction (Zs $\geqq$11.54, ps < .001).

Participant-level circular means: In the DLM condition, the mean position error was -14.4° with a 95% confidence interval [-24.6°, -4.1°] in Experiment 1a (Figure S2.7A) and the mean position error was -2.4° with a 95% confidence interval [-22.7°, -18.0°] in Experiment 1b (Figure S2.6D).

In the PLM condition, the position estimates clustered around the predicted position errors (0°) based on path integration (the dotted red line in Figure S2.7B and S2.7E) in both Experiments 1a and 1b (mean position error = -8.2°, 95% CI [-19.8°, 3.4°] and mean position error = -8.7°, 95% CI [-26.5°, 9.1°], respectively).

In the Conflict condition, the mean position error was 25.0° with a 95% confidence interval [8.2°, 41.8°] in Experiment 1a (Figure S2.7C) and the mean position error was 19.4° with a 95% confidence interval [-6.1°, 45.0°] in Experiment 1b (Figure S2.7F).

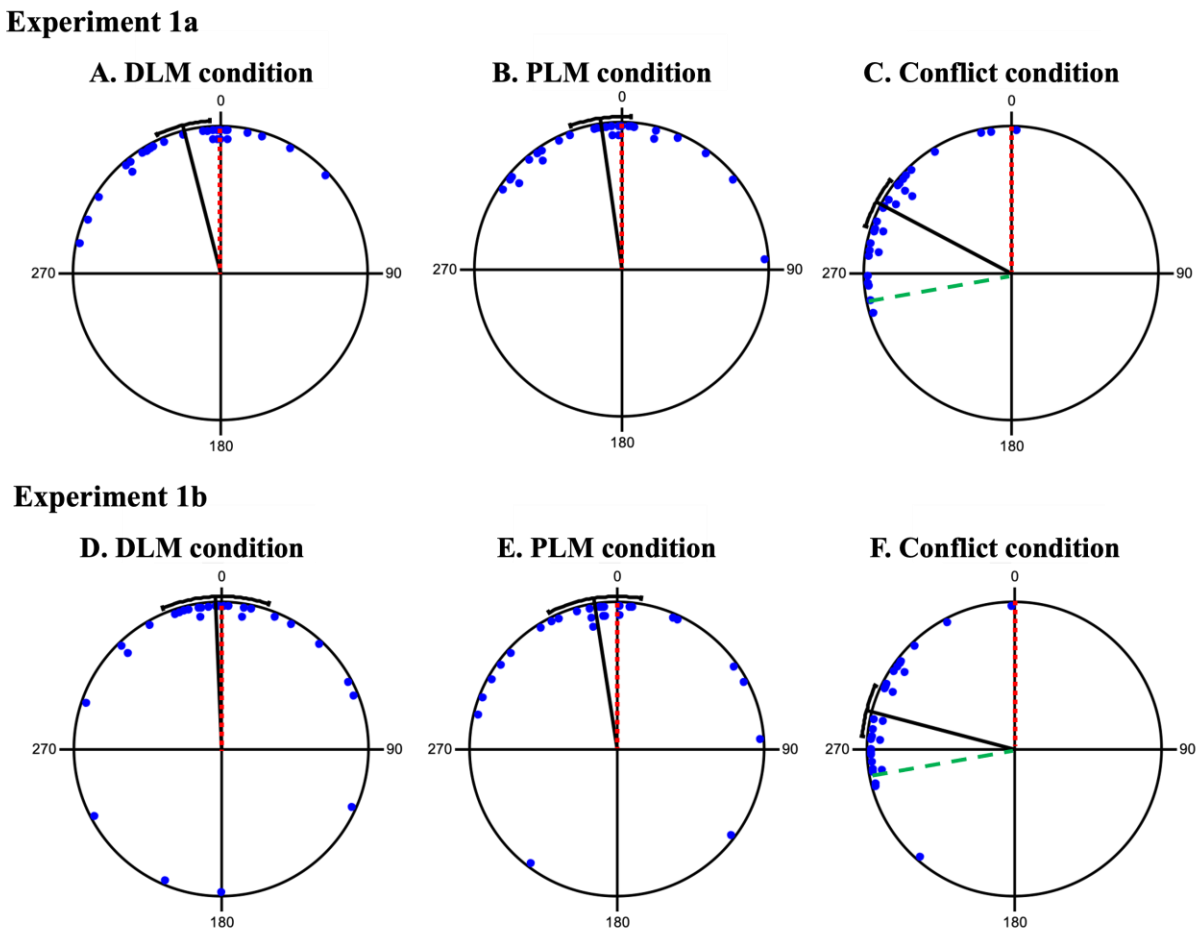

Figure S2.7. Observed and predicted position errors in the DLM (panels A and D), PLM (panels B and E), and Conflict conditions (panels C and F) in Experiments 1a and 1b. Each blue dot indicates one participant-level circular mean of position errors across paths. The solid black line indicates the group-level circular mean of the position errors across participants. The black arc indicates the 95% confidence interval of the group-level circular mean. The red lines indicate the predicted position error (0°) when participants use path integration for position estimates. The dashed green line indicates the predicted position error ($\pi = \theta + \eta$ = -50° + (-50°) = -100°) if participants use the rotated distal landmark for heading estimates and the rotated proximal landmark for homing estimates.

Participant-level circular standard deviation: The means of participant-level circular standard deviations in all conditions are plotted in Figure S2.8. We conducted repeated-measure ANOVA with one within-subject factor (cue condition: DLM, PLM, and Conflict) for Experiment 1a and 1b respectively. There were no significant differences among conditions in Experiment 1a, $F(2, 54) = .21$, $p = .81$, $MSE = 478.76$, $\eta_p^2 = .008$, $BF_{01}=7.99$, indicating that the means of the participant-level SDs of position errors were comparable across all conditions in Experiment 1a.

There was a significant difference among conditions in Experiment 1b, $F(2, 54) = 3.97$, $p = .03$, $MSE = 899.80$, $\eta_p^2 = .128$. In particular, the SD in the PLM condition was significantly larger than that in the Conflict condition, $t(27) = 2.57$, $p = .016$, Cohen's $dz = .49$, but did not differ from that in the DLM condition, $t(27) = 0.96$, $p = .34$, Cohen's $dz = 0.18$, $BF_{01} = 3.27$. The SD in the DLM condition was significantly larger than that in the Conflict condition, $t(27) = 2.45$, $p = .021$, Cohen's $dz = 0.462$.

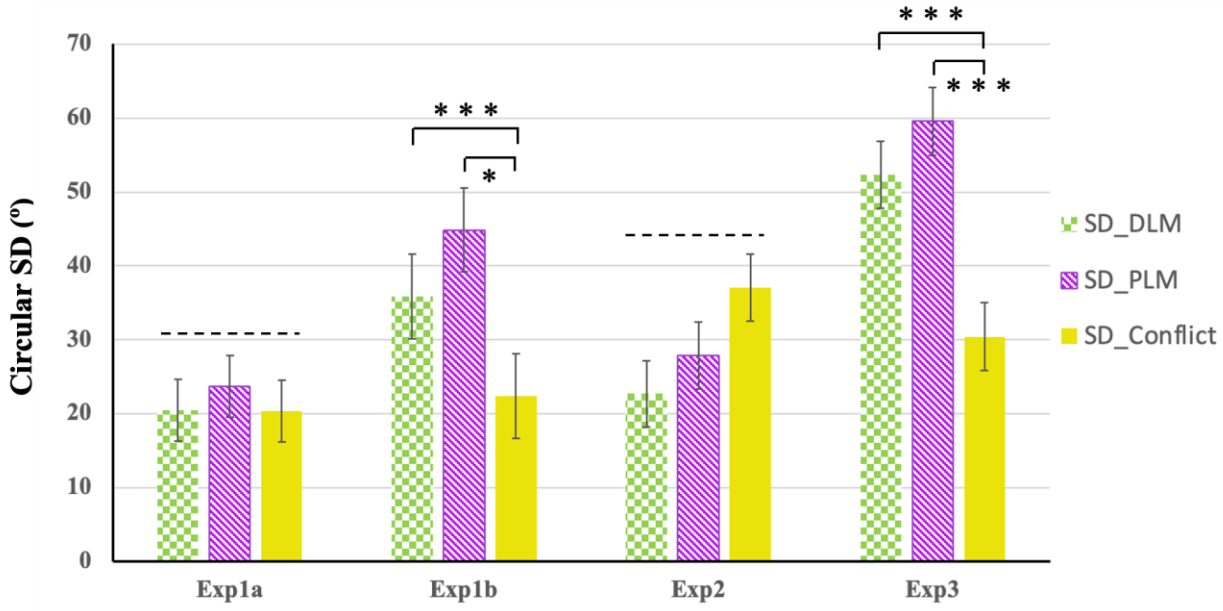

*Figure S2.8. The means of participant-level circular standard deviations of the position errors in all conditions of all experiments. The solid lines represent significant comparisons (.01 < *p < .05, ***p < .001) and the dashed line represents an insignificant comparison (p > .05). Error bars represent ± 1 SE of the means (from the MSE of each repeated-measure ANOVA).*

Position errors of Experiment 2

Participant-level circular means: In the DLM condition, the position estimates clustered around the predicted position errors (0°) based on path integration (the dotted red line in Figure S2.9A) in Experiment 2 (mean position error = -3.1°, 95% CI [-6.6°, .4°]).

In the PLM condition, the position estimates clustered around the predicted position errors (0°) based on path integration (the dotted red line in Figure S2.9B) in Experiment 2 (mean position error = 6.0°, 95% CI [.2°, 11.9°]).

In the Conflict condition, the position estimates clustered around the predicted position errors (0°) based on path integration (the dotted red line in Figure S2.9C) in Experiment 2 (mean position error = -7.1°, 95% CI [-15.0°, .7°]).

Experiment 2

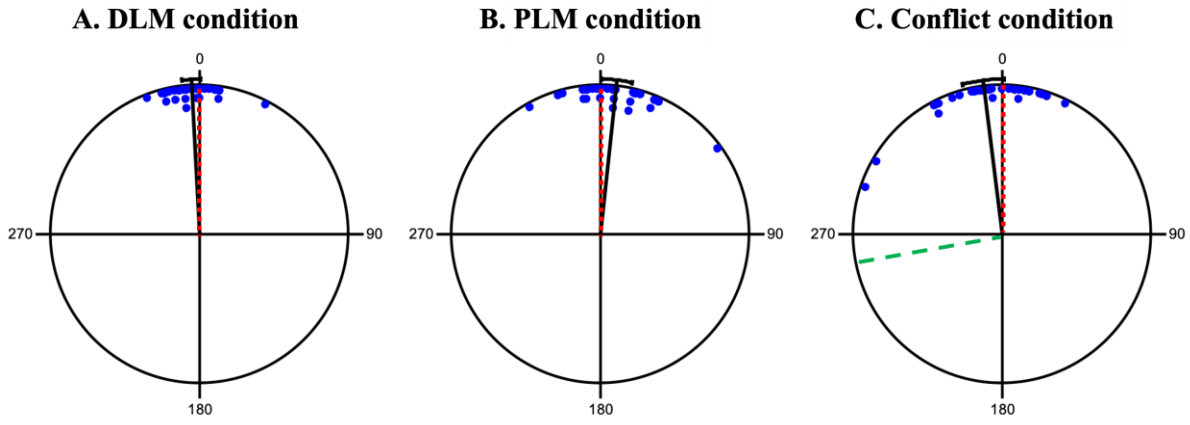

Figure S2.9. Observed and predicted position errors in the DLM (panels A and D), PLM (panels B and E), and Conflict conditions (panels C and F) in Experiments 1a and 1b. Each blue dot indicates one participant-level circular mean of position errors across paths. The solid black line indicates the group-level circular mean of the position errors across participants. The black arc indicates the 95% confidence interval of the group-level circular mean. The red lines indicate the predicted position error (0°) when participants use path integration for position estimates. The dashed green line indicates the predicted position error ($\pi = \theta + \eta$ = -50° + (-50°) = -100°) if participants use the rotated distal landmark for heading estimates and the rotated proximal landmark for homing estimates.

Participant-level circular standard deviation. Participant-level circular standard deviations of all conditions in Experiment 2 are plotted in Figure S2.8. A repeated-measure ANOVA with one within-subject factor (cue condition: DLM, PLM, and Conflict) was conducted. The results show no significant differences among conditions, $F(2, 54) = 2.60$, $p = .08$, $MSE = 567.94$, $\eta_p^2 = .088$, $B_{01}=1.03$, indicating that the SDs of position errors across paths were comparable for all conditions in Experiment 2.

Position errors of Experiment 3

Participant-level circular means. In the DLM condition, the position estimates clustered around the predicted position errors (0°) based on path integration (the dotted red line in Figure S2.10A) in Experiment 3 (mean position error = -6.5°, 95% CI [-22.8°, 9.9°]).

In the PLM condition, the mean position error was -26.6° with a 95% confidence interval [-53.8°, .5°] in Experiment 3 (Figure S2.10B). The predicted position error for the PLM condition (0°) was encompassed in the 95% CI.

In the Conflict condition, the mean position error was -86.1° with a 95% confidence interval [-96.3°, 75.9°] in Experiment 3 (Figure S2.10C).

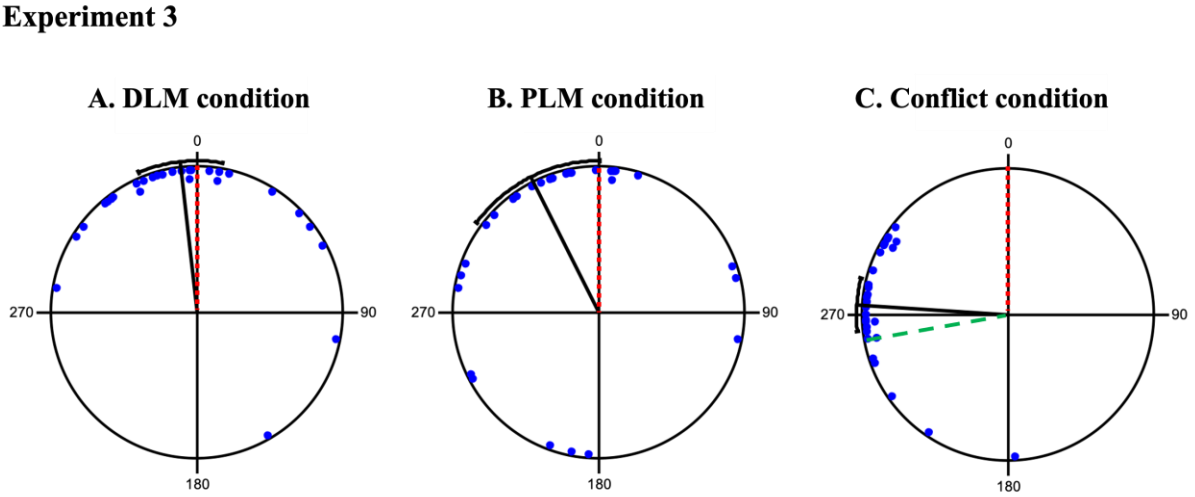

Figure S2.10. Observed and predicted position errors in the DLM (panels A and D), PLM (panels B and E), and Conflict conditions (panels C and F) in Experiments 1a and 1b. Each blue dot indicates one participant-level circular mean of position errors across paths. The solid black line indicates the group-level circular mean of the position errors across participants. The black arc indicates the 95% confidence interval of the group-level circular mean. The red lines indicate the predicted position error (0°) when participants use path integration for position estimates. The dashed green line indicates the predicted position error ($\pi = \theta + \eta$ = -50° + (-50°) = -100°) if participants use the rotated distal landmark for heading estimates and the rotated proximal landmark for homing estimates.

Participant-level circular standard deviation: The means of participant-level circular standard deviations in all conditions are plotted in Figure S2.8. A repeated-measure ANOVA with one within-subject factor (cue condition: DLM, PLM, and Conflict) was conducted. There were significant differences among conditions, $F(2, 54) = 11.04$, $p < .001$, $MSE = 584.54$, $\eta_p^2 = .29$. In particular, the SD in the PLM condition was significantly larger than that in the Conflict

condition, $t(27) = 4.13$, $p < .001$, Cohen's $dz = 0.78$, but was not different from that in the DLM condition, $t(27) = 1.16$, $p = .26$, Cohen's $dz = .22$, $BF_{01} = 2.72$. The SD in the Conflict condition was significantly larger than that in the DLM, $t(27) = 3.64$, $p < .01$, Cohen's $dz = .69$.

Supplementary materials of Chapter 3

Description of the data

Figure S3.1 plots the correct values of the inbound responses in triangle completion of Qi et al. (2021).

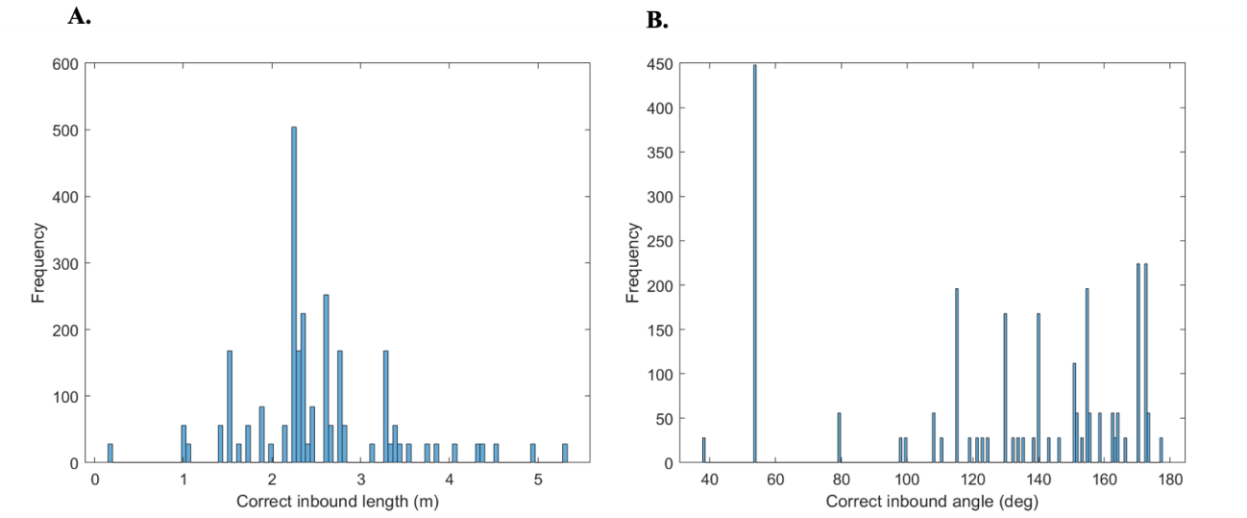

Figure S3.1. The distributions of the correct inbound path lengths (A) and turn angles (B).

Cross-validation without considering participant variable

Cross-validation results of individual folds. All ten folds' cross-validation results based on two different algorithms using participants' responses are summarized separately (model fitting performance in Table S3.1 and model validation performance in Table S3.2).

Table S3.1. Model fitting performance using multiple response locations or only home response locations. Parameters are estimated slopes and intercepts of encoding functions ($\theta_{L\_s}^{enc}$ and $\theta_{L\_i}^{enc}$ for length, $\theta_{A\_s}^{enc}$ and $\theta_{A\_i}^{enc}$ for angle) and execution functions ($\theta_{L\_s}^{exe}$ and $\theta_{L\_i}^{exe}$ for length, $\theta_{A\_s}^{exe}$ and $\theta_{A\_i}^{exe}$ for angle) for three models in the model fitting. The RMSE, maximum log-likelihood, and partial r-squared are goodness-of-fit measures.

Multiple response locations (1st round, subsample 1)											
	Parameters								5×2 Fitting		
Model	$\theta_{L\_s}^{enc}$	$\theta_{L\_i}^{enc}$	$\theta_{A\_s}^{enc}$	$\theta_{A\_i}^{enc}$	$\theta_{L\_s}^{exe}$	$\theta_{L\_i}^{exe}$	$\theta_{A\_s}^{exe}$	$\theta_{A\_i}^{exe}$	RMSE	MaxLogL	Partial R^2
M0	1	0	1	0	1	0	1	0	3.378	-6121.00	0.000
M1	0.96	0.64	0.81	15.49	1	0	1	0	3.269	-6042.04	0.063
M2	1	0	1	0	0.75	1.22	0.77	44.16	3.242	-6023.67	0.079
M3	0.70	0.93	0.85	19.41	0.73	1.08	0.80	39.17	3.208	-5994.13	0.098
Home response locations only (1st round, subsample 1)											
	Parameters								5×2 Fitting		
Model	$\theta_{L\_s}^{enc}$	$\theta_{L\_i}^{enc}$	$\theta_{A\_s}^{enc}$	$\theta_{A\_i}^{enc}$	$\theta_{L\_s}^{exe}$	$\theta_{L\_i}^{exe}$	$\theta_{A\_s}^{exe}$	$\theta_{A\_i}^{exe}$	RMSE	MaxLogL	Partial R^2
M0	1	0	1	0	1	0	1	0	2.922	-1904.77	0.000
M1	0.53	0.94	0.54	12.72	1	0	1	0	2.727	-1854.58	0.129
M2	1	0	1	0	0.48	1.98	0.45	87.29	2.735	-1856.25	0.124
M3	0.28	0.68	0.58	-10.00	1.96	-1.0	0.90	6.56	2.725	-1854.30	0.130
Multiple response locations (1st round, subsample 2)											
	Parameters								5×2 Fitting		
Model	$\theta_{L\_s}^{enc}$	$\theta_{L\_i}^{enc}$	$\theta_{A\_s}^{enc}$	$\theta_{A\_i}^{enc}$	$\theta_{L\_s}^{exe}$	$\theta_{L\_i}^{exe}$	$\theta_{A\_s}^{exe}$	$\theta_{A\_i}^{exe}$	RMSE	MaxLogL	Partial R^2
M0	1	0	1	0	1	0	1	0	2.976	-5799.43	0.000
M1	1.12	0.31	0.77	21.45	1	0	1	0	2.884	-5722.36	0.061
M2	1	0	1	0	0.66	1.34	0.80	38.07	2.865	-5704.63	0.073
M3	0.86	0.73	0.83	21.21	0.66	1.12	0.83	32.42	2.830	-5671.87	0.096
Home response locations only (1st round, subsample 2)											
	Parameters								5×2 Fitting		

Model	$\theta_{L\_s}^{enc}$	$\theta_{L\_i}^{enc}$	$\theta_{A\_s}^{enc}$	$\theta_{A\_i}^{enc}$	$\theta_{L\_s}^{exe}$	$\theta_{L\_i}^{exe}$	$\theta_{A\_s}^{exe}$	$\theta_{A\_i}^{exe}$	RMSE	MaxLogL	Partial R^2
M0	1	0	1	0	1	0	1	0	2.693	-1830.55	0.000
M1	0.87	0.36	0.36	34.38	1	0	1	0	2.517	-1778.07	0.126
M2	1	0	1	0	0.36	2.20	0.47	83.69	2.522	-1779.29	0.123
M3	0.89	0.55	0.32	55.32	0.81	0.59	1.13	-9.98	2.514	-1776.50	0.128

Multiple response locations (2nd round, subsample 1)

	Parameters								5×2 Fitting		
Model	$\theta_{L\_s}^{enc}$	$\theta_{L\_i}^{enc}$	$\theta_{A\_s}^{enc}$	$\theta_{A\_i}^{enc}$	$\theta_{L\_s}^{exe}$	$\theta_{L\_i}^{exe}$	$\theta_{A\_s}^{exe}$	$\theta_{A\_i}^{exe}$	RMSE	MaxLogL	Partial R^2
M0	1	0	1	0	1	0	1	0	3.343	-6074.95	0.000
M1	1.26	0.16	0.73	26.60	1	0	1	0	3.229	-5995.91	0.067
M2	1	0	1	0	0.69	1.38	0.80	40.16	3.212	-5987.98	0.077
M3	1.18	0.26	0.74	31.17	0.75	0.94	0.82	34.20	3.175	-5953.92	0.098

Home response locations only (2nd round, subsample 1)

	Parameters								5×2 Fitting		
Model	$\theta_{L\_s}^{enc}$	$\theta_{L\_i}^{enc}$	$\theta_{A\_s}^{enc}$	$\theta_{A\_i}^{enc}$	$\theta_{L\_s}^{exe}$	$\theta_{L\_i}^{exe}$	$\theta_{A\_s}^{exe}$	$\theta_{A\_i}^{exe}$	RMSE	MaxLogL	Partial R^2
M0	1	0	1	0	1	0	1	0	2.969	-1901.85	0.000
M1	0.91	0.32	0.38	29.54	1	0	1	0	2.760	-1855.84	0.136
M2	1	0	1	0	0.38	2.25	0.44	88.46	2.772	-1858.12	0.128
M3	0.69	0.14	0.35	27.26	1.33	0.11	1.05	-10.0	2.759	-1855.72	0.136

Multiple response locations (2nd round, subsample 2)

	Parameters								5×2 Fitting		
Model	$\theta_{L\_s}^{enc}$	$\theta_{L\_i}^{enc}$	$\theta_{A\_s}^{enc}$	$\theta_{A\_i}^{enc}$	$\theta_{L\_s}^{exe}$	$\theta_{L\_i}^{exe}$	$\theta_{A\_s}^{exe}$	$\theta_{A\_i}^{exe}$	RMSE	MaxLogL	Partial R^2

M0	1	0	1	0	1	0	1	0	3.015	-5838.87	0.000
M1	0.80	0.83	0.84	12.70	1	0	1	0	2.925	-5763.77	0.059
M2	1	0	1	0	0.71	1.20	0.77	41.93	2.900	-5735.84	0.075
M3	0.55	1.18	0.89	14.64	0.67	1.10	0.84	32.75	2.861	-5701.30	0.099

Home response locations only (2nd round, subsample 2)

	Parameters								5×2 Fitting		
Model	$\theta_{L\_s}^{enc}$	$\theta_{L\_i}^{enc}$	$\theta_{A\_s}^{enc}$	$\theta_{A\_i}^{enc}$	$\theta_{L\_s}^{exe}$	$\theta_{L\_i}^{exe}$	$\theta_{A\_s}^{exe}$	$\theta_{A\_i}^{exe}$	RMSE	MaxLogL	Partial R^2
M0	1	0	1	0	1	0	1	0	2.642	-1824.93	0.000
M1	0.44	1.05	0.51	17.71	1	0	1	0	2.482	-1768.70	0.117
M2	1	0	1	0	0.46	1.93	0.48	82.97	2.482	-1768.79	0.117
M3	9.10	17.87	0.84	27.26	0.03	1.97	0.63	66.94	2.479	-1767.48	0.120

Multiple response locations (3rd round, subsample 1)

	Parameters								5×2 Fitting		
Model	$\theta_{L\_s}^{enc}$	$\theta_{L\_i}^{enc}$	$\theta_{A\_s}^{enc}$	$\theta_{A\_i}^{enc}$	$\theta_{L\_s}^{exe}$	$\theta_{L\_i}^{exe}$	$\theta_{A\_s}^{exe}$	$\theta_{A\_i}^{exe}$	RMSE	MaxLogL	Partial R^2
M0	1	0	1	0	1	0	1	0	3.320	-6083.85	0.000
M1	1.05	0.42	0.81	14.42	1	0	1	0	3.227	-6015.45	0.055
M2	1	0	1	0	0.70	1.31	0.83	35.29	3.206	-6001.36	0.067
M3	0.76	0.83	0.86	15.29	0.68	1.16	0.87	26.89	3.179	-5977.51	0.083

Home response locations only (3rd round, subsample 1)

	Parameters								5×2 Fit		
Model	$\theta_{L\_s}^{enc}$	$\theta_{L\_i}^{enc}$	$\theta_{A\_s}^{enc}$	$\theta_{A\_i}^{enc}$	$\theta_{L\_s}^{exe}$	$\theta_{L\_i}^{exe}$	$\theta_{A\_s}^{exe}$	$\theta_{A\_i}^{exe}$	RMSE	MaxLogL	Partial R^2
M0	1	0	1	0	1	0	1	0	2.937	-1908.71	0.000

M1	0.83	0.44	0.57	12.96	1	0	1	0	2.777	-1871.03	0.106
M2	1	0	1	0	0.52	1.84	0.58	68.69	2.782	-1871.64	0.103
M3	0.70	0.26	0.62	6.09	1.11	0.37	0.97	2.39	2.777	-1870.90	0.106

Multiple response locations (3rd round, subsample 2)

	Parameters								5×2 Fitting		
Model	$\theta_{L\_s}^{enc}$	$\theta_{L\_i}^{enc}$	$\theta_{A\_s}^{enc}$	$\theta_{A\_i}^{enc}$	$\theta_{L\_s}^{exe}$	$\theta_{L\_i}^{exe}$	$\theta_{A\_s}^{exe}$	$\theta_{A\_i}^{exe}$	RMSE	MaxLogL	Partial R^2
M0	1	0	1	0	1	0	1	0	3.041	-5854.76	0.000
M1	1.03	0.52	0.77	22.35	1	0	1	0	2.931	-5763.24	0.071
M2	1	0	1	0	0.70	1.27	0.74	47.14	2.906	-5743.56	0.087
M3	0.65	1.07	0.79	27.14	0.68	1.13	0.77	42.32	2.857	-5697.42	0.117

Home response locations only (3rd round, subsample 2)

	Parameters								5×2 Fitting		
Model	$\theta_{L\_s}^{enc}$	$\theta_{L\_i}^{enc}$	$\theta_{A\_s}^{enc}$	$\theta_{A\_i}^{enc}$	$\theta_{L\_s}^{exe}$	$\theta_{L\_i}^{exe}$	$\theta_{A\_s}^{exe}$	$\theta_{A\_i}^{exe}$	RMSE	MaxLogL	Partial R^2
M0	1	0	1	0	1	0	1	0	2.677	-1831.85	0.000
M1	0.54	0.90	0.33	32.72	1	0	1	0	2.461	-1764.61	0.154
M2	1	0	1	0	0.31	2.36	0.43	90.00	2.468	-1766.52	0.149
M3	0.70	1.23	0.29	53.94	0.65	0.67	1.13	-10.00	2.460	-1763.85	0.155

Multiple response locations (4th round, subsample 1)

	Parameters								5×2 Fitting		
Model	$\theta_{L\_s}^{enc}$	$\theta_{L\_i}^{enc}$	$\theta_{A\_s}^{enc}$	$\theta_{A\_i}^{enc}$	$\theta_{L\_s}^{exe}$	$\theta_{L\_i}^{exe}$	$\theta_{A\_s}^{exe}$	$\theta_{A\_i}^{exe}$	RMSE	MaxLogL	Partial R^2
M0	1	0	1	0	1	0	1	0	3.443	-6172.66	0.000
M1	1.28	0.08	0.81	18.80	1	0	1	0	3.352	-6111.46	0.052

M2	1	0	1	0	0.67	1.34	0.78	42.48	3.328	-6096.82	0.066
M3	1.27	0.08	0.83	24.01	0.68	1.10	0.82	35.14	3.295	-6069.04	0.084

Home response locations only (4th round, subsample 1)

	Parameters								5×2 Fitting		
Model	$\theta_{L\_s}^{enc}$	$\theta_{L\_i}^{enc}$	$\theta_{A\_s}^{enc}$	$\theta_{A\_i}^{enc}$	$\theta_{L\_s}^{exe}$	$\theta_{L\_i}^{exe}$	$\theta_{A\_s}^{exe}$	$\theta_{A\_i}^{exe}$	RMSE	MaxLogL	Partial R^2
M0	1	0	1	0	1	0	1	0	3.056	-1945.06	0.000
M1	0.73	0.56	0.38	26.93	1	0	1	0	2.869	-1899.73	0.119
M2	1	0	1	0	0.37	2.23	0.44	90.00	2.872	-1899.84	0.117
M3	1.52	7.13	0.12	64.78	0.40	-3.0	3.19	55.65	2.868	-1899.11	0.119

Multiple response locations (4th round, subsample 2)

	Parameters								5×2 Fitting		
Model	$\theta_{L\_s}^{enc}$	$\theta_{L\_i}^{enc}$	$\theta_{A\_s}^{enc}$	$\theta_{A\_i}^{enc}$	$\theta_{L\_s}^{exe}$	$\theta_{L\_i}^{exe}$	$\theta_{A\_s}^{exe}$	$\theta_{A\_i}^{exe}$	RMSE	MaxLogL	Partial R^2
M0	1	0	1	0	1	0	1	0	2.900	-5730.81	0.000
M1	0.80	0.86	0.78	17.69	1	0	1	0	2.785	-5628.82	0.078
M2	1	0	1	0	0.73	1.23	0.79	39.90	2.767	-5610.79	0.090
M3	0.49	1.27	0.85	15.96	0.70	1.09	0.84	31.88	2.725	-5570.60	0.117

Home response locations only (4th round, subsample 2)

	Parameters								5×2 Fitting		
Model	$\theta_{L\_s}^{enc}$	$\theta_{L\_i}^{enc}$	$\theta_{A\_s}^{enc}$	$\theta_{A\_i}^{enc}$	$\theta_{L\_s}^{exe}$	$\theta_{L\_i}^{exe}$	$\theta_{A\_s}^{exe}$	$\theta_{A\_i}^{exe}$	RMSE	MaxLogL	Partial R^2
M0	1	0	1	0	1	0	1	0	2.540	-1784.59	0.000
M1	0.60	0.81	0.51	19.78	1	0	1	0	2.357	-1726.92	0.139
M2	1	0	1	0	0.47	1.96	0.49	80.44	2.366	-1729.52	0.133

M3	0.82	0.79	0.69	-10.00	0.70	0.37	0.82	21.36	2.356	-1726.83	0.140

Multiple response locations (5th round, subsample 1)

	Parameters								5×2 Fitting		
Model	$\theta_{L\_s}^{enc}$	$\theta_{L\_i}^{enc}$	$\theta_{A\_s}^{enc}$	$\theta_{A\_i}^{enc}$	$\theta_{L\_s}^{exe}$	$\theta_{L\_i}^{exe}$	$\theta_{A\_s}^{exe}$	$\theta_{A\_i}^{exe}$	RMSE	MaxLogL	Partial R^2
M0	1	0	1	0	1	0	1	0	3.108	-5919.57	0.000
M1	1.11	0.24	0.80	16.70	1	0	1	0	3.041	-5866.22	0.043
M2	1	0	1	0	0.70	1.14	0.80	39.54	3.009	-5839.97	0.063
M3	1.07	0.24	0.85	17.29	0.71	0.94	0.85	31.47	2.988	-5820.31	0.076

Home response locations only (5th round, subsample 1)

	Parameters								5×2 Fitting		
	$\theta_{L\_s}^{enc}$	$\theta_{L\_i}^{enc}$	$\theta_{A\_s}^{enc}$	$\theta_{A\_i}^{enc}$	$\theta_{L\_s}^{exe}$	$\theta_{L\_i}^{exe}$	$\theta_{A\_s}^{exe}$	$\theta_{A\_i}^{exe}$	RMSE	MaxLogL	Partial R^2
M0	1	0	1	0	1	0	1	0	2.732	-1849.03	0.000
M1	0.74	0.48	0.45	23.28	1	0	1	0	2.582	-1803.53	0.107
M2	1	0	1	0	0.41	1.97	0.49	80.60	2.586	-1804.16	0.104
M3	2.57	0.88	0.52	23.01	0.25	0.80	0.93	12.41	2.581	-1803.11	0.107

Multiple response locations (5th round, subsample 2)

	Parameters								5×2 Fitting		
Model	$\theta_{L\_s}^{enc}$	$\theta_{L\_i}^{enc}$	$\theta_{A\_s}^{enc}$	$\theta_{A\_i}^{enc}$	$\theta_{L\_s}^{exe}$	$\theta_{L\_i}^{exe}$	$\theta_{A\_s}^{exe}$	$\theta_{A\_i}^{exe}$	RMSE	MaxLogL	Partial R^2
M0	1	0	1	0	1	0	1	0	3.257	-6023.06	0.000
M1	0.98	0.70	0.79	19.58	1	0	1	0	3.118	-5913.01	0.084
M2	1	0	1	0	0.70	1.43	0.77	42.46	3.104	-5907.36	0.092
M3	0.64	1.18	0.88	18.05	0.66	1.30	0.81	35.89	3.052	-5858.41	0.122

Home response locations only (5th round, subsample 2)

	Parameters								5×2 Fitting		
Model	$\theta_{L\_s}^{enc}$	$\theta_{L\_i}^{enc}$	$\theta_{A\_s}^{enc}$	$\theta_{A\_i}^{enc}$	$\theta_{L\_s}^{exe}$	$\theta_{L\_i}^{exe}$	$\theta_{A\_s}^{exe}$	$\theta_{A\_i}^{exe}$	RMSE	MaxLogL	Partial R^2
M0	1	0	1	0	1	0	1	0	2.886	-1889.97	0.000
M1	0.62	0.86	0.43	24.32	1	0	1	0	2.663	-1832.26	0.149
M2	1	0	1	0	0.41	2.25	0.43	90.00	2.669	-1833.68	0.144
M3	8.07	9.90	0.42	24.32	0.08	0.21	1.06	-9.83	2.663	-1832.31	0.149

Table S3.2. Model validation performance using multiple response locations or only home response locations. Parameters are the same as in Table S3.1 from model fitting. The RMSE, maximum log-likelihood, and partial r-squared are generalizability measures, which were calculated by applying the parameters to the test subsamples.

	Multiple response locations (1st round, subsample 1)										
	Parameters								5×2 Validation		
Model	$\theta_{L\_s}^{enc}$	$\theta_{L\_i}^{enc}$	$\theta_{A\_s}^{enc}$	$\theta_{A\_i}^{enc}$	$\theta_{L\_s}^{exe}$	$\theta_{L\_i}^{exe}$	$\theta_{A\_s}^{exe}$	$\theta_{A\_i}^{exe}$	RMSE	MaxLogL	Partial R^2
M0	1	0	1	0	1	0	1	0	3.378	-6121.00	0.000
M1	1.12	0.31	0.77	21.45	1	0	1	0	3.274	-6044.00	0.061
M2	1	0	1	0	0.66	1.34	0.80	38.07	3.247	-6023.54	0.076
M3	0.86	0.73	0.83	21.21	0.66	1.12	0.83	32.42	3.213	-5995.38	0.095
	Home response locations only (1st round, subsample 1)										
	Parameters								5×2 Validation		
	$\theta_{L\_s}^{enc}$	$\theta_{L\_i}^{enc}$	$\theta_{A\_s}^{enc}$	$\theta_{A\_i}^{enc}$	$\theta_{L\_s}^{exe}$	$\theta_{L\_i}^{exe}$	$\theta_{A\_s}^{exe}$	$\theta_{A\_i}^{exe}$	RMSE	MaxLogL	Partial R^2
M0	1	0	1	0	1	0	1	0	2.922	-1904.77	0.000
M1	0.87	0.36	0.36	34.38	1	0	1	0	2.739	-1857.78	0.122

M2	1	0	1	0	0.36	2.20	0.47	83.69	2.739	-1856.74	0.121
M3	0.89	0.55	0.32	55.32	0.81	0.59	1.13	-9.98	2.742	-1858.34	0.119

Multiple response locations (1st round, subsample 2)

	Parameters								5×2 Validation		
Model	$\theta_{L\_s}^{enc}$	$\theta_{L\_i}^{enc}$	$\theta_{A\_s}^{enc}$	$\theta_{A\_i}^{enc}$	$\theta_{L\_s}^{exe}$	$\theta_{L\_i}^{exe}$	$\theta_{A\_s}^{exe}$	$\theta_{A\_i}^{exe}$	RMSE	MaxLogL	Partial R^2
M0	1	0	1	0	1	0	1	0	2.976	-5799.43	0.000
M1	0.96	0.64	0.81	15.49	1	0	1	0	2.889	-5727.83	0.058
M2	1	0	1	0	0.75	1.22	0.77	44.16	2.872	-5710.81	0.069
M3	0.70	0.93	0.85	19.41	0.73	1.08	0.80	39.17	2.835	-5677.57	0.092

Home response locations only (1st round, subsample 2)

	Parameters								5×2 Validation		
Model	$\theta_{L\_s}^{enc}$	$\theta_{L\_i}^{enc}$	$\theta_{A\_s}^{enc}$	$\theta_{A\_i}^{enc}$	$\theta_{L\_s}^{exe}$	$\theta_{L\_i}^{exe}$	$\theta_{A\_s}^{exe}$	$\theta_{A\_i}^{exe}$	RMSE	MaxLogL	Partial R^2
M0	1	0	1	0	1	0	1	0	2.693	-1830.55	0.000
M1	0.53	0.94	0.54	12.72	1	0	1	0	2.530	-1782.19	0.118
M2	1	0	1	0	0.48	1.98	0.45	87.29	2.527	-1780.98	0.119
M3	0.28	0.68	0.58	-10.00	1.96	-1.0	0.90	6.56	2.533	-1783.70	0.115

Multiple response locations (2nd round, subsample 1)

	Parameters								5×2 Validation		
Model	$\theta_{L\_s}^{enc}$	$\theta_{L\_i}^{enc}$	$\theta_{A\_s}^{enc}$	$\theta_{A\_i}^{enc}$	$\theta_{L\_s}^{exe}$	$\theta_{L\_i}^{exe}$	$\theta_{A\_s}^{exe}$	$\theta_{A\_i}^{exe}$	RMSE	MaxLogL	Partial R^2
M0	1	0	1	0	1	0	1	0	3.343	-6074.95	0.000
M1	0.80	0.83	0.84	12.70	1	0	1	0	3.247	-6001.53	0.061
M2	1	0	1	0	0.71	1.20	0.77	41.93	3.215	-5986.01	0.075

M3	0.55	1.18	0.89	14.64	0.67	1.10	0.84	32.75	3.186	-5961.14	0.092

Home response locations only (2nd round, subsample 1)

	Parameters								5×2 Validation		
Model	$\theta_{L\_s}^{enc}$	$\theta_{L\_i}^{enc}$	$\theta_{A\_s}^{enc}$	$\theta_{A\_i}^{enc}$	$\theta_{L\_s}^{exe}$	$\theta_{L\_i}^{exe}$	$\theta_{A\_s}^{exe}$	$\theta_{A\_i}^{exe}$	RMSE	MaxLogL	Partial R^2
M0	1	0	1	0	1	0	1	0	2.969	-1901.85	0.000
M1	0.44	1.05	0.51	17.71	1	0	1	0	2.771	-1856.74	0.129
M2	1	0	1	0	0.46	1.93	0.48	82.97	2.776	-1857.42	0.126
M3	9.10	17.87	0.84	27.26	0.03	1.97	0.63	66.94	2.779	-1858.43	0.124

Multiple response locations (2nd round, subsample 2)

	Parameters								5×2 Validation		
Model	$\theta_{L\_s}^{enc}$	$\theta_{L\_i}^{enc}$	$\theta_{A\_s}^{enc}$	$\theta_{A\_i}^{enc}$	$\theta_{L\_s}^{exe}$	$\theta_{L\_i}^{exe}$	$\theta_{A\_s}^{exe}$	$\theta_{A\_i}^{exe}$	RMSE	MaxLogL	Partial R^2
M0	1	0	1	0	1	0	1	0	3.015	-5838.87	0.000
M1	1.26	0.16	0.73	26.60	1	0	1	0	2.937	-5776.22	0.051
M2	1	0	1	0	0.69	1.38	0.80	40.16	2.904	-5738.89	0.073
M3	1.18	0.26	0.74	31.17	0.75	0.94	0.82	34.20	2.883	-5723.42	0.086

Home response locations only (2nd round, subsample 2)

	Parameters								5×2 Validation		
Model	$\theta_{L\_s}^{enc}$	$\theta_{L\_i}^{enc}$	$\theta_{A\_s}^{enc}$	$\theta_{A\_i}^{enc}$	$\theta_{L\_s}^{exe}$	$\theta_{L\_i}^{exe}$	$\theta_{A\_s}^{exe}$	$\theta_{A\_i}^{exe}$	RMSE	MaxLogL	Partial R^2
M0	1	0	1	0	1	0	1	0	2.642	-1824.93	0.000
M1	0.91	0.32	0.38	29.54	1	0	1	0	2.494	-1772.74	0.109
M2	1	0	1	0	0.38	2.25	0.44	88.46	2.486	-1770.31	0.115
M3	0.69	0.14	0.35	27.26	1.33	0.11	1.05	-10.0	2.497	-1774.01	0.106

Model	$\theta_{L\_s}^{enc}$	$\theta_{L\_i}^{enc}$	$\theta_{A\_s}^{enc}$	$\theta_{A\_i}^{enc}$	$\theta_{L\_s}^{exe}$	$\theta_{L\_i}^{exe}$	$\theta_{A\_s}^{exe}$	$\theta_{A\_i}^{exe}$	RMSE	MaxLogL	Partial R^2
Multiple response locations (3rd round, subsample 1)											
	Parameters								5×2 Validation		
M0	1	0	1	0	1	0	1	0	3.320	-6083.85	0.000
M1	1.03	0.52	0.77	22.35	1	0	1	0	3.232	-6017.62	0.052
M2	1	0	1	0	0.70	1.27	0.74	47.14	3.211	-6005.37	0.064
M3	0.65	1.07	0.79	27.14	0.68	1.13	0.77	42.32	3.190	-5985.37	0.077
Home response locations only (3rd round, subsample 1)											
	Parameters								5×2 Validation		
M0	1	0	1	0	1	0	1	0	2.937	-1908.71	0.000
M1	0.54	0.90	0.33	32.72	1	0	1	0	2.789	-1874.63	0.099
M2	1	0	1	0	0.31	2.36	0.43	90.00	2.788	-1874.16	0.099
M3	0.70	1.23	0.29	53.94	0.65	0.67	1.13	-10.00	2.790	-1874.82	0.098
Multiple response locations (3rd round, subsample 2)											
	Parameters								5×2 Validation		
M0	1	0	1	0	1	0	1	0	3.041	-5854.76	0.000
M1	1.05	0.42	0.81	14.42	1	0	1	0	2.935	-5768.42	0.068
M2	1	0	1	0	0.70	1.31	0.83	35.29	2.911	-5747.98	0.084
M3	0.76	0.83	0.86	15.29	0.68	1.16	0.87	26.89	2.869	-5708.85	0.110
Home response locations only (3rd round, subsample 2)											

	Parameters								5×2 Validation		
Model	$\theta_{L\_s}^{enc}$	$\theta_{L\_i}^{enc}$	$\theta_{A\_s}^{enc}$	$\theta_{A\_i}^{enc}$	$\theta_{L\_s}^{exe}$	$\theta_{L\_i}^{exe}$	$\theta_{A\_s}^{exe}$	$\theta_{A\_i}^{exe}$	RMSE	MaxLogL	Partial R^2
M0	1	0	1	0	1	0	1	0	2.677	-1831.85	0.000
M1	0.83	0.44	0.57	12.96	1	0	1	0	2.475	-1769.70	0.145
M2	1	0	1	0	0.52	1.84	0.58	68.69	2.479	-1770.26	0.142
M3	0.70	0.26	0.62	6.09	1.11	0.37	0.97	2.39	2.475	-1769.72	0.145

Multiple response locations (4th round, subsample 1)

	Parameters								5×2 Validation		
Model	$\theta_{L\_s}^{enc}$	$\theta_{L\_i}^{enc}$	$\theta_{A\_s}^{enc}$	$\theta_{A\_i}^{enc}$	$\theta_{L\_s}^{exe}$	$\theta_{L\_i}^{exe}$	$\theta_{A\_s}^{exe}$	$\theta_{A\_i}^{exe}$	RMSE	MaxLogL	Partial R^2
M0	1	0	1	0	1	0	1	0	3.443	-6172.66	0.000
M1	0.80	0.86	0.78	17.69	1	0	1	0	3.359	-6118.21	0.048
M2	1	0	1	0	0.73	1.23	0.79	39.90	3.329	-6096.64	0.065
M3	0.49	1.27	0.85	15.96	0.70	1.09	0.84	31.88	3.302	-6075.20	0.080

Home response locations only (4th round, subsample 1)

	Parameters								5×2 Validation		
Model	$\theta_{L\_s}^{enc}$	$\theta_{L\_i}^{enc}$	$\theta_{A\_s}^{enc}$	$\theta_{A\_i}^{enc}$	$\theta_{L\_s}^{exe}$	$\theta_{L\_i}^{exe}$	$\theta_{A\_s}^{exe}$	$\theta_{A\_i}^{exe}$	RMSE	MaxLogL	Partial R^2
M0	1	0	1	0	1	0	1	0	3.056	-1945.06	0.000
M1	0.60	0.81	0.51	19.78	1	0	1	0	2.876	-1900.73	0.115
M2	1	0	1	0	0.47	1.96	0.49	80.44	2.876	-1900.38	0.114
M3	0.82	0.79	0.69	-10.00	0.70	0.37	0.82	21.36	2.878	-1901.72	0.113

Multiple response locations (4th round, subsample 2)

	Parameters								5×2 Validation		

Model	$\theta_{L\_s}^{enc}$	$\theta_{L\_i}^{enc}$	$\theta_{A\_s}^{enc}$	$\theta_{A\_i}^{enc}$	$\theta_{L\_s}^{exe}$	$\theta_{L\_i}^{exe}$	$\theta_{A\_s}^{exe}$	$\theta_{A\_i}^{exe}$	RMSE	MaxLogL	Partial R^2
M0	1	0	1	0	1	0	1	0	2.900	-5730.81	0.000
M1	1.28	0.08	0.81	18.80	1	0	1	0	2.794	-5636.87	0.072
M2	1	0	1	0	0.67	1.34	0.78	42.48	2.768	-5611.56	0.090
M3	1.27	0.08	0.83	24.01	0.68	1.10	0.82	35.14	2.743	-5587.92	0.105

Home response locations only (4th round, subsample 2)

	Parameters								5×2 Validation		
Model	$\overline{\theta_{L\_s}^{enc}}$	$\theta_{L\_i}^{enc}$	$\theta_{A\_s}^{enc}$	$\theta_{A\_i}^{enc}$	$\theta_{L\_s}^{exe}$	$\theta_{L\_i}^{exe}$	$\theta_{A\_s}^{exe}$	$\theta_{A\_i}^{exe}$	RMSE	MaxLogL	Partial R^2
M0	1	0	1	0	1	0	1	0	2.540	-1784.59	0.000
M1	0.73	0.56	0.38	26.93	1	0	1	0	2.364	-1730.65	0.134
M2	1	0	1	0	0.37	2.23	0.44	90.00	2.371	-1732.53	0.129
M3	1.52	7.13	0.12	64.78	0.40	-3.0	3.19	55.65	2.365	-1730.73	0.133

Multiple response locations (5th round, subsample 1)

	Parameters								5×2 Validation		
Model	$\overline{\theta_{L\_s}^{enc}}$	$\theta_{L\_i}^{enc}$	$\theta_{A\_s}^{enc}$	$\theta_{A\_i}^{enc}$	$\theta_{L\_s}^{exe}$	$\theta_{L\_i}^{exe}$	$\theta_{A\_s}^{exe}$	$\theta_{A\_i}^{exe}$	RMSE	MaxLogL	Partial R^2
M0	1	0	1	0	1	0	1	0	3.108	-5919.57	0.000
M1	0.98	0.70	0.79	19.58	1	0	1	0	3.057	-5882.08	0.032
M2	1	0	1	0	0.70	1.43	0.77	42.46	3.024	-5855.21	0.053
M3	0.64	1.18	0.88	18.05	0.66	1.30	0.81	35.89	3.010	-5842.31	0.062

Home response locations only (5th round, subsample 1)

	Parameters								5×2 Validation		
	$\overline{\theta_{L\_s}^{enc}}$	$\theta_{L\_i}^{enc}$	$\theta_{A\_s}^{enc}$	$\theta_{A\_i}^{enc}$	$\theta_{L\_s}^{exe}$	$\theta_{L\_i}^{exe}$	$\theta_{A\_s}^{exe}$	$\theta_{A\_i}^{exe}$	RMSE	MaxLogL	Partial R^2

Model											
M0	1	0	1	0	1	0	1	0	2.732	-1849.03	0.000
M1	0.62	0.86	0.43	24.32	1	0	1	0	2.600	-1810.65	0.095
M2	1	0	1	0	0.41	2.25	0.43	90.00	2.602	-1811.29	0.093
M3	8.07	9.90	0.42	24.32	0.08	0.21	1.06	-9.83	2.599	-1810.56	0.095

Multiple response locations (5th round, subsample 2)

	Parameters								5×2 Validation		
	$\theta_{L\_s}^{enc}$	$\theta_{L\_i}^{enc}$	$\theta_{A\_s}^{enc}$	$\theta_{A\_i}^{enc}$	$\theta_{L\_s}^{exe}$	$\theta_{L\_i}^{exe}$	$\theta_{A\_s}^{exe}$	$\theta_{A\_i}^{exe}$	RMSE	MaxLogL	Partial R^2
M0	1	0	1	0	1	0	1	0	3.257	-6023.06	0.000
M1	1.11	0.24	0.80	16.70	1	0	1	0	3.134	-5926.20	0.074
M2	1	0	1	0	0.70	1.14	0.80	39.54	3.118	-5913.54	0.083
M3	1.07	0.24	0.85	17.29	0.71	0.94	0.85	31.47	3.079	-5878.83	0.106

Home response locations only (5th round, subsample 2)

	Parameters								5×2 Validation		
	$\theta_{L\_s}^{enc}$	$\theta_{L\_i}^{enc}$	$\theta_{A\_s}^{enc}$	$\theta_{A\_i}^{enc}$	$\theta_{L\_s}^{exe}$	$\theta_{L\_i}^{exe}$	$\theta_{A\_s}^{exe}$	$\theta_{A\_i}^{exe}$	RMSE	MaxLogL	Partial R^2
Model											
M0	1	0	1	0	1	0	1	0	2.886	-1889.97	0.000
M1	0.74	0.48	0.45	23.28	1	0	1	0	2.680	-1835.94	0.138
M2	1	0	1	0	0.41	1.97	0.49	80.60	2.686	-1836.49	0.134
M3	2.57	0.88	0.52	23.01	0.25	0.80	0.93	12.41	2.681	-1835.76	0.137

AIC and BIC analyses for adjusting the number of free parameters in model fitting.

We used the Akaike information criterion (AIC; Akaike, 1973), Bayesian Information Criterion (BIC; Schwarz, 1978), and the adjustment of the likelihood ratio approach (Glover & Dixon,

2004) to qualify these results, correcting the effect of model complexity (i.e., M3 has more parameters than M1 and M2). The AIC and BIC for a model M_i can be defined as:

AIC_i= -2 log L_i + 2 K_i. (S1)

BIC_i= -2 log L_i + log(N) × K_i. (S2)

Where the L_i is the maximum likelihood of M_i and K_i is the number of free parameters in M_i. In particular, K_3 - K_1 = 4, K_3 - K_2 = 4. N is the number of data, N = 498 × 3 for multiple response locations and N = 498 for home response locations only.

The adjusted maximum likelihood ratio (aLR) indicates the relative likelihood of data under two models, and the aLR in favor of M_i over M_j (i.e., aLR_{ij}) with AIC and BIC values can be written as:

aLR_{ij}^{AIC} = exp ($\frac{AIC_j - AIC_i}{2}$). (S3)

aLR_{ij}^{BIC} = exp ($\frac{BIC_j - BIC_i}{2}$). (S4)

Table S3.3. Adjusted maximum likelihood ratio (aLR^{AIC} and aLR^{BIC}) between models (row model over column model) in model fitting using multiple locations (left) or only home response locations (right).

	Multiple response locations				Home response locations only			
aLR^{AIC}	M0	M1	M2	M3	M0	M1	M2	M3
M1	$7.30 \times 10^{32**}$				$4.70 \times 10^{20**}$			
M2	$1.82 \times 10^{40**}$	$2.49 \times 10^{7**}$			$1.35 \times 10^{20**}$	0.29^{*}		
M3	$1.51 \times 10^{53**}$	$2.11 \times 10^{20**}$	$8.32 \times 10^{12**}$		$1.45 \times 10^{19**}$	0.03^{**}	0.003^{**}	
aLR^{BIC}	M0	M1	M2	M3	M0	M1	M2	M3
M1	$6.95 \times 10^{31**}$				$1.17 \times 10^{20**}$			

M2	$1.73 \times 10^{39**}$	$2.49 \times 10^{7**}$		$3.33 \times 10^{19**}$	0.29^{*}	
M3	$1.45 \times 10^{51**}$	$2.02 \times 10^{19**}$	$8.10 \times 10^{11**}$	$8.89 \times 10^{17**}$	0.008^{**}	0.03^{**}

Note: * indicates clear evidence, i.e., LR > 3 or LR <1/3, and ** indicates strong evidence, i.e., LR > 10 or LR <1/10 (Glover & Dixon, 2004).

The results of aLR in Table S3.3 clearly showed that the bi-component model (M3) is the best model when all three response locations were included in the model fitting. In contrast, although the encoding-error model, execution-error model, and the bi-component model (M1, M2, and M3) are better than the baseline model (M0), the bi-component model (M3) was even worse than the encoding-error and the execution-error models (M1 and M2) when only home response locations were included in the model fitting.

The frequency of the pairwise likelihood ratio in different categories in model recovery. Figure S3.2 plots the frequency of different categories of evidence for the true model in model validation on the 100 sets of simulated response locations. The results showed that the algorithm of using multiple response locations can successfully distinguish the true model from other models. Specifically, when the true model was M1, we got evidence favoring M1 over M2 and M3 with possibilities of 100% and 98% respectively. When the true model was M2, we got evidence favoring M2 over M1 and M3 with possibilities of 100% and 82% respectively. When the true model was M3, we got evidence favoring M3 over M1 and M2 with 100% for both. We never got evidence favoring the other two models over the true model.

In contrast, the algorithm of using home response locations only cannot clearly distinguish the true model from other models. When the true model was M1, we got evidence favoring M1 over M2 and M3 with possibilities of 40% and 52% respectively. When the true model was M2, we got evidence favoring M2 over M1 and M3 with possibilities of 93% and

51% respectively. When the true model was M3, we got evidence favoring M3 over M1 and M2 with possibilities of 37% and 26%. In addition to the relatively low chances to recover the true models, we also got evidence favoring the wrong models over the true model. There was evidence favoring M2 over the true model M1 with a possibility of 6%, evidence favoring M3 over the true model M2 with a possibility of 1%, and evidence favoring M1 and M2 over the true model M3 with possibilities of 9% and 17%.

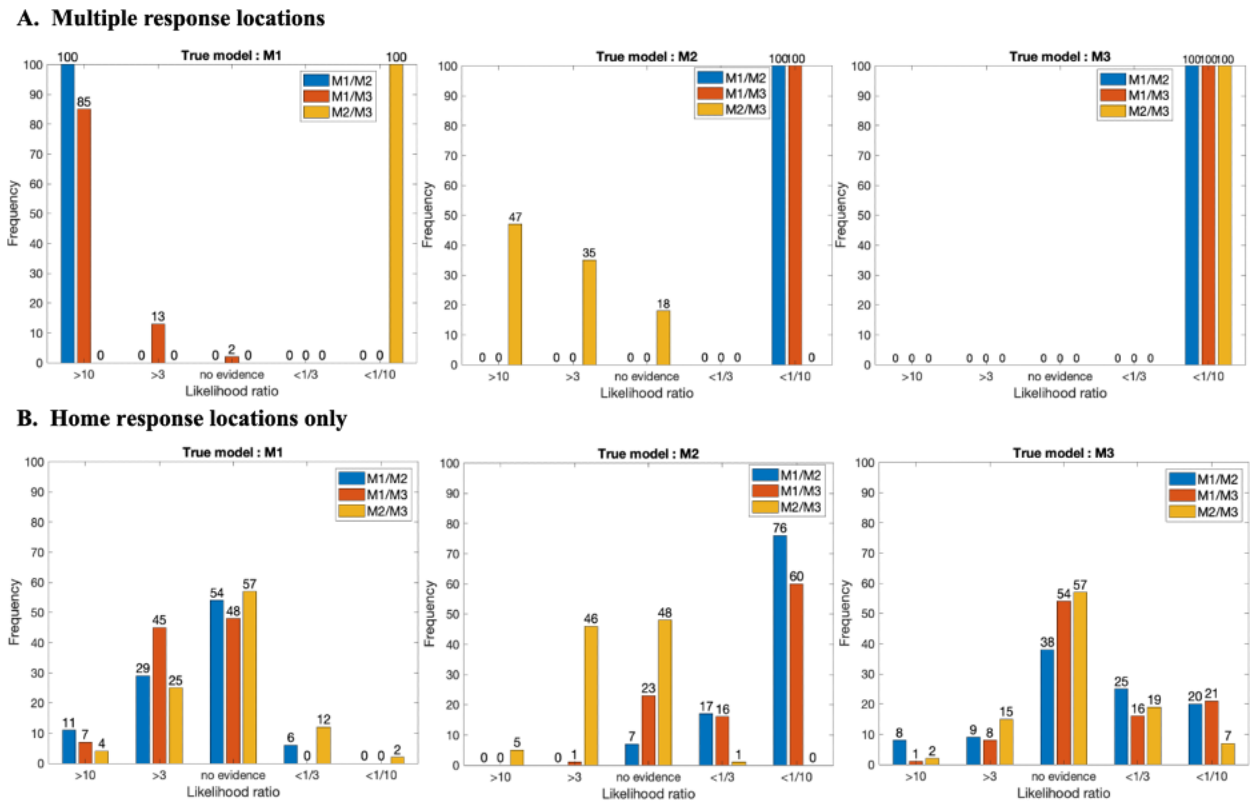

Figure S3.2. Frequency in each category of likelihood ratio in model validation using (A) multiple response locations or (B) home response locations only. These locations are simulated locations from different true models (M1, M2, or M3). Mi/Mj indicates the ratio of model Mi over model Mj. >10 indicates strong evidence supporting Mi, >3 indicates clear evidence supporting Mi, <10 indicates strong evidence supporting Mj, <3 indicates clear evidence supporting Mj.

Values of parameters estimated from real and simulated response locations

Table S3.4 lists the values of parameters estimated for the three models using real data (i.e., true parameters in the upper table) and using the simulated data generated from different models. The simulated data for each model were produced by fixed values of model parameters for all participants (Table 1).

Table S3.4. The similarity between values of parameters based on real response locations (the upper panel) and simulated response locations from different models (the lower panel). S_M1, S_M2, and S_M3 denote the simulated response locations from the true models of M1, M2, and M3 respectively.

	Values of parameters based on real response locations															
	M1				M2				M3							
	$\theta_{L\_s}^{enc}$	$\theta_{L\_i}^{enc}$	$\theta_{A\_s}^{enc}$	$\theta_{A\_i}^{enc}$	$\theta_{L\_s}^{exe}$	$\theta_{L\_i}^{exe}$	$\theta_{A\_s}^{exe}$	$\theta_{A\_i}^{exe}$	$\theta_{L\_s}^{enc}$	$\theta_{L\_i}^{enc}$	$\theta_{A\_s}^{enc}$	$\theta_{A\_i}^{enc}$	$\theta_{L\_s}^{exe}$	$\theta_{L\_i}^{exe}$	$\theta_{A\_s}^{exe}$	$\theta_{A\_i}^{exe}$
	1.04	0.48	0.79	18.38	0.70	1.29	0.78	41.11	0.8	0.78	0.84	20.42	0.6	1.10	0.82	34.21
	Recovered parameters based on simulated locations from each true model															
S_M1	1.04	0.48	0.79	18.37	1.10	0.19	0.87	20.69	1.0	0.53	0.80	17.99	0.9	0.08	0.98	2.54
S_M2	1.39	-.36	0.92	1.55	0.69	1.30	0.78	41.05	1.0	0.00	1.00	0.21	0.6	1.31	0.79	41.06
S_M3	1.06	0.41	0.82	14.91	0.75	1.29	0.78	41.11	0.8	0.78	0.84	20.42	0.6	1.10	0.82	34.21

Effect of participant groups on model validation using the same parameters for all participants

Considering two different compression groups, we examined whether the compression group modulated the model performance. We conducted model validation for each group using the model parameters estimated in model fitting without considering the participant variable (see the parameters in Table 3.1). Tables S3.5-S3.8 show that model validation based on the parameters from the algorithm using home only still could not differentiate the three models in

either compression group. However, model validation based on the parameters from the algorithm using multiple locations showed different results of model comparison in the strong and the weak compression groups. Specifically, for the strong compression group, the bi-component model (M3) was still the best model as indicated by the generalizability measures (RMSE, MaxLogL, and partialR^2) in Table S3.5, RMSEs of individual folds in Table S3.6, the likelihood ratio in Table S3.7 and the results of *Alpaydin's F-test* in Table S3.8. In contrast, for the weak compression group, all three models (M1-M3) even performed worse than the baseline model (M0) (e.g., partial R^2 was negative in Table S3.5). Among the three models, the encoding-error model (M1) appeared to be the best one.

Table S3.5. Mean validation performance across 10 folds for the group with strong (upper) and weak (lower) compression patterns using multiple locations (left) or only home response locations (right). The RMSE, maximum log-likelihood, and partial r-squared are generalizability measures, which were calculated by applying the same parameters for all participants (i.e., the parameters in Table 1 from model fitting).

	Strong compression group					
	Multiple response locations			Home response locations only		
	RMSE	MaxLogL	Partial R^2	RMSE	MaxLogL	Partial R^2
Model						
M0	3.384	-3768.8	0	3.043	-1191.6	0
M1	3.223	-3691.3	0.094	2.765	-1143.2	0.176
M2	3.152	-3651.6	0.133	2.767	-1143.2	0.174
M3	3.114	-3632.7	0.154	2.767	-1143.5	0.174

	Weak compression group					
	Multiple response locations			Home response locations only		
Model	RMSE	MaxLogL	Partial R^2	RMSE	MaxLogL	Partial R^2
M0	2.816	-2168.7	0	2.375	-662.1	0
M1	2.849	-2184.3	-0.024	2.400	-668.6	-0.023
M2	2.903	-2205.2	-0.063	2.400	-668.7	-0.022
M3	2.890	-2200.5	-0.054	2.402	-668.9	-0.024

Table S3.6. RMSEs of individual folds in validation for strong and weak compression groups using two algorithms.

	Strong compression group					
	Multiple response locations			Home response locations only		
RMSE	M1	M2	M3	M1	M2	M3
1st round	2.951	2.889	2.842	2.598	2.598	2.603
	3.473	3.405	3.360	2.928	2.929	2.931
2nd round	3.031	2.955	2.923	2.630	2.620	2.635
	3.427	3.355	3.321	2.912	2.916	2.923
3rd round	2.957	2.890	2.836	2.559	2.567	2.559
	3.494	3.428	3.392	2.982	2.980	2.982
4th round	2.793	2.705	2.678	2.369	2.380	2.370
	3.644	3.577	3.540	3.131	3.131	3.135
5th round	3.350	3.299	3.252	2.888	2.892	2.886

	3.111	3.020	2.997	2.649	2.658	2.648

	Weak compression group					
	Multiple response locations			Home response locations only		
RMSE	M1	M2	M3	M1	M2	M3
1st round	2.791	2.845	2.824	2.420	2.414	2.422
	2.915	2.968	2.955	2.394	2.393	2.399
2nd round	2.778	2.818	2.817	2.253	2.248	2.254
	2.921	2.982	2.961	2.532	2.539	2.536
3rd round	2.897	2.948	2.926	2.317	2.312	2.316
	2.813	2.870	2.876	2.485	2.488	2.487
4th round	2.796	2.875	2.852	2.356	2.357	2.356
	2.889	2.926	2.916	2.451	2.453	2.452
5th round	2.713	2.772	2.747	2.267	2.277	2.272
	2.978	3.029	3.030	2.526	2.520	2.525

Table S3.7. Maximum likelihood ratio (LR) between models (row model over column model) in model validation for the strong (upper) and weak (lower) compression groups using multiple locations (left) or only home response locations (right).

	Strong compression group							
	Multiple response locations				Home response locations only			
LR	M0	M1	M2	M3	M0	M1	M2	M3
M1	$1.93 \times 10^{33**}$				$1.06 \times 10^{21**}$			
M2	$3.40 \times 10^{50**}$	$1.76 \times 10^{17**}$			$1.01 \times 10^{21**}$	0.95—		
M3	$5.52 \times 10^{58**}$	$2.86 \times 10^{25**}$	$1.63 \times 10^{8**}$		$8.16 \times 10^{20**}$	0.77—	0.81—	

	Weak compression group							
	Multiple response locations				Home response locations only			
LR	M0	M1	M2	M3	M0	M1	M2	M3
M1	$1.63 \times 10^{-7**}$				0.0014^{**}			
M2	$1.39 \times 10^{-16**}$	$8.56 \times 10^{-10**}$			0.0013^{**}	$0.89^{—}$		
M3	$1.60 \times 10^{-14**}$	$9.82 \times 10^{-8**}$	114.94^{**}		0.0011^{**}	$0.76^{—}$	$0.86^{—}$	

Note: * indicates clear evidence, i.e., LR > 3 or LR <1/3, and ** indicates strong evidence, i.e., LR > 10 or LR <1/10. — indicates no evidence (Glover & Dixon, 2004).

Table S3.8. Alpaydin's F-test examining the differences in RMSE (dRMSE) between models (the row model minus the column model) for the strong (upper) and weak (lower) compression groups when using multiple locations (left) or only home response locations (right).

	Strong compression group							
	Multiple response locations				Home response locations only			
dRMSE	M0	M1	M2	M3	dRMSE	M0	M1	M2	M3
M1	$-.161^{***}$				M1	$-.278^{***}$			
M2	$-.187^{***}$	$-.071^{**}$			M2	$-.276^{***}$	$.002^{—}$		
M3	$-.270^{**}$	$-.109^{***}$	$-.038^{**}$		M3	$-.275^{***}$	$.003^{—}$	$.000^{—}$	
	Weak compression group							
	Multiple response locations				Home response locations only			
dRMSE	M0	M1	M2	M3	dRMSE	M0	M1	M2	M3
M1	$.033^{—}$				M1	$.025^{—}$			
M2	$.087^{*}$	$.054^{**}$			M2	$.025^{—}$	$-.000^{—}$		
M3	$.074^{—}$	$.042^{*}$	$-.013^{—}$		M3	$.027^{—}$	$.002^{—}$	$.002^{—}$	

Cross-validation considering participant variable (model recovery using varied values of parameters)

Model fitting for different groups. Table S3.9 summarizes the results of model fitting in two different compression groups using two algorithms. The difference in fitting performance (goodness-of-fit measures) between models is most distinct numerically in the strong compression group when multiple response locations were included, and the results suggest that the bi-component model (M3) was the best model.

Table S3.9. Model fitting performance for the strong and weak compression groups. Parameters are estimated from model fitting for each corresponding group. The RMSE, maximum log-likelihood, and partial r-squared are mean goodness-of-fit measures across 10 folds in model fitting.

Model	Strong compression group										
	Multiple response locations										
	Parameters								5×2 Fitting		
	$\theta_{L\_s}^{enc}$	$\theta_{L\_i}^{enc}$	$\theta_{A\_s}^{enc}$	$\theta_{A\_i}^{enc}$	$\theta_{L\_s}^{exe}$	$\theta_{L\_i}^{exe}$	$\theta_{A\_s}^{exe}$	$\theta_{A\_i}^{exe}$	RMSE	MaxLogL	Partial R^2
M0	1	0	1	0	1	0	1	0	3.382	-3770.4	0
M1	1.14	0.49	0.79	15.45	1	0	1	0	3.191	-3681.1	0.110
M2	1	0	1	0	0.60	1.86	0.68	58.50	3.113	-3640.8	0.153
M3	0.64	1.19	0.88	18.69	0.57	1.76	0.72	52.07	3.063	-3613.1	0.180
Model	Home response locations only										
	Parameters								5×2 Fitting		
	$\theta_{L\_s}^{enc}$	$\theta_{L\_i}^{enc}$	$\theta_{A\_s}^{enc}$	$\theta_{A\_i}^{enc}$	$\theta_{L\_s}^{exe}$	$\theta_{L\_i}^{exe}$	$\theta_{A\_s}^{exe}$	$\theta_{A\_i}^{exe}$	RMSE	MaxLogL	Partial R^2
M0	1	0	1	0	1	0	1	0	3.037	-1190.9	0
M1	0.84	0.58	0.46	18.64	1	0	1	0	2.716	-1136.4	0.200

M2	1	0	1	0	0.44	2.42	0.50	81.24	2.725	-1137.7	0.195
M3	2.88	0.84	0.43	12.46	0.72	0.86	1.51	12.50	2.713	-1135.9	0.202

Model	Weak compression group										
	Multiple response locations										
	Parameters								5×2 Fitting		
	$\theta_{L\_s}^{enc}$	$\theta_{L\_i}^{enc}$	$\theta_{A\_s}^{enc}$	$\theta_{A\_i}^{enc}$	$\theta_{L\_s}^{exe}$	$\theta_{L\_i}^{exe}$	$\theta_{A\_s}^{exe}$	$\theta_{A\_i}^{exe}$	RMSE	MaxLogL	Partial R^2
M0	1	0	1	0	1	0	1	0	2.817	-2169.2	0
M1	0.86	0.46	0.80	21.2	1	0	1	0	2.787	-2158.9	0.021
M2	1	0	1	0	0.85	0.46	1.00	2.96	2.807	-2166.7	0.007
M3	0.81	0.56	0.80	21.9	0.92	0.17	1.04	-1.73	2.778	-2155.8	0.028

Model	Home response locations only										
	Parameters								5×2 Fitting		
	$\theta_{L\_s}^{enc}$	$\theta_{L\_i}^{enc}$	$\theta_{A\_s}^{enc}$	$\theta_{A\_i}^{enc}$	$\theta_{L\_s}^{exe}$	$\theta_{L\_i}^{exe}$	$\theta_{A\_s}^{exe}$	$\theta_{A\_i}^{exe}$	RMSE	MaxLogL	Partial R^2
M0	1	0	1	0	1	0	1	0	2.379	-662.8	0
M1	0.51	0.69	0.44	33.0	1	0	1	0	2.300	-653.0	0.067
M2	1	0	1	0	0.44	1.43	0.44	84.44	2.304	-653.6	0.062
M3	1.54	11.7	2.25	17.8	0.58	0.06	2.24	17.13	2.293	-652.2	0.071

Model validation for different groups. Table S3.10 summarizes the validation performance of RMSEs in all ten folds for two different compression groups using two algorithms.

Table S3.10. RMSEs of individual folds in validation for strong and weak compression groups using two algorithms.

Strong compression group

	Multiple response locations			Home response locations only		
RMSE	M1	M2	M3	M1	M2	M3
1st round	3.438	3.366	3.319	2.934	2.930	2.934
	2.976	2.873	2.842	2.535	2.546	2.536
2nd round	3.436	3.341	3.317	2.905	2.912	2.907
	2.966	2.906	2.842	2.572	2.574	2.572
3rd round	2.879	2.774	2.734	2.422	2.423	2.423
	3.562	3.473	3.436	3.051	3.053	3.050
4th round	3.350	3.272	3.234	2.920	2.931	2.926
	3.119	2.990	2.956	2.576	2.595	2.604
5th round	3.117	3.039	2.996	2.544	2.543	2.544
	3.298	3.214	3.166	2.931	2.943	2.932

Weak compression group

	Multiple response locations			Home response locations only		
RMSE	M1	M2	M3	M1	M2	M3
1st round	2.788	2.803	2.777	2.334	2.330	2.333
	2.842	2.819	2.836	2.322	2.314	2.319
2nd round	2.681	2.695	2.672	2.360	2.370	2.364
	2.925	2.934	2.927	2.281	2.278	2.284
3rd round	2.790	2.737	2.785	2.390	2.397	2.329
	2.907	2.890	2.915	2.329	2.328	2.329
4th round	2.825	2.855	2.828	2.360	2.359	2.359
	2.790	2.805	2.787	2.282	2.276	2.338

5th round	2.862	2.867	2.850	2.474	2.476	2.472
	2.732	2.756	2.726	2.155	2.155	2.230

The frequency of the pairwise likelihood ratio in different categories in model recovery. After producing 100 sets of simulated response locations using varied values of parameters, the frequency of different categories of evidence for the true model in model validation are represented in Figure S3.3. The results showed that the algorithm of using multiple response locations can successfully distinguish the true model from other models. Specifically, when the true model was M1, we got evidence favoring M1 over M2 and M3 with possibilities of 100% and 64% respectively. When the true model was M2, we got evidence favoring M2 over M1 and M3 with possibilities of 100% and 84% respectively. When the true model was M3, we got evidence favoring M3 over M1 and M2 with 100% for both. We never got evidence favoring the other two models over the true model.

In contrast, the algorithm of using home response locations only cannot clearly distinguish the true model from other models. When the true model was M1, we got evidence favoring M1 over M2 and M3 with possibilities of 14% and 26% respectively. When the true model was M2, we got evidence favoring M2 over M1 and M3 with possibilities of 50% and 38% respectively. When the true model was M3, we got evidence favoring M3 over M1 and M2 with possibilities of 7% and 0%. In addition to the relatively low chances to recover the true models, we also got evidence favoring the wrong models over the true model. There was evidence favoring M2 and M3 over the true model M1 with a possibility of 42% and 27% respectively, evidence favoring M1 and M3 over the true model M2 with a possibility of 20%

and 10% respectively, and evidence favoring M1 and M2 over the true model M3 with possibilities of 5% and 13%.

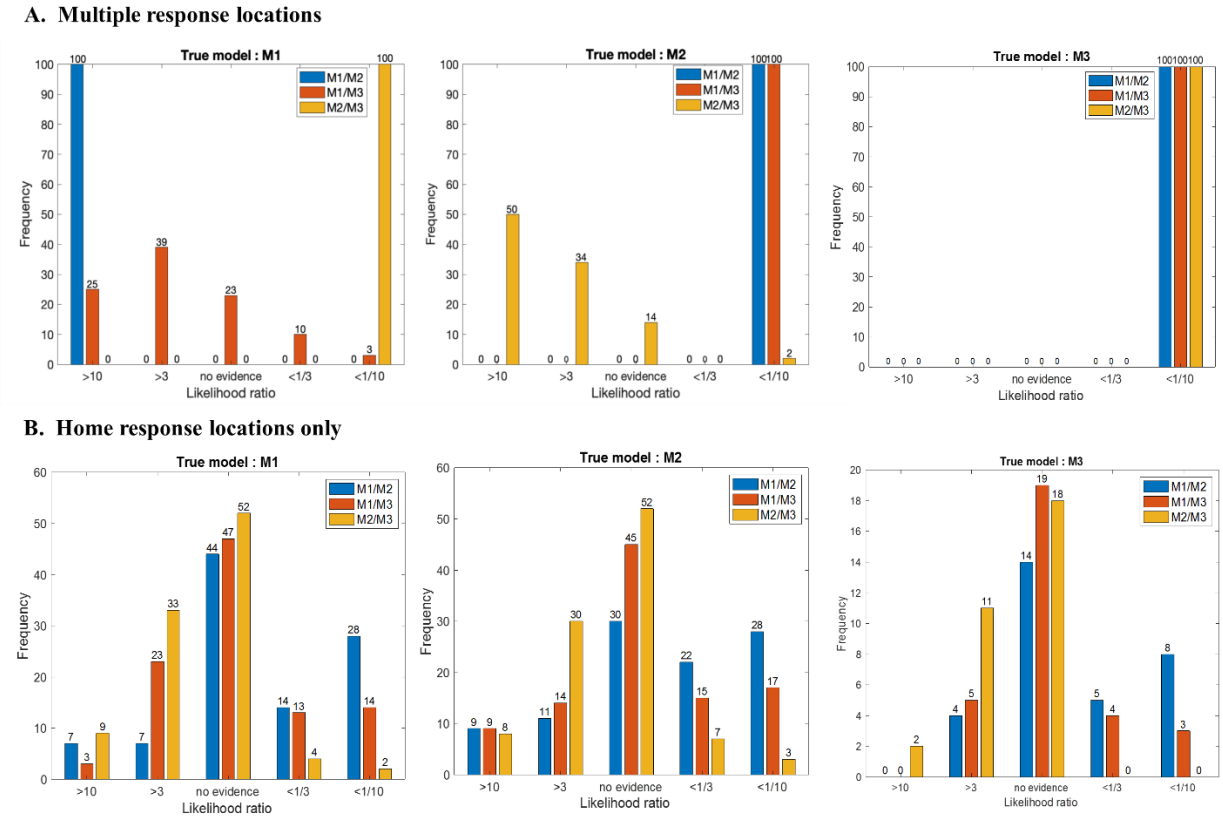

Figure S3.3. Frequency in each category of likelihood ratio in model validation using (A) multiple response locations or (B) home response locations only. These locations are simulated locations from different true models (M1, M2, or M3). Mi/Mj indicates the ratio of model Mi over model Mj. >10 indicates strong evidence supporting Mi, >3 indicates clear evidence supporting Mi, <10 indicates strong evidence supporting Mj, <3 indicates clear evidence supporting Mj.

Values of parameters estimated from real and simulated response locations.

Table S3.11 lists the values of parameters estimated for the three models using real data (i.e., true parameters in the upper table) and using the simulated data generated from different models. The

simulated data for each model were produced by varied values of model parameters considering the participants' differences in compression patterns.

Table S3. 11. The similarity between values of parameters based on real response locations (the upper panel) and simulated response locations from different models (the lower panel). S_M1, S_M2, and S_M3 denote the simulated response locations from the true models of M1, M2, and M3 respectively.

	True parameters based on real data															
	M1				M2				M3							
	$\theta_{L\_s}^{enc}$	$\theta_{L\_i}^{enc}$	$\theta_{A\_s}^{enc}$	$\theta_{A\_i}^{enc}$	$\theta_{L\_s}^{exe}$	$\theta_{L\_i}^{exe}$	$\theta_{A\_s}^{exe}$	$\theta_{A\_i}^{exe}$	$\theta_{L\_s}^{enc}$	$\theta_{L\_i}^{enc}$	$\theta_{A\_s}^{enc}$	$\theta_{A\_i}^{enc}$	$\theta_{L\_s}^{exe}$	$\theta_{L\_i}^{exe}$	$\theta_{A\_s}^{exe}$	$\theta_{A\_i}^{exe}$
	1.04	0.48	0.79	18.38	0.70	1.29	0.78	41.11	0.82	0.78	0.84	20.42	0.69	1.10	0.82	34.21
	Recovered parameters based on simulated data															
S_M1	1.07	0.48	0.80	17.78	1.07	0.21	0.85	23.60	1.06	0.45	0.79	18.44	0.96	0.06	0.97	4.76
S_M2	1.25	-.30	0.93	1.73	0.59	1.20	0.79	40.61	0.98	0.01	1.00	-.09	0.60	1.21	0.79	40.83
S_M3	1.04	0.29	0.81	16.66	0.67	1.04	0.74	45.00	0.96	0.50	0.84	19.09	0.64	0.93	0.81	34.86

Bibliography

Able, K. P. (1991). Common themes and variations in animal orientation systems. *American Zoologist, 31*(1), 157-167.

Akaike, H. (1973). Information theory and an extension of the maximum likelihood principle. In B. N. Petrov & F. Caski (Eds.), *Second international symposium on information theory* (pp. 267-281). Budapest: Akademiai Kiado.

Alpaydm, E. (1999). Combined 5× 2 cv F test for comparing supervised classification learning algorithms. *Neural Computation*, *11*(8), *1885-1892*.

Arlot, S., & Celisse, A. (2010). A survey of cross-validation procedures for model selection. *Statistics Surveys, 4*, 40-79.

Bakker, N. H., Werkhoven, P. J., & Passenier, P. O. (1999). The effects of proprioceptive and visual feedback on geographical orientation in virtual environments. *Presence, 8*(1), 36–53.

Bakker, N. H., Werkhoven, P. J., & Passenier, P. O. (2001). Calibrating visual path integration in VEs. *Presence, 10*(2), 216–224.

Batschelet, E. (1981). *Circular statistics in biology*. London, UK: Academic Press.

Benhamou, S., & Poucet, B. (1998). Landmark use by navigating rats (Rattus norvegicus) contrasting geometric and featural information. *Journal of Comparative Psychology, 112*(3), 317-322.

Benhamou, S., & Séguinot, V. (1995). How to find one's way in the labyrinth of path integration models. *Journal of Theoretical Biology, 174*(4), 463-466.

Boles, L. C., & Lohmann, K. J. (2003). True navigation and magnetic maps in spiny lobsters. *Nature, 421*(6918), 60-63.

Brown, J. E., & Skaggs, W. E. (2002). Concordant and discordant coding of spatial location in populations of hippocampal CA1 pyramidal cells. *Journal of Neurophysiology, 88*(4), 1605-1613.

Buckley, M. G., Haselgrove, M., & Smith, A. D. (2015). The developmental trajectory of intramaze and extramaze landmark biases in spatial navigation: An unexpected journey. *Developmental Psychology, 51*(6), 771-791.

Bullens, J., Nardini, M., Doeller, C. F., Braddick, O., Postma, A., & Burgess, N. (2010). The role of landmarks and boundaries in the development of spatial memory. *Developmental Science, 13*(1), 170-180.

Chan, E., Baumann, O., Bellgrove, M. A., & Mattingley, J. B. (2012). From objects to landmarks: the function of visual location information in spatial navigation. *Frontiers in Psychology, 3*, 304.

Chen, X., McNamara, T. P., Kelly, J. W., & Wolbers, T. (2017). Cue combination in human spatial navigation. *Cognitive Psychology, 95*, 105-144.

Cheng, K., & Newcombe, N. S. (2005). Is there a geometric module for spatial orientation? Squaring theory and evidence. *Psychonomic Bulletin & Review, 12*, 1-23.

Cheng, K., Shettleworth, S. J., Huttenlocher, J., & Rieser, J. J. (2007). Bayesian integration of spatial information. *Psychological Bulletin, 133*(4), 625-637.

Cheng, K., & Spetch, M. L. (1998). Mechanisms of landmark use in mammals and birds. In S. Healy (Ed.), *Spatial representation in animals* (pp. 1–17). New York, NY: Oxford University Press.

Chrastil, E. R., & Warren, W. H. (2014). Does the human odometer use an extrinsic or intrinsic metric?. *Attention, Perception, & Psychophysics, 76*(1), 230-246.

Chrastil, E. R., & Warren, W. H. (2017). Rotational error in path integration: Encoding and execution errors in angle reproduction. *Experimental Brain Research, 235*(6), 1885-1897.

Chrastil, E. R., & Warren, W. H. (2021). Executing the homebound path is a major source of error in homing by path integration. *Journal of Experimental Psychology: Human Perception and Performance, 47*(1), 13-35.

Collett, M., & Collett, T. S. (2000). How do insects use path integration for their navigation?. *Biological Cybernetics, 83*(3), 245-259.

Collett, M., Collett, T. S., & Wehner, R. (1999). Calibration of vector navigation in desert ants. *Current Biology, 9*(18), 1031-1034.

Cressant, A., Muller, R. U., & Poucet, B. (1997). Failure of centrally placed objects to control the firing fields of hippocampal place cells. *Journal of Neuroscience, 17*(7), 2531-2542.

Cressant, A., Muller, R. U., & Poucet, B. (1999). Further study of the control of place cell firing by intra-apparatus objects. *Hippocampus, 9*(4), 423-431.

Dietterich, T. G. (1998). Approximate statistical tests for comparing supervised classification learning algorithms. *Neural Computation, 10*(7), 1895-1923.

Doeller, C. F., & Burgess, N. (2008). Distinct error-correcting and incidental learning of location relative to landmarks and boundaries. *Proceedings of the National Academy of Sciences, 105*(15), 5909-5914.

Douglas, R. M., Alam, N. M., Silver, B. D., McGill, T. J., Tschetter, W. W., & Prusky, G. T. (2005). Independent visual threshold measurements in the two eyes of freely moving rats and mice using a virtual-reality optokinetic system. Visual Neuroscience, 22(5), 677-684.

Du, Y., Mou, W., & Zhang, L. (2020). Unidirectional influence of vision on locomotion in multimodal spatial representations acquired from navigation. *Psychological Research, 84*(5), 1284-1303.

Dyer, F. C., Berry, N. A., & Richard, A. S. (1993). Honey bee spatial memory: Use of route-based memories after displacement. *Animal Behaviour, 45*(5),1028-1030.

Ekstrom, A. D. (2015). Why vision is important to how we navigate. *Hippocampus, 25*(6), 731-735.

Etienne, A. S., & Jeffery, K. J. (2004). *Path integration in mammals*. Hippocampus, 14(2), 180-192.

Etienne, A. S., Maurer, R., Boulens, V., Levy, A., & Rowe, T. (2004). Resetting the path integrator: A basic condition for route-based navigation. *Journal of Experimental Biology, 207*(9), 1491-1508.

Etienne, A. S., Maurer, R., & Séguinot, V. (1996). Path integration in mammals and its interaction with visual landmarks. *Journal of Experimental Biology, 199*(1), 201-209.

Etienne, A. S., Teroni, E., Hurni, C., & Portenier, V. (1990). The effect of a single light cue on homing behaviour of the golden hamster. *Animal Behaviour, 39*(1), 17-41.

Fujita, N., Klatzky, R. L., Loomis, J. M., & Golledge, R. G. (1993). The encoding-error model of pathway completion without vision. *Geographical Analysis, 25*(4), 295-314.

Foo, P., Warren, W. H., Duchon, A., & Tarr, M. J. (2005). Do humans integrate routes into a cognitive map? Map-versus landmark-based navigation of novel shortcuts. *Journal of Experimental Psychology: Learning, Memory, and Cognition, 31(2)*, 195-215.

Friedman, A., & Kohler, B. (2003). Bidimensional regression: Assessing the configural similarity and accuracy of cognitive maps and other two-dimensional data sets. *Psychological Methods, 8*(4), 468-491.

Gallistel, C. R. (1990). *The organization of learning.* The MIT Press.

Gladwin, T. (1970) *East is a big bird*. Cambridge, MA., Harvard University Press.

Glover, S., & Dixon, P. (2004). Likelihood ratios: A simple and flexible statistic for empirical psychologists. *Psychonomic Bulletin & Review, 11*(5), 791-806.

Goodridge, J. P., & Taube, J. S. (1995). Preferential use of the landmark navigational system by head direction cells in rats. *Behavioral Neuroscience, 109*(1), 49-61.

Harootonian, S. K., Ekstrom, A. D., & Wilson, R. C. (2022). Combination and competition between path integration and landmark navigation in the estimation of heading direction. *PLoS Computational Biology, 18*(2), e1009222.

Harootonian, S. K., Wilson, R. C., Hejtmánek, L., Ziskin, E. M., & Ekstrom, A. D. (2020). Path integration in large-scale space and with novel geometries: Comparing vector addition and encoding-error models. *PLoS Computational Biology, 16*(5), e1007489.

He, Q., & McNamara, T. P. (2018). Spatial updating strategy affects the reference frame in path integration. *Psychonomic Bulletin & Review, 25*(3), 1073-1079.

Hebb, D. O. (1938). Studies of the organization of behavior. I. Behavior of the rat in a field orientation. *Journal of Comparative Psychology*, *25*(2), 333-352.

Hebb, D. O. (1949). *The organization of behaviour*. Wiley-Interscience, New York.

Hermer, L., & Spelke, E. S. (1994). A geometric process for spatial reorientation in young children. *Nature, 370*(6484), 57–59.

Hughes, R. N., & Blight, C. M. (1999). Algorithmic behaviour and spatial memory are used by two intertidal fish species to solve the radial maze. *Animal Behaviour, 58*(3), 601-613.

Huttenlocher, J., Hedges, L. V., & Duncan, S. (1991). Categories and particulars: Prototype effects in estimating spatial location. *Psychological Review, 98*(3), 352-376.

Jacobs, L. F., & Schenk, F. (2003). Unpacking the cognitive map: the parallel map theory of hippocampal function. *Psychological Review, 110*(2), 285-315.

Jordan, M. I. (2003). *An Introduction to Probabilistic Graphical Models.* Chapter 13, Unpublished manuscript. Department of Statistics, University of California. https://people.eecs.berkeley.edu/~jordan/prelims/chapter13.pdf

Kearns, M. J., Warren, W. H., Duchon, A. P., & Tarr, M. J. (2002). Path integration from optic flow and body senses in a homing task. *Perception, 31*(3), 349-374.

Kelly, J. W., McNamara, T. P., Bodenheimer, B., Carr, T. H., & Rieser, J. J. (2008). The shape of human navigation: How environmental geometry is used in maintenance of spatial orientation. *Cognition, 109*(2), 281-286.

Klatzky, R. L., Beall, A. C., Loomis, J. M., Golledge, R. G., & Philbeck, J. W. (1999). Human navigation ability: Tests of the encoding-error model of path integration. *Spatial Cognition and Computation, 1*(1), 31-65.

Klatzky, R. L., Loomis, J. M., Beall, A. C., Chance, S. S., & Golledge, R. G. (1998). Spatial updating of self-position and orientation during real, imagined, and virtual locomotion. *Psychological Science, 9*(4), 293-298.

Klatzky, R. L., Loomis, J. M., Golledge, R. G., Cicinelli, J. G., Doherty, S., & Pellegrino, J. W. (1990). Acquisition of route and survey knowledge in the absence of vision. *Journal of Motor Behavior, 22*(1), 19-43.

Knierim, J. J. (2002). Dynamic interactions between local surface cues, distal landmarks, and intrinsic circuitry in hippocampal place cells. *Journal of Neuroscience, 22*(14), 6254-6264.

Knierim, J. J., & Hamilton, D. A. (2011). Framing spatial cognition: Neural representations of proximal and distal frames of reference and their roles in navigation. *Physiological Reviews, 91*(4), 1245-1279.

Kravitz, D. J., Saleem, K. S., Baker, C. I., Ungerleider, L. G., & Mishkin, M. (2013). The ventral visual pathway: An expanded neural framework for the processing of object quality. *Trends in Cognitive Sciences, 17*(1), 26-49.

Layne, J. E., Barnes, W. J. P., & Duncan, L. M. (2003). Mechanisms of homing in the fiddler crab Uca rapax 2. Information sources and frame of reference for a path integration system. *Journal of Experimental Biology, 206*(24), 4425-4442.

Learmonth, A. E., Nadel, L., & Newcombe, N. S. (2002). Children's use of landmarks: Implications for modularity theory. *Psychological Science, 13*(4), 337-341.

Lee, S. A., & Spelke, E. S. (2010). A modular geometric mechanism for reorientation in children. *Cognitive Psychology, 61*(2), 152-176.

Lei, X., & Mou, W. (2023). Visual re-anchoring in misaligned local spaces impairs global path integration. *Journal of Experimental Psychology: Learning, Memory, and Cognition*. *49*(5), 728-742.

Lew, A. R. (2011). Looking beyond the boundaries: Time to put landmarks back on the cognitive map?. *Psychological Bulletin, 137*(3), 484-507.

Loomis, J. M., Klatzky, R. L., Golledge, R. G., Cicinelli, J. G., Pellegrino, J. W., & Fry, P. A. (1993). Nonvisual navigation by blind and sighted: Assessment of path integration ability. *Journal of Experimental Psychology: General*, 122(1), 73-91.

Loomis, J. M., Klatzky, R. L., Golledge, R. G., & Philbeck, J. W. (1999). Human navigation by path integration. In R. G. Golledge (Ed.), *Wayfinding: Cognitive mapping and other spatial processes* (pp. 125–151). Baltimore, MD: Johns Hopkins University Press.

Lu, R., Yu, C., Li, Z., Mou, W., & Li, Z. (2020). Set size effects in spatial updating are independent of the online/offline updating strategy. *Journal of Experimental Psychology: Human Perception and Performance, 46*(9), 901-911.

May, M., & Klatzky, R. L. (2000). Path integration while ignoring irrelevant movement. *Journal of Experimental Psychology: Learning, Memory, and Cognition, 26*(1), 169–186.

McNamara, T. P., & Chen, X. (2022). Bayesian decision theory and navigation. *Psychonomic Bulletin & Review*, *29*, 721-752.

Mittelstaedt, H., & Mittelstaedt, M. L. (1982). Homing by path integration. In F. Papi & H. G. Wallraff (Eds.), *Avian navigation* (pp. 290–297). Springer-Verlag.

Mittelstaedt, M. L., & Glasauer, S. T. E. F. A. N. (1991). Idiothetic navigation in gerbils and humans. *Zool. Jb. Physiol*, *95*, 427-435.

Mittelstaedt, M. L., & Mittelstaedt, H. (1980). Homing by path integration in a mammal. *Die Naturwissenschaften, 67*(11), 566-567.

Mou, W., & Zhang, L. (2014). Dissociating position and heading estimations: Rotated visual orientation cues perceived after walking reset headings but not positions. *Cognition, 133*(3), 553-571.

Muller, R. U., & Kubie, J. L. (1987). The effects of changes in the environment on the spatial firing of hippocampal complex-spike cells. *Journal of Neuroscience, 7*(7), 1951-1968.

Müller, M., & Wehner, R. (1988). Path integration in desert ants, Cataglyphis fortis. *Proceedings of the National Academy of Sciences, 85*(14), 5287-5290.

Nadel, L., & Haupbach, A. (2006). Species comparisons in development: The case of the geometric 'module'. *Processes of Change in Brain and Cognitive Development: Attention and Performance XXI*, 499-511.

Nardini, M., Jones, P., Bedford, R., & Braddick, O. (2008). Development of cue integration in human navigation. *Current Biology, 18*, 689–693.

Negen, J., Bird, L. A., King, E., & Nardini, M. (2020). The difficulty of effectively using allocentric prior information in a spatial recall task. *Scientific Reports*, *10*(1), 7000.

Newman, P. M., Qi, Y., Mou, W., & McNamara, T. P. (2023). Statistically optimal cue integration during human spatial navigation. *Psychonomic Bulletin & Review*, 1-22.

O'Keefe, J., & Nadel, L. (1978). *The hippocampus as a cognitive map* (Vol. 3, pp. 483-484). Oxford: Clarendon Press.

O'Keefe, J., & Speakman, A. 1. (1987). Single unit activity in the rat hippocampus during a spatial memory task. *Experimental Brain Research, 68*, 1-27.

Padilla, L. M., Creem-Regehr, S. H., Stefanucci, J. K., & Cashdan, E. A. (2017). Sex differences in virtual navigation influenced by scale and navigation experience. *Psychonomic Bulletin & Review, 24*, 582-590.

Parron, C., Poucet, B., & Save, E. (2004). Entorhinal cortex lesions impair the use of distal but not proximal landmarks during place navigation in the rat. *Behavioural Brain Research, 154*(2), 345-352.

Pecchia, T., & Vallortigara, G. (2010). View-based strategy for reorientation by geometry. *Journal of Experimental Biology, 213*(17), 2987-2996.

Péruch, P., May, M., & Wartenberg, F. (1997). Homing in virtual environments: Effects of field of view and path layout. *Perception, 26*(3), 301–311.

Petzschner, F. H., & Glasauer, S. (2011). Iterative Bayesian estimation as an explanation for range and regression effects: A study on human path integration. *Journal of Neuroscience, 31*(47), 17220-17229.

Petzschner, F. H., Maier, P., & Glasauer, S. (2012). Combining symbolic cues with sensory input and prior experience in an iterative Bayesian framework. *Frontiers in Integrative Neuroscience*, *6*, 58.

Raschka, S. (2018). MLxtend: Providing machine learning and data science utilities and extensions to Python's scientific computing stack. *Journal of Open Source Software, 3*(24), 638.

Refaeilzadeh, P., Tang, L., & Liu, H. (2009). Cross-validation. *Encyclopedia of Database Systems, 5*, 532-538.

Renaudineau, S., Poucet, B., & Save, E. (2007). Flexible use of proximal objects and distal cues by hippocampal place cells. *Hippocampus, 17*(5), 381-395.

Rieser, J. J. (1989). Access to knowledge of spatial structure at novel points of observation. *Journal of Experimental Psychology: Learning, Memory, and Cognition*, *15*(6), 1157-1165.

Rieser, J. J., Ashmead, D. H., Talor, C. R., & Youngquist, G. A. (1990). Visual perception and the guidance of locomotion without vision to previously seen targets. *Perception, 19*(5), 675-689.

Rieser, J. J., & Rider, E. A. (1991). Young children's spatial orientation with respect to multiple targets when walking without vision. *Developmental Psychology, 27*(1), 97-107.

Roy, C., Wiebusch, D., Botsch, M., & Ernst, M. O. (2023). Did it move? Humans use spatio-temporal landmark permanency efficiently for navigation. *Journal of Experimental Psychology: General, 152*(2), 448-463.

Saint Paul, U. V. (1982). Do geese use path integration for walking home? In F. Papi & H. G. Wallraff (Eds.), *Avian navigation* (pp. 298–307). Springer.

Sampaio, C., Jones, M., Engelbertson, A., & Williams, M. (2020). Bayesian priors in estimates of object location in virtual reality. *Psychonomic Bulletin & Review, 27*, 1309-1316.

Séguinot, V., Maurer, R., & Etienne, A. S. (1993). Dead reckoning in a small mammal: the evaluation of distance. *Journal of Comparative Physiology A, 173*, 103-113.

Schwarz, G. (1978). Estimating the dimension of a model. *The Annals of Statistics*, 461-464.

Shapiro, M. L., Tanila, H., & Eichenbaum, H. (1997). Cues that hippocampal place cells encode: Dynamic and hierarchical representation of local and distal stimuli. *Hippocampus, 7*(6), 624-642.

Souman, J. L., Frissen, I., Sreenivasa, M. N., & Ernst, M. O. (2009). Walking straight into circles. *Current Biology, 19*(18), 1538-1542.

Stevens, S. S., & Greenbaum, H. B. (1966). Regression effect in psychophysical judgment. *Perception & Psychophysics, 1*(5), 439-446.

Taboga, Marco (n.d.). *Multivariate normal distribution - Maximum Likelihood Estimation*. StatLect. https://www.statlect.com/fundamentals-of-statistics/multivariate-normal-distribution-maximum-likelihood.

Tanila, H., Shapiro, M. L., & Eichenbaum, H. (1997). Discordance of spatial representation in ensembles of hippocampal place cells. *Hippocampus, 7*(6), 613-623.

Taube, J. S. (2007). The head direction signal: origins and sensory-motor integration. *Annual Review of Neuroscience, 30*, 181-207.

Taube, J. S., & Burton, H. L. (1995). Head direction cell activity monitored in a novel environment and during a cue conflict situation. *Journal of Neurophysiology, 74*(5), 1953-1971.

Tcheang, L., Bülthoff, H. H., & Burgess, N. (2011). Visual influence on path integration in darkness indicates a multimodal representation of large-scale space. *Proceedings of the National Academy of Sciences, 108*(3), 1152-1157.

Teghtsoonian, R., & Teghtsoonian, M. (1978). Range and regression effects in magnitude scaling. *Perception & Psychophysics, 24*(4), 305-314.

Valerio, S., & Taube, J. S. (2012). Path integration: how the head direction signal maintains and corrects spatial orientation. *Nature Neuroscience, 15*(10), 1445-1453.

Wallace, D. J., Greenberg, D. S., Sawinski, J., Rulla, S., Notaro, G., & Kerr, J. N. (2013). Rats maintain an overhead binocular field at the expense of constant fusion. *Nature, 498*(7452), 65-69.

Wang, L., & Mou, W. (2020). Effect of room size on geometry and features cue preference during reorientation: Modulating encoding strength or cue weighting. *Quarterly Journal of Experimental Psychology, 73*(2), 225-238.

Wang, L., Mou, W., & Dixon, P. (2018). Cue interaction between buildings and street configurations during reorientation in familiar and unfamiliar outdoor environments. *Journal of Experimental Psychology: Learning, Memory, and Cognition, 44*(4), 631-644.

Wang, R. F. (2016). Building a cognitive map by assembling multiple path integration systems. *Psychonomic Bulletin & Review, 23*(3), 692-702.

Wang, R. F., & Brockmole, J. R. (2003). Human navigation in nested environments. *Journal of Experimental Psychology: Learning, Memory, and Cognition*, *29*(3), 398-404.

Wang, R. F., & Spelke, E. S. (2000). Updating egocentric representations in human navigation. *Cognition, 77*(3), 215-250.

Warren, W. H. (2019). Non-euclidean navigation. *Journal of Experimental Biology, 222*(jeb187917), 1–10.

Warren, W. H., Kay, B. A., Zosh, W. D., Duchon, A. P., & Sahuc, S. (2001). Optic flow is used to control human walking. *Nature Neuroscience, 4*(2), 213-216.

Warren, W. H., Rothman, D. B., Schnapp, B. H., & Ericson, J. D. (2017). Wormholes in virtual space: From cognitive maps to cognitive graphs. *Cognition, 166*, 152-163.

Wartenberg, F., May, M., & Péruch, P. (1998). Spatial orientation in virtual environments: Background considerations and experiments. In C. Freska, C. Habel, & K. F. Wender (Eds.), *Spatial cognition* (pp. 469–489). Springer.

Wehner, R., Michel, B., & Antonsen, P. (1996). Visual navigation in insects: Coupling of egocentric and geocentric information. *Journal of Experimental Biology, 199*(1), 129-140.

Wehner, R., & Srinivasan, M. V. (1981). Searching behaviour of desert ants, genus Cataglyphis (Formicidae, Hymenoptera). *Journal of Comparative Physiology, 142*, 315-338.

Wehner, R., & Wehner, S. (1986). Path integration in desert ants. Approaching a long-standing puzzle in insect navigation. *Monitore Zoologico Italiano-Italian Journal of Zoology, 20*(3), 309-331.

Wiener, J. M., Berthoz, A., & Wolbers, T. (2011). Dissociable cognitive mechanisms underlying human path integration. *Experimental Brain Research, 208*(1), 61-71.

Wiener, J. M., & Mallot, H. A. (2006). Path complexity does not impair visual path integration. *Spatial Cognition and Computation, 6*(4), 333-346.

Wilson, P. N., & Alexander, T. (2008). Blocking of spatial learning between enclosure geometry and a local landmark. *Journal of Experimental Psychology: Learning, Memory, and Cognition, 34*(6), 1369-1376.

Wittlinger, M., Wehner, R., & Wolf, H. (2006). The ant odometer: Stepping on stilts and stumps. *Science, 312*(5782), 1965-1967.

Yamamoto, N., Meléndez, J. A., & Menzies, D. T. (2014). Homing by path integration when a locomotion trajectory crosses itself. *Perception, 43*(10), 1049-1060.

Yoder, R. M., Clark, B. J., & Taube, J. S. (2011). Origins of landmark encoding in the brain. *Trends in Neurosciences, 34*(11), 561-571.

Yoganarasimha, D., Yu, X., & Knierim, J. J. (2006). Head direction cell representations maintain internal coherence during conflicting proximal and distal cue rotations: Comparison with hippocampal place cells. *Journal of Neuroscience, 26*(2), 622-631.

Youngstrom, I. A., & Strowbridge, B. W. (2012). Visual landmarks facilitate rodent spatial navigation in virtual reality environments. *Learning & Memory, 19*(3), 84-90.

Zhang, L., & Mou, W. (2017). Piloting systems reset path integration systems during position estimation. *Journal of Experimental Psychology: Learning, Memory, and Cognition, 43*(3), 472-491.

Zhang, L., & Mou, W. (2019). Selective resetting position and heading estimations while driving in a large-scale immersive virtual environment. *Experimental Brain Research, 237*(2), 335-350.

Zhang, L., Mou, W., Lei, X., & Du, Y. (2020). Cue combination used to update the navigator's self-localization, not the home location. *Journal of Experimental Psychology: Learning, Memory, and Cognition. 46*(12), 2314-2339.

Zhao, M., & Warren, W. H. (2015a). Environmental stability modulates the role of path integration in human navigation. *Cognition, 142*, 96-109.

Zhao, M., & Warren, W. H. (2015b). How you get there from here: Interaction of visual landmarks and path integration in human navigation. *Psychological Science, 26*(6), 915-924.

Zhou, R., & Mou, W. (2016). Superior cognitive mapping through single landmark-related learning than through boundary related learning. *Journal of Experimental Psychology: Learning, Memory, and Cognition, 42*(8), 1316.

Zugaro, M. B., Tabuchi, E., & Wiener, S. I. (2000). Influence of conflicting visual, inertial and substratal cues on head direction cell activity. *Experimental Brain Research, 133*, 198-208.